CRANFIELD UNIVERSITY

CRANFIELD HEALTH

PhD Thesis

Academic Years 2008-2011

Joanne Louise Holmes

SCANNING ELECTROCHEMICAL MICROSCOPY FOR THE CHARACTERISATION OF SURFACES MODIFIED WITH BIOLOGICAL MOLECULES

Supervisor: Professor Séamus P. J. Higson

Presented February 2011

This thesis is submitted in partial fulfilment of the requirements for the degree of Doctor of Philosophy (PhD)

“Pressure is nothing more than the shadow of great opportunity."

Michael Johnson

Acknowledgements

First and foremost I would like to extend my gratitude to my supervisor, Professor Seamus Higson for all his support over the past three years – not only for his academic input, but also for his unerring enthusiasm and energy for what he does. Thanks also go to other senior members of the group – Dr. Frank Davis and Dr. Stuart Collyer for their technical and moral input. Thanks are also due to Dr. Michael Cauchi for his technical insights into my project and Professor Joe Lunec for his belief and support in me as an individual.

Thank you to all my family and my many friends for their input and influences throughout my life.

Finally the love and support of my partner Dave who has believed in me and gives me continual hope in everything I do.

Declaration

This is a declaration to certify that no portion of the work referred to in this thesis has been submitted in support of an application for another degree or qualification of this or any other university, or institute of learning.

The results detailed in Chapter 5 have contributed to a joint publication in *Analytica Chemica Acta*, (2011), In Press; this paper is included in the appendix of this thesis.

Joanne Louise Holmes

February 2011

Abstract

This thesis describes a novel fabrication procedure for microelectrodes to be used with the scanning electrochemical microscope (SECM), the characterisation of a variety of novel impedance based immunosensors, and the characterisation of a novel oligonucleotide biosensor.

The thesis firstly describes the development of a protocol for the fabrication of reproducible microelectrodes characterised to identify suitability in use with the SECM.

The thesis then describes the use of SECM in feedback mode to interrogate a variety of antibody-polyelectrolyte films determining whether the changes observed by impedance were detectable by SECM. A screen printed carbon ink surface was patterned with an array of biotinylated polyethyleneimine (PEI) which was exposed to Neutravidin and then the biotinylated antibody of interest. Using ferrocenecarboxylic acid as the redox couple, the array was interrogated by SECM, scanning before and following exposure to a series of concentrations of the complementary antigen and a non-complementary antigen. Upon the exposure of the PEI/Neutravidin/biotinylated antibody array to the antigen, the feedback current over the functionalised region was observed to change. The change observed increased as the concentration of the antigen exposed to the array was increased showing linear correlation. On exposure of the array to a non-complementary antigen, only a small change in the feedback current was observed. NSE, PSA, Ciprofloxacin and NTx were all investigated with limits of detection of 0.5 pg ml^{-1}, 1 pg ml^{-1}, 0.1 ng ml^{-1} and 1 nM respectively.

Finally using a similar method as employed above, SECM was utilised in the detection of binding events of short oligonucleotides. Once again scans were conducted before and after exposure to both complementary and non-complementary oligonucleotide sequences and by subtraction absolute changes in feedback current were determined. On exposure to the complementary oligonucleotide sequence a change in feedback was observed when the array was exposed to the non-complementary oligonucleotide sequence, as with the antibody/antigen array, only a small change in the feedback current was observed.

Table of Contents

List of figures i

Abbreviations x

1. Research rationale and Aims and Objectives 1
    1.1 Research Rationale 2
    1.2 Aims and Objectives 5

2. Introduction and literature review 6
    2.1 Electrochemistry 7
        2.1.1 Electron transfer and energy levels 7
        2.1.2 The Electrical Double Layer 11
        2.1.3 The electrochemical cell and electrodes 14
        2.1.4 Working electrodes (WE) 17
        2.1.5 Reference electrodes (RE) 17
        2.1.6 Counter electrodes (CE) 18
    2.2 Mass Transport 18
        2.2.1 Diffusion 19
        2.2.2 Convection 21
        2.2.3 Migration 22
    2.3 Microelectrodes 23
        2.3.1 Definition 23
        2.3.2 Microelectrode behaviour 24
        2.3.3 Advantages of microelectrodes 30
    2.4 Review of microelectrode fabrication methodologies 32
        2.4.1 Disk microelectrodes 32
        2.4.2 Hemispherical microelectrodes 34
        2.4.3 Ring-disk microelectrodes 34
        2.4.4 Finite Conical (Etched) microelectrodes 35

2.4.5 Microelectrodes by Microfabrication 36
2.5 Scanning electrochemical microscopy 37
2.5.1 Feedback mode 39
2.5.2 Substrate generation / tip collection mode 41
2.5.3 Tip generation / substrate collection mode 41
2.5.4 Penetration mode 42
2.6 Application of SECM to biological systems 43
2.6.1 DNA imaging by SECM 44
2.6.2 Enzymes 47
2.6.3 Living cells 51
2.6.4 Mammalian cells 55
2.6.5 Combined SECM instrumentation 56
2.6.4 Conclusions and future outlook 57

3. Materials and methods 59
3.1 Introduction 60
3.1.1 Reagents 60
3.1.2 Materials 61
3.1.3 Equipment 61
3.1.4 Solution preparation 62
3.2 Antibody/Antigen sensor characterisation methodology 62
3.2.1 Additional reagents 62
3.2.2 Substrate 63
3.2.3 Biotinylation of IgG 63
3.2.4 Polyelectrolyte film deposition 65
3.2.5 PEI/neutravidin/biotinylated antibody film formation 65
3.2.6 SECM interrogation and antibody/antigen binding detection 66
3.3 Oligonucleotide sensor characterisation methodology 67
3.3.1 Additional reagents 67
3.3.2 Substrate 67
3.3.3 Polyelectrolyte film deposition 68

3.3.4 PEI/neutravidin/biotinylated oligonucleotide film formation 68
3.3.5 SECM interrogation and hybridisation detection 68
3.4 Scanning Electrochemical Microscope (SECM) Instrumentation 69
3.4.1 Uniscan SECM270 69
3.4.2 XYZ stage 70
3.4.3 Probe clamp 71
3.4.4 Potentiostats 71
3.4.5 Software 72
3.5 Scanning Electrochemical Microscope experiment capabilities 73
3.5.1 Cyclic voltammetry 73
3.5.2 Approach curve macro 74
3.5.3 Area scan 75
3.5.4 Sloping scan macro 75
3.6 Three-Dimensional Representation of the Data 79
3.7 ELISA protocol 79

4. Microelectrode Fabrication and Characterisation 81
4.1 Introduction 82
4.2 Fabrication of microelectrode probes for SECM 83
4.2.1 Equipment 83
4.2.2 Method 83
4.3 Microelectrode characterisation 87
4.3.1 Optical Microscopy 87
4.3.2 Cyclic voltammetry 88
4.4 Conclusions 91

5. Characterisation of an immunosensor for the detection of neuron specific enolase by SECM 93
5.1 Introduction 94
5.2 Results and Discussion 97
5.2.1 Carbon electrode substrate 97
5.2.2 Characterisation of carbon inks by SECM 98
5.2.3 Polyelectrolyte films 102
5.2.4 Antibody biotinylation – UV spectrum profile 106
5.2.5 Interrogation of film integrity by SECM 108
5.2.6 Methodology of antigen/antibody binding experiments 110
5.2.7 Control experiments 111
5.2.8 Detection of antigen/antibody binding by SECM 113
5.3 Conclusions 118

6. Characterisation of an immunosensor for the detection of prostate specific antigen by SECM 120
6.1 Introduction 121
6.2 Results and Discussion 126
6.2.1 Detection of antigen/antibody binding by SECM 126
6.2.2 Detection of antigen/antibody binding by ELISA 132
6.3 Conclusions 133

7. Characterisation of an immunosensor for the detection of NTx by SECM 135
7.1 Introduction 136
7.2 Results and Discussion 139
7.2.1 Detection of antigen/antibody binding by SECM 139
7.3 Conclusions 146

8. Characterisation of an immunosensor for the detection of ciprofloxacin by SECM 147
8.1 Introduction 148

8.2 Results and Discussion 151
8.2.1 Detection of antigen/antibody binding in buffer by SECM 151
8.2.2 Detection of antigen/antibody binding in milk by ELISA 155
8.3 Conclusions 161

9. Characterisation of DNA biosensor by SECM 163
9.1 Introduction 164
9.2 Results and Discussion 168
9.2.1 Detection of oligonucleotide binding by SECM 168
9.3 Conclusions 175

10. General conclusions 176

11. Suggestions for further work 180

12. References 183

Appendices 214

Appendix 1: Paper 215

Appendix 2: Poster of Work 221

Appendix 2: Poster of Work 222

Appendix 4: Programme written in MatLab for 3D Visualization
of SECM sloping Marco Scan Results 223

List of figures

Figure No.	Legend	Page
2.1	Schematic diagram illustrating the pathway of a general electrode reaction.	8
2.2	Free energy profile for a single electron reduction of species $O_{(aq)}$.	10
2.3	Schematic diagram illustrating the principle of oxidation and reduction of species X. The molecular orbits shown are the highest energy filled orbitals and the lowest energy vacant orbitals.	11
2.4	Schematic diagram of the electrical double layer.	13
2.5	A) Two electrode cell; B) Three electrode cell with a counter/auxiliary electrode.	15
2.6	A schematic illustrating potential drop between working and auxiliary electrodes in solution and iR_u measured at the reference electrode.	16
2.7	Schematic diagram illustrating the concentration gradient from right to left and diffusion from left to right.	19
2.8	Schematic detailing the growth of the diffusion layer into bulk solution with time.	21
2.9	Schematic diagram detailing the nomenclature used when describing microelectrodes.	24
2.10	Schematic illustrating planar diffusion at a macroelectrode and hemispherical diffusion at a hemispherical microelectrode.	25

2.11	Schematic diagram illustrating the flattening of a hemispherical microelectrode to a disc conformation.	27
2.12	Schematic detailing the growth of the diffusion layer into bulk solution with time from a microelectrode.	28
2.13	Schematic diagram illustrating the difference in the faradaic current response to variation in applied potential for a macroelectrode (A) and a microelectrode (B).	29
2.14	Schematic diagram illustrating cross section of disk electrode geometry.	32
2.15	Schematic diagram illustrating cross section of hemispherical electrode geometry.	34
2.16	Schematic diagram illustrating cross section of ring-disk electrode geometry.	34
2.17	Schematic diagram illustrating cross section of finite cone electrode geometry.	35
2.18	Schematic diagram depicting the instrumentation necessary in SECM.	38
2.19	Schematic of the basic principles of SECM: When the microelectrode tip is A) far from substrate, diffusion leads to a steady-state current $i_{T\infty}$; B) near a conductive substrate feedback diffusion leads to $i_T > i_{T\infty}$; C) near an insulating substrate hindered diffusion leads to $i_T < i_{T\infty}$.	40
2.20	Schematic representation of the SECM detection method used by Wain & Zhou (2008).	46

2.21	Schematic diagram detailing imaging of cells by detection of reduction in oxygen concentration in close proximity of the immobilised cell compared to detection in bulk solution.	52
2.22	A) Positive feedback is observed as a hydrophobic reduced species generated at the tip diffuses through the cell membrane before being re-oxidised by a different intracellular redox centre within the cell. B) Positive feedback observed as a result of a hydrophobic mediator diffusing to the cell membrane where it is re-oxidised by ET occurring across the cell membrane. C) Schematic illustrating the potentiometric measurement of the pH profile around a single cell.	54
3.1	Schematic representation of the immobilisation of the antibody onto the screen-printed carbon surface.	66
3.2	Photographs of the Uniscan SECM270.	70
3.3	SECM software main menu for selection of experiment to take place.	72
3.4	Experiment configuration for conducting a cyclic voltammetry.	74
3.5	Schematic diagrams depicting the movement of the microelectrode probe (A) during an area scan; (B) the scanning and tip recovery paths respectively.	75
3.6	Series of approach curves allowing substrate slope to be calculated.	76
3.7	Experiment configuration for conducting a sloping area macro scan allowing an area scan to be conducted over a sloped surface.	77
3.8	Area scan over sloped glass substrate using the (A) area scan macro and (B) the sloping scan macro.	78

4.1	Optical Micrograph of a pulled capillary.	84
4.2	Optical image showing Pt-quartz fibre.	84
4.3	Optical image showing the dimensions of the tip of an electrode.	85
4.4	Optical micrograph of pulled capillary with Pt-quartz fibre.	85
4.5	Optical image of an 8μm Pt-quartz microdisk electrode.	87
4.6	Optical image of an 8**μ**m Pt-quartz microdisk microelectrode.	88
4.7	Series of cyclic voltammograms in differing mediators and concentrations. CVs conducted in; A) ferrocenemonocarboxylic acid, B) potassium ferricyanide (III) and C) hexaammineruthenium (III) chloride.	89
4.8	Series of cyclic voltammograms in differing mediators and concentrations. CVs conducted in mediators with concentrations of A) 5mM, B) 2.5mM and C) 1mM.	90
5.1	An optical image of the carbon paste electrode used in the study.	97
5.2	(a) 3D representation of the data obtained from an Area scan over border between carbon (red/green/yellow region) substrate and millinex printing substrate (dark blue region); (b) Linescan across border at a tip position of 400microns.	99
5.3	(a) 3D representation of the data obtained from area scan images of a carbon ink electrode. Current hotspots show areas of raised topography and/or increased conductivity arising from the heterogeneous nature of the carbon ink used; (b) SEM image of a carbon ink electrode surface.	100

5.4	Schematic of the arrangement of carbons within graphite.	102
5.5	Schematic illustration of patterned biotinylated polyelectrolyte film which allows the monitoring of the change in background current over an unmodified surface against the change in feedback response over PEI/biotinylated antibody modified carbon.	104
5.6	Elution profiles obtained following biotinylation (NSE MAb).	106
5.7	Photograph of biotinylated polyethylenimine deposition on carbon electrode by pulled microcapillary using the XYZ micro-positioning stage of the SECM270.	107
5.8	3D representation of the data obtained from consecutive area scans over biotinylated PEI array on carbon at (a) T=0 min; (b) T=200 min; (c) T=500 min using 5mM ferrocenecarboxylic acid.	109
5.9	3D representation of the data obtained from an area scan of PEI/neutravidin/biotinylated antibody arrays on screen printed carbon electrode (a) before and (b) following rinsing and 30 mins exposure to control solution (water); (c) absolute change in measured current.	112
5.10	3D representation of the data obtained from a SECM area scan of a PEI/neutravidin/biotinylated antibody array on a screen-printed carbon electrode; (a) following exposure to biotinylated antibody NSE; (b) following further exposure to complementary NSE antigen at 200 pg ml^{-1}; (c) absolute change in measured current.	114

5.11 (a) Mean changes of a twelve dot array scan (n = 12) taken over PEI/neutravidin/biotinylated antibody surface area to various antigen concentrations (no error bars are included for clarity); (b) Calibration plot showing changes in current measured (n = 12) vs. NSE concentration. Error bars show the standard deviation between the 12 individual dots. 117

6.1 3D representation of the data obtained from a SECM scan of a PEI/neutravidin/biotinylated antibody array on a screen-printed carbon electrode; (a) following exposure to biotinylated antibody PSA; (b) following further exposure to complementary PSA antigen at 200 pg ml^{-1}. 127

6.2 Line plot of a PEI/neutravidin/biotinylated antibody array on a screen-printed carbon electrode; before and after exposure to complementary PSA antigen at 200 pg ml^{-1}. 128

6.3 (a) 3D representation of the data obtained from a SECM scan of a PEI/neutravidin/biotinylated antibody array on a screen-printed carbon electrode, showing absolute change in feedback after exposure; (b) line plot of absolute change in feedback after exposure to PSA antigen at 200 pg ml^{-1}. 129

6.4 (a) Mean changes of a twelve dot array scan (n = 12) taken over PEI/neutravidin/biotinylated antibody surface area to various antigen concentrations (no error bars are included for clarity); (b) Calibration plot showing changes in current measured (n = 12) vs. PSA concentration. 131

6.5 PSA ELISA (where) showing the calibration plot using the standards provided representing a range of antigen concentration in the ng ml^{-1} (n = 12). 132

7.1 3D representation of the data obtained from a SECM scan of a PEI/neutravidin/biotinylated antibody array on a screen-printed carbon electrode; (a) following exposure to biotinylated antibody NTx, (b) following further exposure to complementary NTx antigen at 100 nM. 140

7.2 Line plot of a PEI/neutravidin/biotinylated antibody array on a screen-printed carbon electrode; before and after exposure to complementary NTx antigen at 100 nM. 141

7.3 (a) 3D representation of the data obtained from a SECM scan of a PEI/neutravidin/biotinylated antibody array on a screen-printed carbon electrode, showing absolute change in feedback after exposure; (b) line plot of absolute change in feedback after exposure to NTx antigen at 100 nM. 142

7.4 (a) Mean changes of a twelve dot array scan (n = 12) taken over PEI/neutravidin/biotinylated antibody surface area to various antigen concentrations (no error bars are included for clarity); (b) Calibration plot showing changes in current measured (n = 12) vs. NTx concentration. 144

7.5 Calibration plot showing changes in current measured vs. non-complementary PSA antigen concentration. 145

8.1 Chemical structure of ciprofloxacin 148

8.2 (a) 3D representation of the data obtained from a SECM scan of a PEI/neutravidin/biotinylated antibody array on a screen-printed carbon electrode, showing absolute change in feedback after exposure; (b) line plot of absolute change in feedback after exposure to ciprofloxacin antigen at 100 pg ml^{-1}. 152

8.3	(a) Mean changes of a twelve dot array scan (n = 12) taken over PEI/neutravidin/biotinylated antibody surface area to various antigen concentrations (no error bars are included for clarity); (b) Calibration plot showing changes in current measured (n = 12) vs. ciprofloxacin concentration.	154
8.4	(a) 3D representation of the data obtained from a SECM scan of a PEI/neutravidin/biotinylated antibody array on a screen-printed carbon electrode, showing absolute change in feedback after exposure; (b) line plot of absolute change in feedback after exposure to ciprofloxacin antigen at 500 pg ml^{-1}.	156
8.5	Shows cyclic voltammograms of screen printed carbon electrodes before and after exposure to semi-skimmed milk (a) shows results for bare carbon surface; (b) shows results attained aftert the carbon surface has been coated with biotinylated PEI.	158
8.6	(a) Mean changes of a twelve dot array scan (n = 12) taken over PEI/neutravidin/biotinylated antibody surface area to various antigen concentrations (no error bars are included for clarity); (b) Calibration plot showing changes in current measured (n = 12) vs. ciprofloxacin concentration in milk. (Note, the y scale is inverted compared to that in Figure 8.3b).	160
9.1	Schematic illustrating principle of DNA biosensor	165

9.2 (a) 3D representation of the data obtained from a SECM scan of a PEI/avidin/biotinylated oligonucleaotide array on a screen-printed carbon electrode showing absolute change in feedback after exposure to complementary oligonucleotide sequence; (b) Line plot of a PEI/avidin/biotinylated oligonucleotide array on a screen-printed carbon electrode; before and after exposure to complementary oligonucleotide sequence. 170

9.3 (a) 3D representation of the data obtained from a SECM scan of a PEI/avidin/biotinylated oligonucleaotide array on a screen-printed carbon electrode showing absolute change in feedback after exposure to non complementary oligonucleotide sequence; (b) Line plot of a PEI/avidin/biotinylated oligonucleotide array on a screen-printed carbon electrode; before and after exposure to non-complementary oligonucleotide sequence. 172

9.4 Linescans illustrating difference in feedback response after exposure to complementary and non-complementary oligonucleotide sequences. 173

Abbreviations

Term	Description
a	tip radius in SECM (μm)
A	geometric electrode area (cm2)
Ab	antibody
AC	alternating current (V)
AFM	Atomic Force Microscopy
Ag	antigen
Au	gold
BSA	bovine serum albumin
C	capacitance (Farads, F)
Co(x=0)	concentration of species O at a distance x = 0 from the electrode
Co∞	concentration of species O in bulk solution
CV	Cyclic voltammetry
CVD	chemical vapour deposition
CT	charge transfer
d	tip to substrate distance
D	diffusion coefficient (cm2/s)
Dp	diaphorase
E	potential of an electrode versus a reference
E^0	standard potential
EBL	electron beam lithography
ET	electron transfer
ELISA	enzyme linked immunosorbant assay
F	Faraday's constant (9.6 x 104 Cmol-1)
FB	feedback mode
FIB	focussed ion beam
GΦ	Gibbs Free energy of transition state
ΔG_{red}^{Φ}	Gibbs Free energy change in reduction reaction

ΔG_{ox}^{Φ}	Gibbs Free energy change in oxidation reaction
GC	generation collection mode
GDH	glucose dehydrogenase
GOx	glucose oxidase
HOMO	highest occupied molecular orbital
HRP	horseradish peroxidase
i_c	oxidative current (A)
i_l	limiting current
i_r	reductive current (A)
i_s	substrate current (A)
i_T	tip current (A)
$i_{T\infty}$	tip current in bulk solution
IHP	inner Helmholtz plane
J	diffusional flux (molcm-2s-1)
K_{ox}	first order heterogenous rate constant for the reductive ET reaction
K_{red}	first order heterogenous rate constant for the oxidative ET reaction
L	normalised tip to substrate distance
MB	Methylene blue
m_O	mass transfer coefficient
n	number of electrons involved in electrode reaction
NSE	neuron specific enolase
NTx	N-terminal cross-linked telopeptide of type I collegen
O	oxidised form of a redox couple (O → R + ne-)
OHP	outer Helmholtz plane
PBS	phosphate buffer solution
PEI	polyethyleneimine
PSA	prostate specific antigen
qe	charge on an electrode (C)
qs	charge in solution (C)
rg	ratio of radius of insulating sheath to radius of electroactive area
r_{disk}	radius of a microdisk electrode

$r_{hemisphere}$	radius of a hemispherical electrode
R	a) Reduced form of a redox couple (O → R + ne-)
	b) Resistance
	c) gas constant ($Jmol^{-1}k^{-1}$)
R_u	uncompensated resistance
RE	reference electrode
ROS	reactive oxygen species
SCFM	scanning confocal microscope
SECM	Scanning Electrochemical Microscopy
SG/TC	substrate generation/tip collection mode
SHE	standard hydrogen electrode
SNPs	single nucleotide polymorphisms
TBS	trizma base solution
TIA	Transient Ischaemic Attack
UME	ultramicroelectrode
WE	working electrode
x	distance from electrode (cm)
X	X axis on SECM stage
Y	Y axis on SECM stage
Z	Z axis on SECM stage

Symbols

α	transfer coefficient
δ_j	diffusion layer thickness for species j
η	overpotential (E-Eeq)
σ_d	charge density of diffuse layer
σ_i	charge density arising from IHP
σ_s	charge density on solution side of double layer
Φ_e	electrostatic potential of electrode
Φ_s	electrostatic potential of solution
Φ_{REF}	electrostatic potential of reference electrode
$\Delta\Phi$	electrostatic potential drop

Chapter 1
Research Rationale
Aims and Objectives

1. Research Rationale and Aims and Objectives

1.1 Research Rationale

The scanning electrochemical microscope (SECM) was first described in 1989 (Bard *et al*, 1989) as an instrument that could examine chemistry at high resolution near interfaces. The apprach is based on electrochemical monitoring reactions that occur at small electrodes (the tips) as they are scanned in close proximity to a surface. Scanning electrochemical microscopy is capable of probing surface reactivity allowing for the collection of high resolution electrochemical data at a range of surfaces. The primary aim of this research programme was to explore the ability of SECM to interrogate biologically modified surfaces.

SECM offers several and significant advantages over other microscopic techniques. A particular feature of SECM in imaging applications, compared to other types of scanning probe microscopy, is that the response observed can be interpreted based on rigorous and modeled theory, and hence the measured current can be employed to estimate the tip-substrate distance. Moreover, SECM can be used to image the surfaces of different types of substrates, both conductors and insulators, immersed in solutions. Biological samples being tested do not require complex and lengthy pre-treatment and as the technique is not optically based the approach does not suffer from interference from factors such as background fluorescence. In addition samples may be interrogated repeatedly since the imaging process is non-destructive in nature and unlike the scanning electron microscope (SEM) there is no need for a vacuum to be applied and therefore less concern relating to the introduction of unwanted artefacts.

The technique has been previously applied to a large number of bioanalytical problems (Wittstock *et al*, 2001; 2007 Gyurcsanyi *et al*, 2004; Edwards *et al*, 2006; Amemiya *et al*, 2006; Sun *et al*, 2007; Roberts *et al*, 2009). SECM has previously been used successfully to investigate diffusion through biological membranes, respiratory and intracellular redox

activity of cancerous cells, topography of neurons and has also proved useful in quality control applications of the development and manufacture of biosensing devices (Yasukawa *et al*, 1998; Liu *et al*, 2001; Takii *et al*, 2003; Uitto and White, 2003).

Within the work to be carried out in this project, two different avenues of SECM application will be described. The first area of investigation to take part is the development in the use of SECM in the detection of antibody/antigen interactions. Contemporary formats for detecting either antibodies (HIV tests) or antigens (pregnancy tests) include ELISA, lateral flow auto analysers, both of which are limited in their sensitivity since they rely on being able to label one of the molecules in order to gain a visual response, comprising either colour, fluorescence or radio-labelling based approaches. Often these tests are not able to reach certain levels of sensitivity either due to the label being too large, steric hindrance or not being able to find a matching antibody (in the case of a sandwich ELISA).

The second area of research involving further development of a DNA biosensor previously developed within the group (Davis *et al*, 2005a; Robert *et al*, 2009) involved the use and development of SECM as a tool in the detection of DNA hybridisation in polyelectrolyte films. Electrochemical approaches to the detection of DNA hybridisation promise to offer significant advantages over the established optical detection methods based on the use of fluorescent labels – potentially offering high sensitivity, cost effectiveness and synergy with microfabrication technologies. Whilst the electrochemical labelling approach offers much in the development of rapid sensing technologies, there is much scope for the direct, label-less detection of DNA hybridisation by electrochemical methods. By removing the necessity for labelling, sensors offer the promise of faster responses while requiring fewer reagents so making them an extremely attractive route for investigation. The work outlined in this project looks at the detection of the binding event of short oligonucleotides.

The quality of the images obtained by SECM is highly dependent on the quality of the microelectrode probes used. It was, therefore important to establish a working fabrication protocol for the production of robust, sensitive and reproducible microelectrodes with

small critical dimensions. This was one of the main aims in the first year of the research programme.

Once the fabrication method for the production of microelectrodes had been carried out it was established that the sensitivity and spatial resolution of the electrodes was greater than that previously experienced. It was then necessary to establish a working platform for the immunosensor so that comparison could be made between previous work undertaken within the group (Barton *et al*, 2008a, 2008b, 2009: Tsekenis *et al*, 2008a, 2008b; Garifallou *et al*, 2007). Once a suitable method for the preparation of the array on the screen printed carbon ink surfaces had been established, it was possible to interrogate oligonucleotides-polyelectrolyte and various antibody-polyelectrolyte films to determine whether the changes observed by impedance were detectable by SECM.

The results reported herein to date have so far at the time of writing led to two posters, one paper (see Appendices) and an oral presentation. Other papers are presently in preparation.

Holmes JL, Davis F, Higson SPJ. Scanning Electrochemical Microscopy Used In The Interrogation Of Label-Free Antibody/Antigen Interactions. 20th World Congress on Biosensors, Glasgow, 2010 (Oral presentation).

Holmes JL, Davis F, Collyer SD, Higson SPJ (2011) A new application of scanning electrochemical microscopy for the label-free interrogation of antibody-antigen interactions *Anal Chim Acta* In press.

1.2 Aims and Objectives

1. To develop a methodology by which robust microelectrodes of small critical dimensions may be fabricated.

2. To characterise a variety of immunosensors previously developed within the group (Barton *et al*, 2008a, 2008b, 2009: Tsekenis *et al*, 2008a, 2008b; Garifallou *et al*, 2007) and in doing so, investigate the potential of SECM in the detection of antibody/antigen binding events.

3. To characterise an oligonucleotide biosensor previously developed within the group (Davis *et al*, 2005a; Roberts *et al*, 2009) and in doing so, investigate the potential of SECM to detect DNA hybridisation in polyelectrolyte films.

Chapter 2

Introduction and literature review

2. Introduction and literature review

This chapter aims to provide an introduction to a number of electrochemical factors of relevance to the scanning electrochemical microscope. This is followed by an overview of scanning electrochemical microscopy (SECM) as an analytical technique, concluding with a discussion of the advantages offered by SECM to the study of a number of biological systems.

2.1 Electrochemistry

2.1.1 Electron transfer and energy levels

Electrons may transfer between the molecule and an electrode in either direction as demonstrated in Equation 2.1 using $Fe^{2+/3+}$ as an example. The molecule in solution can be reduced by accepting an electron from the electrode or it can become oxidized by donating an electron to the electrode. When Fe^{3+} is reduced at the electrode/solution interface, the passage of current through the cell converts Fe^{3+} to Fe^{2+} and this results in an increased concentration of Fe^{2+} at the electrode.

$$Fe^{3+} + e^- \rightleftharpoons Fe^{2+} \qquad \textbf{Equation 2.1}$$

The reason for this is due to the fact that the rate of reduction is greater than the rate at which the reactant may be replenished by diffusion from the bulk solution to the interfacial region.

$$O + ne^- \underset{K_{ox}}{\overset{K_{red}}{\rightleftharpoons}} R \qquad \textbf{Equation 2.2}$$

In the above reaction (Equation 2.2) it can be concluded that a series of steps causes the conversion of the oxidized species O, to a reduced form R. This electrode reaction rate is controlled by two main processes: these are mass transfer, the transport of reactants to, and products from, the electrode surface (e.g., of O from the bulk solution to the electrode surface); and the rate of electron transfer at the electrode surface (rate-determining electrode kinetics). However it is also important to consider chemical reactions either preceding or following the electron transfer. These can include both homogenous processes, such as protonation and dimerization, and heterogeneous processes, including catalytic decomposition, on the electrode surface. Other surface reactions may also occur such as adsorption or desorption (Figure 2.1).

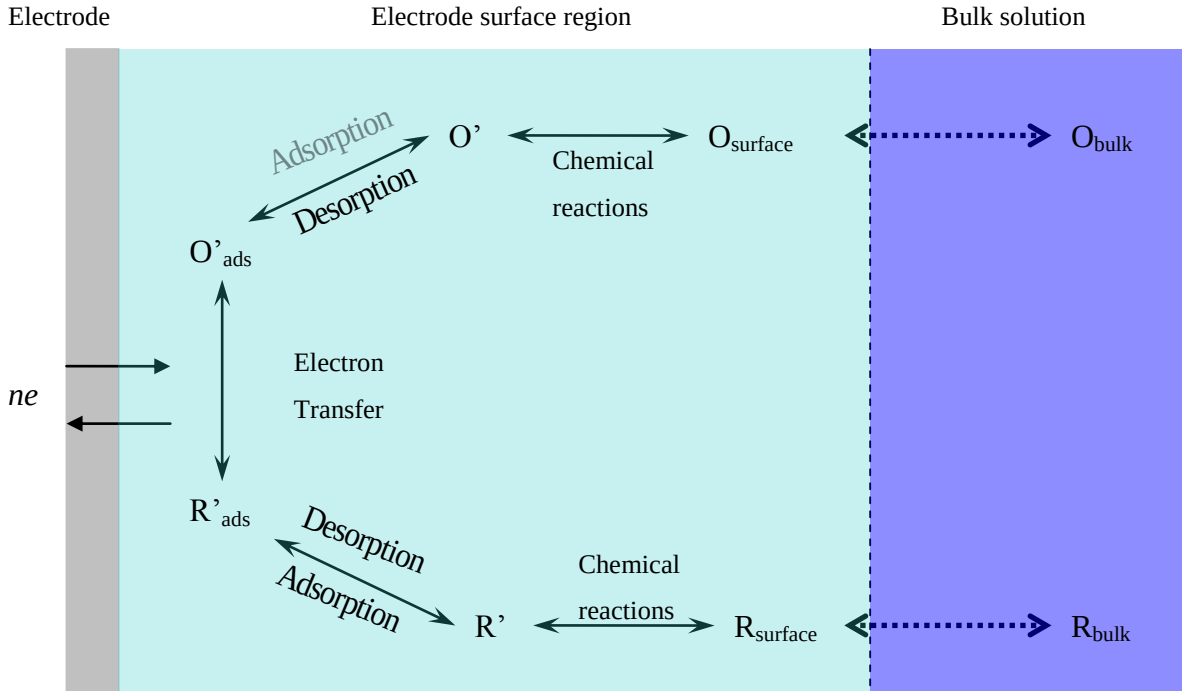

Figure 2.1: Schematic diagram illustrating the pathway of a general electrode reaction.

The rate constant for some of these processes is dependent upon the potential. The electrons in an electrode have a maximum energy distributed proximal to the Fermi level, which is the energy of the highest occupied molecular orbital (HOMO), where electrons may only be supplied or received at energy levels around this level. However, if an external potential is applied, the Fermi level may be altered to either supply electrons to, or

remove electrons from, the electrode. For the reduction of a molecule in solution to take place, it is necessary for electrons in the electrode to have a minimum amount of energy in order to be transferred from the electrode to the receptor molecule, O; for oxidation to occur, the electrons in the donor orbital of R must be at least equal to or higher than that of the Fermi level of the electrodes. To study the relationship between a species' energy levels and their partiality to donate or receive electrons, it is necessary to quantify the potential dependence of the heterogeneous rate constant for the electron transfer reaction. In the reaction given above (Equation 2.2), it is assumed that there are finite quantities of O and R present in the solution and that K_{red} and K_{ox} describe the first order heterogeneous rate constants for the reductive and oxidative electron transfer reactions.

The electron transfer process (ET) is assumed to act in an analogous manner to chemical rate processes and it is therefore possible to describe it using the transition state model, which has been described at length by Compton *et al* (1994) (Figure 2.2). The model shows the ET reaction as one that occurs via a path involving two reactants ($O_{(aq)} + e^-$) and one product ($R_{(aq)}$). The reactants must overcome an energy barrier for the reaction to occur, the height of which is given by G^{Φ}, the transition state. Transition state theory predicts that the rate of the reduction reaction, k_{red} will be given by:

$$k_{red} = Af \exp\left(\frac{-\Delta G^{\Phi}_{red}}{RT}\right) \qquad \textbf{Equation 2.3}$$

Where A = geometric electrode area (cm^2)

ΔG^{Φ}_{red} = Gibbs Free energy change in reduction reaction

R = gas constant ($Jmol^{-1}k^{-1}$)

T = absolute temperature (°K)

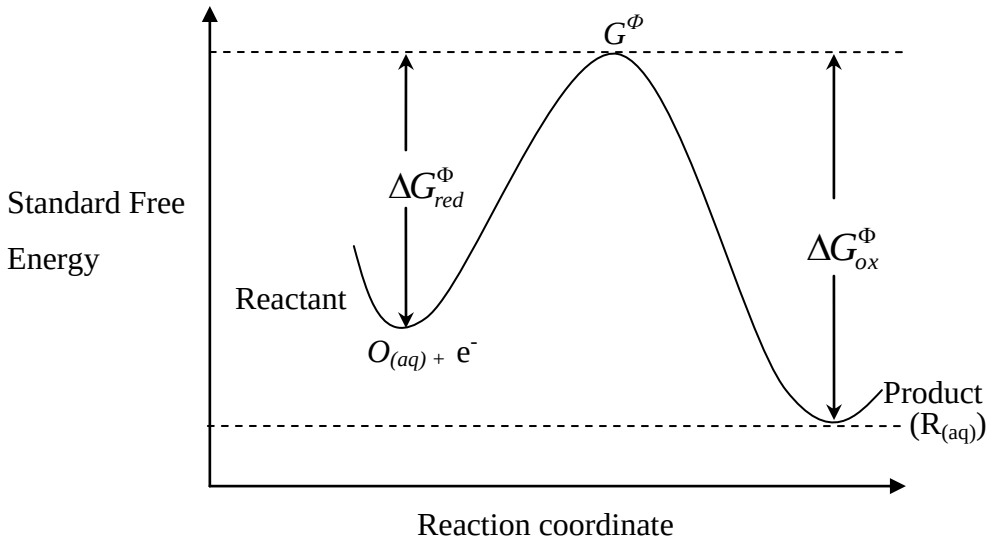

Figure 2.2: Free energy profile for a single electron reduction of species $O_{(aq)}$.

Electrochemical reactions can be influenced by altering the energy levels of the electrode, such as changing the interfacial potential. When the applied potential is equal to that of the equilibrium potential / open circuit potential, no current flows through the system. By forcing the electrode to a more negative potential, the energy of the electrons within the electrode phase become raised, which, depending on the energy state of the species in the electrolyte phase, can result in the transfer of the electrons from the electrode into vacant electronic states on species in the electrolyte (Figure 2.3). This current is termed a reduction current. The flow of electrons in solution moving towards a more favourable energy level on the electrode results in the creation of an oxidation current. The critical potentials at which these processes occur are related to the standard potentials, E^0, for the specific chemical substances in the system.

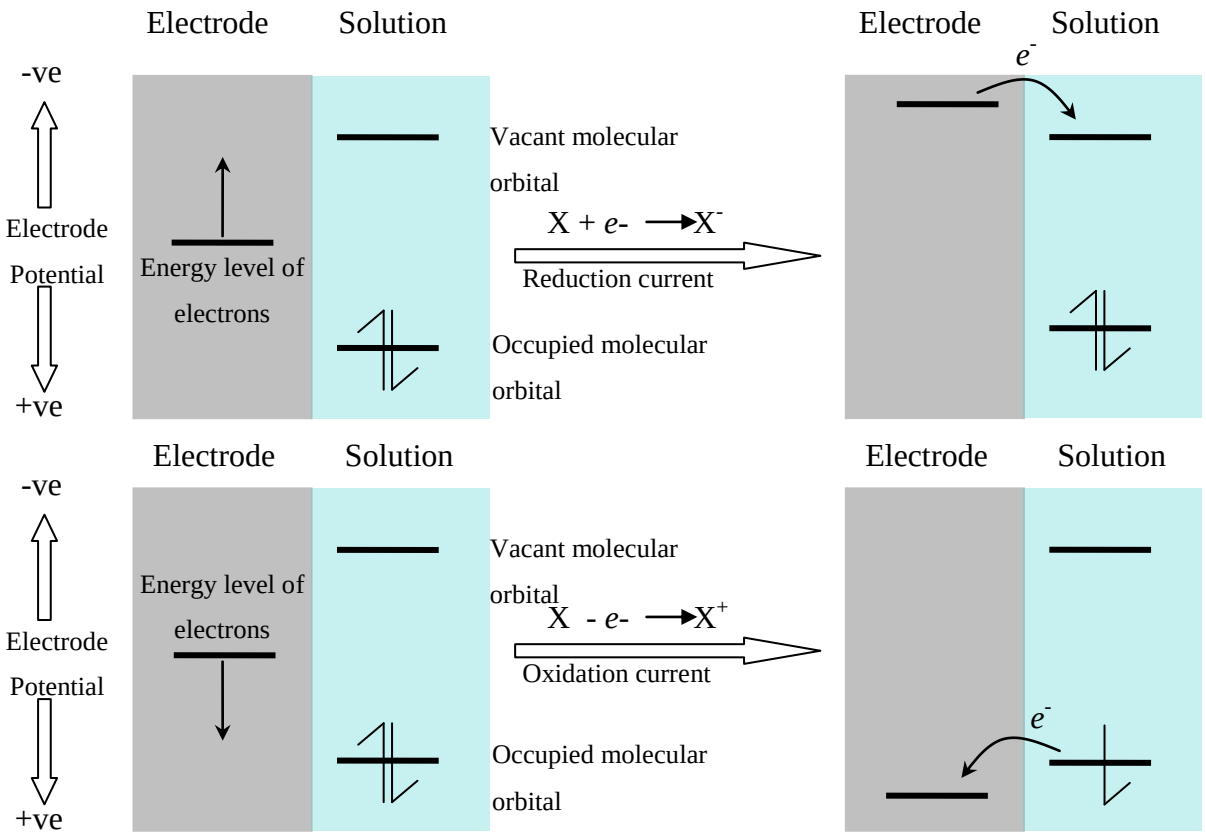

Figure 2.3: Schematic diagram illustrating the principle of oxidation and reduction of species X. The molecular orbits shown are the highest energy filled orbitals and the lowest energy vacant orbitals.

2.1.2 The Electrical Double Layer

The electrical double layer is the array of charged species and oriented dipoles at the electrode-solution interface, thought to be made up of several layers (see Figure 2.4). The inner layer located closest to the electrode contains solvent molecules that are specifically adsorbed on the electrode surface. This inner layer can also be referred to as the 'compact', 'Helmholtz' or 'Stern' layer. The locus of the electrical centres of the specifically adsorbed ions is called the inner Helmholtz plane (IHP), which is located a distance x_1 from the electrode surface. It is important, however, to state that although the IHP may be dominated by solvent molecules, some ionic or uncharged species from the electrolyte solution may also possibly penetrate this region as a result of the loss of the

solvation shell and become 'specifically adsorbed' to the electrode surface (in this instant the term 'specific' is used to account for the fact that the interaction occurs only for certain ions or molecules and is generally unrelated to the charge on the ion) (Grahame, 1947). The total charge density from specifically adsorbed ions in this inner layer is σ^i ($\mu C/cm^2$). Solvated ions are able to approach the electrode to a distance of x_2 only, making the locus of these centres the outer Helmholtz plane (OHP). The interaction of these solvated ions and the electrode are relatively weak as it involves only long-range electrostatic forces, making their interaction independent of the chemical properties of the ions. These ions are said to be nonspecifically adsorbed and due to the thermal agitation and subsequent Brownian motion, these are distributed in a three-dimensional region called the diffuse layer, where the OHP extends into the bulk of the solution. The charge density of this diffuse layer, given by σ^d, contributes to the total charge density on the solution side of the double layer, σ^S so that (Chapman, 1913):

$$\sigma^S = \sigma^i + \sigma^d = -\sigma^e \qquad \textbf{Equation 2.4}$$

As highlighted by Stern (1924), the structure of the double layer can affect the rates of the electrode process; for example if we consider a non-specifically adsorbed electroactive species which can only approach the electrode to the OHP then this results in the potential it experiences being less than the potential between the electrode and the solution (potential drop).

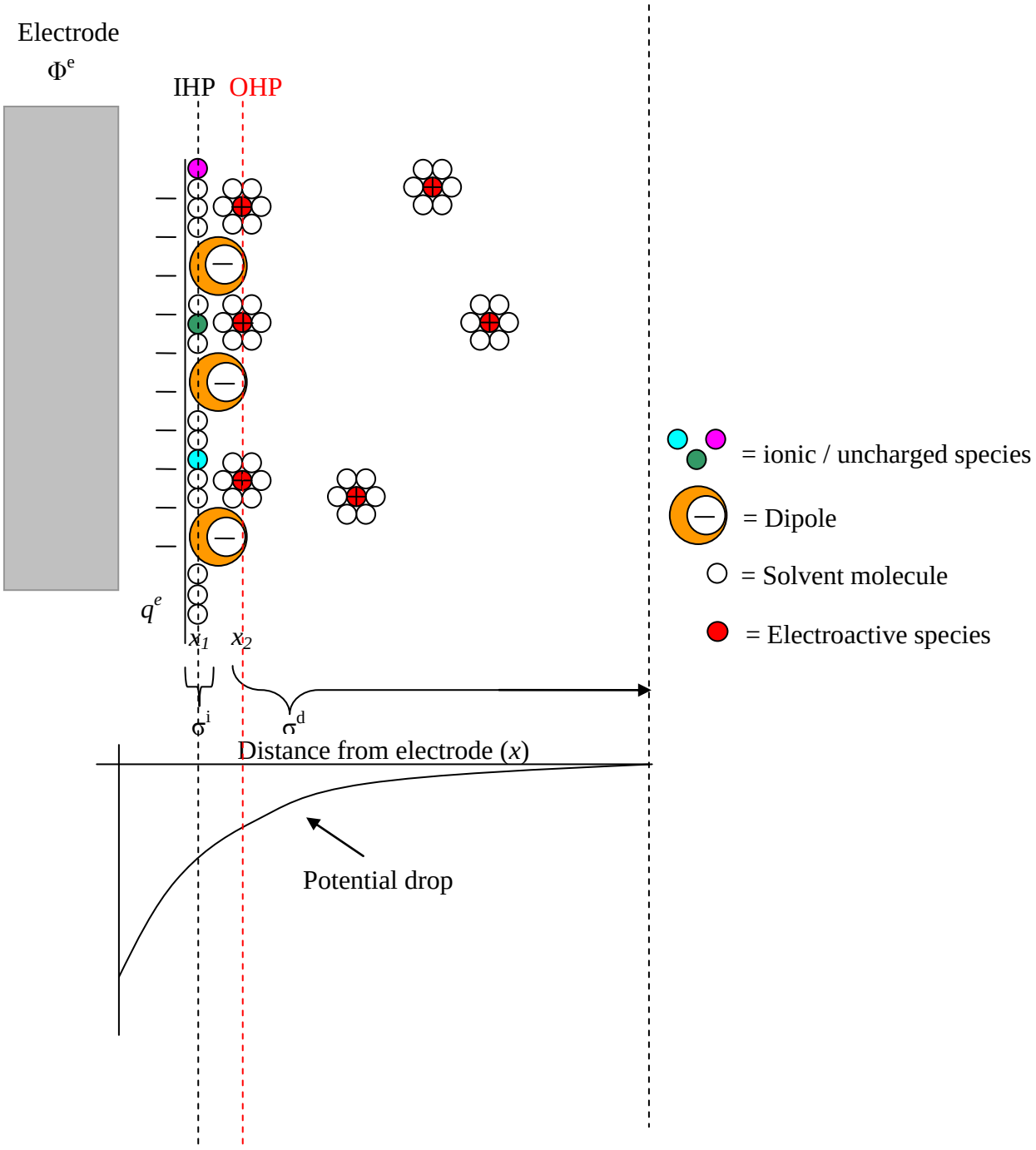

Figure 2.4: Schematic representation of the electrical double layer.

2.1.3 The electrochemical cell and electrodes

An apparatus assembly necessary for an electrochemical experiment consists of a container vessel in which at least two independent electrodes are immersed in a solution containing the electroactive species of interest and an electrolyte. These electrodes are then linked through solution as well as through external connectors to form an electrical circuit (Figure 2.5). The working electrode (WE) is the electrode at which the reaction of interest occurs and the reference electrode (RE) is present to provide a stable and fixed potential. Therefore, when a potential (E) is applied between the two electrodes, the potential drop between the WE and the solution can be defined according to the following equation (Equation 2.5).

$$\mathrm{PotentialDrop}(\Delta\Phi) = \Phi_e - \Phi_s \qquad \textbf{Equation 2.5}$$

Where Φ_e = electrostatic potential of electrode

Φ_s = electrostatic potential of solution

In this two electrode arrangement, complementary oxidation and reduction reactions occur at each electrode. However, while a two electrode arrangement will often suffice, where a tiny current is passed, in the case of larger electrodes, problems arise with potential drop.

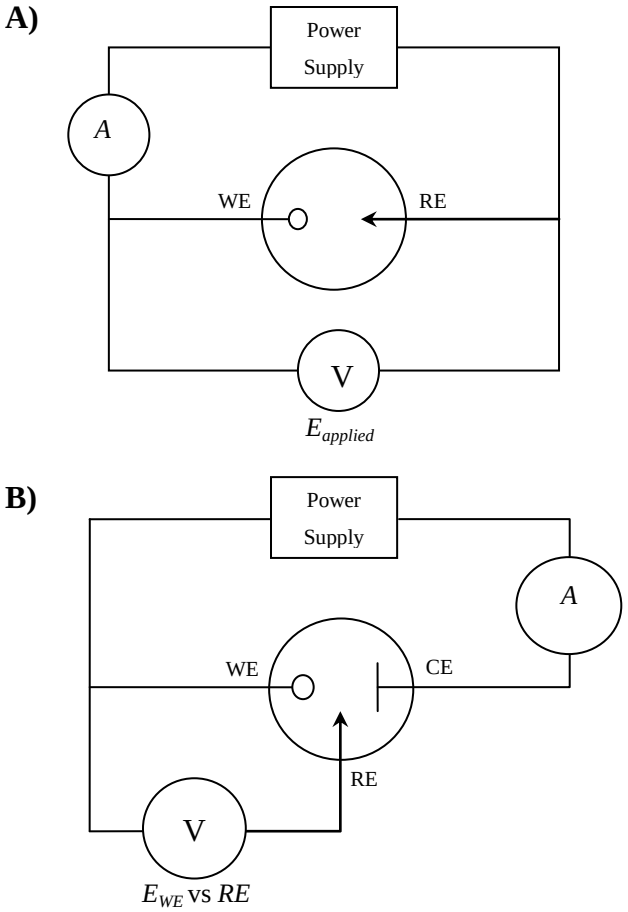

Figure 2.5: A) Two electrode cell; B) Three electrode cell with a counter/auxiliary electrode.

When a potential (E) is applied to a two electrode system, a finite current flows between the RE and WE, where E may be split into three components:

$$E = (\Phi_e - \Phi_S) + iR_S + (\Phi_s - \Phi_{REF}) \qquad \textbf{Equation 2.6}$$

The first term refers to the over-potential required to drive the redox reaction at the WE/solution interface, the second term refers to the potential drop due to the passage of current through solution (where i = current flowing, R_s = solution resistance), and the final term refers to the potential drop at the RE/solution interface which is fixed via the chemical composition of the chosen reference solution.

The current flowing is small in the case of a small electrode resulting in the second term being almost negligible and allowing it to be ignored. This point, combined with the fact that the potential drop at the RE is constant, means that any changes in E may be reflected directly in the driving force applied to the WE. However, in the case of larger electrodes, solution resistance becomes a more significant element as changes in E do not solely control the potential at the working electrode. Issues arising from this problem may be overcome by the use of a third electrode, a 'counter' or 'auxiliary' electrode (CE). In this arrangement, the current is passed between the WE and the CE and the potential of the working is monitored with respect to the reference electrode. The potentiostat controls the potential applied to the WE and maintains the potential across the electrodes regardless of the current measured. This therefore, allows the assurance that the only current which flows is that between the working electrode and the counter electrode. However, it is prudent to note that not all the iR_S term is removed from the reading – if the reference electrode is not precisely (in the terms of distance) at the WE surface a fraction of iR_S will be present in the measured potential. This fraction is defined as iR_u where R_u is uncompensated resistance. This concept is illustrated schematically in Figure 2.6.

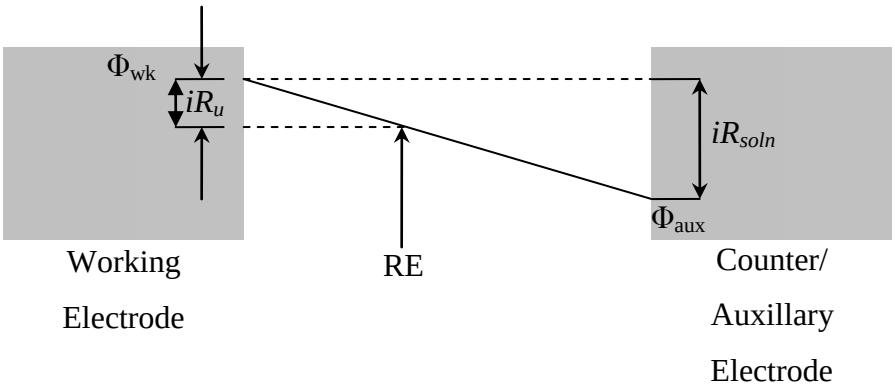

Figure 2.6: A schematic illustrating potential drop between working and auxiliary electrodes in solution and iR_u measured at the reference electrode.

2.1.4 Working Electrodes (WE)

If the WE is to be used under non-equilibrium conditions then it is necessary for the WE to be a good electron conductor. Therefore, WEs are often precious inert metals such as platinum (Pt) or gold (Au) however, carbon in its various forms is being increasingly used to reduce the costs of electrode materials. It is essential that the electrode remains inert through the potential range over which the electrochemical experiment is to be conducted. Within the realms of SECM, the resolution of the information that may be obtained about the electrochemistry of a surface is very much determined by the physicochemical properties of the microelectrode probe.

2.1.5 Reference Electrodes (RE)

The standard hydrogen electrode (SHE) is the RE used for the calculation of the standard electrode potentials. However, as a result of its size impracticality in being used for all reactions, a number of other electrodes have been developed which are more suited to the analysis of electrochemical reactions occurring in smaller volumes. Examples of these include the saturated calomel electrode (SCE) and the silver/silver chloride (Ag/AgCl) electrode. The silver/silver chloride electrode is commonly used in electrochemical measurements; for example it is usually used as the internal reference electrode in pH meters. The electrode functions as a redox electrode and the reaction is between the silver metal (Ag) and its chloride salt (AgCl).

The Nernst equation below shows the dependence of the potential of the silver-silver(I) chloride electrode on the activity or effective concentration of chloride-ions:

$$E = E^{O} - \frac{RT}{F} Ina_{cl^-} \qquad \textbf{Equation 2.7}$$

For this reaction ($AgCl_{(s)} + e^- \rightleftharpoons Ag_{(s)} + Cl^-$) the standard electrode potential E^0 against the standard hydrogen electrode is 0.230 V ± 10 mV. Ideally, on the application of a potential to the WE, no current should cross the RE/solution interface and they should be able to exhibit a stable potential difference that can be referred to.

2.1.6 Counter Electrodes (CE)

The role of the CE, also called an auxiliary electrode, is to make a connection to the electrolyte so that a current can be applied to the WE. Therefore it provides a sink/supply of electrons and also to minimise any potential drop, resulting in the CE being a degree larger than that of the WE. It is necessary for the CE to be placed at a sufficient distance from the WE so as to prevent the diffusion of unwanted reaction products from the CE to the WE in cases where the products of the reaction occurring at the CE should not be allowed to reach the WE. Typically the CE, like the WE is fabricated out of inert conductivity materials, such as Pt.

2.2 Mass Transport

Mass transport is the term used to describe the movement of a reactant to and from an electrode surface. It is known that other physical processes may contribute to the overall kinetics of a reaction and that in order for a reaction to occur, the reactant molecule must be transported from the bulk solution towards the electrode interface and that the reaction products, once formed, will themselves diffuse away from the electrode. The overall reaction rate is limited by the slowest step. Therefore, a reaction can be controlled by either the kinetics of electron transfer or by the rate at which the material is brought to or from the electrode through mass transport. Three modes of mass transport are found to be of great significance; these are diffusion, convection and migration and will be discussed in greater detail.

2.2.1 Diffusion

Diffusion may be described as the natural movement of species down a concentration gradient – from a region of high concentration to a region of low concentration. Diffusion arises from uneven concentration distributions - and the driving forces behind the diffusion phenomenon are entropy-based which work to smooth out the differences in reactant concentration. Therefore the rate of diffusion at a given point in solution is dependent on the concentration gradient at that particular location (Figure 2.7).

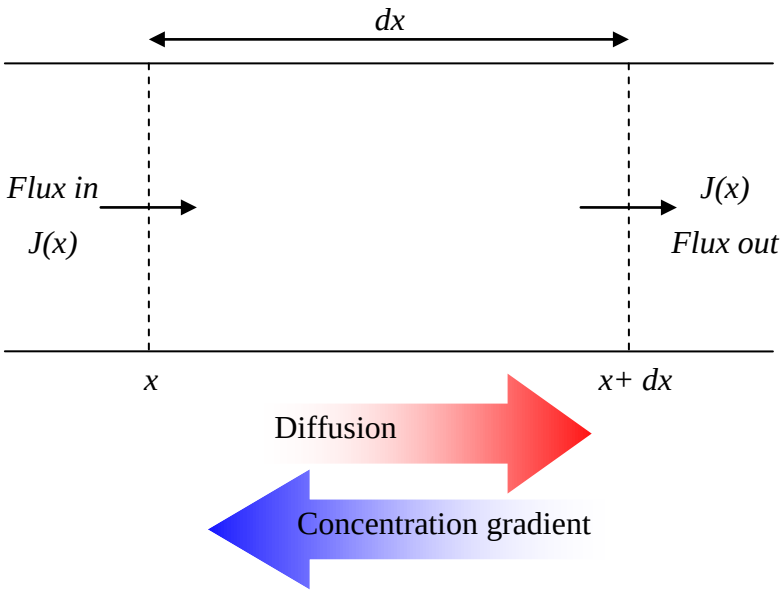

Figure 2.7: Schematic diagram illustrating the concentration gradient from right to left and diffusion from left to right.

Ficks first law of diffusion (1885) described diffusion mathematically. He successfully demonstrated that the diffusional flux, J (the number of moles of material diffusing through a unit area per second) is equal to the negative of the product of the concentration gradient ($\partial[C]/\partial x$) and the diffusion coefficient (D), the latter of which is a unique characteristic of the diffusing molecule in that particular solvent (Equation 2.8).

$$J = \frac{-D\partial[C]}{\partial x} \qquad \textbf{Equation 2.8}$$

Ficks first law of diffusion is then extended in to Ficks second law of diffusion (Equation 2.9). This enables the prediction of concentration changes of electroactive material close to an electrode surface at a specific point in space and time – where $\partial[C]/\partial t$ represents the concentration of the species of interest with respect to space and time and $\partial^2[C]/\partial x^2$ is the concentration gradient.

$$\frac{\partial[C]}{\partial t} = D\left(\frac{\partial^2[C]}{\partial x^2}\right) \qquad \textbf{Equation 2.9}$$

This equation may then be used to derive the Cottrell equation (Equation 2.10) giving the variation in Faradaic current as a function of time where n is the number of electrons transferred in the oxidation or reduction of the species per mol, F= Faraday's Constant, A= electrode area (cm^2) and $[C]_\infty$ is the concentration of the electroactive species of interest in bulk solution.

$$i = nFAJ = \frac{nFAD^{1/2}[C]_\infty}{(\pi t)^{1/2}} \qquad \textbf{Equation 2.10}$$

Now consider the following redox couple:

$$O + ne \Leftrightarrow R$$

When electrolysis of O begins, its concentration falls to a value less than in the bulk solution at the electrode surface ($C_o(x=0) < C_{O\infty}$). As the concentration gradient grows it acts to force a flux of unreacted O from bulk solution towards the electrode surface. As the electrolytic process proceeds, consuming more and more O, the diffusion layer grows as depicted in Figure 2.8.

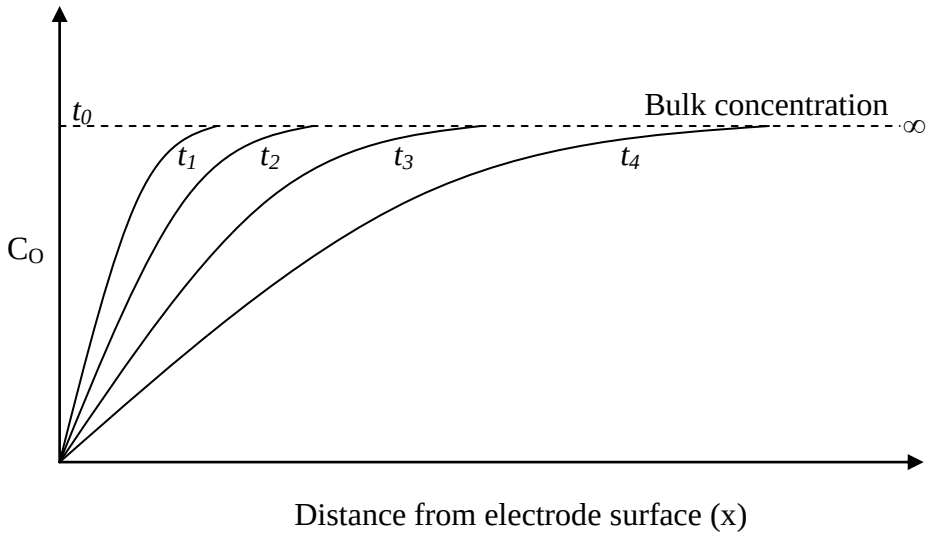

Figure 2.8: Schematic detailing the growth of the diffusion layer into bulk solution with time.

2.2.2 Convection

Convection occurs when the application of a mechanical force or energy causes the movement of a species within a solution. There are two forms of convection – natural convection and forced convection.

The first form of convection is natural convection. Natural convection arises as a result of thermal gradients or differential densities within solution and can be present in any solution. Thermal gradients may arise within electrolysis reactions because of the exo- or endo-thermicity of the process. Differential densities can be present due to the electrode reaction creating concentrations of products near the electrode of different density to those of the reactants in the bulk solution.

The second type of movement is forced convection and is a result of the application of kinetic energy into the system by, for example, stirring or pumping.

In electrochemical systems which incorporate larger electrodes, natural convection can lead to limitations in the distance that the diffusion layer may extend into the bulk solution. Therefore it can be determined that the larger the convective forces, the smaller the resulting diffusion layer. In large electrodes, natural convection may become a significant problem. Therefore, in some electrochemical experiments an element of forced convection is deliberately applied. This causes the swamping of contributions from natural convection and enables reproducible experiments involving measurements past the 10-20 second boundary.

2.2.3 Migration

The third mass transport mechanism encountered within electrochemistry is migration and may be defined as the movement of charged species through a medium under the influence of an applied potential gradient. The mechanism is due to the drop in electrical potential between the two electrodes inducing the movement of ions to and from the electrode, with the effect of maintaining the charge balance between electrodes. Whilst the interplay of migration and electrolysis can give rise to a complex physical transport process, experiments may be performed under conditions where migration can be neglected. This is made possible by the presence of an inert supporting electrolyte which enables the passage of charge and diminishes any potential gradients that may arise in the electrochemical cell. With the addition of electrolytic ions, there is a slight redistribution of the different cations and anions, which the supporting electrolyte is comprised of - and this has the effect of maintaining near electrical neutrality in the entire interfacial region.

It can be difficult to determine the contribution of each process to the observed faradaic current when all three processes are taking place in one system. Therefore, to counter this problem, electrochemical experiments can be designed so that there is one principal component of mass transport in action. An example of this is the avoidance of migration and convection by the use of an excess of inert electrolyte in the mediator solution and the prevention of stirring, respectively.

2.3 Microelectrodes

2.3.1 Definition

The introduction of microelectrodes, occurring principally through the independent work of Wightman, Fleischmann and co-workers circa 1970 -1990 (Ponchon *et al*, 1979; Fleischmann *et al*, 1985), represents one of the greatest advancements in the world of electrochemistry and continues to change electrochemical science as they improve and develop over time. A microelectrode may be defined as an electrode that has a characteristic surface dimension smaller than the thickness of the diffusion layer on the timescale of the electrochemical experiment (Dayton *et al*, 1980). However, this definition does not take into account any kinetic parameters of the electroanalytical technique employed and therefore a definition specifying only the geometric dimension is inappropriate. It follows that a better definition is:

> "…*any electrode whose characteristic dimension is, under the given experimental conditions, comparable to or smaller than the diffusion layer thickness, δ. Under these conditions, a steady state or pseudo steady state (cylindrical electrodes) is attained*." (Myers, 2006)

An ultramicroelectrode (UME) may be defined as an electrode with a critical dimension of <25 μm (Wang, 2001), but no less than 10 nm - since it has been previously demonstrated that electrodes with dimensions lower than this limit behave differently from theoretical expectations based on larger electrodes (Zoski, 2000, 2002). A schematic diagram detailing the nomenclature used when describing microelectrodes is given in Figure 2.9.

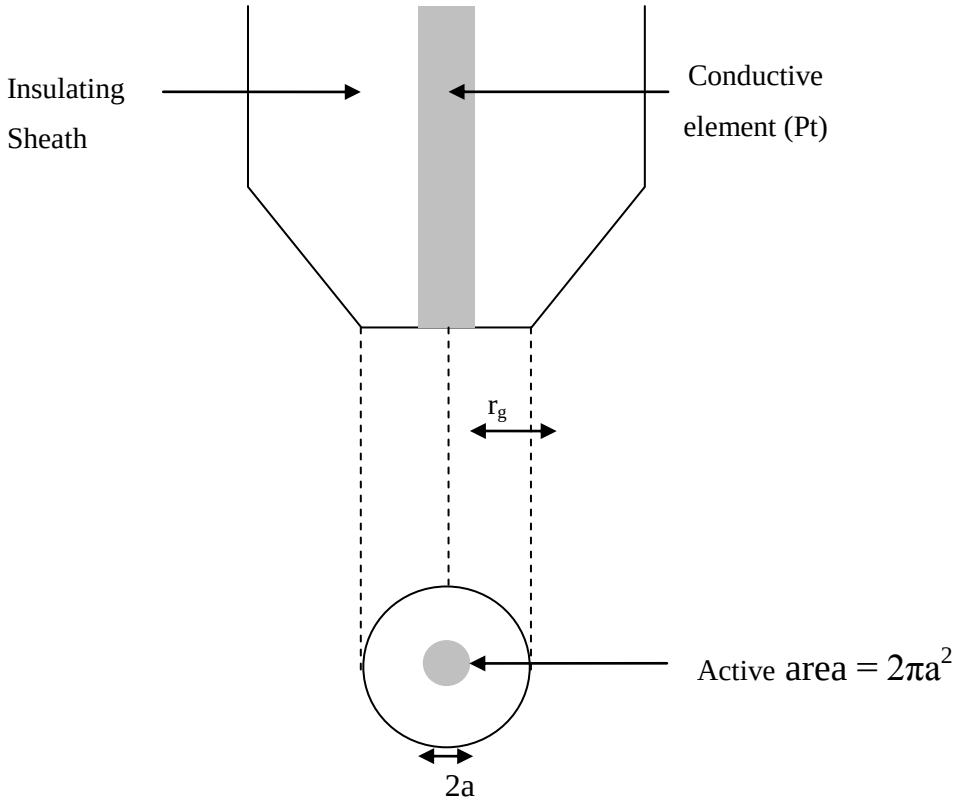

Figure 2.9: Schematic diagram detailing the nomenclature used when describing microelectrodes**.**

2.3.2 Microelectrode behaviour

Although microelectrodes have been used within the field of electrochemical science for over 25 years, as is often the case with new developments of tools and techniques, their true potential and use has only started to be realised. The ability of microelectrodes to produce a substantial amount of information about a number of different systems, such as living, chemical and physiochemical, has only recently begun to be demonstrated and understood.

A significant problem arising from macroelectrodes is that of the diffusion to and from the surface as the diffusion occurs at a much slower rate than convection. As a result, current fluctuations will occur if convective forces are not eliminated from the system - and these fluctuations will not be attributed to any known experimental variable and so a significant

error component may be introduced to the data. However, this problem can be overcome if the convection force is completely eliminated or alternatively if the rate of diffusion is enhanced to a level significantly larger than that of convection. This can be achieved using microelectrodes.

The current measured at a microelectrode is significantly lower than that measured at a conventional macroelectrode, often involving measurements at nano-amp levels or below. Microelectrodes induce only a tiny amount of electrolysis in solution due to the minute currents being passed through them. Therefore, the diffusion layer of microelectrodes is very thin (in the order of micrometers) resulting in the concentration gradient induced across them being very high. This means that the rate of mass transport to the microelectrode is much greater when compared to that of macroelectrodes. The current measured is also highly dependent on the geometry of the microelectrode (Zoski, 1990, 2002).

The variation of current at a hemispherical electrode (Figure 2.10) with time, derived from the Cottrell equation, is as follows:

$$i = nFAD[C]_{\infty}\left[\frac{1}{(\pi Dt)^{1/2}} + \frac{1}{r}\right] \qquad \textbf{Equation 2.11}$$

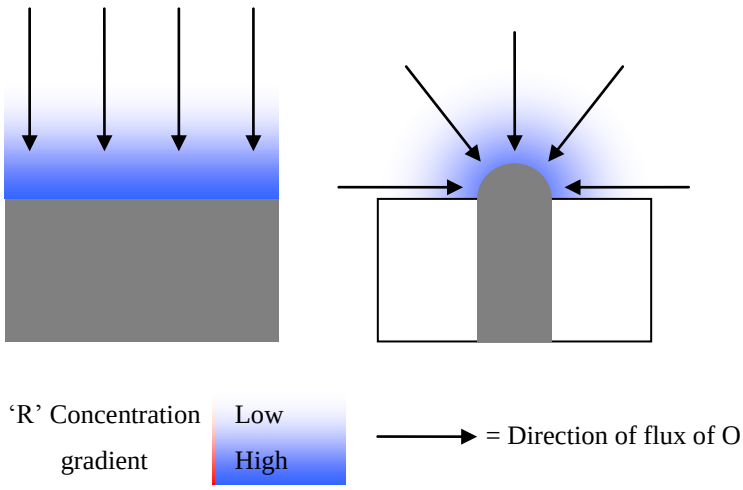

Figure 2.10: Schematic illustrating planar diffusion at a macroelectrode and hemispherical diffusion at a hemispherical microelectrode.

Where r is the radius of the sphere and A is given by $4\pi r^2$ and $2\pi r^2$ for a sphere and a hemisphere respectively. The limiting current is reached in a hemispherical microelectrode substantially faster than for the limiting current to be reached in a planar microelectrode. As a result of this, the term t is suppressed, yielding the following equation which describes the current at a hemispherical microelectrode:

$$i = \frac{nFAD[C]_\infty}{r_{hemisphere}} = 2\pi nr_{hemisphere}FD[C]_\infty \qquad \textbf{Equation 2.12}$$

In SECM, as with other electrochemical experimental arrangements the embedded disk electrode is the main geometry employed. However, if the hemispherical dimension is close to that of the diffusion layer thickness, the resultant current will be the same if the hemisphere were to be flattened into a disc shape (Oldham and Zoski, 1988).

The Cottrell equation describing the planar diffusion of electroactive species towards an electrode predicts that the application of a sufficient electrical potential to the electrode causes products of the redox reaction to form a diffusion gradient extending from the electrode surface out into solution to a point where $C_O \rightarrow C_{O\infty}$. However, the concentration profile observed is quite different in relation to a microelectrode (Figure 2.11).

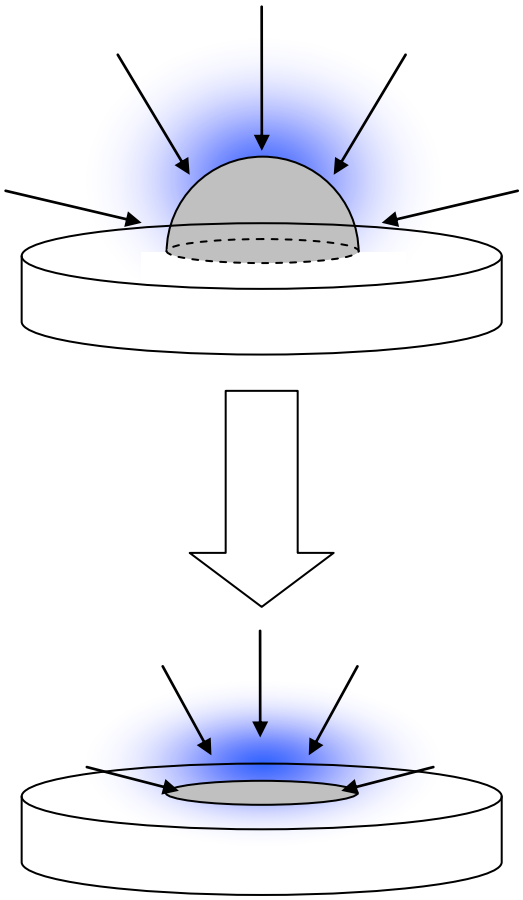

Figure 2.11: Schematic diagram illustrating the flattening of a hemispherical microelectrode to a disc conformation.

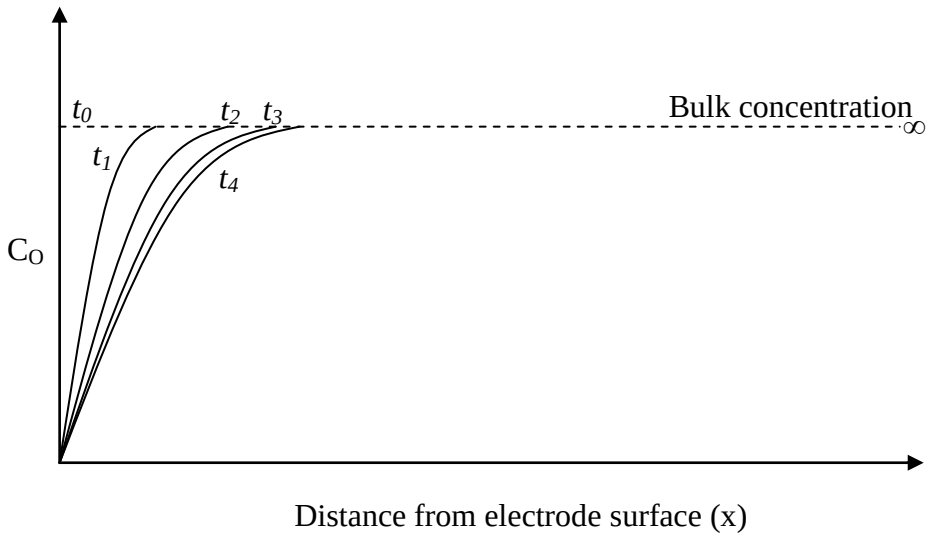

Figure 2.12: Schematic detailing the growth of the diffusion layer into bulk solution with time from a microelectrode.

At the onset of electrolysis the diffusion layer is similar to that observed at a planar microelectrode, however the diffusion layer then extends out into the solution adopting an expanding hemispherical conformation. This results in the diffusion taking place in both the planar direction and radially, and as a consequence of this bi-lateral diffusion the flux of electroactive species to the electrode surface is substantially greater than that observed at a typical macro-electrode (Figure 2.12).

Due to this enhanced rate of mass transport, when the electrode is scanned from a potential causing no electrolysis of the electroactive species towards a potential that does cause electrolysis, the faradaic current that results from the oxidation or reduction of the species displays a sigmoidally shaped response (Figure 2.13).

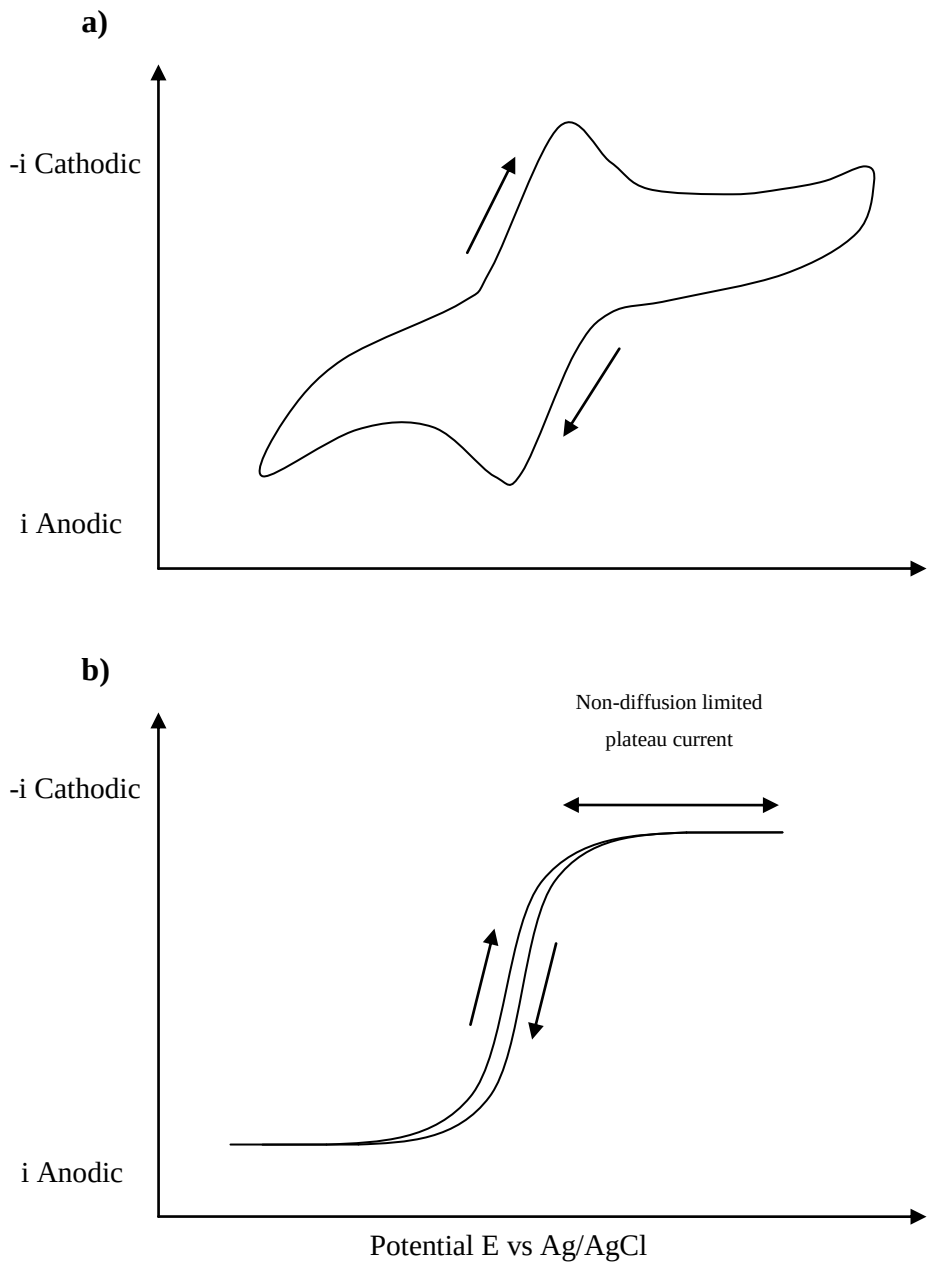

Figure 2.13: Schematic diagram illustrating the difference in the faradaic current response to variation in applied potential for a macroelectrode (a) and a microelectrode (b).

2.3.3 Advantages of microelectrodes

The advantages of microelectrodes will be discussed here in terms of their use with SECM experimentation. A very low dependence on hydrodynamic conditions (i.e. stir independence) is induced by having a relatively small, thin diffusion layer at the microelectrode which means that when the electrode is brought into close proximity to the substrate of interest for scanning (in the case of SECM), the "sensing" is performed within the diffusion layer. This means, when the microelectrode is scanning over the substrate in the presence of mediator solution, the current observed can be attributed to the properties of the substrate, mediator and tip - and not the movement of the tip through the mediator solution. When taking into account the rate at which the experiment is occurring, if the experiment is running faster than the rate of mass transport, then the electrochemical results will reflect the rate of the slowest step in the process which will therefore provide information on the rate of diffusion in the solution only. Due to the properties of a microelectrode, the increased rate of mass transport is less likely to have an effect on the result of the experiment and much faster chemical steps are available for study by electrochemical methods.

A further advantage of using microelectrodes is a reduced iR or "ohmic drop" effect. In electrochemical experiment a considerable distortion factor in the derivation of data is brought about by the ohmic effect. The ohmic drop is brought about as the current that flows through a solution generates a potential that opposes the applied potential. The true potential (E) can be calculated using the formula below, i.e. by subtracting the product of current (i) and resistance R from the applied potential (Eapp) (Equation 2.13).

$$E = E_{app} - iR \qquad \textbf{Equation 2.13}$$

When using conventional macroelectrodes there are fairly large iR distortions, since the current is relatively large (due to the large surface area), especially in highly resistive solutions such as organic solvents or aqueous systems with no added electrolytes. These problems are avoided when using microelectrodes, and for this reason experiments in these

situations can be often performed. This is due to two reasons, the first being that the distribution of the current passing through a solution in the vicinity of the electrode surface is different at the microelectrode, and this results in enhanced electrochemical behaviour. The second is that micoelectrodes that are performing near or at a steady state show minimal iR problems when compared to electrodes which are operating under planar diffusion. This has been shown by Bruckstein (1987), who showed that the iR drop is insignificant and independent of the geometry and size of the electrode with conditions under which true steady-state currents are observed.

Sweeping the electrode potential whilst monitoring the current gives information about electrode processes. The effect of changing potential, in addition to electrolysis, changes the ionic distribution of the electrolyte (background or otherwise) near the electrode surface, thus causing a charging current to flow which can mask the phenomena under investigation. Microelectrodes have a much smaller electrode area which gives rise to significantly smaller transient changes; this is due to the faradaic-to-charging current ratio, i_f/i_c which increases with the reciprocal of the characteristic dimensions. It therefore follows that microelectrode systems will suffer less distortion from "capacitative charging". This means that the rate at which the potential is swept can be made greater in a microelectrode system (Munteanu, 2002).

In summary, microelectrodes show the following advantageous capabilities:

- Can quickly achieve a steady state for a faradaic process
- Improved $i_{F/}i_c$ allows rapid scan rates
- Minimised ohmic drop minimises risk of signal distortion
- Improved signal to noise ratio as a result of minimal charging current
- The smaller size of microelectrodes allows measurements in very small solution volumes

2.4 Review of microelectrode fabrication methodologies

2.4.1 Disk microelectrodes

Figure 2.14: Schematic diagram illustrating cross section of disk electrode geometry.

Pulled Pt Wires/Pipette puller

One procedure for fabricating microelectrodes of less than 2 μm diameter involves employment of a pipette puller. Platinum (Pt) wire can be inserted into an open glass capillary and often local heating is introduced to the glass capillary with the inserted platinum wire. The wire and glass capillary can then be pulled simultaneously leading to an extreme decrease of its diameter and a tight seal of the Pt wire within the glass capillary (Pendley, 1990; Zhang, 1999; Katemann and Schuhmann, 2002). It is possible to program the pipette puller controlling the temperature and strength of pulling of the glass capillary. This has the effect of reproducing small microelectrodes with a very uniform shape (Figure 2.14). After pulling it is necessary for the metal core to be exposed and this can be performed by micropolishing (Shao and Mirkin, 1998). With the introduction of laser pipette pullers, electrodes with dimensions down to 10 nm have been reported using quartz capillaries and 25 μm hard Pt wire (Katemann and Schumann, 2002).

Gold Microbead Microelectrodes

Gold microbeads of diameters down to 1.5 μm have been used in the construction of disposable microelectrodes with diameters of 5 μm and smaller (Miles *et al*, 1997). A micropipette puller is used to pull pyrex capillaries that are uniformed in shape and opening dimension. Gold beads in solution are then injected into the lumen of the pyrex capillary which can then be heated at 120 ˚C to enable the evaporation of the water from the capillary before heating for a further 2 hours at 580 ˚C allowing the gold microbeads to sinter into a solid mass. An advantage is the reduced cost in the manufacture of these microelectrodes due to the microbeads being inexpensive and the fact that they are available in smaller dimensions than their respective wires.

Microelectrode fabrication by Chemical Vapour Deposition (CVD)

Microelectrodes have also been fabricated by chemical vapour deposition (CVD), which involves an insulating film being deposited on a carbon fibre or metal wire from a gas phase precursor. Film formation occurs by the deposition of silica from a $SiCl_4$, H_2 and O_2 gas phase onto a resistively heated carbon fibre or metal wire (Zhao *et al*, 1995). Due to the presence of a temperature gradient near the extremes of the wire or fibre, deposition rates are variable. This has the effect of generating an insulating covering of a uniform and concentric film that tapers down to the bare fibre/metal tip. Carbon fibre disk microelectrodes of 5 μm and 10 μm have been fabricated using this technique with silica films ranging from 1-600 μm in thickness (Zhao *et al*, 1995).

CVD offers many advantages including the geometry of the microelectrode being highly predictable and therefore conforming to theoretical predictions due to the concentric deposition of the film according to the temperature gradient. Also due to the nature of deposition, there is no need for sealants as required in other fabrication methodologies and finally, by altering the precursor formulae, one is able to cover an array of electrode materials of differing physiochemical properties with films of different thicknesses and properties.

2.4.2 Hemispherical microelectrodes

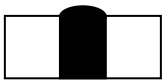

Figure 2.15: Schematic diagram illustrating cross section of hemispherical electrode geometry.

Demaille *et al* (1997) constructed spherical gold microelectrodes with diameters of 1-30 μm by self assembly of Au nanoparticles and 1,9-nonanedithiol molecules at the tip end of glass micropipettes. The spherical geometry of these fabricated tips were perfectly controlled and reproducible, and their electrochemical properties are the same as for solid metallic Au, showing ideal micro-electrode behaviour (Figure 2.15).

2.4.3 Ring-disk microelectrode

Figure 2.16: Schematic diagram illustrating cross section of ring-disk electrode geometry.

Carbon disk microelectrodes

As previously described, Zhao *et al* (1995) reported a 10 μm diameter carbon fibre insulated with a Si film by CVD. Based on this method ring-disk microelectrodes with tip diameters down to 25-30 μm have been fabricated. Once desired thickness of silica is deposited using CVD methodology a layer of pyrolytic carbon can be deposited from acetone. The silica coating process can then be repeated to insulate the newly deposited Carbon ring layer. The ring disk microelectrode is then prepared by cutting the end of the coated fibre at a position that produces the desired outside diameter for the analytical tip and polished (Figure 2.16).

Au/Pt ring disk

More recently, glass encapsulated Pt disk microelectrodes have been fabricated with the tip sharpened until the required Rg ratio was reached (Liljheroth *et al*, 2002). A thin Au film was sputtered onto a continuously rotated tip producing a thin Au film of about 500 nm in thickness. This outer ring is then insulated and exposed by polishing with aluminium oxide grinding paper.

2.4.4 Finite Conical (Etched) microelectrodes

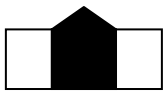

Figure 2.17: Schematic diagram illustrating cross section of finite cone electrode geometry.

A number of papers have documented the fabrication of microelectrodes $\leq$ 10 nm using electrochemical etching of metal wires over the last couple of decades (Penner *et al*, 1989; Lee *et al*, 1991; Mirkin and Bard, 1992; Conyers, 2000; Macpherson and Unwin, 2000; Sun *et al*, 2001). The electrochemical etching method involves anodic dissolution of a metal as a result of the application of an AC voltage (Lee *et al*, 1991). An alternating voltage is applied between a microwire and a Pt coil, in which the microwire is centrally located, to try and ensure symmetrical etching. The tip sharpness of the microelectrode is dependent on the etching current and length of time etching is allowed to proceed. Once the etching process is completed, the tips are washed and the wire is then coated with an insulating material to create a microelectrode with a very small area (Figure 2.17). There are a number of different coating techniques employed including dipping the wire into a varnish (Gewirth and Bard, 1988) or molten alkali metal (Zhang and Kanatzidis, 1994), translating the tip through a bead of molten glass (Penner *et al*, 1989) or the deposition of electrophoretic paints (Macpherson and Unwin, 2000; Lee *et al*, 2002). Although the

etching process allows the fabrication of very small tips, the conformity and reproducibility of microelectrodes using this method is very low and uncertainty often remains as to the exact shape of the resultant electrode (Thiebaud *et al*, 2000).

2.4.5 Microelectrodes by microfabrication

It has become necessary for microelectrode fabrication techniques to focus on generating smaller probes with reproducible and exact geometries to keep up with the requirements of the technologies that make use of them. Thiebaud *et al* (2000) employed a technique involving the use of Si anisotropic etching and thin-film Pt deposition to fabricate highly conformed Pt-tip microelectrodes. These microelectrodes are primarily used for extracellular monitoring of brain slices in vitro but the technique may one day be applied in the fabrication of tips for other applications such as the scanning electrochemical microscope (SECM). Another reported technique is the batch-microfabrication of SECM-AFM probes. This techniques uses direct write electron beam lithography (EBL) producing sharp atomic force microscopy (AFM) tips with a triangular-shaped electrode at the apex with a base width of 1μm and a height of just 0.65 μm (Dobson *et al*, 2005).

2.5 Scanning electrochemical microscopy

Scanning electrochemical microscopy (SECM) is a surface scanning probe technique allowing the collection of high resolution electrochemical data over a wide range of surfaces. SECM involves the measurement of the current through a microelectrode when it is held or moved in a solution in the surrounding area of a substrate. SECM makes use of many of the unique electrochemical properties of microelectrodes as described previously within this chapter. These include the hemispherical diffusion profile of solutes towards a microelectrode and the stir independence of microelectrode responses. Substrate, which can be solid surfaces of different types (e.g. glass, metal, polymer, biological material) or liquids (e.g. mercury, immiscible oil), perturb the electrochemical response of the tip, and this perturbation provides information about the nature and properties of the substrate. Engstrom *et al* and Liu *et al* in the late 1980's demonstrated the ability of microelectrodes to probe diffusion layers and the study of conductor and semi-conductor surfaces was carried out (Engstrom *et al*, 1986; Liu *et al*, 1986).

The SECM instrument is composed of an electrochemical cell, a translational stage capable of high resolution movement in the X,Y and Z planes (sub-micron), a bipotentiostat for the accurate control of the potential applied at the tip and/or the substrate, a hardware interface enabling the control of both cell and stage, and a PC which ideally provides an easy to use interface with the hardware as well as allowing the experimenter to control the parameters of the SECM experiment (Figure 2.18). Further details of the instrumentation are given in Chapter 3.

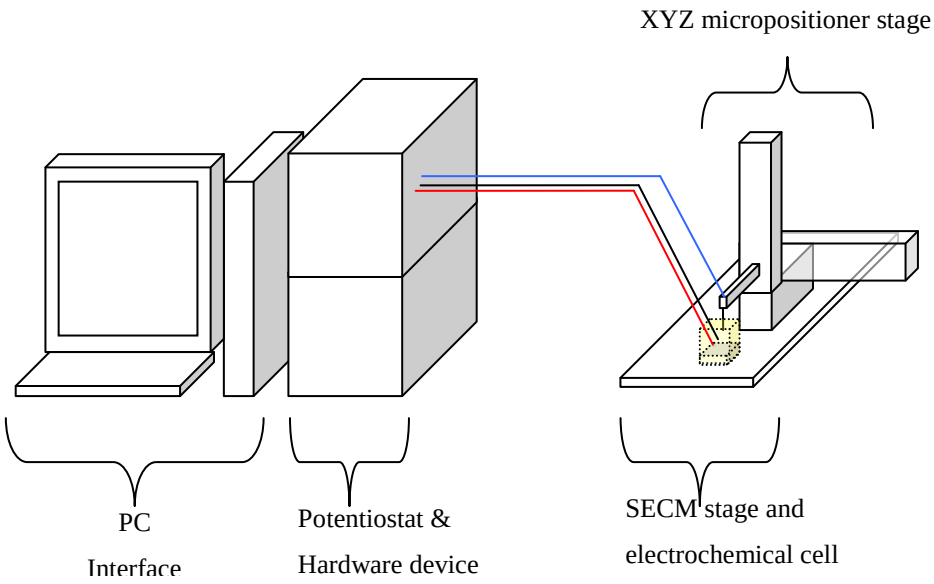

Figure 2.18: Schematic diagram depicting the instrumentation necessary in SECM.

Bard and co-workers carried out many experiments in the early years of SECM development leading to theoretical descriptions of (i) how the faradaic current measured at the tip may be described as a function of substrate charge transfer properties (ii) the relationship between the faradaic current detected at the tip and the tip to substrate distance, and (iii), the relationship between mass transport and homogenous reaction kinetics in the inter tip-substrate gap (Liu *et al*, 1986; Kwak and Bard 1989a, 1989b; Bard *et al*, 1989, 1990, 1991, 1992; Unwin and Bard, 1991).

In a typical SECM experiment, the microelectrode probe (as the working electrode) is immersed in a mediator solution (such as ferrocene carboxylic acid) along with a reference and counter electrode. There are three main SECM principles that may then be employed to collect data about the electrochemical properties of the substrate. These are the feedback mode (FB), generation collection mode (GC) and penetration mode.

2.5.1 Feedback mode

When a microelectrode is biased at a potential sufficient to drive an electron transfer reaction at the tip, a small faradaic current is generated, the magnitude of which is dependent on the radius of the active area and is termed 'i_T'. The current observed when the microelectrode tip is a relatively infinite distance away from the substrate – i.e. in bulk solution, is termed $i_{T\infty}$. Under these conditions the current is driven by the hemispherical flux of the species from the bulk solution to the tip (Figure 2.19a). When a tip is brought into close proximity to the substrate, moving through the mediator solution, the faradaic current may be observed to change. If the substrate is conductive, or, more accurately, has a high rate of heterogeous electron transfer, such as a carbon surface, the electroactive species reduced (or oxidized) at the microelectrode tip diffuses to the substrate and is recycled as it donates electrons to (or receives electrons from) the conductive substrate (Figure 2.19 B). As a result of this recycling, the rate at which fresh mediator molecules arrive at the microelectrode is increased to a rate greater than that due to diffusional processes only, resulting in an increase in tip current ($i_T > i_{T\infty}$). This increase of current with distance is known as 'positive feedback'. The equation for the tip current as a function of the normalised tip to substrate distance, L is as follows (where $L = d/a$) (Kwak and Bard, 1989b) (Equation 2.14).

$$(i_T / i_{T\infty}) = 0.68 + 0.7838/L + 0.3315\exp(-1.0672/L) \qquad \textbf{Equation 2.14}$$

When the tip approaches the surface of an insulating substrate, such as glass or plastic, the diffusion of the mediator to the tip of the microelectrode is hindered, resulting in the rate of diffusion becoming a limiting factor (Figure 2.19 C). Therefore, as the microelectrode approaches distances increasingly less than the depth of the diffusion layer, the tip current is observed to drop exponentially. This reduction in tip current with distance to the substrate is termed 'negative feedback' ($i_T < i_{T\infty}$), where the normalised current is given by (Kwak and Bard, 1989b) (Equation 2.15).

$$(i_T / i_{T\infty}) = \frac{1}{0.292 + 1.515/L + 0.655\exp(-2.4035/L)}$$ **Equation 2.15**

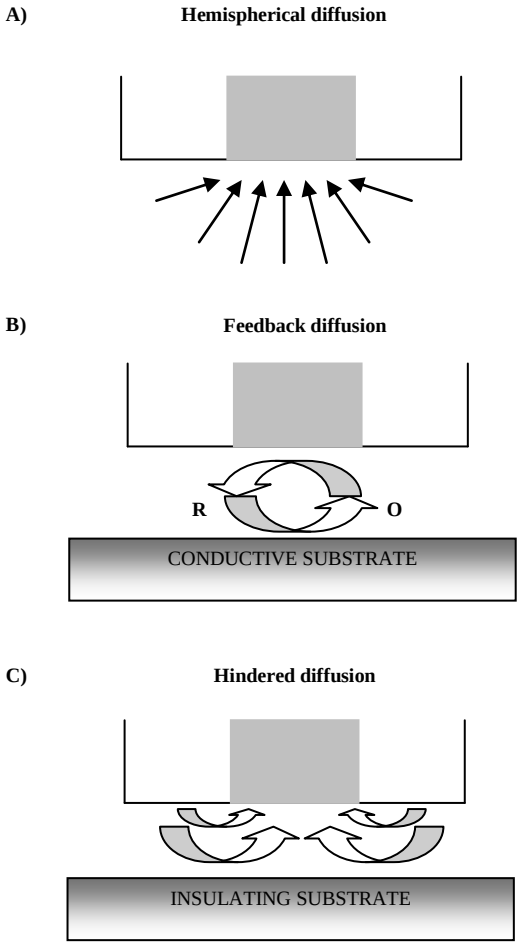

Figure 2.19: Schematic of the basic principles of SECM: When the microelectrode tip is A) far from substrate, diffusion leads to a steady-state current $i_{T\infty}$; B) near a conductive substrate feedback diffusion leads to $i_T > i_{T\infty}$; C) near an insulating substrate hindered diffusion leads to $i_T < i_{T\infty}$.

2.5.2 Substrate generation / tip collection mode (SG/TC)

This method is the more frequently employed of the collection-generation modes and involves the spatial and temporal mapping of concentration profiles of species being studied. Theories for linear or hemispherical diffusion that relate concentration vs. time and spatial coordinates can be used to calculate kinetic parameters of chemical and electrochemical processes, as well as mass transport coefficients (Bard & Faulkner, 2001).

Systems that are frequently studied by SG/TC include enzymatically patterned surfaces (Whittstock, 2001). For example, the activity of immobilized horseradish peroxidase for reduction of H_2O_2 to water using ferrocenemethanol in solution as an electron-donor can be studied by amperometric detection of ferrocene methanol cations. Furthermore, the oxidation of glucose by oxygen on immobilized glucose oxidase can be studied. The tip can be used as an amperometric oxygen sensor, by reducing O_2 to H_2O or H_2O_2, to map O_2 concentration profiles (Carano *et al*, 2003). Using this method it has been possible to monitor the respiration of living organisms (Kaya *et al*, 2001), and the catalytic activity for oxygen reduction of electro- and photo-catalysts (Fonseca *et al*, 2003).

2.5.3 Tip generation / substrate collection mode (TG/SC)

This method is similar to the feedback mode of the SECM (Fernandez and Bard, 2003). In the TG/SC mode, the collector is the substrate while the tip is used to locally generate the species which is measured. Here, the microelectrode tip is held at a potential where an electrode reaction occurs and the substrate is held at a different potential where the product of the tip reaction will react and thus be collected. In the majority of cases the substrate is infinitely larger than the tip, yielding a collection efficiency, given by $i_s/i_{t,}$ of 1 (100 %) for a stable tip-generated species, R. If R reacts, i_s/i_t becomes smaller and its change with separation, d, allows the determination of the rate constant of the homogenous reaction (Bard and Mirkin, 2001).

TG/SC has been almost exclusively used in combination with feedback experiments for studying coupled homogenous chemical reactions following electron-transfer in the tip-substrate gap (Zhou *et al*, 1992). The counter electrode will be affected by any side reaction in the gap, which makes it a useful parameter to monitor and calculate chemical reaction rates. More recently this method has been applied to the study of electrode reactions using a constant-current variant (Fernandez and Bard, 2003, 2004). The electro-reduction of dissolved oxygen on various materials was studied using this method. The imaging capabilities of this method can be exploited for the imaging of large arrays of catalyst spots as it is less dependent on the tip-substrate distance.

2.5.4 Penetration mode

In penetration mode, the SECM microelectrode tip is translated through the substrate of interest to obtain spatially resolved electrochemical information. An example of this was demonstrated by Csoka *et al* (2003a) who used the SECM to investigate concentration profiles of oxygen and hydrogen peroxide in a biosensor devised for the detection of sucrose in glucose containing samples by Scheller and Renneberg (1983). The multilayer electrode comprised a glucose-eliminating outer layer of glucose oxidase and catalase together with a sucrose detecting inner layer of invertase, mutarotase and glucose oxidase. The analytical signal of interest was the current obtained from the oxidisation of the hydrogen peroxide generated by the enzymatic reaction. Using the SECM technique, it was possible to measure enzymatic activity, activity ratios and reaction layer thickness, as well as sucrose and glucose concentrations.

The different approaches to SECM imaging have their associated advantages. In feedback mode, the reaction at the surface only occurs if the tip is in close proximity to the reaction site, whether it be the simple recycling of a mediator species or involvement of the redox species in an enzymatic reaction, generating the necessary reactants. However, in SG/TC mode, the reaction under observation occurs at the electrode surface regardless of the presence of the microelectrode tip. Therefore, the microelectrode is imaging the diffusion layer, i.e. the products of the reaction at the substrate, when scanned across a surface. As a

result of the accumulation of these products, the microelectrode shows greater sensitivity but lower resolution than SECM in feedback mode.

2.6 Application of Scanning Electrochemical Microscopy to Biological systems

The scanning electrochemical microscope has been applied to a diverse array of bio-analytical problems and is capable of providing quantitative information about the topography and electrochemical properties of a surface. In contrast to other microscopic techniques the SECM does not require biological samples to undergo complex pre-treatment, with a sample only having to be submerged in a mediator solution or thin film. Additionally SECM does not experience problems such as background fluorescence since the technique is not optically based. A further advantage of SECM is that the system under interrogation may be numerically modelled, allowing the subsequent capture of information relating to the kinetics of the reaction under observation. This makes SECM distinctively suitable for the study of biological specimens as it is possible for them be studied under simulated conditions close to those experienced *in-vivo* and interrogated repeatedly due to the non-destructive nature of the imaging process. SECM has allowed numerous, distinctly different bioanalytical problems to be tackled, and these have included: the imaging of methyl viologen permeability in bovine cartilage (Gonsalves *et al*, 2000); the determination of the electroosmotic flow of ions through mouse and human skin (Bath *et al*, 2000; Uitto and White, 2003); convective flow rates through dentine (Macpherson and Unwin, 2005); bone reabsorption by osteoclasts (Berger *et al*, 2001); the interrogation of redox activities of cancer cells; and as a quality control tool for biosensor fabrication.

A significant limitation to SECM imaging however is the slow scanning speed, and hence low sample throughput, although this is common to most scanning probe techniques. The use of a microelectrode probe as opposed to a lens also creates difficulties. An example of this is that for positive feedback to occur, the tip must be positioned within one critical

dimension of the working electrode from the surface under interrogation, giving rise to the problem of tip crash and the potential damage of the tip and substrate. It is important to remember that SECM cannot be directly compared to other imaging technologies as the technique does not directly image these biological entities, but the processes in which they are involved. For example, when SECM is used to image an enzyme immobilised on a surface, it is the enzyme mechanism and the behaviour of products, co-factors or substrates that it is imaging and not the enzyme itself. The technique gives complementary information that can lead to an improved understanding of the images obtained by other techniques, such as fluorescence.

2.6.1 DNA Imaging by SECM

There has been a great deal of progress and development of fabrication techniques of DNA microarrays and their associated high-throughput DNA microarray chip detectors. For the study, diagnosis and treatment of genetic disease, as well as the identification of SNPs (single nucleotide polymorphisms), the reliable detection of mismatched base pairs is critical. Of the many assays proposed for large scale mutational analysis, those which employ "DNA chips" have been the most widely investigated. Current techniques employed in this field often rely on the detection of a label tagged on to the target sequence on the formation of a duplex between the probe sequence (on the chip) and targets in the sample analyte (which may have a flourophore or a chemiluminesent label). However, the size, complexity and capital-intensive nature of these techniques represent major drawbacks, allowing for the development of alternative methods of detecting hybridisation events (Turcu, 2004a).

As a consequence of this, the employment of SECM techniques in studying hybridisation events is extremely appealing. This is due to the fact that the detection level is potentially sufficiently low for most applications involving gene expression, and SECM detection is relatively inexpensive and substrate general. With regards to its suitability in comparison to other modes of scanning probe microscopy, it represents the most viable approach because of the congruency of the spatial resolution of SECM tips with dimensions of

microarray wells or spots. For example, microarrays printed by ink jet technology produce droplets ~67 μm in diameter, which is well within the resolution capabilities of an SECM (down to sub micron). The simplest form of nucleic acid detection has been described by Wang and Zhou (2002), who exploited the intrinsic electrochemical properties of the guanine residue in the DNA duplex. Surface-confined DNA molecules were detected through the guanine oxidation induced by the tip-generated $Ru(bpy)^{3+}$:

$$Ru(bpy)_3^{2+} \rightarrow Ru(bpy)_3^{3+} + e^- \text{ (at the tip of the UME)}$$

$$Ru(bpy)_3^{3+} + \text{guanine} \rightarrow Ru(bpy)_3^{2+} + \text{guanine}^+ \text{ (at the substrate surface)}$$

On the application of a sufficient potential at the tip, $Ru(bpy)_3^{3+}$ is generated which diffuses to the substrate, irreversibly oxidising the guanine residues on the immobilised substrate. This then generates $Ru(bpy)_3^{2+}$ for re-oxidation at the tip. In this way positive feedback is observed over the surface confined DNA molecules. A disadvantage of this approach is that due to the irreversible oxidisation of the guanine residue, the same surface cannot be repeatedly scanned (Wang and Zhou, 2002).

A second method for imaging DNA and the hybridisation event is in the use of electrochemically active labels. Yamashita *et al* (2001) investigated the SECMs applicability to visualising DNA microarrays using an amino based ligand to immobilise DNA duplexes on glass in a mediator solution of ferrocenyl naphthalene. This ligand was concentrated on the double stranded DNA region of the DNA array only, meaning that because of the ligand's electrochemistry, it can interact with the scanning tip to generate a signal. The DNA hybridisation detection levels of this system, however, were significantly less than those reported for alternative, existing techniques. Further to this, a study using the silver staining approach in combination with SECM to image a DNA microarray was reported (Wang *et al*, 2002). In this study silver nanoparticles were deposited at sites where hybridisation had occurred as they themselves conjugate onto the biotin/streptavidin-colloidal gold conjugate that had been sequentially constructed at the initial site of hybridisation. This resulted in an area over which positive feedback could

occur as a consequence of mediator recycling at the site of silver deposition. Therefore it was possible for the SECM to detect the hybridisation events. It was additionally revealed that by altering the hybridisation temperature, highly sequence-specific DNA analysis was possible down to the level of a single base-pair mismatch.

Wain and Zhou (2008) employed the use of the SECM in the imaging of DNA microarrays fabricated on gold substrates using methylene blue (MB) as a redox-active intercalator. Their work demonstrated that MB, intercalated between base pairs of immobilised ds-DNA, was electrochemically reduced via electron transfer from the underlying gold substrate, and the product then reoxidized in solution by SECM tip-generated ferricyanide (Figure 2.20). This resulting feedback current allowed a heterogeneous electron-transfer rate constant for the MB-intercalated DNA to be deduced. This resulted in DNA microarray spots being detected at a level of 14 fmol/spot for ds-DNA consisting of 15 base pairs. The method also discriminated between single- and double-stranded DNA, indicating its potential use as a hybridisation sensor for disease diagnoses (Wain and Zhou, 2008).

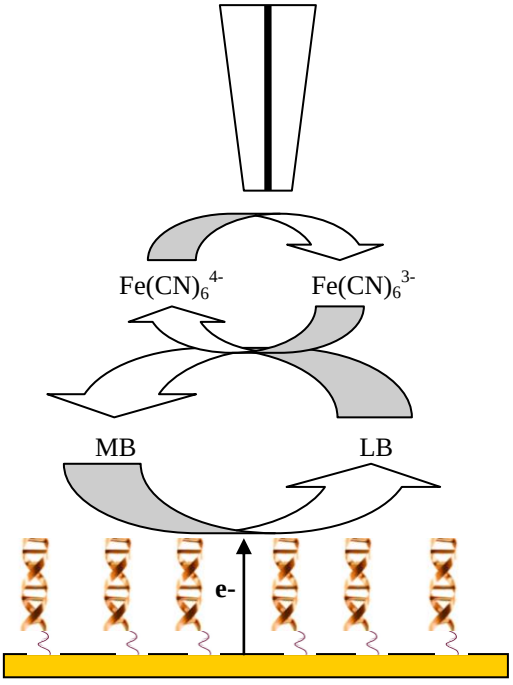

Figure 2.20: Schematic representation of the SECM detection method used by Wain & Zhou (2008) (MB = methylene blue, LB = leucomethylene blue).

A significant caveat of current approaches to imaging DNA microarrays is the use of numerous reagents which is a costly and time consuming factor. Exploiting the highly negatively charged properties of the sugar phosphate back bone of DNA, Turcu and co-workers, were able to develop an electrostatic approach to visualising the status of surface bound DNA probes (Turcu *et al*, 2004a, 2004b). The detection of hybridisation was achieved through coulomb interactions between the negatively charged sugar phosphate back bone of the immobilised oligonucleotide and the free diffusing redox mediator. Using $[Fe(CN)_6]^{3-}$ as a mediator, it was found that when the tip was scanned across a gold electrode functionalised with DNA, the tip current dropped as a result of the repulsive forces, preventing the diffusion of the mediator to the gold electrode beneath for recycling. Additional differences were found between the repulsive forces of ssDNA dots and dsDNA, indicating that the increase in repellent charges due to duplex formation is sufficient for detection by their repellent mode of SECM operation. Previously within our group (Roberts *et al*, 2009) microarrays of polyethyleneimine (PEI) films were deposited on screen-printed carbon substrates using the SECM. Single stranded herring DNA was electrostatically adsorbed at the surface of the polyethyleneimine and the further adsorption of complementary single stranded DNA on the surface was observed, using hexaamine ruthenium chloride as a mediator, to give rise to substantial decreases in interfacial impedance at the surface as measured by increases of tip current of the order of 1-2 nA (6%). Conversely, adsorption of DNA from alternate species, i.e. salmon ssDNA on herring ssDNA, yielded much smaller changes in tip current of 0.2 nA.

2.6.2 Enzymes

In recent years a trend towards the development of miniaturised analytical devices has evolved and it is within this area that there is much scope for the use of SECM in the fabrication (with regards to substrate patterning), characterisation and optimisation of enzyme based sensing systems. Through the determination of enzymatic activity, it is possible for the SECM to be used to characterise a variety of different sensors with various applications, from those using enzymes as a label for a binding event through to sensors in which the enzyme forms the primary recognition element (Turcu *et al*, 2005; Zhang *et al*,

2006). By obtaining spatially resolved data relating to the distribution of electrochemical activity on the sensor substrate, it is possible for the effectiveness of the patterning technique to be established and any possible problems associated with cross talk between different sensing regions being detected (Strike *et al*, 1999). The SECM has been previously used in the validation of an ink-jet microdispensing technique for the production of a sensor with differently composed sensing regions (Turcu *et al*, 2005) demonstrating its usefulness within this area.

It is possible for an immobilised enzyme to be imaged by SECM in either feedback or SG/TC mode of operation. Enzyme mediated feedback imaging, or 'enzyme-mediated positive feedback', involves the replacement of the enzymes co-factor, or 'electron acceptor', by a mediator. Zhao and Wittstock (2005), demonstrated the use of feedback imaging through mediator regeneration by using the catalysis of glucose to gluconolactone by glucose dehydrogenase (GDH), using the redox active mediator ferrocenemethanol as a cofactor. Biotinylated GDH was immobilised on streptavidin coated paramagnetic microbeads at a surface concentration of 2.8×10^6 molecules/$4\pi r_{bead}^2$ (1.8×10^{-11} mol cm^{-2}) and deposited in a well defined, mound-shaped 100 μm diameter microspot. Polarised at a potential of +400 mV at a scan height of 30 μm above the surface, the scan was conducted in a buffered solution of Ca^{2+}, D-glucose and $FcCH_2OH$. Positive feedback was obtained as a result of the reduction of the ferroceniummethanol (Fc) complex that occurs with the oxidation of glucose and its subsequent diffusion to the tip. On the removal of the D-glucose from the system, the feedback signal was halted:

$$\text{D-Glucose} + (3\text{-n})M_{ox} \longrightarrow \text{D-gluconolactone} + (3\text{-n})M_{red} + 2H^+ \ (n = 1,2)$$

The second mode of imaging enzymatic activity, substrate generation / tip collection (SG/TC) mode, is different to the feedback mode in that it does not involve the use of a mediator but rather the direct reduction or oxidation of the enzymatic product. Within this method the microelectrode tip is scanned across the specimen surface to produce a map of the local concentration of a molecule generated or consumed by the enzyme. In contrast to

the feedback mode, the biochemical process in this mode is independent of the presence of the tip. A distinct advantage of GC over the feedback mode is that the background current detected at the tip is negligible, increasing the signal to noise ratio by allowing any change in the faradaic current to be attributed to enzymatic activity (Kranz *et al,* 1997; Oyamatsu *et al*, 2003a).

However, despite its high sensitivity, this technique does suffer from a lack of spatial resolution due to the diffuse distribution of the biocatalytic products, which diffuse away from the substrate down a concentration gradient into the surrounding medium thereby preventing an accurate determination of the location of the enzyme. Another disadvantage of this technique arises when the process at the tip is reversible which means that there may be a feedback component to the current. It is possible to overcome this problem, however, by increasing the tip-to-substrate distance or by using a potentiometric tip which does not perturb the local concentration of the reactant. The sensitivity of the GC mode may be enhanced by increasing the concentration of the generated product, which may be achieved by minimising the volume of solution between the tip and the substrate. A possible problem in doing this is that the diffusion of the substrate or cofactor from bulk to the enzyme may be physically hindered by the tip. As a result of this a lowering of the tip current similar to that observed when approaching an insulating substrate may occur (Zhao and Wittstock, 2004b).

An immunoassay was designed by Zhang *et al* (2006) to detect the circulating CA15-3 antigen, a specific marker of breast cancer, with the aim of simplifying the conventional costly, complex and time consuming assays that are currently adopted to detect this molecule. By interrogating horseradish peroxidase by SECM in GC mode, Zhang and co-workers, used this information to develop an immunoassay for this antigen. The assay which involves the sandwiching of the antigen between an antibody immobilised on a streptavidin coated plate and an antibody labelled with horseradish peroxidase. Once exposed to H_2O_2 and hydroquinone, HRP catalyses the reduction of hydrogen peroxide to water via the oxidation of hydroquinone to benzoquinone which then diffuses to the microelectrode and is reduced, thus generating a faradaic current. The SECM has also been

used in other immunosensors and immunoassays involving the use of a variety of other enzyme linked systems including biotinylated glucose oxidase (Wijayawardhana *et al*, 2000a) and alkaline phosphatase (Wijayawardhana *et al*, 2000b).

To design optimal, efficient devices it can also be necessary to determine the distribution of the different electroactive species inside the differently made, sized and formed reaction layers during their operation. To allow for the optimisation of the biosensor, it is possible to make these determinations using the SECM. The SECM is so effective and useful within this area of research that it is often used as a quality control technique. For instance, in a series of papers by Csoka *et al* (2003), SECM has been used to calculate the distribution of enzyme products within a less complex glucose oxidase biosensor in order to determine the optimum polymer:enzyme ratio in a wired enzyme electrode, as well as quantifying the effectiveness of an interference-eliminating layer, and also for the determination of the reaction layer thickness to give an optimum enzyme response (100 µm). This research helped to demonstrate the capability of SECM in determining the distribution of different species within the reaction layer of biosensors and this could allow their optimisation by the alteration of the structure of the sensor.

By using SECM in feedback mode, the visualisation of redox hydrogel-based micropatterened complex biosensor architectures was achieved (Niculescu *et al*, 2004), and by using high spatial resolution through the use of $K_4[Fe(CN)_6]$ as the electroactive mediator, the biochemical activity of immobilized enzyme microstructures was determined.

In 2001 Wittstock produced a comprehensive review of techniques that are available for immobilizing enzymes onto different substrates and these include enzyme-modified patterned monolayers, polymer and metal microstructures. The SECM studies that were published after this review detailing new immobilisation combinations include: horseradish peroxidase and glucose oxidase immobilisation on amino- thiol- and disulphide- functionalised gold patterned by a variety of soft lithographic techniques (Wilhelm and Wittstock, 2002; Wilhelm and Wittstock, 2003; Oyamatsu *et al*, 2003b; Gaspar, 2001); 'wired' spots of bilirubin oxidase (laccase) in a redox hydrogel (Fernandez,

et al, 2004); horseradish peroxidise in β-Cyclodextrin (Wang *et al*, 2004); biotinylated β-Galactosidase on streptavidin coated paramagnetic beads (Zhao and Wittstock, 2004a); and GOx immobilisation on biotinylated polypyrrole films deposited by SECM in direct mode (Evans *et al*, 2005; Kranz *et al*, 1997).

In addition to this, lactate oxidase, LOx has recently been seen to absorb directly on glassy carbon and highly ordered pyrolytic graphite. This has been detected by SECM and AFM, thus giving promise for the development of these materials as platforms for a biosensor for lactate, an important analyte in food and clinical science (Parra *et al*, 2006).

2.6.3 Living cells

Whereas other microscopic techniques require complex preparations for imaging of living cells to be achieved, often resulting in artifacts being produced, the SECM has the advantage of being able to image living specimens under *in-vivo* conditions. Combined with its ability to interrogate substrates non-invasively, SECM offers a unique approach to the study of intracellular processes with high spatial resolution (Yotter and Wilson, 2004). In 1990 Lee *et al* investigated the photosynthetic activity of a number of plant leaf structures using SECM, monitoring the concentration profiles of oxygen evolved during photosynthesis and also their topography via negative feedback imaging using potassium ferricyanide (Lee *et al*, 1990). After this initial application of SECM to a biological substrate, the technique has been developed and applied to a variety of biological systems including the application to living cells obtaining information on the processes that occur within them.

Yasukawa *et al* (1998) monitored the depletion of molecular oxygen in the immediate environment of cells as they respire. Oxygen is present at higher concentrations in bulk solution than the immediate vicinity of a respiring cell as oxygen is consumed by the cell resulting in a decrease in concentration. By placing an electrode in close proximity to a respiring cell, the faradaic current measured from the reduction of oxygen near the specimen is less than that recorded by the electrode in bulk solution (Figure 2.21).

However, in the case of a photosynthetic cell, oxygen concentration around the cell increases as the cell is producing oxygen. This approach has been used in the study of plant physiology (Tsionsky *et al*, 1997); with the SECM's ability to obtain high resolution electrochemical maps of a surface, the activity of single stomata and their effects of cadmium induced stress on the plant *Brassica juncea* has been successfully monitored (Zhu *et al*, 2005). Garay *et al* (2004) also illustrated its diversity as a bioanalytical tool by undertaking the study of the chemical analysis of tree rings by modifying the amino groups on the wood surface with glucose oxidase, using a shear force feedback approach. Garay *et al* (2004) succeeded in obtaining topographical and chemical composition information about the sample wood surface obtained from the spruce, *Picea abies*, with the results being comparable to the more classical analyses of the wood.

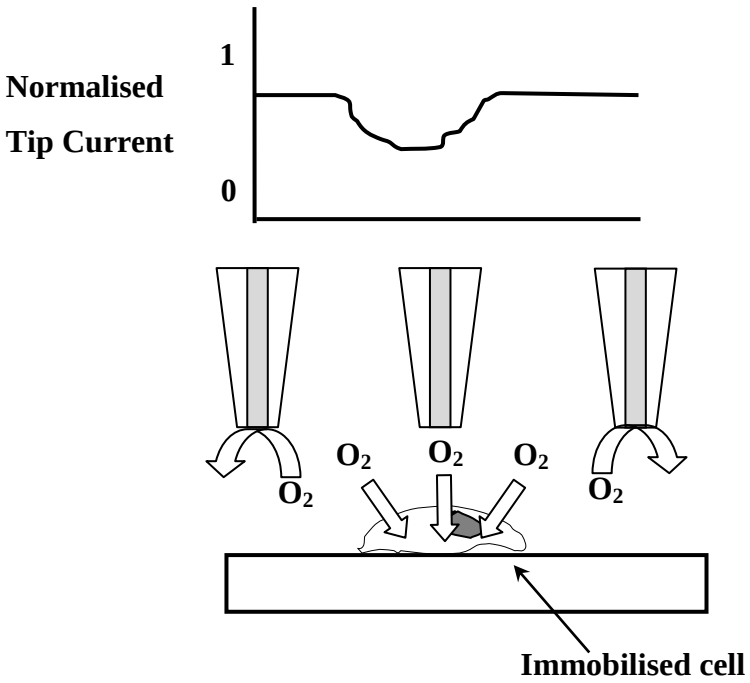

Figure 2.21: Schematic diagram detailing imaging of cells by detection of reduction in oxygen concentration in close proximity of the immobilised cell compared to detection in bulk solution.

Oxygen was also utilised in a study of the differentiation process of human monocytic cell lines. Leukocytes play a pivotal role in the immune system and produce reactive oxygen species (ROS), ($O_2^{\bullet-}$, H_2O_2 and OH^-) during "respiratory burst". This involves the conversion of molecular oxygen to $O_2^{\bullet-}$ by NADPH oxidase in human monocytic leukaemia cells. Using SECM, the rate of ROS production was found to be reflective of the cellular differentiation process and when combined with chemiluminescence methodologies, could represent an easy approach to monitoring the differentiation process in real time (Kasai *et al*, 2005).

These approaches demonstrated above have not included the use of electroactive mediators, such as redox active species that act as intermediaries between the microelectrode probe and the substrate under interrogation. The main advantage of this methodology is that the use of potentially harmful reagents can be avoided, allowing for conditions to be maintained which are as close as possible to those experienced *in-vivo*. Whilst this type of experiment has its uses studying cellular respiration, their value in probing cellular biology and physiology has proved somewhat limited. Therefore, the scope for the development of alternative techniques is great. Simply by introducing a mediator to the system it could be possible to interrogate the topography of cells, changes in morphology and changes in intracellular processes - as well as the mixed intracellular potentials, concentration and location of redox centres (Liu *et al*, 2000). A schematic detailing some of the ways in which mediators of differing hydrophobicities may be utilised to interrogate living cells are shown in Figure 2.22.

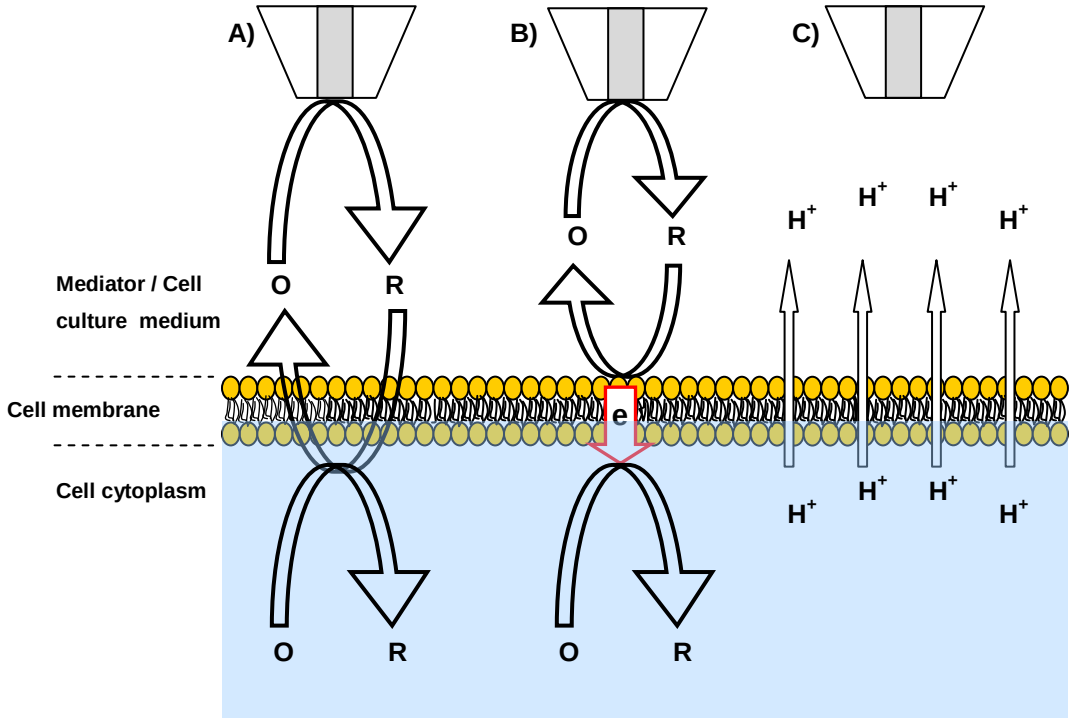

Figure 2.22: A) Positive feedback is observed as a hydrophobic reduced species generated at the tip diffuses through the cell membrane before being re-oxidised by a different intracellular redox centre within the cell. B) Positive feedback observed as a result of a hydrophobic mediator diffusing to the cell membrane where it is re-oxidised by ET occurring across the cell membrane. C) Schematic illustrating the potentiometric measurement of the pH profile around a single cell.

Takahashi *et al* (2009) evaluated the inner and outer functions of single living cells using an optical fiber-nanoelectrode probe with a shear force feedback system. Using this probe it was possible to detect and induce electrochemical and photochemical reactions simultaneously. HeLa cells were transfected with two expression vectors including secreated alkaline phosphatase (SEAP) and green fluorescent protein (GFP). Simultaneous topography, fluorescent and electrochemical images of these transfected HeLa cells were obtained in constant distant and constant height modes. In the constant-height mode when the probe moved above the HeLa cell, there was an observed increase in intensity of the electrochemical reaction which was due to the oxidation of p-aminopropiophenone (PAPP) generated by an enzyme reaction of SEAP. However, the constant-distance mode allowed

for a greater contrast as the concentration of SEAP was higher near the cell. This combination of fluorescent and electrochemical measurements shows great potential for analyzing the dynamics of cellular membrane proteins (Takahashi *et al*, 2009).

2.6.4 Mammalian cells

Through the use of mediators with differential hydrophobicities, it has become possible to investigate the intracellular redox potential of cells and the redox reactions which take place within them. The topography and intracellular redox behaviour of metastatic and non-metastatic breast cell lines has been investigated using a range of hydrophilic mediators, namely $Ru(NH_3)_6^{3/2+}$, $Fe(CN)_6^{3/4-}$ and $Ru(CN)_6^{3/4-}$ (Liu *et al*, 2001). When comparing the metastatic and non-metastatic cell lines they were observed to exhibit significantly different intracellular redox behaviour with normal, healthy MCF-10A cells regenerating napthoquinone at a faster rate than the metastatic MDA-MB-231 cells. It was established, using SECM in combination with single cell chronocoulometry, that differences in the redox activity between non-transformed breast cells and metastatic breast cells were due to different concentrations of redox-active moieties in the cells and that the same intracellular moieties participate in the oxidation of all three quinols used as mediators. The occurrence of mediator regeneration within the cell raised the question of whether specific redox events are confined to specific spatial localities in the cell (Liu *et al*, 2001). The capability of SECM to detect activity was also demonstrated by Takii *et al* (2003) employing SECM techniques in the characterisation of spatial distribution of respiratory activity in PC12 neuronal cells. Oxygen reduction current was used as an indicator of respiratory intensity; areas where negative feedback was obtained were correlated to areas of high respiratory activity as the cell consumed oxygen. Employing this technique, mitochondria location in the axon could also be identified together with the role of neuronal growth factor (NGF) in mitochondrion distribution and excitation (Takii *et al*, 2003). A limitation of this study is the inability to image the axon and cell body simultaneously due to the height differential. However, this problem was overcome by Takahashi *et al* (2006) by utilizing the 'standing approach mode', a feedback mechanism

allowing the simultaneous imaging of PC12 cell topography and respiratory activity for the first time (Takahashi *et al*, 2006).

Feng *et al* (2003) highlighted that SECM may also be applied to larger fields of cells to good effect. Metastatic breast cells were loaded with fluorescent nanospheres and placed in a densely packed monolayer with unlabelled normal breast cells. By measuring the redox activity of a heterogeneous field of cells, it was possible to identify cancerous cells and so identify malignant cells in human tissues. The fluorescent images and SECM profiles were superimposed and showed that the SECM was capable of differentiating between the two closely packed cell lines (Feng *et al*, 2003).

SECM has also been utilized for the in situ detection of membrane glycans on adherent cells using BGC-823 human gastric carcinoma (BGC cells as the model (Xue *et al*, 2010). The localized surface interaction on the cell was controlled by poly(dimethylsiloxane) (PDMS) membrane and HRP-tagged lectins were specifically bound to cell membrane glycans to catalyse the oxidation of ferrocenylmethanol (FMA) by H_2O_2 to FMA^+. Using a substrate generation/tip collection (SG/TC) mode it was possible to determine that the expression levels for cell-surface glycans were statistically different and that when compared with flow cytometric assay the same differences were observed Xue *et al*, 2010).

2.6.5 Combined SECM Instrumentation

As a stand alone instrument the SECM is unique in the information it can provide; in combination with other imaging techniques, the SECM becomes a very powerful tool. For instance, it may be possible to address the problem of differentiating the variation in current due to surface reactivity from that due to surface topography. Zhou *et al* in 2001 used the SECM, in combination with a scanning chemi-luminescence microscope (SCLM), to generate electrochemical/chemiluminesence maps of HRP activity; the SECM image, which is based on the reduction current of oxygen, gives information on the topography of the area of enzyme immobilisation, whereas the SCLM images, which are generated based on the detection of localised chemiluminesence, show the activity and distribution of the immobilised enzyme. A further example of this combined approach was

demonstrated by Oyamatsu *et al* (2003b) in which the SECM was hybridized to a Scanning Confocal Microscope (SCFM) system, and this was undertaken to image diaphorase (Dp) patterns generated by spotting, laser induced patterning and patterning through the electrogeneration of HOBr in order to deactivate the immobilised enzyme. In this system the SCFM is capable of imaging Dp alone, unlike the SECM which can only generate an image when NADH is introduced to the system - and when used in combination these techniques are capable of imaging the localised enzyme and the *activity* of the enzyme only.

2.6.6 Conclusions and future outlook

The SECM has become an invaluable tool for studying living cells, as samples require little or no pre-treatment - and the high resolution imaging of the electrochemical processes under in-situ conditions has become a key tool on the interrogation of a variety of biological systems. The SECM has also been used extensively to study transmembrane processes and the role of trans-membrane pumps. The SECM has moreover been used in a number of studies investigating the redox behaviour of cells, using mediators with different hydophobicities. With the fabrication of smaller and smaller electrodes, there is the possibility the techniques could be used to further interrogate intracellular domains – and in this concept Takahashi *et al* (2006), for example, have reported the successful imaging of biological samples using an electrode with an effective radius of just 35 nm. Using these small electrodes, it may be possible to determine the locus of enhanced mitochondrial activity within a cell. However, since electrodes with progressively smaller critical dimensions may exhibit electrochemical behaviour that departs from existing models, development of the accompanying theory must be developed alongside.

As the SECM may be used to non-invasively monitor cellular status, it is thought that it will be increasingly used as an effective research tool within drug discovery. In this context the SECM has already been used to demonstrate its usefulness in monitoring cellular respiration by measuring the oxygen oxidation current in the vicinity of a living cell.

There is a strong trend towards the exploitation of developments in manufacturing techniques to allow the miniaturisation of biological devices such as biosensors, micro-fluidic devices and "lab-on-a-chip" sensing technologies. Whilst these techniques do exist, it is of great importance that the technique is sufficiently flexible to characterise the resulting product appropriately. Using SECM it is possible to locate immobilised entities, determine their spatial distribution and to interrogate the movement of substrates and products in and around the functionalised surface. The technique therefore, proves to be a versatile system for application to sensor development, not only in their characterisation and quality control of sensing systems, but also in their fabrication via the controlled direct deposition of polymers and other biosensor scaffolds. The SECM's capability to pattern substrates, either by selective desorption of self assembled monolayers or by the localised deposition of polymers, has significant implications for the construction of multi-enzyme arrays.

The SECM is a powerful tool which could be exploited to detect DNA hybridization. Reasons for this technique being a lead contender in this field include: the sensors themselves being able to be exploited as micro-fabrication techniques; the technique potentially offering great sensitivity; and the approach is also being highly cost effective. The spatial resolution that the SECM offers has great potential for the development of DNA microarray sensing systems to rival the benchmark fluorescent approach currently used.

SECM is a powerful tool for particular applications as a stand-alone technique. However, when combined with other imaging tools such as atomic force and confocal microscopy, the power and resolution of the technique, in terms of information provided, is very much enhanced.

Chapter 3
Materials and Methods

3. Materials and methods

3.1 Introduction

This chapter provides details of the materials and methods employed in the preparation of mediator solutions and the fabrication of substrates for interrogation by SECM. The protocol for each type of SECM experiment is also described.

3.1.1 Reagents

Disodium hydrogen orthophosphate, potassium chloride, dihydrogen sodium orthophosphate (all 'AnalaR' grade) were purchased from BDH (Poole, Dorset, UK). Potassium ferricyanide, hexamine ruthenium chloride, ferrocenecarboxylic acid, poly-L-lysine, Polyethyleneimine (PEI) (50% solution) and albumin serum bovine (BSA) were all purchased from Sigma Aldrich (Gillingham, Dorset, UK).

Immunoprobe™ biotinylation kits containing 0.1M sodium phosphate buffer, 0.01 M phosphate buffered saline (PBS) (NaCl 138mM; KCl 27mM; pH 7.4 at 25ºC), biotinamidohexanoic acid sulfo-N-hydroxysuccinimde (BAC-Sulfo-NHS), pronase, affinity purified avidin, dimethylsulfoxide and 10 mM 2-(4-Hydroxyphenylazo) benzoic acid (HABA) in 10 mM NaOH were also purchased from Sigma-Aldrich (Gillingham, Dorset, UK). All chemicals were supplied as analytical grade and therefore were used without further purification.

Free PSA ELISA kit containing antibody-coated microtiter 96 microtitre plate, sample diluent, reference standards (0, 0.1, 0.5, 2.0, 5.0 and 10.0 ng/ml) f-PSA, enzyme conjugate reagent, TMB subtrate, stop solution and wash buffer (50X) were purchased from Diagnostic Automation Inc (Calabasas, CA, USA).

3.1.2 Materials

Epoxy resin (Araldite®) and Acheson Electrodag conductive silver paint were purchased from AGAR Scientific Limited. Platinum-quartz fibres were obtained from Thomas Recording GmbH, Germany. All wires, crocodile clips and other consumer electronics were purchased from Maplin Electronics (Luton, Bedfordshire, UK). Conductive inks (carbon type 422SS and Ag/AgCl type 6088SS) were obtained from Acheson Industries Europe and printed onto Melinex plastic sheets. Superfrost® microscope slides were obtained from Menzel-Glaser GmbH & Co, Germany.

3.1.3 Equipment

Scanning Electrochemical Microscope (SECM)

A Uniscan Instruments Ltd SECM270 was used for all SECM experiments. Further information is given later within this chapter with regards to the instrument specifictions.

Scanning Electron Microscope (SEM)

A scanning field emission gun scanning electron microscope (SFEG SEM, model XL30, FEI, Netherlands), was used for all SEM imaging.

Digital Multimeter

A hand held ASYC II MX 54C (Metrix Electronics, Hamps., UK) digital multimeter was used to verify electrical conductivity during points of the microelectrode fabrication process.

Microscopy

An Olympus SZX12 bifocal microscope (max 90X magnification) (Wolf Laboratories Limited, York, UK) and a Schott KL 1500 LCD (Myer Instruments, Houston, USA) light source were used for image capturing

Pipette Puller

A Narishige PP-830 pipette puller (Narishige International Limited, London, UK) was used in the fabrication of microelectrodes.

Electrode polishing

Electrode surfaces were polished using the Narishige EG-400 microgrinder (Narishige International Limited, London, UK). Silicon carbide grinding discs, lapping paper and alumina powder were obtained from Buehler (Windsor, Berkshire, UK).

3.1.4 Solution preparation

Unless stated otherwise, all solutions were prepared using water from the Elga Purelab UHQ-II water system (Vivendi Water Systems, High Wycombe, Buckinghamshire, UK).

3.2 Antibody/Antigen sensor characterisation methodology

3.2.1 Additional reagents

Monocolonal antibodies against Neuron Specific Enolase (NSE), Prostrate specific antigen (PSA) were developed and supplied by Canag Diagnostics, Ltd. (Gothenburg, Sweden). NSE and PSA antigen were also developed and supplied by Canag Diagnostics, Ltd. (Gothenburg, Sweden).

Monoclonal antibody against ciprofloxacin was purchased from Abcam (Cambridge, Cambridgeshire, UK). Ciprofloxacin ≥ 98.0% (HPLC) was purchased from Sigma Aldrich (Poole, Dorset, UK).

Monoclonal antibody against N-terminal cross linked telopeptide (NTx) was developed and supplied by Unipath Ltd (Bedford, Bedfordshire, UK). The NTx antigen concentration

range were standards provided as part of a commercially available ELISA from Wampole Laboratories (Princeton, NJ, USA).

All antibodies and antigen were supplied with sodium azide as preservative.

3.2.2 Substrate

A screen printed electrode was used as the substrate in this series of experiments (obtained from Microarray Ltd). Commercial graphite paste-based carbon ink product code: 7102, Silver/silver chloride (product code: 5874), and dielectric ink (product code: 5018) were all purchased from DuPont Microcircuit Materials (Bristol, Avon, UK).

3.2.3 Biotinylation of IgG

The primary application of the ImmunoProbe Biotinylation kit is the preparation of biotin labeled monoclonal antibodies which may be used in ELISA, immunoblotting, immunohistochemistry and other immunosensing techniques. The kit may also be used for conjugation of biotin to other proteins, peptide hormones or cytokines.

Biotinylation is often performed with N-hydroxysuccinimide (NHS) esters of biotin or biotinamidohexanoic acid (biotinAC, BAC) (Wilchek and Bayer, 1990). The extended spacer arm from the hexanoic acid improves the interaction between avidin and biotinylated macromolecules, overcoming steric hindrance present at the biotin binding sites of avidin (Green *et al*, 1971).

With the Sigma ImmunoProbe Kit, biotinylation is performed with BAC-SulfoNHS. This derivative is soluble in water and biotinylation proceeds at near neutral pH values. The reagent is particularly useful when mild reaction conditions are required for the biotinylation of sensitive biomolecules such as antibodies, enzymes and cell surface proteins (Suter and Butler, 1986; Gretch *et al*, 1987).

The following procedure describes the preparation of biotin-labelled IgG. The molar ratio in the reaction mixture 10:1 of biotinylation reagent (BAC-SulfoNHS, MW = 556.8) to IgG (MW = 150,000). These ratios result, in most cases, in 4-6 moles of biotin per mole of protein, respectively. This procedure can be modified if a protein of a different molecular weight or a different amount of IgG is used in the labeling reaction. The level of biotin labelling may vary from one protein to another, in part due to the different number of lysine residues available for modification.

A sodium phosphate buffer sachet was reconstituted with 5 ml of deionised water to 0.1 M. The IgG sampler (a-PSA, a-NTx, a-NSE, a-ciprofloxacin) for biotinylation was prepared at 1 mg ml^{-1} in 0.1 M sodium phosphate buffer. 30 µl of DMSO was used to dissolve 5 mg of BAC-SulfoNHS. 0.1 M sodium phosphate buffer was then added to a final volume of 0.5 ml and the solution was vortexed well. The resulting concentration of BAC-SulfoNHS solution was 10 mg ml^{-1}. 38 µl (ratio 10:1) of the BAC-SulfoNHS was immediately added to 1 ml of the IgG solution with gentle stirring. The reaction mixture solution was incubated with gentle stirring for a further 30 minutes at room temperature or for 2 hours at 2-8 ºC.

To separate the conjugate from the reactants, 1 litre of 0.01 M PBS was prepared for the fast gel-filtration step. The gel filtration column (Sephadex G-25M), with a bed volume of 9.1 ml and bed height of 5 cm, was supported over a 100 ml beaker. The cap was removed from the top of the column. The lower tip of the column was cut open and the excess liquid was allowed to flow through. The column was then equilibrated with 30 ml of PBS (6 x 5 ml). The reaction mixture (IgG with BAC-SulfoNHS) was applied to the column and the flow-through was collected as Fraction 1. The column was then eluted with 9 x 1 ml of PBS and the flow through was collected as Fractions 2-10. The gel-filtration column was then washed with a further 30 ml of PBS (6 x 5 ml) and as such may then be regenerated up to five times.

The protein presence was monitored by measuring the absorbance at 280 nm in the UV/visible spectrophotometer. An elution profile was obtained and the fractions

displaying a clear peak at 280 nm (thus containing the protein) were pooled. Working aliquots of 100 µl were stored frozen at -20 ºC until they were required during the latter stages of sensor fabrication utilizing the biological affinity attachment bridges for their specifically orientated immobilisation. Using the methods described above PEI was also biotinylated.

3.2.4 Polyelectrolyte film deposition

A borosilicate glass capillary was drawn to an internal diameter between 20-100 µm using the Narashige PP-830 pipette puller. This capillary was then filled with a 1% (v/v) solution of biotinylated PEI solution and fixed into the clamp of the XYZ stage on the SECM270. The screen printed electrode was fixed onto the platform and levelled before positioning under the polymer-filled microcapillary. The microcapillaries were lowered at a rate of 5µm per step to lightly touch the carbon substrate via the use of a combination of eye and microscope viewing. At this point a small droplet of the PEI solution was transferred from the capillary to the carbon surface. Following deposition, the microcapillary was then retracted and translated away to a fixed distance in the X or Y axis for the deposition of another PEI dot. Using this technique, a polyelectrolyte array was fabricated. After patterning, excess PEI was rinsed from the surface with an excess of RO (reverse osmosis) H_2O and allowed to air dry.

3.2.5 PEI/neutravidin/biotinylated antibody film formation

Once the area was dry 20 µl of Neutravidin (10 mg ml^{-1} in water) was placed on the dotted microarray covering the entire array surface for 1 hour, followed by rinsing with water. Again the area was allowed to air dry before 20 µl of the biotinylated antibody of interest (~0.2 mg ml^{-1} in water, 1 hour) was then added covering the entire array followed by further rinsing. Finally non-specific interactions were blocked by BSA (10^{-6} mol L^{-1} in PBS, 1 hour).

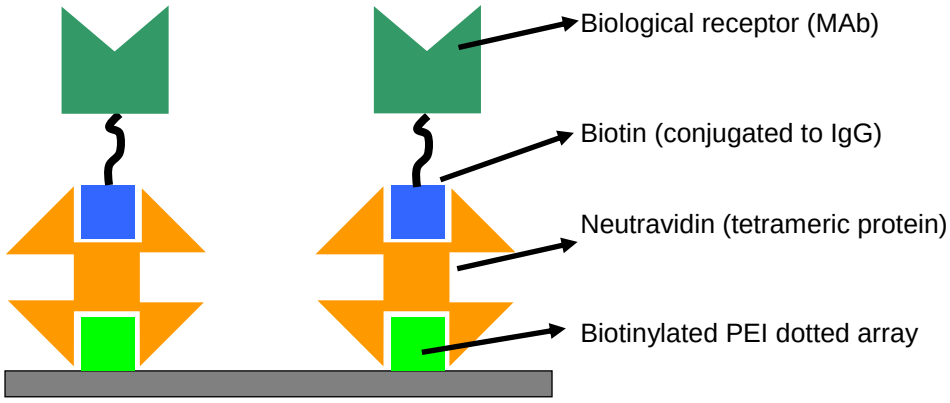

Figure 3.1: Schematic representation of the immobilisation of the antibody onto the screen-printed carbon surface.

This approach for biomolecule immobilisation provides orientation specific attachment (Figure 3.1) of a layer of receptors at the surface of the biotinylated PEI.

3.2.6 SECM interrogation and antibody/antigen binding detection

The patterned PEI/neutravidin/biotinylated antibody substrate described above was first fixed to the SECM stage and the substrate levelled. The microelectrode probe, reference electrode and counter electrode were then positioned above the area of interest. 1 ml of 5 $mmol^{-1}$ ferrocenecarboxylic acid was then introduced to the system, which was sufficient enough in volume to both cover the functionalised area and to immerse the working, reference and counter electrodes. The microelectrode probe was then moved to an inert (Melinex) region of the substrate and an approach curve conducted so as to allow the positioning of the probe relative to the substrate. The approach curve was stopped at i_T = 0.5 i_∞ and a linescan conducted to locate the carbon substrate – indicated by a large increase in the faradaic current observed at the tip as a result of positive feedback. The area scan was then conducted at i_T = 0.5 i_∞. After tip positioning, the tip was then set to the relevant potential and scanned across the substrate at a step rate of 10 μm per step.

After the first area scan experiment was conducted, the tip was retracted a known safe distance from the substrate. The mediator solution was then removed and the substrate gently rinsed with UHQ water before applying a solution containing complementary antigen over a range of concentrations or a non-complementary antigen. After exposure for 1 hour, the antigen solution was then removed and the substrate again rinsed before the re-introduction of fresh mediator solution. A second area scan experiment was then conducted over the same functionalised area as measured previously. The tip current data from the area scan before exposure was then subtracted from the tip current data following this exposure. Throughout all these experiments the sample substrate does not move at all, i.e. all exposures, rinsing steps etc. are performed with the sample *in situ.* It is worth noting here that after each exposure and rinsing step the Petri dish is refilled with fresh mediator solution and the tip exactly repositioned, made possible using the XYZ micro-positioning stage of the SECM270. This allows precise and reproducible imaging of the same area of the electrode.

3.3 Oligonucleotide sensor characterisation methodology

3.3.1 Additional reagents

Oligonucleotide sequences Sp_cap1 (sequence 5' – 3' TTTTAACAGCCCCTCGACAC (20)), the complementary oligonucleotide Sp_rep1 (sequence 5' – 3' GTGTCGAGGGGCTGTTAAAA (20)) and the non-complementary oligonucleotide Sp_rep2 (sequence 5' – 3' GATAGACTCGCAGTTTCTAGAC (22)) were provided by Dr. Barry Glynn (National University of Ireland, Galway, Ireland).

3.3.2 Substrate

A screen printed electrode was used as the substrate in this series of experiments (obtained from Microarray Ltd). Conductive inks (carbon type 422SS and Ag/AgCl type 6088SS) were obtained from Acheson Industries Europe and printed onto Melinex plastic sheets.

3.3.3 Polyelectrolyte film deposition

Biotinylated PEI deposition was undertaken using the method previously described in section 3.2.4.

3.3.4 PEI/neutravidin/biotinylated oligonucleotide sequence film formation

Once the area was dry 20 µl of neutravidin (10 mg ml^{-1} in water) was placed on the dotted microarray covering the entire array surface for 1 hour, followed by rinsing with water. Again the area was allowed to air dry before 20 µl of the biotinylated oligonucleotide sequence Sp_cap1 (sequence 5' – 3' TTTTAACAGCCCCTCGACAC (20)) (100 pmol $µl^{-1}$, nuclease-free water) was added covering the entire array (1 hour), followed by further rinsing. Finally non-specific interactions were blocked by BSA (10^{-6} mol L^{-1} in PBS, 1 hour).

3.3.5 SECM interrogation and hybridisation detection

Interrogation was performed as described in Section 3.2.6.

3.4 Scanning Electrochemical Microscope (SECM) Instrumentation

3.4.1 Uniscan SECM270

The Uniscan SECM270 is a scanning electrochemical microscope that may be used in the modification, characterisation and interrogation of a variety of substrates on a sub-micrometer scale. The system composes a bi-potentiostat (two PG580R potentiostats), a precision xyz micro-positioning stage and the SECM270 control unit for motion control (Figure 5.1). With the aid of Uniscan's Windows based control and analysis software provided and downloaded onto a connected PC, it is possible to control all experimental variables detailing the movement of the tip and the potential applied to the system.

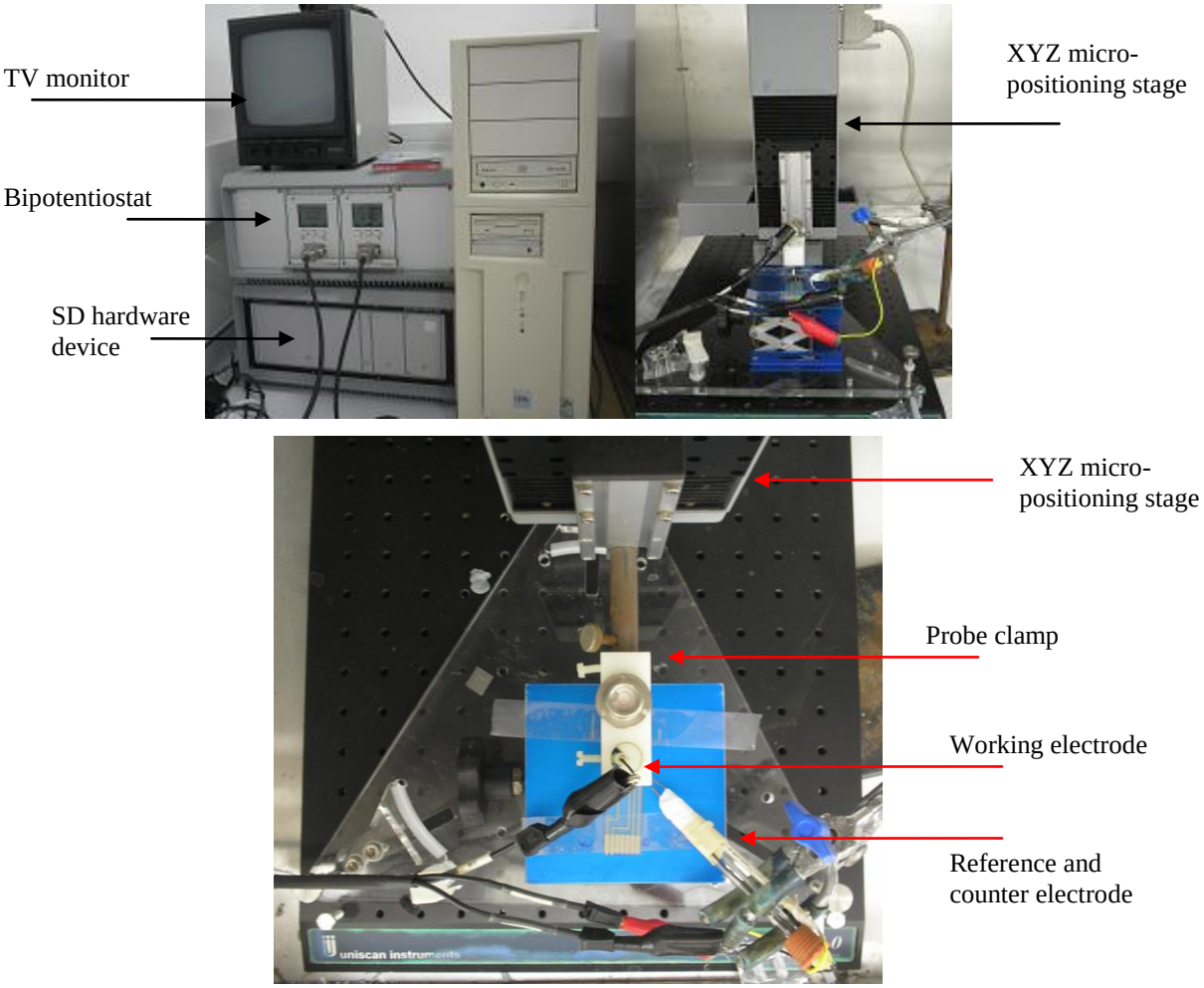

Figure 3.2: Photographs of the Uniscan SECM270.

3.4.2 XYZ stage

The precision micropositioner in the SECM270 is composed of precision motors on fine pitch lead screws allowing a combination of speed, accuracy and excellent reproducibility. The reproducibility of a scan is essential in time-dependent work – when a scan is conducted, the user must be confident that after the required time period, the scan will be conducted over exactly the same region as the first experiment. Each motor on each axis has a resolution of 100 nm and is capable of scanning at a rate of 2 mm per second. One aspect of the SECM technique is that images or scans may be acquired over relatively large distances; the SECM270 maximum scan range is 70 mm in all X, Y and Z

dimensions. By the use of linear encoders, the user is fully aware of the position of the probe at all times via readout of the sensor position given in the toolbar of the user interface.

3.4.3 Probe clamp

The probe clamp is the point of contact between the XYZ stage and the microelectrode probe; as such, it must provide a firm point of contact without risking damaging the probe while providing a reproducible positioning mechanism. In SECM experiments, the tip is translated in all X, Y and Z axes. During this movement, it is essential that there is no movement of the tip due to creep or slippage at the fixing point in the clamp. The number of connection points and rotational joints in this assembly results in noticeable movement when inserting the probe. Any movement in this region during scanning may introduce the possibility of variation in tip current not being attributable to variations in substrate activity or topography.

3.4.4 Potentiostats

To use the instrument for interrogating biased substrates and to allow the experimenter flexibility in their experimental design, there are two Uniscan PG580R potentiostats incorporated into the Uniscan SECM270. The user may specify the electrochemical parameters of the experiment, via the PC interface and by direct manual control. The PG580R have been designed with relatively low limits, a maximum current of ±10mA and a potential range of ± 2V for both potentiostats (i.e. substrate and probe potentiostats); this is because currents measured at microelectrodes are very small in comparison to those measured at larger, planar electrodes used in more general electrochemical experiments.

Prior to running an experiment, the user may set the experimental parameters and adjust potentiostat settings. With respect to the latter, this concerns setting the default, initial potential and the current range – the range across which the system will record the current passing at the working electrode, which may be between 1 pA and 10 mA.

3.4.5 Software

The user interface software is Uniscan's Windows based control and analysis software. The interface is highly intuitive (Figure 3.3), and very effective for specifying experiment type, experimental parameters, potentiostat settings and probe position, however, its ability to perform post-data acquisition analysis is limited.

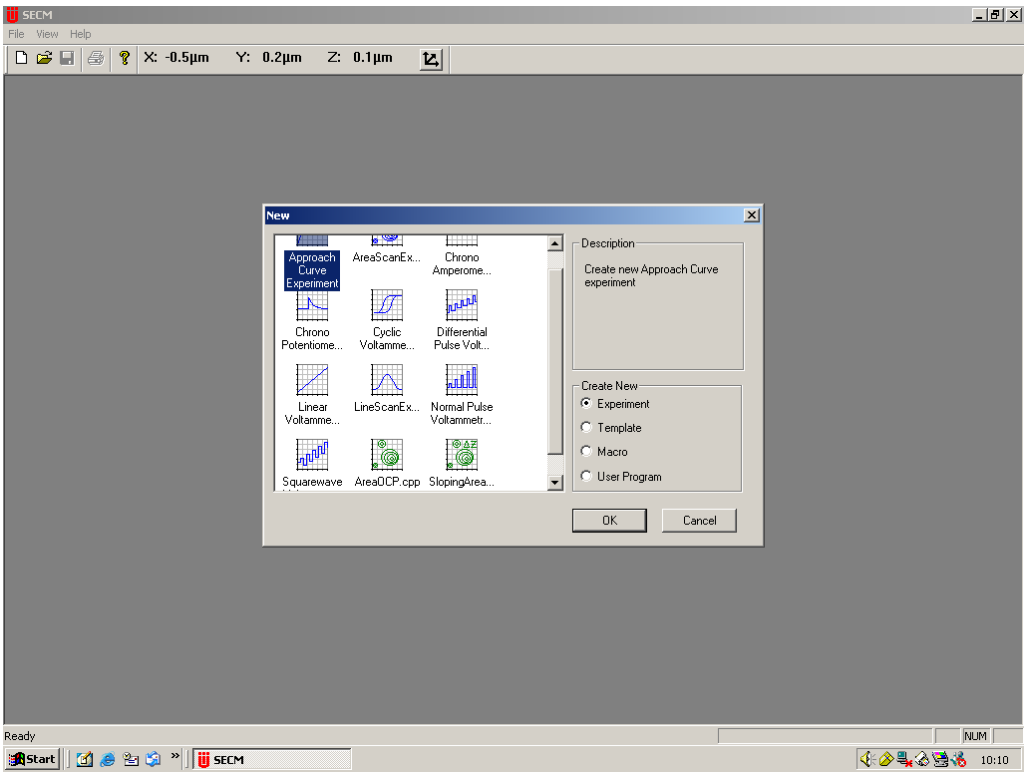

Figure 3.3: SECM software main menu for selection of experiment to take place.

3.4 Scanning Electrochemical Microscope (SECM) experiment capabilities

The SECM is capable of a wide variety of electrochemical experiments. Relating to SECM specifically, the user may conduct line scans, approach curves and area scans. Recent additions also include a sloping scan macro. Outside SECM applications, the user may conduct a number of other, general electrochemical experiments including cyclic voltammetry, chronoamperomtery, chronopotentiometry, square-wave voltammetry, normal pulse voltammetry and differential pulse voltammetry.

3.5.1 Cyclic voltammetry

The cyclic voltammetry (CV) experiment is an important part of the SECM as it allows characterisation of electrochemical processes of a given microelectrode and ensures the microelectrodes' behaviour compares with that theoretically expected. To conduct a cyclic voltammetry experiment the user must stipulate in particular the sweep potentials, sweep rate and the number of cycles required (Figure 3.4).

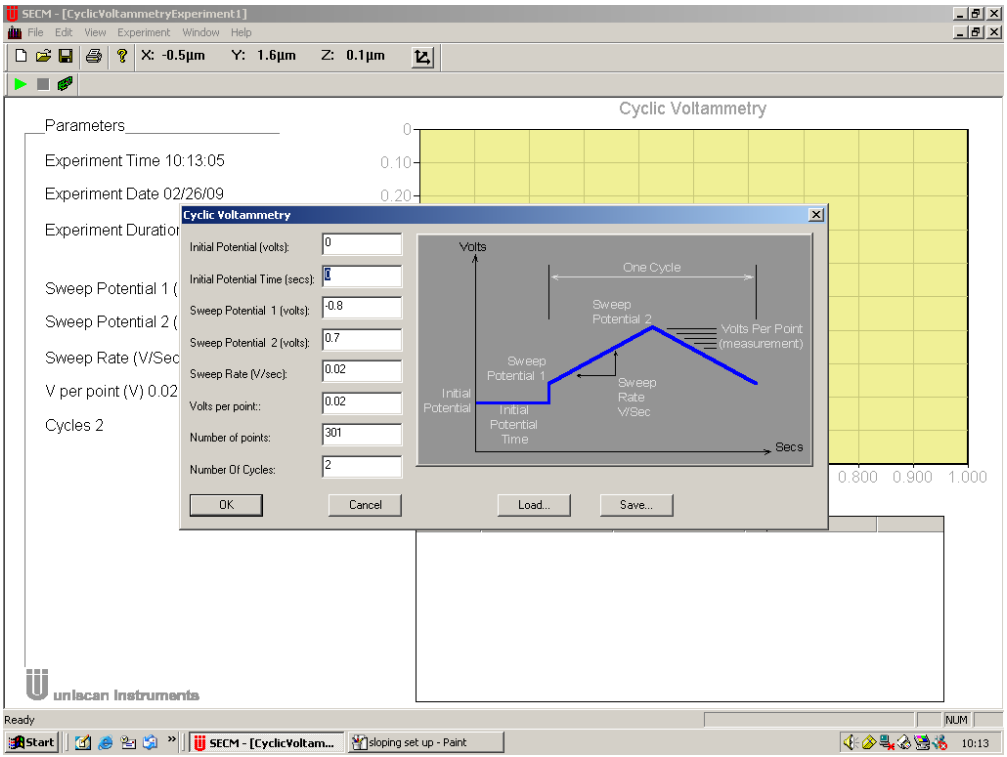

Figure 3.4: Experiment configuration for conducting a cyclic voltammetry.

3.5.2 Approach curve macro

To conduct an approach curve, the user stipulates the distance of the scan, tip potential and the step size required. It is necessary when carrying out an approach curve for the user to continually monitor the tip current and to halt the experiment manually before the tip comes into direct contact with the surface causing possible damage to the tip. To prevent unnecessary damage to the microelectrodes a possible solution is to develop a functionality which would permit the user to stipulate a particular current value or at a specific i_{∞} / i_T value at which the approach curve should and can be halted.

3.5.3 Area scan

In an SECM area scan, the probe tip is translated across a substrate of interest generating a map of the electrochemical activity or topography of a specified area of that substrate. In the SECM270, the tip is moved repeatedly from left to right in the X axis and moved incrementally in the Y axis after each sweep (Figure 3.5). After each linescan, the potential applied to the tip is switched off, the tip repositioned on the left hand side of the scan area (recovery sweep) and the potential is then re-applied for another scan. This can have the effect of creating a high current area on the left hand side of the area scan due to the brief occurrence of a charging current.

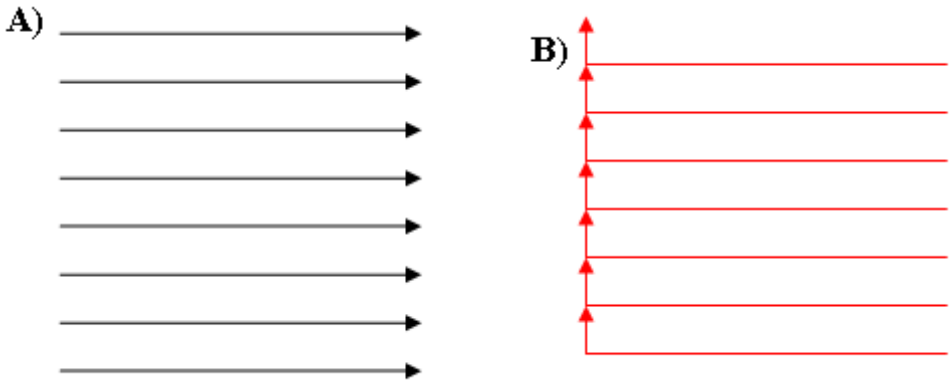

Figure 3.5: Schematic diagrams depicting the movement of the microelectrode probe (A) during an area scan; (B) the scanning and tip recovery paths respectively.

3.5.4 Sloping Scan macro

A problem associated with recording SECM area scans is the difficulty in differentiating variation in tip current due to variations in topography and those due to variation in the electrochemical properties of the surface. To combat this problem, the sloping area macro exists allowing the user to conduct an area scan over a sloped but topographically flat substrate. This results in any variation in current due to the slope of the substrate being accounted for so preventing such variation from masking the signal current. The slope of the substrate in the X and Y axes is calculated by conducting approach curves the distance

of the area scan requirements from the origin in both the X and Y dimensions as in Figure 3.6.

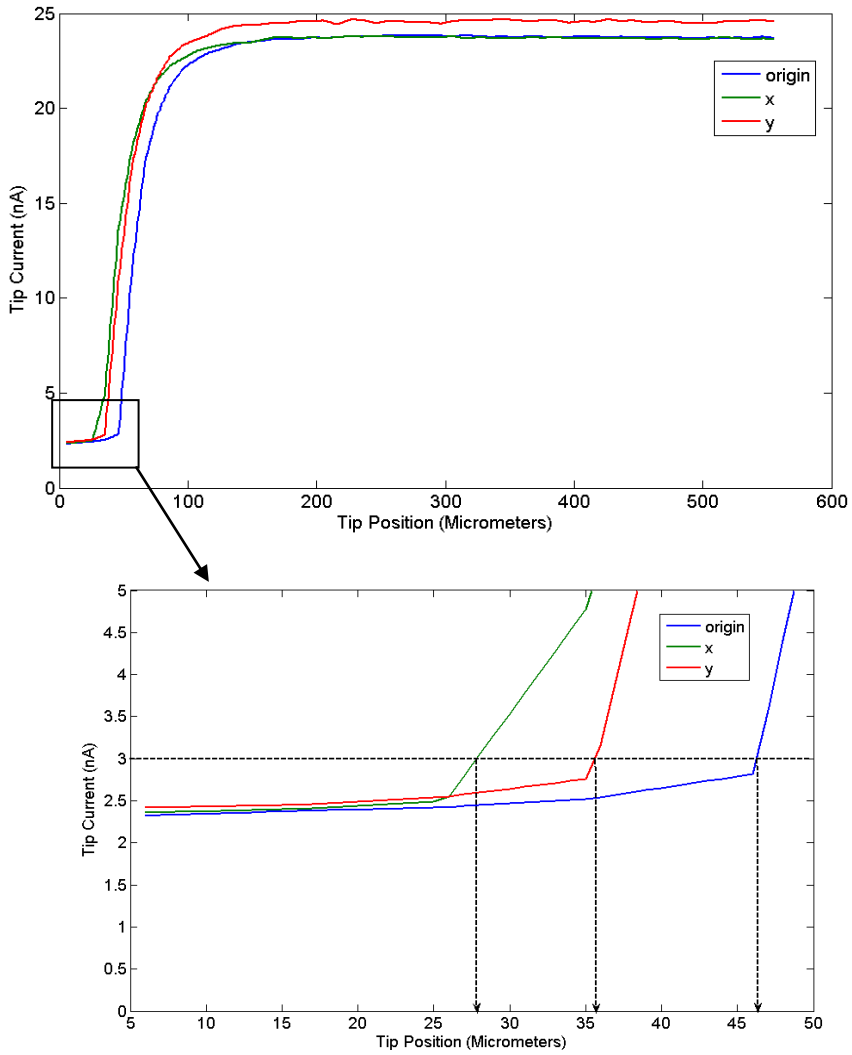

Figure 3.6: Series of approach curves allowing substrate slope to be calculated.

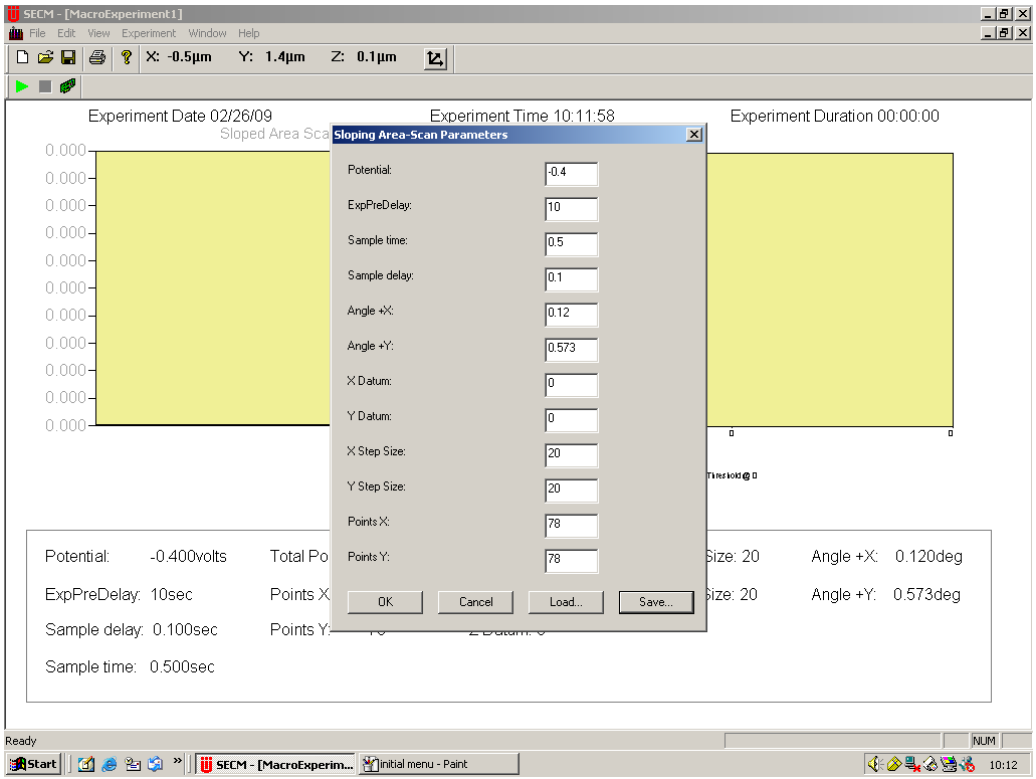

Figure 3.7: Experiment configuration for conducting a sloping area macro scan allowing an area scan to be conducted over a sloped surface.

By calculating the point at which a specific current value is reached, it is possible for the tip to substrate distance to be estimated. This then allows the slope in the X and Y axes to be calculated by trigonometric methods. These values are then entered into the macro configuration and the scan conducted, whereby the microelectrode probe is moved in the respective direction in the Z plane with movement along the X or Y axis (Figure 3.7). The effectiveness of this technique in eliminating substrate slope is demonstrated in Figure 3.8.

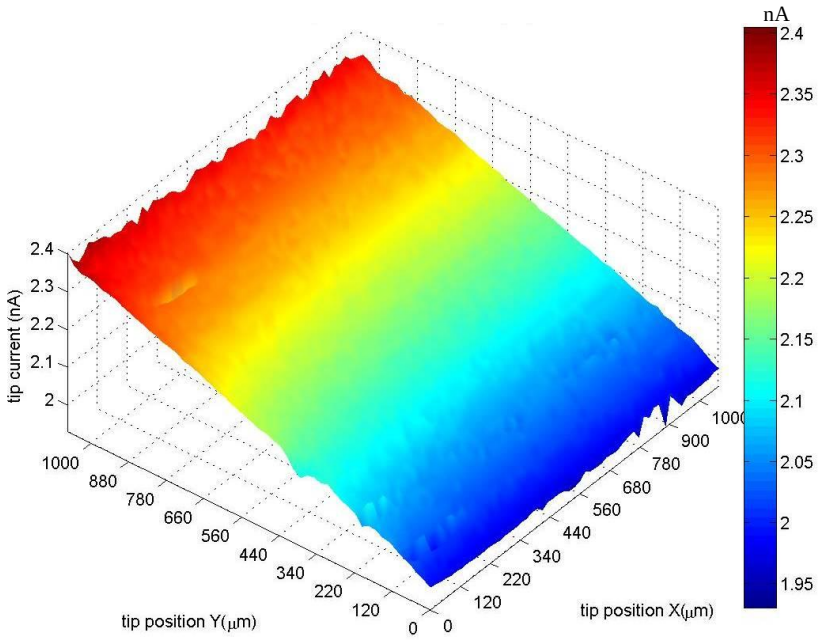

A)

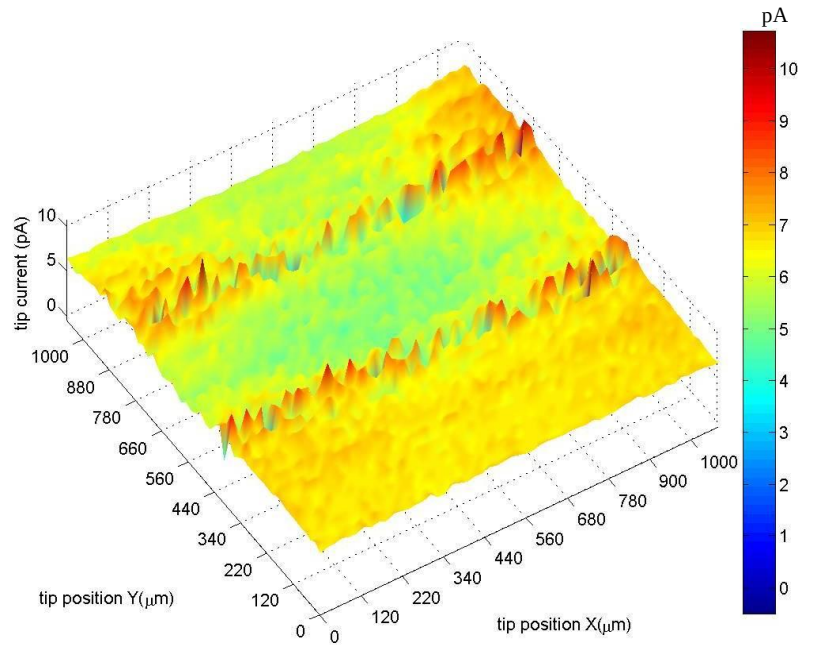

B)

Figure 3.8: Area scan over sloped glass substrate using the (A) area scan macro and (B) the sloping scan macro**.**

3.6 Three-Dimensional Representation of the Data

The software that controls the SECM instrument does not deliver sufficient information with regards to the surface areas of the scanned electrodes. To allow for the three-dimensional viewing of the data, and thus to permit the user to view as much information with regards to the changes occurring in the tip current, a script was written in Matlab (2008a, Mathworks Inc., USA). The script (see Appendix 4) permits the data to be imported, processed, and visualized in three dimensions, thus allowing a more user friendly representation of the data. The script also enables the user to specify plot characteristics, such as camera viewing angle, perspective, in addition to setting axis values and units, and also to reverse the axes.

3.7 ELISA protocol

The principle for the PSA ELISA is a solid phase two-site immunoassay. An anti-f-PSA monoclonal antibody is pre-coated on the surface of the micotitre wells and another anti-PSA monoclonal antibody labelled with horse radish peroxidise (HRP) is used for the detection. The free PSA molecules present in a standard solution are sandwiched between the two antibodies. Following the formation of the coated antibody-antigen-antibody-enzyme complex, the antibody enzymes are removed by washing. The HRP activity bound in the wells is then assayed by a colourmetric reaction. The intensity of the colour formed is proportional to the concentration of the f-PSA present in the standards.

A brief description of the assay procedure follows:

Into the appropriate wells 100 µl of standards and controls were aliquoted, followed by 100 µl of the sample diluent. This was then mixed for 10 seconds on an orbital shaker and then incubated at 37 °C for 1 hour. After incubation the plate was emptied the wells were

then rinsed 5 times with the buffer provided (1X washing buffer). 200 µl of enzyme conjugate reagent was then added to each well, mixed for 5 seconds on the orbital shaker and then incubated for 1 hour at 37 °C. The washing procedure was then repeated, 100 µl of TMB solution was then added to each well, this was then mixed for 10 seconds on the orbital shaker and incubated for 20 minutes at room temperature in the dark. The reaction was then stopped by adding 100 µl of the stop solution to each well. The plate was then placed on the orbital shaker for 30 seconds after which the optical density was measured at 450 nm.

Chapter 4
Microelectrode Fabrication and Characterisation

4. Microelectrode Fabrication and Characterisation

4.1 Introduction

A key parameter in any SECM study is the quality of the microelectrode used. Poorly constructed microelectrodes will impact on the signal to noise ratio, the spatial resolution of an area scan and may impact on the reproducibility of an experiment. The methodology for the fabrication of high quality probes exhibiting reproducible electrochemical behaviours is therefore of paramount importance. The subsequent characterisation of microelectrodes following fabrication is an essential step in determining whether an individual electrode exhibits good microelectrode behaviour (i.e. as close as possible to 'ideal' with respect to behaviour as predicted by microelectrode theory). By conducting a variety of electrochemical approaches it is also possible to quantify the area of the active electrode and the thickness of the insulating sheath in which it is embedded.

4.2 Fabrication of microelectrode probes for SECM

This section describes the methodology for the fabrication of embedded disk microelectrodes suitable for use with the Uniscan SECM 270. The methodology used allows for standard, robust electrodes with a small Rg ratio and excellent geometry which reproducibly exhibit microelectrode behaviour in accordance with microelectrode theory. The fabrication of electrodes using platinum-quartz (Pt-quartz) fibres will be described followed by a description of methods employed in their characterisation.

4.2.1 Equipment

Pipette pulling was achieved by the use of a Narashige pipette puller.

4.2.2 Method

A glass capillary (1.5 mm O.D x 0.86 mm I.D) was pulled with a 250 g weight whilst being heated at 99.8 ºC at its midsection using the pipette puller. On reaching the point at which the capillary is elastic and may be pulled, the descending weight is allowed to pull the capillary to the end of its axis of travel. The weight is lowered gently and not allowed to fall. The capillary should be pulled so that the thickness of the capillary is minimal, so as not to increase the Rg ratio, with the pulled region of the probe being as short as possible increasing the robustness of the probe (Figure 4.1).

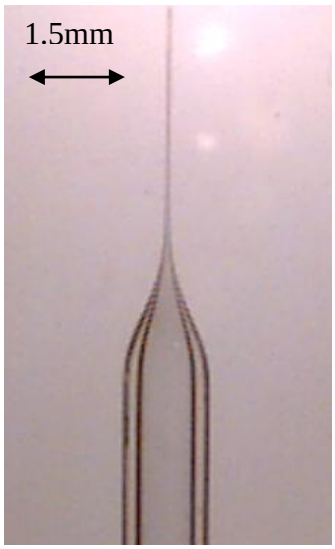

Figure 4.1: Optical Micrograph of a pulled capillary.

Pt-quartz fibres were obtained from Thomas Recording GmbH. The Pt core is highly centred in the quartz fibre, with high reproducibility of Rg ratios offering excellent geometry, reducing the need for bevelling and limiting polishing requirements to produce an electrode with the required positioning (Figure 4.2).

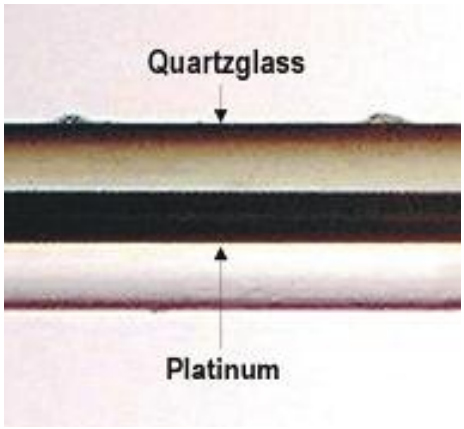

Figure 4.2: Optical image showing Pt-quartz fibre.

The Pt-quartz fibres used had the dimensions of Pt 8 µm and quartzglass 85 µm giving an Rg ratio of 10-11 (Figure 4.3).

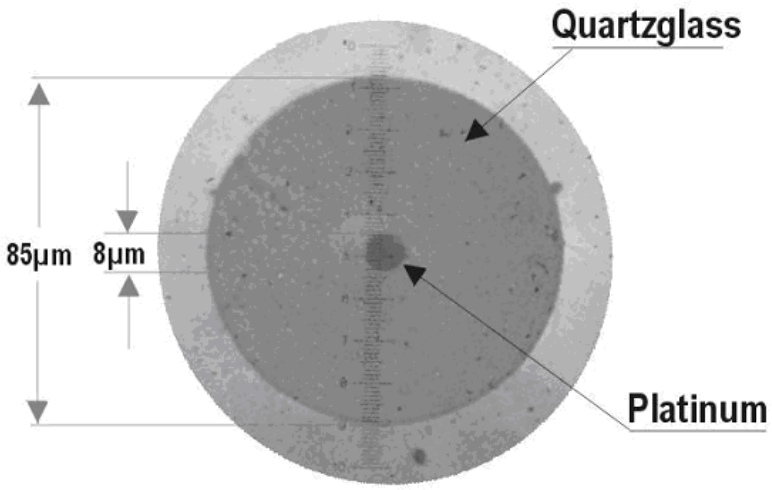

Figure 4.3: Optical image showing the dimensions of the tip of an electrode.

The Pt-quartz fibre was then cut to a length of approximately 5-10 mm and placed into a pulled capillary. The fibre is moved into the finely drawn out section of the capillary and down to the tip by gently tapping the capillary. A mark is then made at the furthest point along the tip where the fibre reaches (Figure 4.4).

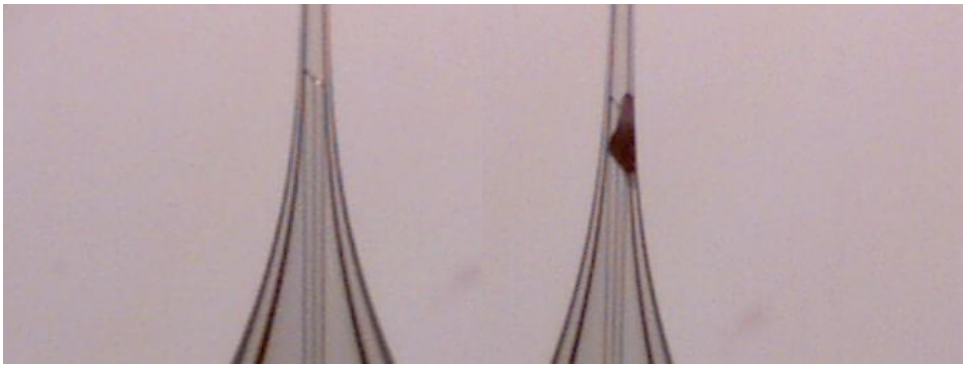

Figure 4.4: Optical micrograph of pulled capillary with Pt-quartz fibre.

The fibre is then removed allowing the tip to be cut to length and polished before replacing the Pt-quartz fibre. The fibre is then sealed in place by placing the pulled capillary with fibre into the nichrome wire coil. On heating, a vacuum was applied to the open end of the capillary to draw the heated glass around the Pt-quartz fibre, encapsulating it in the insulating glass sheath. The electrode was then inspected to ensure the wire was completely sealed.

As well as increasing the robustness of a probe the geometry of the electrode after sealing is improved by maintaining a short pulled region of the capillary. This also reduces the risk of a 'teardrop' tip. Once this is achieved, the tip is then gently polished using different grades of Buehler Apex-Met II silicon carbide grinding paper.

The next step allows an electrical connection between the embedded Pt-quartz fibre and an electrical lead. This is difficult to achieve as the conductive area at the end of the Pt-quartz fibre to which an electric connection may be made is very small. To combat this problem silver conductive paint was used. The Pt-quartz fibre was fixed to some stripped multicore wires by covering the entire assembly with conductive silver paint ensuring complete covering of the conductive end. This assembly is then secured by gently wrapping thread seal tape around the area; this also thickens the area for enabling a tight fit when securing into the lumen of another capillary. An electrical connection is then made by soldering the stripped multicore wires to another multicore wire and the completed article placed within a larger-bored capillary (2.4 mm O.D x 2.0 mm I.D). This increases the robustness of the electrode and reduces the risk of damage during clamping in the SECM stage or transit. To ensure the tip is secure and that the area remains sealed where the two capillaries overlap, epoxy resin is applied. The end where the wire protrudes is then also sealed using epoxy resin.

4.3 Microelectrode characterisation

Following fabrication, microelectrodes were characterised by cyclic voltammetry and their Rg ratios calculated by both measurement and comparison with simulated negative feedback approach curves.

4.3.1 Optical Microscopy

To ensure the microelectrodes produced had the desired geometries (i.e. active embedded disk centrally located in insulating glass sheath), optical micrographs were taken using Video Capture software (Figure 4.5 and Figure 4.6). If the disk was found to be non-centrally positioned, it was polished further to obtain the required geometry. If the microelectrode is not directly in the centre of the insulating substrate in which it is embedded, the resulting mass flow of the mediator solution in a horizontal direction *may* contribute to an additional current component.

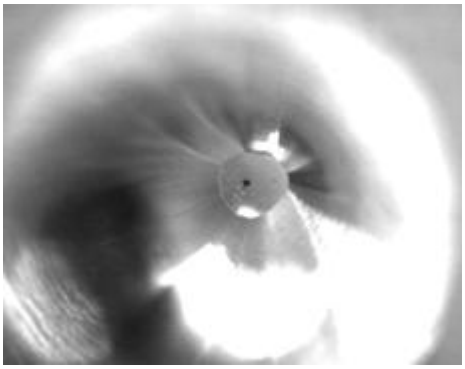

Figure 4.5: Optical image of an 8μm Pt-quartz microdisk electrode.

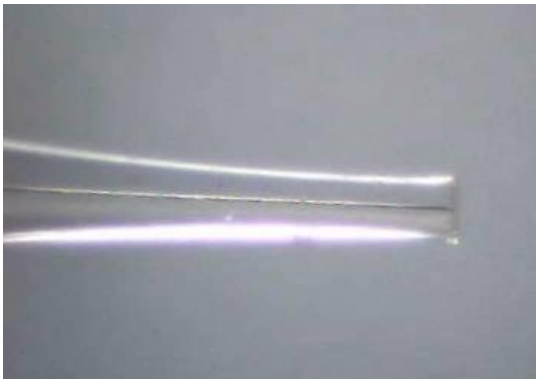

Figure 4.6: Optical image of an 8μm Pt-quartz microdisk microelectrode.

4.3.2 Cyclic Voltammetry

Cyclic voltammograms are one of the simplest electrochemical techniques that can be employed for the characterisation of electrochemical processes (Cannes *et al*, 2002; Bollo *et al*, 2003). Cyclic voltammograms were therefore conducted using a variety of different mediators at different concentrations with the aim of comparing the microelectrodes' behaviour with that theoretically expected. Mediators used include ferricyanide, hexamine ruthenium chloride and ferrocenecarboxylic acid. Representative cyclic voltammograms are given in Figures 4.7 and 4.8.

As the current measured at an electrode is a function of its area, the current measured at a microelectrode is significantly lower than that at a conventional macroelectrode (often nano-amps or below). By virtue of passing minute currents, microelectrodes induce very little electrolysis in solution. As a result, the diffusion layer associated with microelectrodes is very thin, (in the order of micrometers) meaning that the concentration gradient induced across them is correspondingly very high. Consequently, the rate of mass transport, namely diffusion, to the microelectrode is much greater than for macroelectrodes, leading to an absence of the 'diffusion limited' peak in the oxidation phase of the cyclic voltammogram for the microelectrode. It is this difference that allows one to make inferences concerning the quality of a microelectrode and for it to be used in a SECM system.

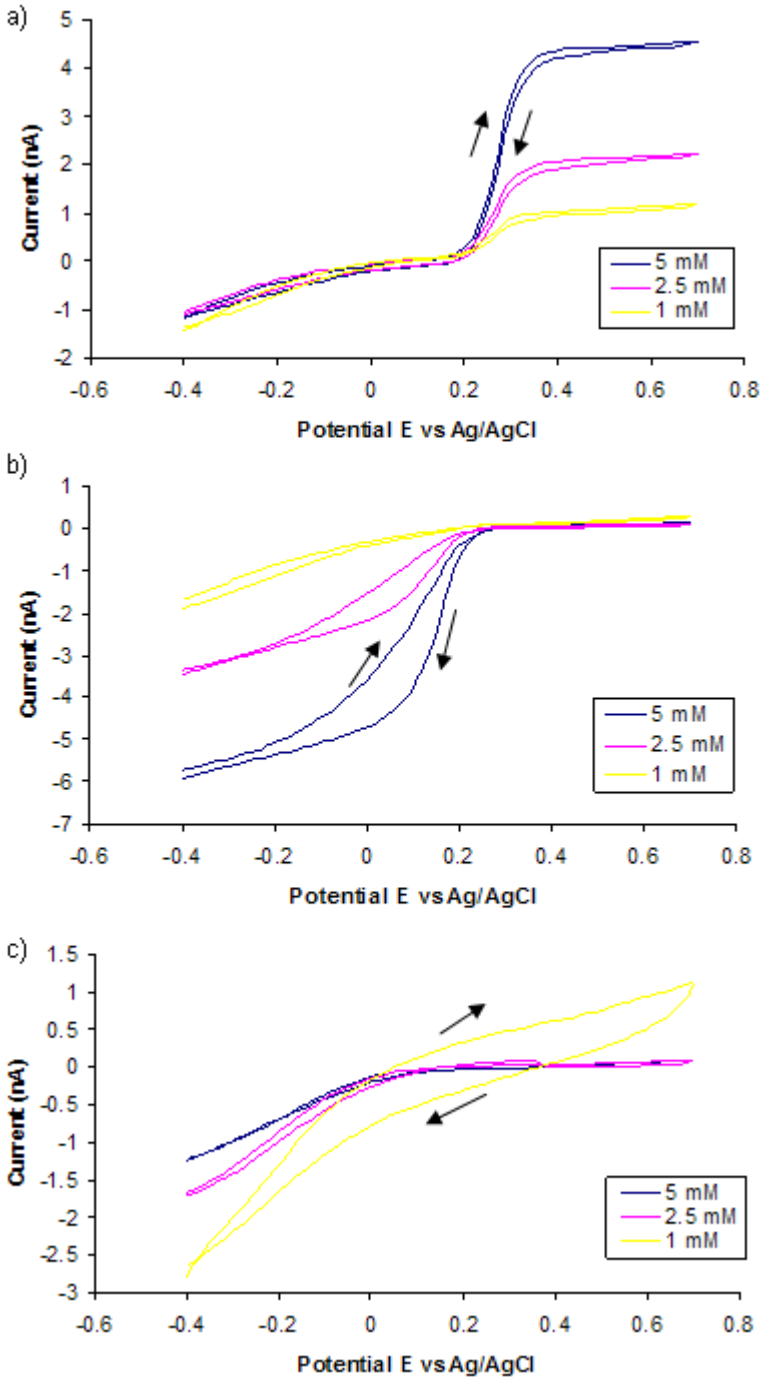

Figure 4.7: Series of cyclic voltammograms in differing mediators and concentrations. CVs conducted in; (a) ferrocenemonocarboxylic acid, (b) potassium ferricyanide (III) and(c) hexaammineruthenium (III) chloride.

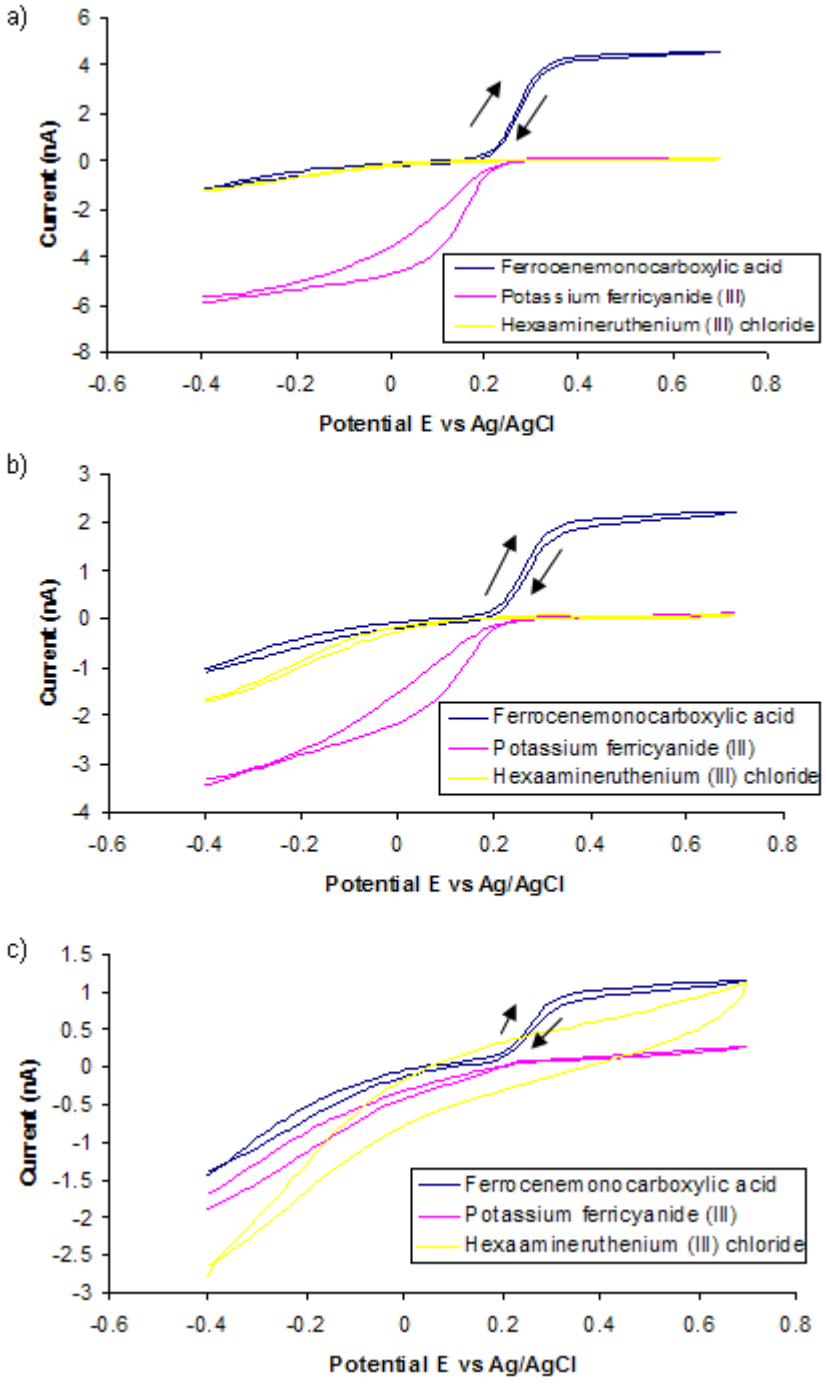

Figure 4.8: Series of cyclic voltammograms in differing mediators and concentrations. CVs conducted in mediators with concentrations of (a) 5mM, (b) 2.5mM and (c) 1mM.

The electrode is initially polarised at a potential that is insufficient to initiate the oxidation reaction (-0.4 V), but on sweeping the potential to 0.7 V at a sweep rate of 50 mVs^{-1}, the tip current is observed to increase to a plateau current. This current arises as the reduced form of the redox couple is oxidised to form the oxidised species. The sigmoidal plateau current with no diffusion limited peak, demonstrated best with ferrocenemonocarboxylic acid across all molarities, is a clear indication of microelectrode behaviour.

4.4 Conclusions

The production of robust, well characterised electrodes represents a key step in this work as the quality of data obtained is directly dependent on the quality of the electrode used. The development of a reproducible methodology for the fabrication of electrodes is reported here. The fragile nature of the Pt-quartz fibres used make polishing exceptionally difficult and problems were encountered at times with getting an electrical connection between the Pt-quartz fibre and the wire which was to be connected to the potentiostat cabling. The geometry of the tips is relatively consistent as there is very little deviation in the fibres position relative to the insulating glass surround during sealing with the technique applied. Bevelling the tip to produce a microelectrode with an even smaller Rg ratio was found to be extremely difficult, often resulting in damage to the tip. Therefore, this step was not included in the protocol as the risk of damaging the microelectrode tip was too great.

The robust construction of these probes makes them suitable for use with the clamping mechanism used on the SECM270. By taking aspects of existing electrode designs and incorporating them into a single model, an electrode with a unique combination of desirable qualities has been produced.

However, it is important to note that the quality of the electrodes produced by this methodology is highly dependent on the skill of the individual involved in the fabrication process. Therefore, minimising the human element in the process would increase the reproducibility of the microelectrodes produced. One possible area for minimising variability in the microelectrodes is in the initial step of pulling the capillary for the insertion of the Pt-quartz fibre. A laser pipette puller would enable the simultaneous pulling of Pt in glass, to allow the controlled manufacture of Pt disk electrodes with diameters down to the nanometer range so as to give a much higher level of reproducibility.

Chapter 5
Characterisation of an immunosensor for the detection of neuron specific enolase by SECM

5. Characterisation of an immunosensor for the detection of neuron specific enolase by SECM

5.1 Introduction

Stroke is clinically defined as a rapidly developing syndrome of vascular origin that manifests itself in focal loss of cerebral function. Strokes are caused by the blood supply to the brain being suddenly interrupted (ischemic) or when a blood vessel in the brain bursts, spilling blood into the spaces surrounding the brain cells (hemorrhagic). The symptoms of stroke include: numbness, weakness or paralysis on one side of the body (signs of this may be a drooping arm, leg or lower eyelid, or a dribbling mouth), slurred speech or difficulty finding words or understanding speech, sudden blurred vision or loss of sight, confusion or unsteadiness and/or a severe headache. Stroke is a manifestation of vascular injury to the brain, which is commonly secondary to atherosclerosis or hypertension. Stroke is the most common devastating neurological disease and the second most common cause of neurological disability (Adamson *et al*, 2004) after dementia.

It is vital to promptly diagnose strokes as any delays in diagnosis and resultant medical intervention may contribute to clinical deterioration and disability. Early diagnosis enables more effective emergency intervention such as anti-platelet and / or neuroprotective therapy to be administered resulting in better prognoses of the disease outcome. Successful treatment of stroke requires rapid state diagnosis and any delay in achieving accurate diagnosis wastes the limited amount of time available in which the brain can respond to reperfusion, significantly increasing the risk of haemorrhage even after most of the permanent injury has occurred (National Institute of Neurological Disorders and Stroke, 1995; Kwiatkowski *et al*, 1999; Marler, 1999; Marler *et al*, 2000).

Transient Ischaemic Attack **(**TIA) is a short-lived episode of focal neurological deficit which often precedes the cerebral infarction of a stroke. It occurs when the blood supply to part of the brain is briefly interrupted, and is typically accompanied by permanent brain damage - albeit normally less severely than results from a stroke. TIA symptoms are similar to those of stroke but do not last for as long, often disappearing within an hour, although they may persist for up to 24 hours. Patients who have suffered a TIA have a greater risk of having a future stroke and about one third of patients who suffer a TIA will typically suffer from an acute stroke in the future (UK Office of National Statistics Health Statistics, 2001). However, because symptoms of TIA are short term, many patients do not recognise the event and fail to perceive the event as warning of a potentially impending stroke.

TIA is therefore a very interesting aspect of investigation for the scientist in terms of an obvious need for identifying the underlying systemic changes in the brain and spinal cord throughout the TIA. A precise understanding also enables the development of varying diagnostics that permit and validate the effective intervention of the appropriate thrombolytic therapy so as to prevent subsequent damage. This can significantly increase the recovery of a patient enabling little or no disability provided there is the close monitoring of patients identified as high risk (National Institute of Neurological Disorders and Stroke, 1995; Kwiatkowski *et al*, 1999; Marler *et al*, 1999; Marler *et al*, 2000).

Current diagnostic methods for stroke include costly and time-consuming procedures such as noncontrast-computed tomography (CT) scan, electrocardiogram, magnetic resonance imaging (MRI) and angiography. At this time, there are no rapid diagnostic methods that can differentiate and identify a TIA, or predict delayed neurological deficits, often detected at a time after the onset concurrent with the presentation of symptoms. Accordingly, there is a present need in the area for a rapid, sensitive and specific diagnostic assay for stroke and TIA which is able to differentiate stroke type and identify those at greatest risk for delayed neurological deficits. For such an assay to be developed it, has been necessary for research to be undertaken in the identification and use of diagnostic markers for stroke and cerebral injury. Enolase is a 78 kDa homo- or heterodimeric cytosolic protein produced

from [α], [β], and [γ] subunits. Enolase can be present as [α][α], [β][β], [α][γ], and [γ][γ] isoforms. The [α] subunit is found in glial cells and most other tissues, the [β] subunit in muscle tissue, and the [γ] subunit mainly in neuronal and neuroendocrine cells (Quinn *et al*, 1994). The [γ][γ] enolase isoform is most specific for neurons, and is therefore referred to as neuron-specific enolase (NSE). NSE is predominantly found in neurons and neuroendocrine cells, but also present in platelets and erythrocytes. Serum NSE is reportedly elevated after all stroke types, including TIAs, which are cerebral in origin and are thought to predispose an individual to having a more severe stroke at a later date (Isgro *et al*, 1997).

Elevations of NSE in serum can be attributed to cerebral injury due to physical damage or ischemia caused by infarction or cerebral haemorrhage, coupled with increased permeability of the blood brain barrier. The serum concentration of NSE has also been reported to correlate with the extent of damage (infarct volume) and neurological outcome (Martens *et al*, 1998). Additionally, a secondary elevation of serum NSE concentration may be an indicator of delayed neuronal injury resulting from cerebral vasospasm (Laskowitz *et al*, 1998). NSE, which has a biological half-life of 48 hours and is normally detected in serum at an upper limit of 12.5 ng ml^{-1} (160 pM), is typically elevated after stroke and cerebral injury. Serum NSE is elevated after 4 hours from onset, with concentrations reaching a maximum between 1-3 days after onset (Missler *et al*, 1997). After the serum concentration reaches its maximum (maybe > 300 ng ml^{-1}, 3.9 nM), it gradually decreases to normal concentrations over approximately one week.

This chapter describes the development of an immunosensor and its interrogation using the scanning electrochemical microscope. The fabrication of this immunosensor is described in the material and methods section. By interrogating the same system using SECM, valuable insights may be obtained regarding the fabrication of the immunosensor and the applicability of SECM to detecting antibody/antigen interactions. SECM offers a route for non-contact electrochemical interrogation, negating the need for hard-wired electrodes; this in turn offers the potential for developing an array based approach which may be interrogated via a scanning probe tip.

Thus, the aim of the work presented in this Chapter is to conduct a preliminary investigation into whether SECM may be used to detect neuron specific enolase at low concentrations.

5.2 Results and Discussion

5.2 1 Carbon electrode substrate

The carbon ink screen printed electrodes used in this series of experiments was the same as that used in a study by other members of the team previously (Davis *et al*, 2005a). An image of the sensor used is given below (Figure 5.1).

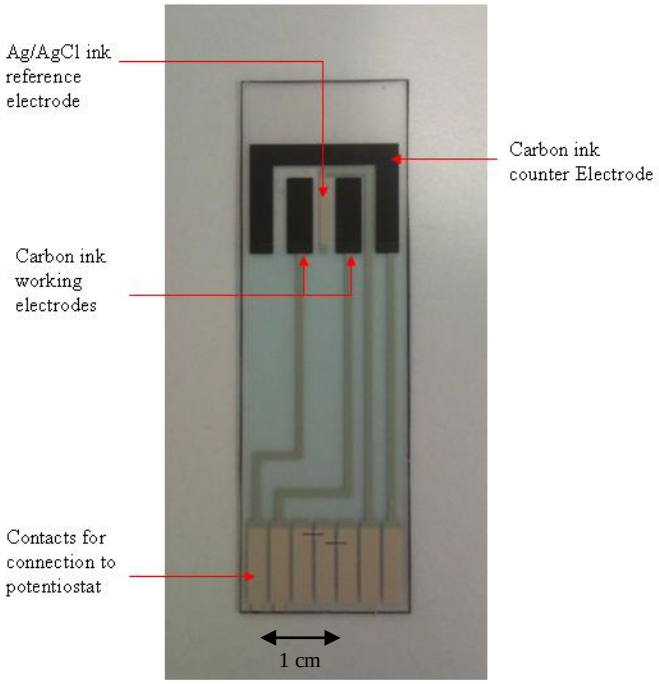

Figure 5.1: An optical image of the carbon paste electrode used in the study.

Screen printed electrodes are now the substrate of choice for a wide range of sensing applications. This is due to the ease at which the electrodes are fabricated allowing mass

production of inexpensive yet highly reproducible biosensing devices (Alvarez-Icaza and Bilitewski, 1993).

There are two main stages carried out in the production of screen printed electrodes, the first of these being the deposition of the conductive film and this is achieved by forcing a conductive ink through a patterned screen. The second stage is the curing phase, performed by either heating or photocuring. It is during this step that the solvent within the ink evaporates. This process is then repeated a number of times depending on how complex the pattern is (Svancara *et al*, 1996a). Silver based inks are generally used for reference electrodes, whilst carbon or metallic inks (e.g. Pt, Au, Ag) are used for the working and counter electrodes of the sensor.

There are a number of advantages associated with the use of carbon inks. One of these advantages is the fact that they exhibit lower background currents over a wider potential window than metal electrodes; this has the effect of improving the signal/noise ratio and lowers the detection limits of the system under investigation (Niwa and Tabei, 1994; Gilmartin and Hart, 1995). The graphite based carbon electrodes are also extremely robust allowing them to be used in turbulent conditions (Wring and Hart, 1990). Moreover, they are extremely cost effective, making them ideal for single use applications.

5.2.2 Characterisation of carbon inks by SECM

In general, carbon inks are composed of graphite particles bound by a polymer and a selection of additives which allow the dispersion, printing and adhesion of the ink to the base substrate (Adams, 1958; Svancara *et al*, 1996a, 1996b; Grennan *et al*, 2000). It is as a result of this heterogeneous composition that there is a great deal of topographical variation in the conductivity of the electrodes produced. These heterogeneities were investigated by SECM.

Prior to each area scan, the microelectrode tip was positioned at a height where the tip current was equal to half of that obtained in bulk solution. The area scans shown in this chapter were performed using 2.5 mM ferrocene-monocarboxylic acid. On scanning

across the carbon/Melinex border, an increase in the tip current is observed as a consequence of positive feedback due to the recycling of the ferrocenecarboxylic redox couple at the conductive substrate (Figure 5.2). On further interrogation of the carbon substrate at a decreased tip to substrate distance, (Figure 5.3), it is evident that there is a considerable degree of variation in the feedback response.

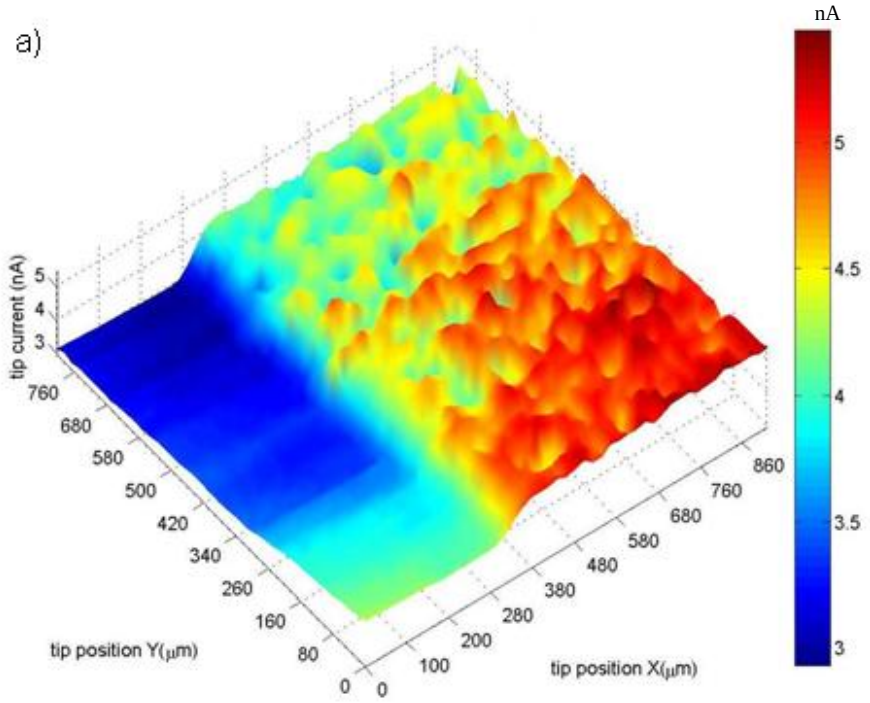

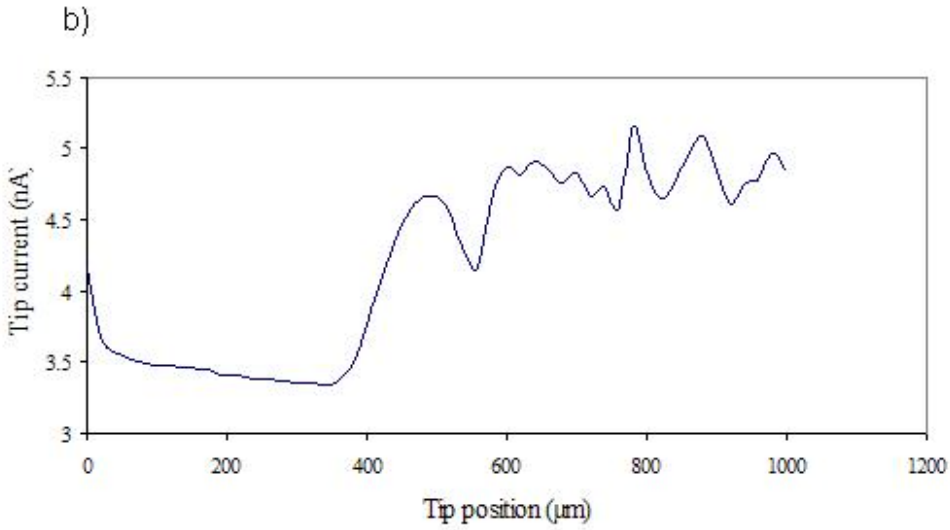

Figure 5.2: (a) 3D representation of the data obtained from an Area scan over border between carbon (red/green/yellow region) substrate and Melinex printing substrate (dark blue region); (b) Linescan across border at a tip position of 400microns.

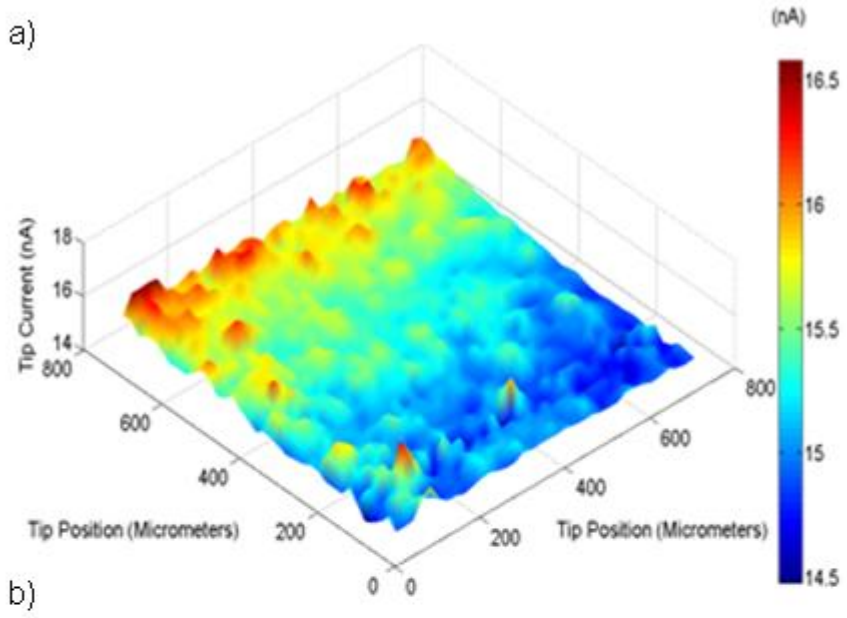

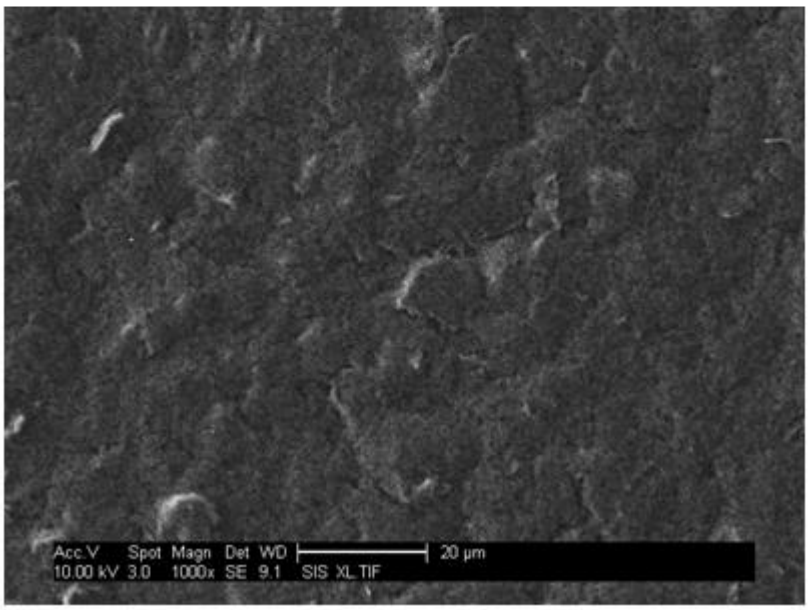

Figure 5.3: (a) 3D representation of the data obtained from area scan images of a carbon ink electrode. Current hotspots show areas of raised topography and/or increased conductivity arising from the heterogeneous nature of the carbon ink used; (b) SEM image of a carbon ink electrode surface.

In Figure 5.2 there is a slight increase in current in the Y dimension which is most probably due to substrate slope, however, this is kept to a minimum by utilising the sloping scan macro as described in Chapter 3. In doing so, variation in current due to the slope of the substrate is to a degree accounted for, preventing such variation from masking the signal current.

It is possible that the observed heterogeneity in Figure 5.3a, is due to variation in the conductivity of the substrate, arising as a result of the composition of the carbon ink (Figure 5.3b). Electrical conductivity within the bulk system occurs by physical contact between graphite particles, providing a conductive route through the polymeric medium, although an alternative mechanism involving indirect electron tunnelling between proximal particles has also been previously suggested (Svancara and Vytras, 2000). It is possible that even though the addition of conductive particles such as carbon black are added to the ink to enhance conductivity, regions of higher conductivities and higher rates of heterogeneous charge transfer may still exist as a result of the physical properties of graphite. Graphite consists of carbon atoms arranged in a hexagonal sheet, with each atom covalently bound to three other surrounding atoms; the remaining fourth electron is donated to a delocalised system of electrons between sheets (see Figure 5.4). As a result of this delocalised system, there is high electron mobility parallel to the plane of the sheets, yielding excellent conductivity – of the order of ~0.1 Ωcm (McCreery, 1991). This is in contrast to the conductivity of graphite across the sheets – of the order of ~$1x10^{-4}$ Ωcm. As a result of this differential conductivity, the edge plane of graphite exhibits excellent conductivity, whilst the basal plane is highly insulating. Considering that there is no mechanism by which to orientate the graphite particles in the carbon ink, the result of this differential conductivity is a surface with highly heterogenous charge transfer, with some areas exhibiting higher rates of heterogeneous rates of charge transfer than others.

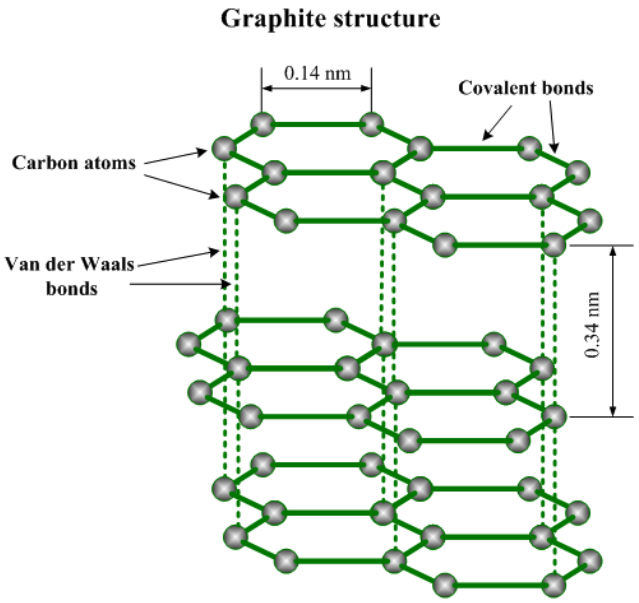

Figure 5.4: Schematic of the arrangement of carbons within graphite.

A further possible reason for the observed heterogeneity in feedback response is the variation in the topography of the substrate. When the tip is translated across the substrate, raised regions are closer to the tip, resulting in an enhanced positive feedback effect as the distance across which the recycled mediator has to travel is less than for areas that are topographically further away from the tip. This may either be as a result of the topography of the underlying Melinex substrate, variation caused by the screen printing process, or be due to variations in the size of particles incorporated into the ink.

5.2.3 Polyelectrolyte films

Polyelectrolyte films have been used extensively in the preparation of biosensing elements. Films such as these may be assembled by taking advantage of the strong forces of attraction between oppositely charged polyelectrolytes, a technique first reported by Decher *et al* (1992).

The stable immobilisation of macromolecular biomolecules on conductive microsurfaces with complete retention of their biological recognition properties is a crucial problem for the commercial development of miniaturised biosensors (Turner *et al*, 1987; Cosnier, 1999). Most conventional procedures of biomolecule immobilisation such as cross-linking, covalent binding and entrapment in gels or membranes suffer from low reproducibility and a poor spatially controlled deposition.

The orientation of immobilised antibody can be random and therefore the availability of antigen binding sites and hence subsequent stable complex formation is hindered. Within the literature, an attempt to overcome this issue has been initially to electrogenerate functionalised conducting polymers. Then the attachment of biomolecules to the polymer surface can be obtained by covalent binding to adequate functional groups (Schuhmann *et al*, 1990, 1993; Willner *et al*, 1992; Rockel *et al*, 1994; Korri-Youssoufi *et al*, 1997).

Another approach is to electropolymerise functionalised conducting polymers. Then the attachment of biomolecules to the surface can be obtained by affinity of the biomolecule at the functional group. This approach enables optimum conditions to be utilised throughout the fabrication.

However, while these are suitable approaches for sensor preparation for impedimetric analysis, it is not appropriate for the preparation of electrodes to be interrogated by SECM. The reason for this was that by imaging a homogenously treated surface, it is not possible to compare a modified region with an unmodified region. Any changes in the tip current may be due to changes in the background current and not due to changes in the charge transfer properties of the modified substrate. It was therefore decided that for SECM interrogation, the polyelectrolyte film should be patterned in an array format. By producing this pattern, background changes in the feedback current could be determined by comparing the feedback signals over unmodified carbon and for this reason an affinity immobilisation system was undertaken (Figure 5.5).

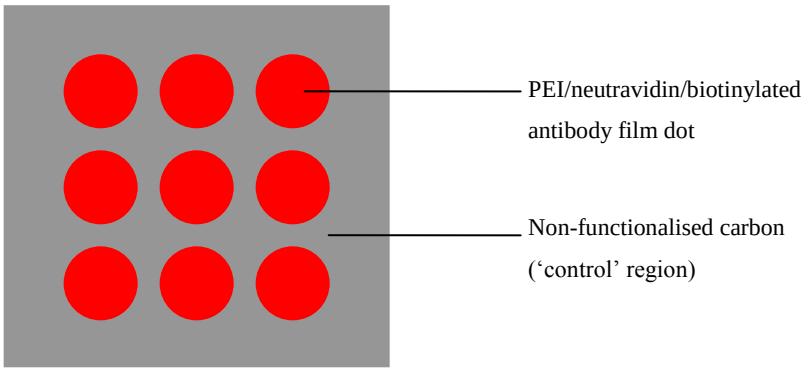

Figure 5.5: Schematic illustration of patterned biotinylated polyelectrolyte film which allows the monitoring of the change in background current over an unmodified surface against the change in feedback response over PEI/biotinylated antibody modified carbon.

As well as facilitating antibody-antigen interactions, an affinity immobilisation system would also preserve the complete biological properties of the biomolecules unlike immobilisation via electropolymerised entrapment - or via covalent binding following electropolymerisation.

Due to the high affinity constant of the avidin-biotin interaction (association constant $K_a = 10^{15}$ M^{-1}) (Wilchek and Bayer, 1988), this coupling system has been used for protein immobilisation on biotinylated polymer films. The attachment of proteins is achieved via the simple formation of an avidin-biotin bridge with biotinylated proteins or avidin-conjugated proteins via a non-covalent bond (Vermette *et al*, 2003).

The high affinity interaction of avidin-biotin leads to an affinity-driven immobilisation protocol of biomolecules solely involving a single attachment point that fully retain their biological activity (Gitlin *et al*, 1988a, 1988b). More interestingly, binding of a protein monolayer displaying excellent accessibility to each immobilised protein has been recently achieved by using avidin-biotin bridges between electropolymerised biotinylated polypyrrole films and biotinylated antibodies (Ouerghi *et al*, 2002).

Avidin (pI of 10.5, ~67 kDa, 5.6 x 5 x 4 nm) is a basic glycoprotein, consisting of 10% carbohydrate (Hiller *et al*, 1987) and it is composed of 4 x 128 amino acid residue chains (Hiller *et al*, 1987). The avidins (including streptavidin and neutravidin) all have weights in the region of ~60 kDa and are tetrameric, with one biotin binding site per monomer (Green, 1964). Neutravidin biotin-binding protein is a superior replacement for avidin when non-specific binding must be minimized. Neutravidin is a modified avidin derivative that combines several key features to provide a biotin-binding protein with exceptionally low non-specific binding properties. The Neutravidin protein does not contain carbohydrate, thus eliminating the potential for binding to lectins. The deglycosylation of Neutravidin does not compromise or impact the stability or biotin-binding activity of the protein (Hiller *et al*, 1987).

The relatively neutral isoelectric point (6.3 +/- 0.3) of neutravidin is achieved through modification of charged groups on the surface of the protein. This modification ensures that sufficient lysines remain available on the surface of neutravidin, so that protein conjugates can still be successfully prepared through traditional amine-reactive chemistries and as mentioned, the neutral pI minimises nonspecific adsorption. The specific activity for biotin-binding is approximately 14 μg/mg of protein, which is near the theoretical maximum activity (Unson *et al*, 1999; Wojciechoski *et al*, 1999; Glover and McHenry, 2001; Guo *et al*, 2001; Claypool *et al*, 2002).

The simplest way of using the avidin-biotin reagents is to use a biotinylated surface, add on the tetrameric avidin, and then add on the biotinylated antibody. There are many biotinylation reagents available with a range of functional groups for attachment, and various spacer arms. The biotinylating agent used herein was biotin 3-sulfo-N-hydroxysuccinimide ester. Biotinylation of antibody was performed in accordance with Chapter 3 (materials and methods) and the biotinylated capture bio components were stored frozen at -20 ºC until required for further use.

5.2.4 Antibody biotinylation – UV spectrum profile.

Following the biotinylation of NSE antibodies (according to section 3 materials and methods) UV spectroscopy is employed to obtain an elution profile. A clear peak at 280 nm indicates the presence of protein in the fraction. In this case fractions 4, 5 & 6 exhibited peaks and were therefore pooled. Figure 5.6 shows a representative elution profile obtained for monoclonal anti NSE antibodies following biotinylation at 1 mg ml^{-1}.

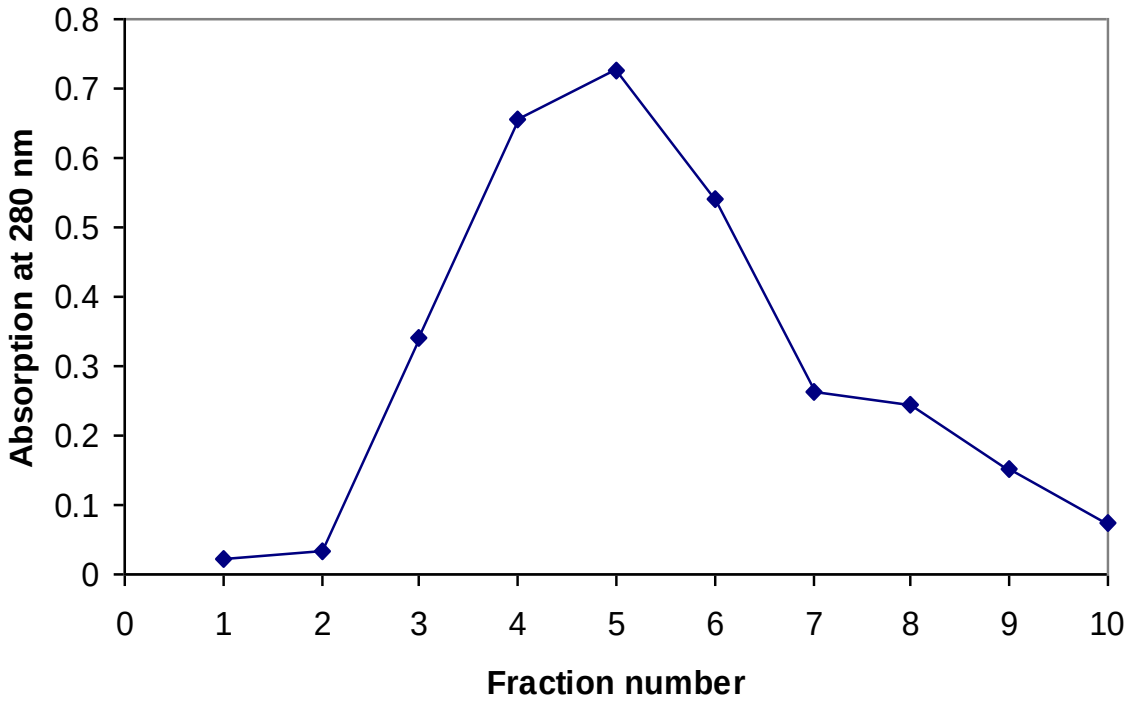

Figure 5.6: Elution profiles obtained following biotinylation (NSE MAb).

Approximately 6 moles of biotin were bound to each mole of protein (Ab) following the Avidin-HABA assay. Biotinylated antibodies were then attached to free biotin groups on the PEI using Neutravidin as a coupling reagent.

As described in the methods section (Chapter 3) the patterned array was achieved using the SECM micro-positioning XYZ stage. A capillary was filled with the biotinylated polyelectrolyte (polyethylenimine – PEI) and lowered towards the carbon substrate (Figure 5.7). By observing the small meniscus at the tip of the pulled capillary, it was possible to determine the point at which contact was made and when the deposition of the PEI droplet was achieved. After deposition, the tip was retracted and moved in the X or Y direction respectively and the process repeated.

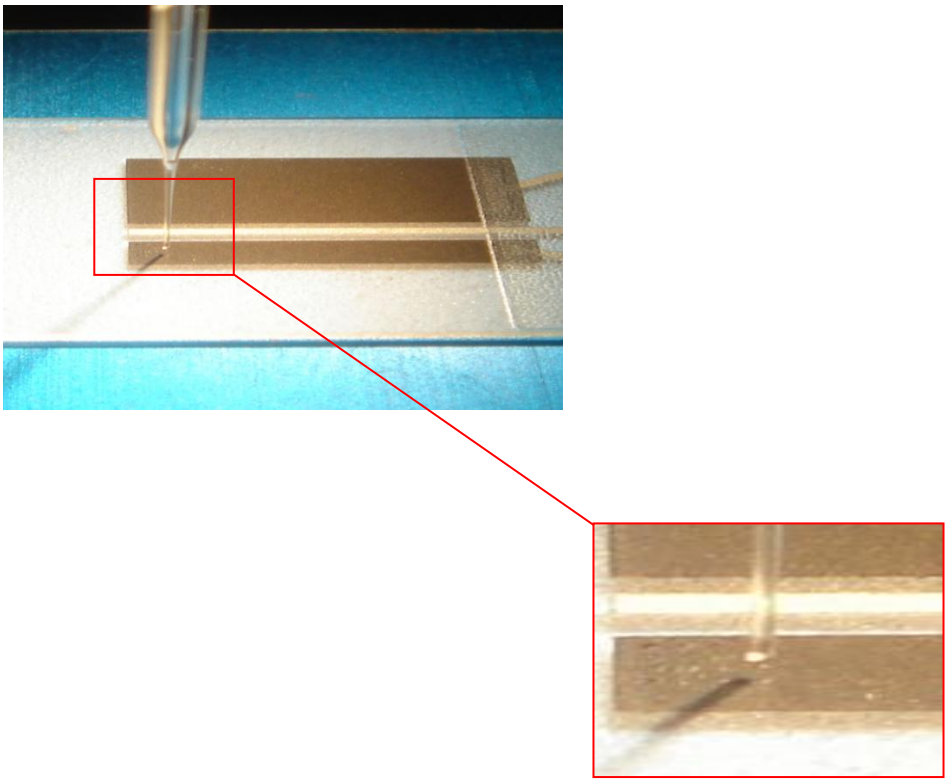

Figure 5.7: Photograph of biotinylated PEI deposition on carbon electrode by pulled microcapillary using the XYZ micro-positioning stage of the SECM270.

5.2.5 Interrogation of film integrity by SECM

To determine the stability of the PEI film to the scanning process during multiple scans, the biotinylated PEI film was scanned repeatedly over a period of time. If the integrity of the film was put at risk by the scanning process, it would not be possible to determine whether any changes occurring in the film were due to DNA hybridisation or not in future experiments. With reference to Figure 5.8, it is apparent that over the course of three area scans in which the PEI film was submerged in ferrocenecarboxylic acid mediator, the image became slightly distorted. Initially it was thought that this noise may have been a result of the degradation of the film, but since the distortion is seen to occur across the entire region, it was established that it was due to the precipitation of the ferrocenecarboxylic acid from solution. We determined that providing fresh mediator is used for each scan and the area rinsed well to remove any precipitated material, no distortion was observed.

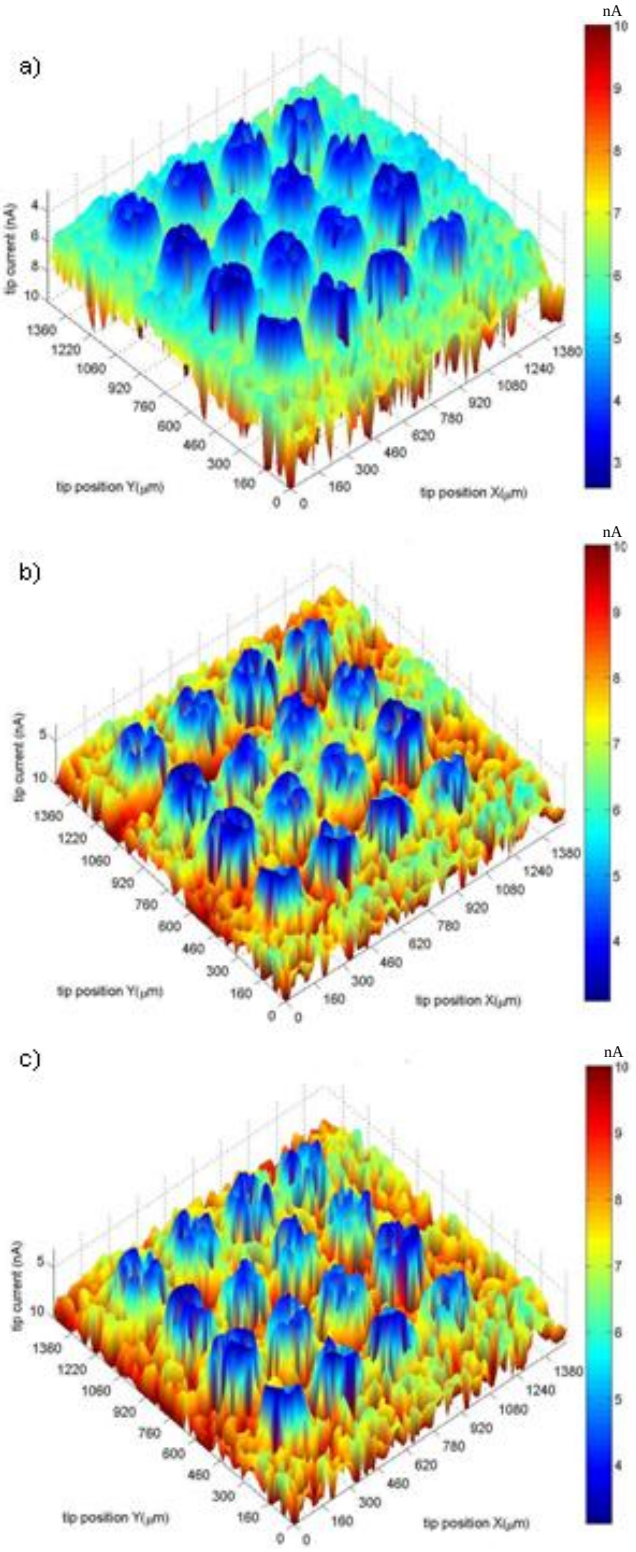

Figure 5.8: 3D representation of the data obtained from Consecutive area scans over biotinylated PEI array on carbon at (a) T=0 min; (b) T=200 min; (c) T=500 min using 5mM ferrocenecarboxylic acid.

5.2.6 Methodology of antigen/antibody binding experiments

A screen-printed carbon electrode substrate was placed in a plastic petri dish and exposed to 5 mmol l^{-1} mediator solution. The SECM working electrode tip and counter and reference electrodes were then immersed into the mediator solution. Prior to undertaking an area scan over the antibody/PEI functionalized regions, an approach curve experiment was conducted over the polycarbonate - non-conductive region of the substrate to estimate the tip-to-substrate distance (Tip Potential (E) = +0.45 V vs. Ag/AgCl; step size = 10 µm). The tip was positioned at a distance at which the measured current was half that of the observed current with the tip a few mm distant from the surface of the screen printed electrode (effectively infinite on this scale); this was to allow for the variation in topography and the height differential between this non-carbon region and the slightly raised carbon electrode surface - while also serving to reduce the risk of tip crash. After tip positioning, an area scan over the functionalised region was conducted with a step size of 10 µm. At no point in the experiment was the substrate touched; this allowed any change in the observed tip current to be attributed solely to changes in the charge transfer properties of the surface. In all cases the tip diameter was 8.5 µm; the scan rate used was 10 µm per step throughout and there was no potential applied to the substrate.

After the first area scan experiment was conducted, the tip was retracted a known safe distance from the substrate. The mediator solution was then removed and the substrate gently rinsed with UHQ water before applying a solution containing complementary antigen over a range of concentrations or a non-complementary antigen. After exposure for 1 hour, the antigen solution was then removed and the substrate again rinsed before the re-introduction of fresh mediator solution. A second area scan experiment was then conducted over the same functionalised area as measured previously. The tip current data from the area scan before exposure was then subtracted from the tip current data following this exposure. Throughout all these experiments the sample substrate does not move at all, i.e. all exposures, rinsing steps etc are performed with the sample *in situ.* It is worth noting here that after each exposure and rinsing step the Petri dish is refilled with fresh mediator solution and the tip exactly repositioned, made possible using the XYZ micro-positioning

stage of the SECM270. This allows precise and reproducible imaging of the same area of the electrode. Differences in the pH of samples tested would have very little effect as the area of interest is rinsed well and the scan is conducted in the coupled buffer solution.

5.2.7 Control experiments

To ensure that changes occurring on the sensor surface were directly related to the binding of antibody and antigen, and not due to interference of mediator solution or poor stability of the substrate, surface scans were undertaken of the antibody modified dotted arrays (Figure 5.9a). The modified surface displays an array of peaks which correspond to decreases in the tip current. This can be accounted for by the polymer/antibody composite acting as a barrier to mediator diffusion to the surface, thereby diminishing the current since polyelectrolytes are known to act as barriers to ion migration (Schönhoff, 2003).

After this initial scan, samples were incubated in purified water for 30 mins in parallel to the immunochemical exposures but in the absence of antigen. Following rinsing, fresh mediator solution was introduced. A scan of this surface is shown in Figure 5.9b. Subtraction of the data from Figure 5.9a from 5.9b (Figure 5.9c) clearly shows only minimal variations, indicating that minimal changes in background current are seen and that there is no loss of material from the surface. Other techniques employed to dot down the array were investigated. These included the direct dotting of antibody onto the carbon surface, once again the SECM micro-positioning XYZ stage was utilised and a capillary filled with the antibody was lowered towards the carbon substrate depositing a small amount of the antibody onto the carbon surface. However, this did not produce effective results as the attraction of the antibody directly onto the carbon proved to be unstable and deterioration of the array could be visualised as the scan progressed.

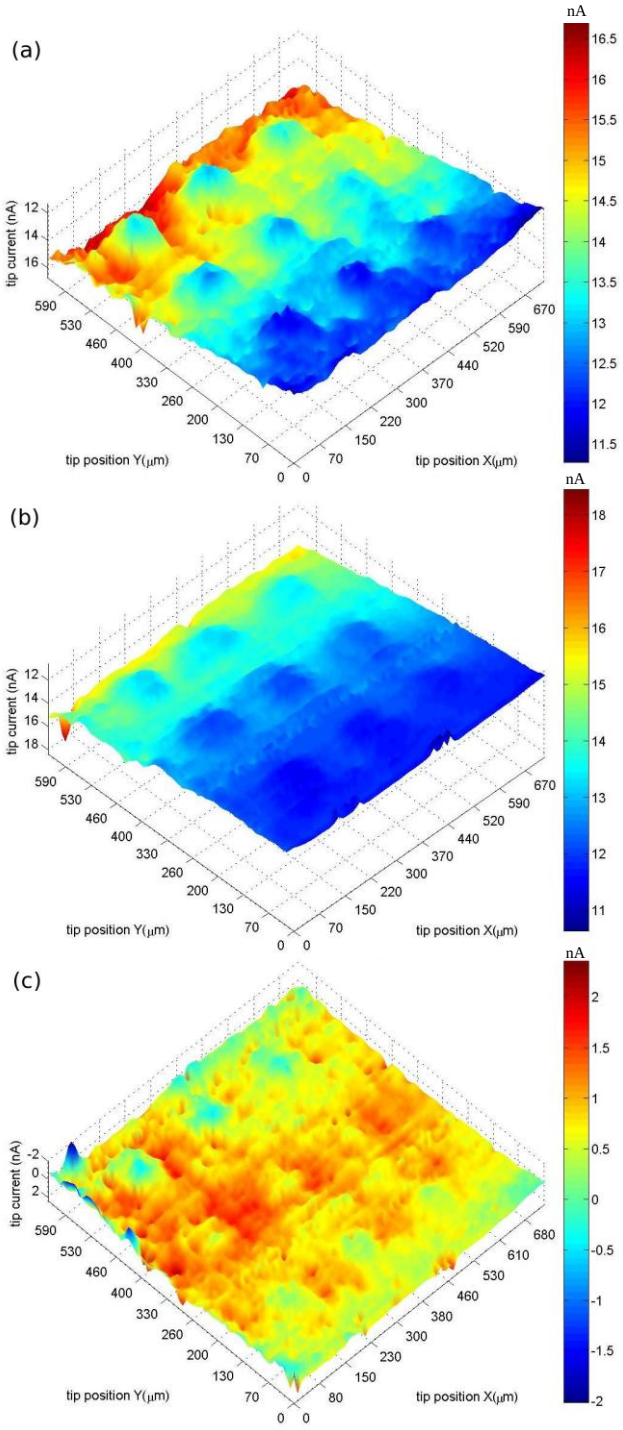

Figure 5.9: 3D representation of the data obtained from an area scan of PEI/neutravidin/biotinylated antibody arrays on screen printed carbon electrode (a) before and (b) following rinsing and 30 mins exposure to control solution (water); (c) absolute change in measured current.

5.2.8 Detection of antigen/antibody binding by SECM

Binding experiments were performed by soaking the modified antibody dotted arrays in solutions of varying concentrations of the complementary antigen for 30 mins, followed by scanning in fresh mediator solution. A control was also run using 5 pg ml^{-1} PSA to ensure changes could be related to specific antigen/antibody binding rather than simple non-specific absorption of proteins to surfaces. Binding experiments were carried out using NSE solution with concentrations ranging from 500 fg ml^{-1} - 200 pg ml^{-1} in water. Detailed results (Figures 5.10a – c) are presented for the exposure to 200 pg ml^{-1}. Figure 5.10a depicts the scan over the dotted array before incubation, with Figure 5.10b showing the scan taken after exposure to 200 pg ml^{-1} NSE. Figure 5.10c shows the difference between the two scans indicating changes to the tip current over both the carbon surface and the dotted substrate. Figure 5.10c shows that across the whole of the array there is a general increase in measured tip current. The change in tip current is, however, seen to be greater in the areas of the PEI/neutravidin/biotinylated antibody dots than for the untreated carbon surface.

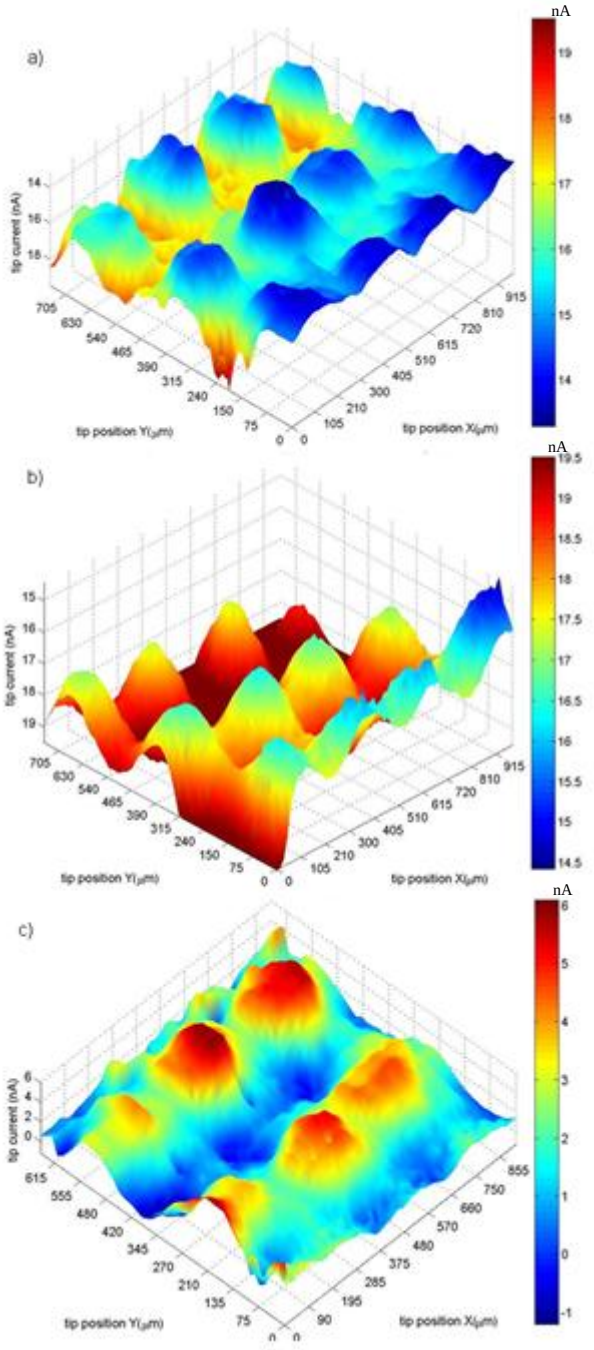

Figure 5.10: 3D representation of the data obtained from an SECM scan of a PEI/neutravidin/biotinylated antibody array on a screen-printed carbon electrode; (a) following exposure to biotinylated antibody NSE; (b) following further exposure to complementary NSE antigen at 200 pg ml^{-1}; (c) absolute change in measured current.

NSE is known to have both positively and negatively charged areas on the surface of the protein (Chai *et al*, 2004). The cationic areas of the protein are capable of electrostatically attracting the ferrocene carboxylic acid (which is anionic at pH 7 due to ionisation of the acid group), thereby increasing the flux of the mediator to the microelectrode tip. There is also the possibility of hydrophobic interactions between the ferrocene unit and any hydrophobic regions of the NSE protein. These could effectively increase the concentration of ferrocene carboxylic acid at the surface and thus enhance the current flow.

Evidence for this type of behaviour comes from earlier work on DNA where the charge on the mediator is found to determine the electrochemical response at the surface. DNA is an anionic polymer due to the presence of phosphate groups and when an anionic mediator is utilised (ferricyanide), increasing the amount of DNA at the surface by hybridisation led to a decrease in current transfer due to repulsion and inhibition of mediator diffusion (Turcu *et al*, 2004a). However when a cationic hexaamine ruthenium mediator was used, increasing the amount of DNA led to an increase in current transfer (Roberts *et al*, 2009). This is thought to be due to the cationic mediator associating with the anionic DNA, thereby increasing the local concentration of mediator at the surface and enhancing electron transfer between the surface and the probe tip. In a similar fashion the binding of antigen causes a localised increase of mediator (in this case ferrocene carboxylic acid) by the same principle and leads to increased current transfer.

The results demonstrate that NSE is bound at the surface in greater concentration in the modified areas, indicating that specific binding is indeed occurring. There appears to be some non-specific binding as shown by the increase in current over the unmodified carbon surface however, this non-specific binding was only observed at the highest concentration of 200 pg ml^{-1} and not when investigating the lower antigen concentrations. Further confirmation was obtained by control experiments with PSA which showed a low level of non-specific binding over the entire surface but no specific binding to the anti-NSE; this is demonstrated in Figure 5.11a.

In each investigation, an array of twelve dots were imaged with a surface profile being obtained for each separate dot. The twelve profiles could be combined to give a mean peak magnitude response for these dots. Figure 5.11a shows the mean trace for a number of samples which have been exposed to a variety of concentrations of NSE and it is clear that an increase in binding as the concentration of antigen increases can be seen. For 200 pg ml^{-1}, the dot profile appears larger and this is believed to be due to saturation of the area resulting in a much greater level of non-specific binding being observed. Figure 5.11b shows a calibration profile obtained by plotting the peak mean dot responses with respect to antigen concentration. A linear relationship (R^2 = 0.97) can be seen between the response and the log of the concentration in the range 0.5 pg ml^{-1} to 200 pg ml^{-1}. This demonstrates the capability for this technique to detect and quantify the presence of a target in solution.

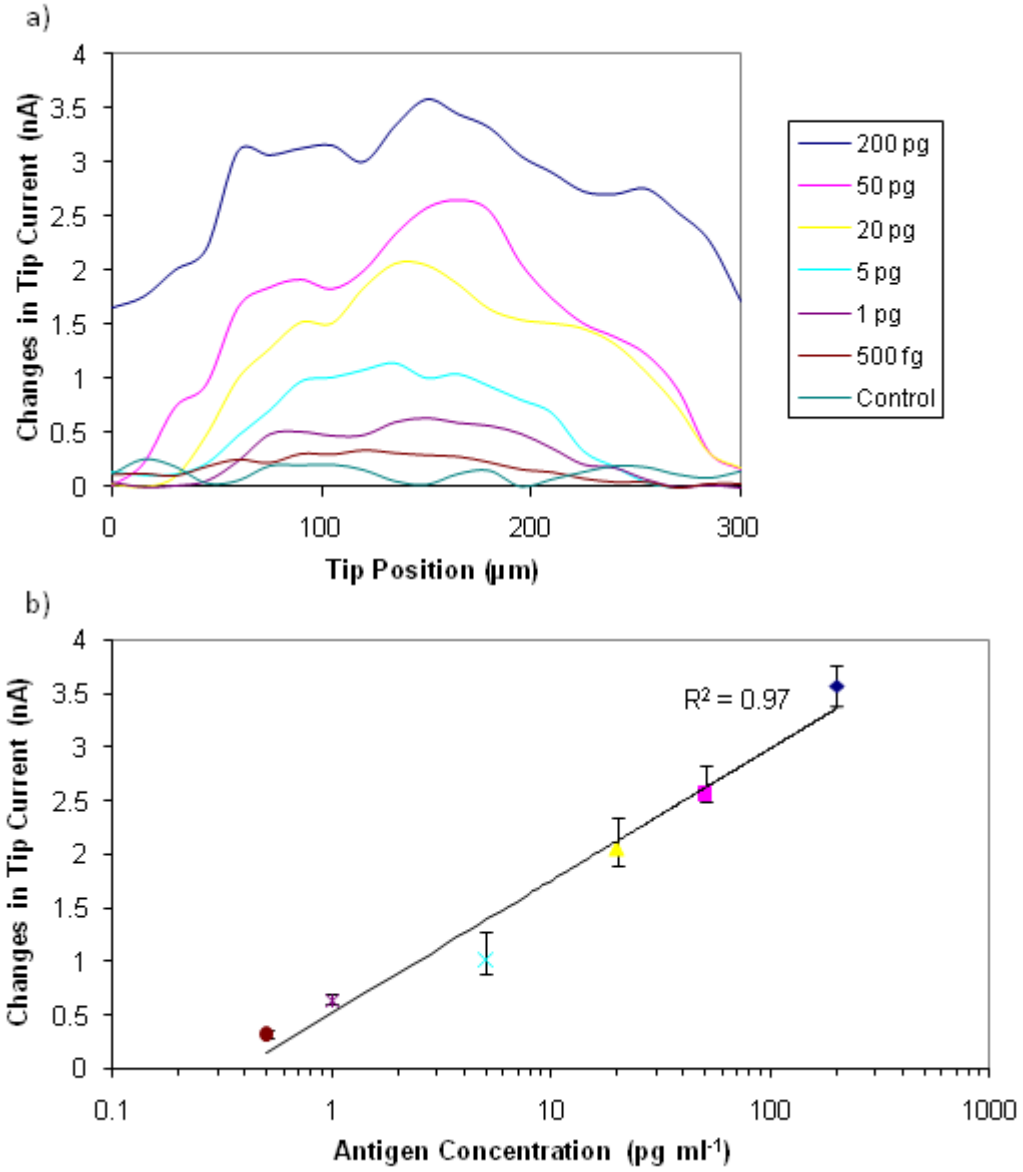

Figure 5:11 (a) Mean changes of a twelve dot array scan (n = 12) taken over PEI/neutravidin/biotinylated antibody surface area to various antigen concentrations (no error bars are included for clarity); (b) Calibration plot showing changes in current measured (n = 12) vs. NSE concentration. Error bars show the standard deviation between the 12 individual dots.

5.3 Conclusions

The main aim of this chapter was to explore the ability of the SECM to characterise a previously optimised impedance based immunosensor developed within the group (Barton *et al* 2008a). It was previously demonstrated that the immunosensor gave a corrected linear response from 1 to 50 pg ml^{-1} with saturation occurring above these concentrations. The limit of detection of the anti-NSE-NSE immunosensor system was found to be 0.5 pg ml^{-1}, and there was an ability to discriminate at a concentration of 1 pg ml^{-1} NSE.

A polyelectrolyte film was constructed using biotinylated PEI, exposed to Neutravidin and then the biotinylated antibody of interest, which in this case was NSE. Using the area scan macro the insulating properties of the polyelectrolyte film were investigated. After the characterisation of the carbon/biotinylated PEI array the complete platform was interrogated by SECM. To do this an area scan of the biotinylated PEI/neutravidin/biotinylated antibody array was undertaken before and after exposure to a variety of concentrations of the complementary antigen NSE. After exposure to the antigen an increase in current was observed over the modified areas, whereas little change was observed over the non-modified carbon surface, thus indicating the binding of NSE to the modified regions. As the antigen concentration exposed to the array increased there was also an increase in the changes in tip current observed. To ensure that the binding events were specific to the antigen of interest scans were also conducted before and after exposure to the non-complementary antigen PSA showing a low level of non-specific binding over the entire array not just specific to the modified regions.

The limits of detection for NSE in this experiment are comparable to those obtained with sonochemically microfabricated arrays (Barton *et al*, 2008a) - and substantially lower than obtained for similar systems based on macroelectrodes (Garifallou *et al*, 2007; Tsekenis *et al*, 2008a, 2008b). The results observed using the SECM were also able to detect binding events at concentrations as low as 0.5 pg ml^{-1} but it was possible to show discrimination at higher concentrations than those observed with sonochemically microfabricated arrays

with detection of up to 200 pg ml^{-1}. A corrected linear response was demonstrated with an R^2 value of 0.97 between 0.5 – 200 pg ml^{-1}.

The low limits of detection for NSE illustrate the potential use of the SECM for the labeless detection of markers for TIA as results are of clinical significance. Currently ELISA permits the quantification of elevated levels of NSE in human serum following stroke from approximately 1 - 150 ng ml^{-1} (μg L^{-1}) NSE (Canag Diagnostics, Diagnostic Automation, Inc).

Previous work has succeeded in imaging layers of immobilised antibodies, however their technique required the use of enzyme modified antigens and also only reported the use of excess labelled antigen whereas our technique is label free and is capable of producing a calibration curve (Wittstock *et al*, 1995).

This work has been published and can be found in the Appendices (Holmes *et al*, 2011 Anal. Chim. Acta).

Chapter 6
Characterisation of an immunosensor for the detection of prostate specific antigen by SECM

6. Characterisation of an immunosensor for the detection of prostate specific antigen by SECM

6.1 Introduction

The prostate gland is an accessory sex gland and is made up of fibrous, muscular and stromal tissue surrounded by connective tissue. The gland is 3 - 4 cm long is 3 - 5 cm wide, walnut in shape and has an average adult weight of 20 grams. However, when it becomes cancerous it can grow and weigh up to 150 grams or more. At birth the gland is pea size and during the first few years leading to puberty grows rapidly. Once puberty is reached, the growth slows until the third decade when growth of the gland stops entirely (Rous, 1988). In some men however, this is not the end of the prostatic enlargement. In 60% of men in their sixties and 80% of men in their eighties, benign prostatic hyperplasia (BPH) develops (Roehrborn *et al*, 1999). The symptoms of BPH are an increase in the prostate volume, symptoms of prostatism and obstruction in the bladder outlet flow (Bosch *et al*, 1995).

A number of disorders can occur in the prostate gland like BPH, prostatitis and prostate cancer. Prostatitis is inflammation of the prostate gland and can be caused by non-bacterial and bacterial infections, causing pain and urinary obstruction. Non-bacterial forms of prostatitis are common and can be sexually transmitted (Naslund, 1993). The prostate gland is situated in the pelvic area and is located between the urinary bladder and urethral sphincter. The gland surrounds the urethra, which has two ejaculatory ducts, situated just above the urethral sphincter (Rous, 1988). The prostate is made up of three lobes – two being lateral and one middle. The lateral lobes are the same size separated by a deep notch, and the middle is small, transverse and is normally triangular or round (Gray, 1994). The gland consists of glandular and muscular tissue made up of two cell types, epithelial cells and stromal cells. The epithelial cells make up the glandular structures and

are involved in producing prostatic secretion, while the stromal cells make up the connective and muscular part of the gland and aid in ejaculation. The gland has numerous blood vessels, which form a sheath cover. Underneath this cover there are 30 - 50 branched tubuloalveolar glands, and these empty their content into the prostatic urethra via the excretory ducts (Kierszenbaum, 2002).

When spermatozoa and fluids from the seminal vesicles pour though the ejaculation ducts into the prostatic urethral, the prostate releases 13 - 33% of its own prostatic fluid. This milky secretion produced by the prostate is at pH 6.5 and contains fibrinolysin, which aids in liquefaction of the semen. Zinc, amylase, prostate specific antigen (PSA), acid phosphatase, calcium and other factors are all also present (Kierszenbaum, 2002). This mixture combines with the rest of the secretory fluids to form the ejaculation fluid; these help in nourishment and transportation of the sperm, as well as making the uterine environment more favourable.

Prostate cancer is well documented as being a major killer in men accounting for 40,000 deaths (Adams *et al*, 2001). In England and Wales most cases of prostate cancer arise in individuals over the age of 65, and in 1997 prostate cancer accounted for 17% of all cancer malignancies occurring (Quinn and Babb, 2002). The National Statistic office published, in 2002 for 1999, that prostate cancer incident rates exceeded that of lung cancer for the first time in twenty years; this included both the new and the directly age-standardised rates.

Prostate cancer is a highly variable disease. It can range from being highly aggressive and malignant killing the individual, to slow growing and never malignant and not killing the individual (Nash and Melezinek, 2000). Prostate cancer normally occurs within the glandular portion of the cells (epithelial cells), with 70% of prostate cancer arising in the peripheral zone, 15 - 20% in the transitional zone and 15 - 20% in the central zone (Spence and Johnson, 2001). Prostatic intraductal neoplasia (PIN) is very rare with 5% of prostate

cells becoming PIN, this being due to proliferation of cells located in the ducts and acini and as well as being associated with basal cell layer disruption (Belldegrun *et al*, 1998).

Malignant adenocarcinomas occur 90% of the time in the peripheral or outer part of the prostate gland, so digital rectal examination (DRE) can easily identify this condition (Rous, 1988). Prostatic adenocarcinomas are rare in men under 50 years of age but occur 50% of the time in men in their eighties, although these are normally small and insignificant. While BPH is a non-invasive form and is due to abnormal proliferation of glandular cells, malignant adenocarcinoma is more advanced, with the cells having irregular edges and an irregular appearance compared to normal cells in their locality (King, 2000). This type of cancer can spread out of its area of production and can cause the formation of secondary tumours, which can become life threatening.

Currently diagnostic methods for prostate cancer involve measurements of prostate specific antigen (PSA) and digital rectal examination (DRE). Once the individual has been identified as having either elevated PSA, or abnormal prostate by DRE, they will be further evaluated by a transrectal ultrasound (TRUS) and in serious cases a prostatectomy may need to be performed. Even with combined use of DRE, PSA and TRUS biopsy, about 40% of men considered to have localised tumours will already have extraprostatic disease (Clements *et al*, 1999). Also 75% of men showing elevated PSA who have a biopsy taken do not have cancer, which causes false positive results, while 20% of patients that do have cancer go unnoticed due to false negative results.

Individuals who have prostatic cancer, typically show elevated PSA levels. PSA is a 33 Kda glycoprotein and is a member of the Kallikreins family; this family is made up of three glycoproteins and these are human glandular kallikrein 1, human glandular kallikrein 2, and human glandular kallikrein 3 (PSA) (Diamandis, 1998). In 1971 Hara *et al* extracted a protein from the human seminal fluid, then Wang *et al* (1979) purified the protein from prostatic tissue identifying it as PSA. PSA is produced by the prostatic secretory epithelium and is one of the most abundant proteins in seminal plasma found at

levels of 0.2 - 5.0 mg/ml; these are a million folds higher than serum levels, which are 0.1 - 4.0 ng/ml (Nash and Melezinek, 2000).

PSA is measured via a blood test and if PSA levels are above the normal range (0.1 - 4.0 ng ml^{-1}), the individuals are identified as possible candidates for having prostate cancer. PSA has enhanced detection of prostate cancer, but there are still uncertainties on how specific it is especially between the ranges of 4 - 10 ng/ml, and moreover only has 25 - 30% specificity in identifying BPH from prostate cancer (Adams *et al*, 2001). It is already known that prostatisis, prostatic massage, needle biopsy, trauma, inflammation, BPH, acute bacterial prostatisis and urinary retention all elevate PSA levels (Belledgrun *et al*, 1998), and therefore a new technique for diagnosis is needed to reduce the number of false positive and negative results.

Due to inaccuracies in measuring PSA, numerous methods have been tried to improve detection methods, and in this context for PSA density, PSA velocity, age specific PSA and PSA forms have all been identified as possible focus for further investigation.

PSA is known to be exposed to a number of protease inhibitors and form complexes with them. In serum, 80 - 90% of PSA is bound to these protease inhibitors such as alpha 1 antichymotrypsin (ACT) or alpha 2 macroglobulin (A2M) while only a small percentage (10 - 20%) is the free/unbound PSA (Chan and Sokoll, 1999).

There is a strong correlation between the amount of free and complexed PSA, with the percentage of free to total PSA supposed to reduce in prostate cancer patients (Stenman *et al*, 1991). However, the percentage of free to total PSA is affected by inflammation and therefore total PSA and free PSA fails to differentiate between cancerous and non-cancerous prostatic diseases (Jung *et al*, 1998).

Although numerous attempts have been made to try and improve the use of PSA, it is still problematic in its predictive use - and PSA alone misses 25% of prostate cancers

(Goldstein and Messing, 1998). PSA is now believed not to be organ specific, with PSA being detected at low levels in the endometrium, breast tissue, adrenal and renal carcinomas (Van der Cruijsen-Koeter *et al*, 2001). PSA furthermore rises in individuals that injure the prostate gland, in men as they get older, and also after sexual activity. When men undergo biopsy due to elevated PSA, two thirds are shown to have no apparent cancer leading to unwarranted stress and anxiety - as well as increased risk of infection and bleeding (Hanks and Scardino, 1996).

Even though all these inaccuracies have been identified, PSA is still currently used for diagnosis, even though the sensitivity of PSA serum testing is not sufficient (Pannek *et al*, 1997). The problem is that even though it is so ineffective there are no other methods for non-invasive monitoring of prostate cancer, and therefore until a new effective approach can be implemented, this approach will still be used.

DRE is an invasive procedure involving the doctor inserting a finger into the anus and feeling the prostate for an abnormal shape or structure. If an abnormality is found then the patient may be admitted for a transrectal ultrasound (TRUS) and in serious cases a prostatectomy is performed. DRE alone misses approximately 40% of prostate cancers (Goldstein and Messing, 1998). Once prognosis involving PSA and/or DRE has occurred, it is important that the actual progression of cancer is assessed, so that the grading and staging can be calculated. TRUS involves a probe with a mounted needle being inserted into the rectum; this probe produces an image of the internal architecture of the gland and aids in diagnosis of cancer (Belledgrun *et al*, 1998). The probe does this by emitting sound waves that bounce off the area in view creating a picture. However, TRUS does not only identify prostate cancer it also detects BPH and prostatitis (Van der Cruijsen-Koeter *et al*, 2001), and so it is important for needle aspirations to be taken so that correct analysis and diagnosis of the gland can occur.

This chapter describes the development of an immunosensor and its interrogation using the scanning electrochemical microscope. The fabrication of this immunosensor is described

in the material and methods section. By interrogating the same system using SECM, valuable insights may be obtained regarding the fabrication of the immunosensor and the applicability of SECM to detecting antibody/antigen interactions. SECM offers a route for non-contact electrochemical interrogation, negating the need for hard-wired electrodes; this in turn offers the potential for developing an array based approach which may be interrogated via a scanning probe tip.

In brief, the aim of the work presented in this chapter is to conduct a preliminary investigation into whether SECM may be used to detect prostate specific antigen at low concentrations and results are compared to those of established ELISA procedures.

6.2 Results and Discussion

6.2.1 Detection of antigen/antibody binding by SECM

Binding experiments were performed as previously described in Chapter 5. Scans were conducted of the modified antibody dotted arrays and then exposed to varying concentrations of the complementary antigen for 30 mins, followed by a second scan in fresh mediator solution. A control was also run using 5 pg ml^{-1} NSE to ensure changes could be related to specific antigen/antibody binding rather than simple non-specific absorption of proteins to surfaces. Binding experiments were carried out using PSA solution with concentrations ranging from 1 pg ml^{-1} - 200 pg ml^{-1} in a phosphate buffer solution. Detailed results (Figure 6.1) are presented for the exposure to 200 pg ml^{-1}. Figure 6.1a depicts the scan over the dotted array before incubation, with Figure 6.1b showing the scan taken after exposure to 200 pg ml^{-1} PSA.

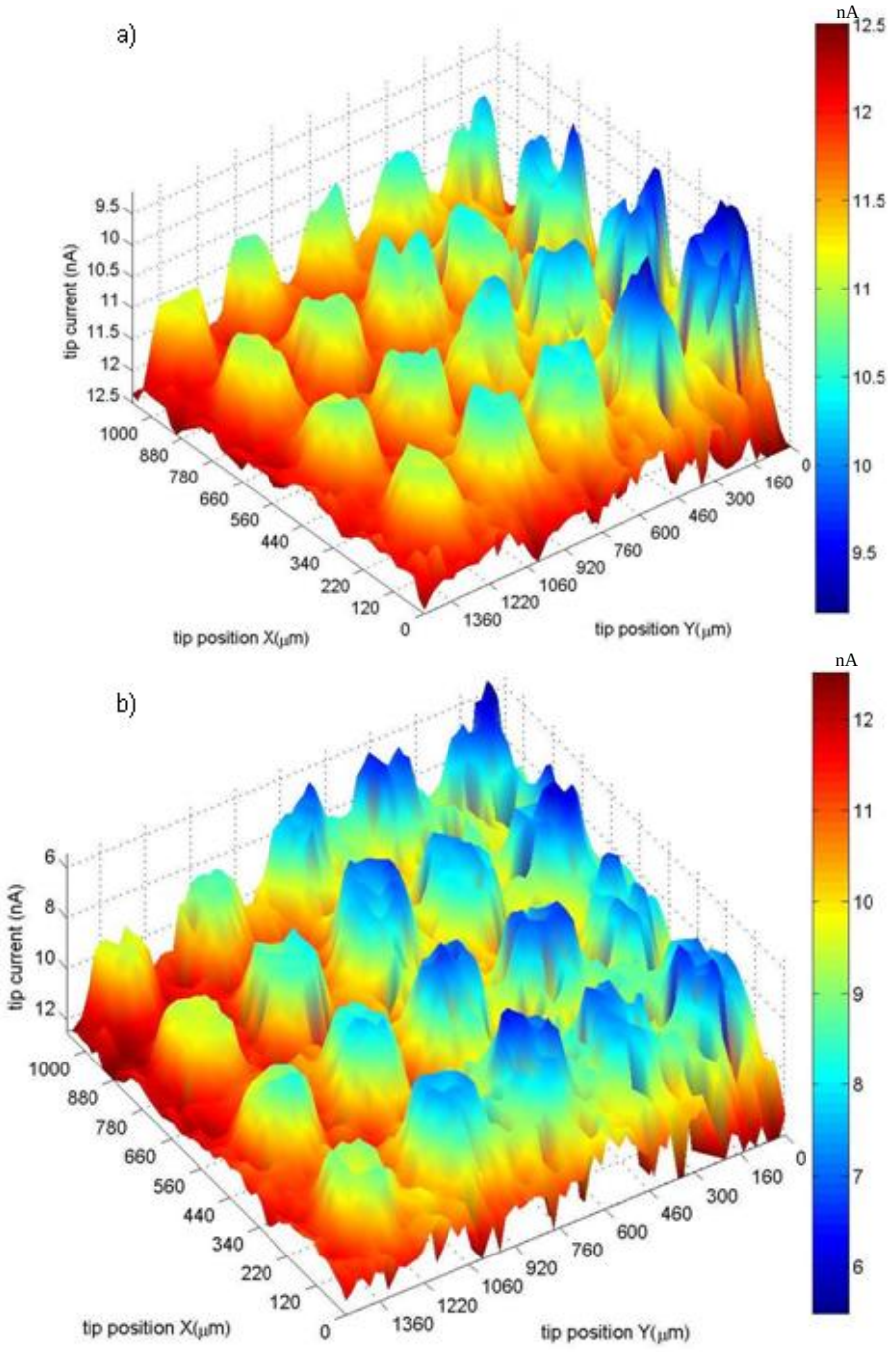

Figure 6.1: 3D representation of the data obtained from a SECM scan of a PEI/neutravidin/biotinylated antibody array on a screen-printed carbon electrode; (a) following exposure to biotinylated antibody PSA; (b) following further exposure to complementary PSA antigen at 200 pg ml^{-1}.

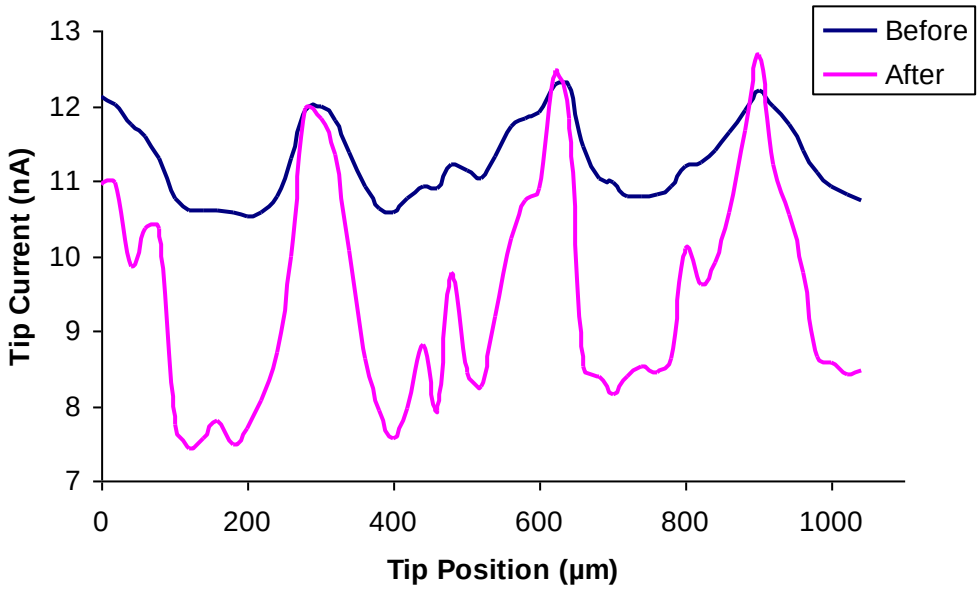

Figure 6.2: Line plot of a PEI/neutravidin/biotinylated antibody array on a screen-printed carbon electrode; before and after exposure to complementary PSA antigen at 200 pg ml^{-1}.

Figure 6.2 is a line plot showing the difference between the two scans. It is clear that there are changes to the tip current over the modified dotted substrate, with a clear decrease in current measured being observed. Also it is worth noting that only very small changes in current are observed on the untreated carbon surface. Figure 6.3a shows the absolute change in feedback across the whole array while Figure 6.3b shows the absolute change in feedback of the line plots shown in Figure 6.2. The results demonstrate that PSA is bound at the surface in greater concentration in the modified areas, indicating that specific binding is indeed occurring. There appears to be very little non-specific binding occurring as demonstrated by the lack of change in current over the unmodified carbon surface. Further confirmation was obtained by control experiments with NSE which showed a low level of non-specific binding over the entire surface but no specific binding to the anti-PSA; this is demonstrated in Figure 6.4a.

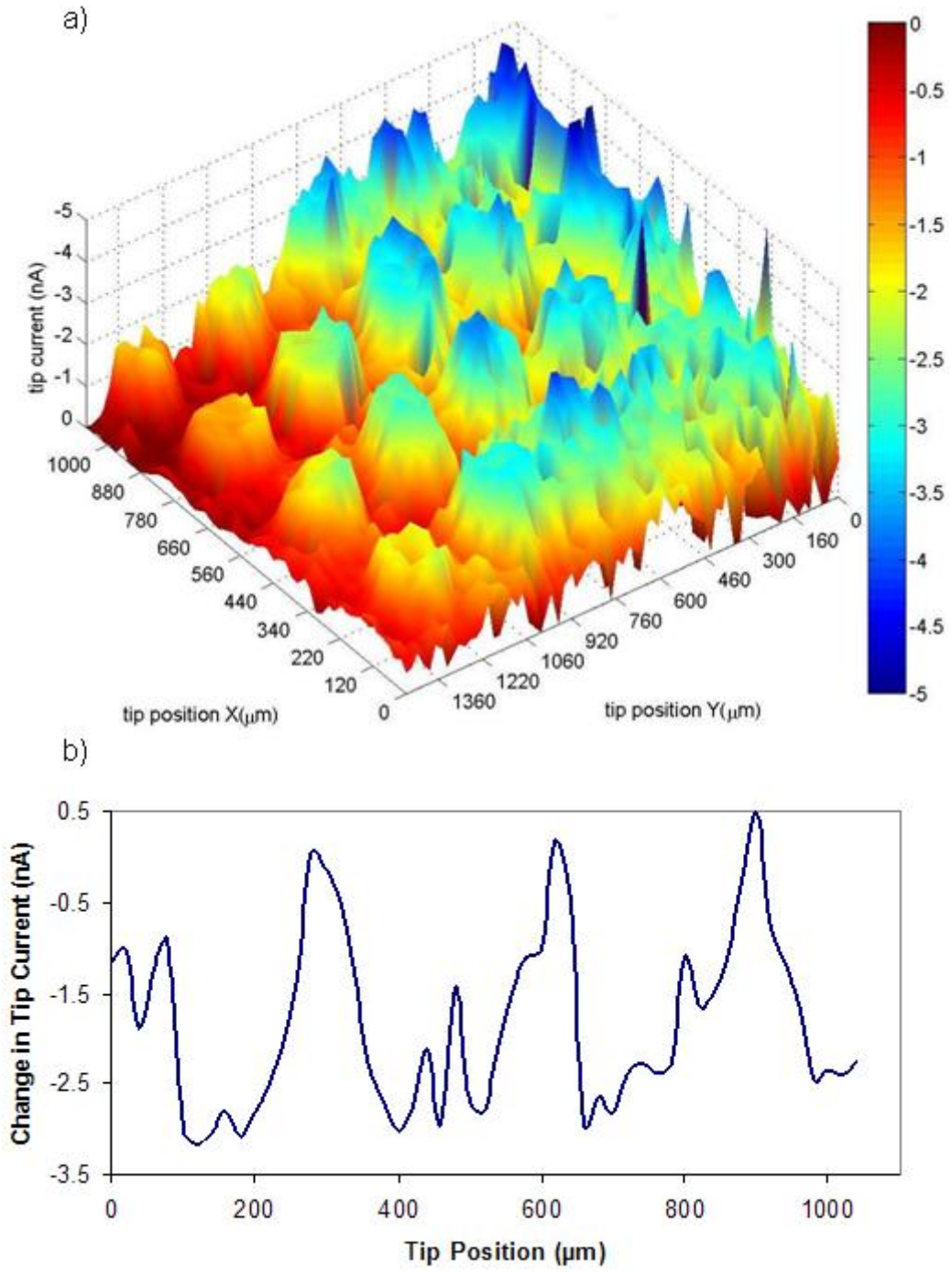

Figure 6.3: (a) 3D representation of the data obtained from a SECM scan of a PEI/neutravidin/biotinylated antibody array on a screen-printed carbon electrode, showing absolute change in feedback after exposure; (b) line plot of absolute change in feedback after exposure to PSA antigen at 200 pg ml^{-1}.

In each investigation, an array of twelve dots were imaged with a surface profile being obtained for each separate dot. The twelve profiles could be combined to give a mean peak magnitude response for these dots. Figure 6.4a shows the mean trace for a number of samples which have been exposed to a variety of concentrations of PSA and it is clear that an increase in binding as the concentration of antigen increases can be seen. This results in a change in the current being measured with a decrease being observed over the modified areas. This is to be expected as binding of the protein to the modified areas will result in a decrease in flux to the tip resulting in the observed decreases in current observed. Figure 6.4b depicts a calibration profile obtained by plotting the peak mean dot responses with respect to antigen concentration. A linear relationship ($R^2 = 0.94$) can be seen between the response and the log of the concentration in the range 1 pg ml^{-1} to 100 pg ml^{-1} which decreases to 0.84 when including 200 pg ml^{-1}. A logarithmic relationship has also been found between ac impedance and antigen concentration in previous immunosensor work (Barton *et al*, 2008b). This demonstrates the potential for this technique to detect and quantify the presence of a target in solution.

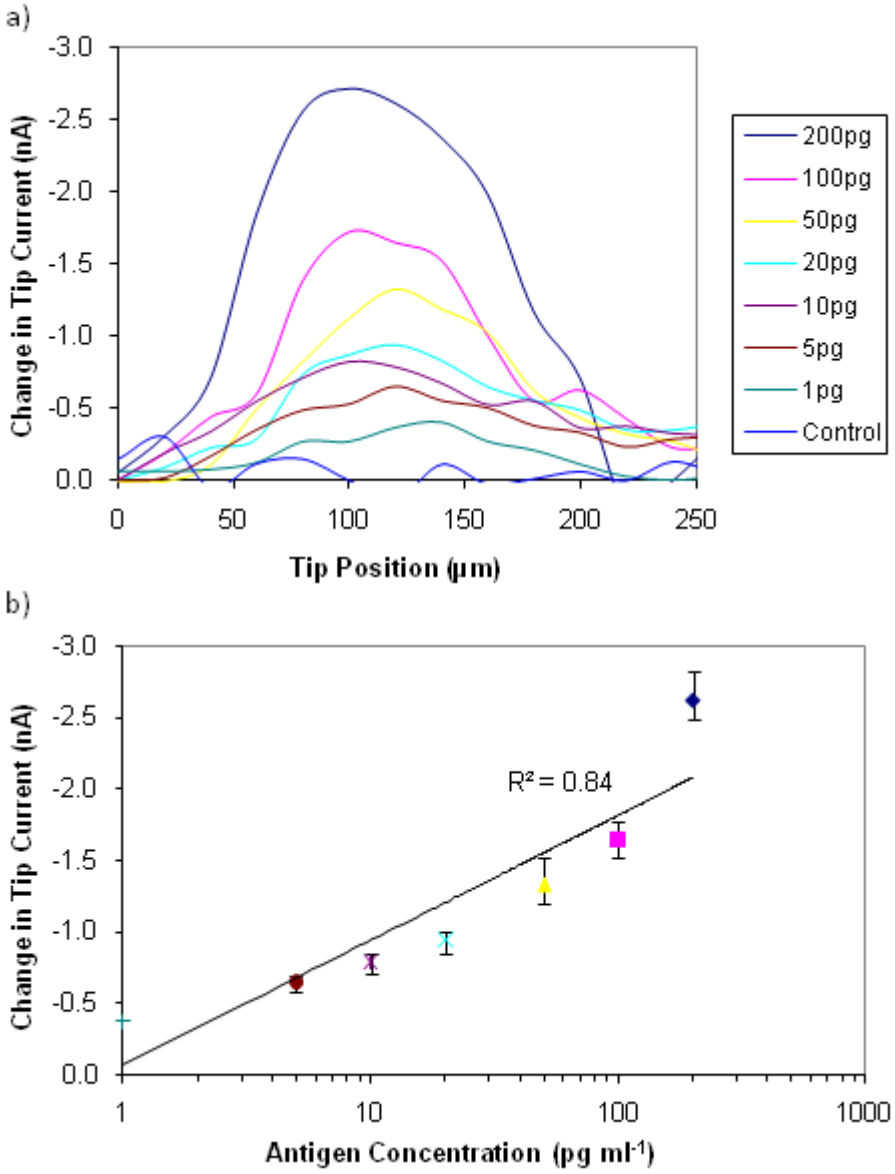

Figure 6.4: (a) Mean changes of a twelve dot array scan (n = 12) taken over PEI/neutravidin/biotinylated antibody surface area to various antigen concentrations (no error bars are included for clarity); (b) Calibration plot showing changes in current measured (n = 12) vs. PSA concentration.

6.2.2 Detection of antigen/antibody binding by ELISA

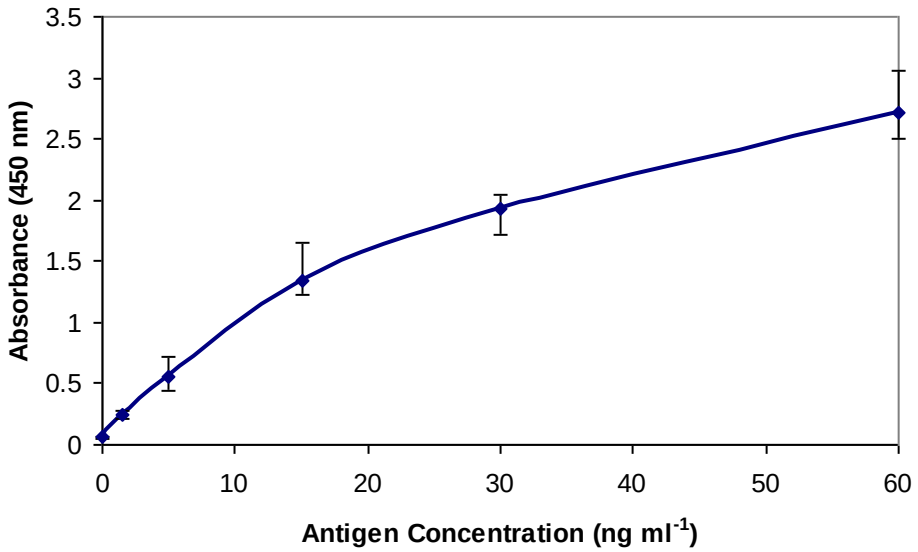

Figure 6.5: PSA ELISA (where) showing the calibration plot using the standards provided representing a range of antigen concentration in the ng ml^{-1} (n = 12).

An ELISA was undertaken (according to Chapter 3 materials and methods) to compare detection levels with the SECM. As depicted in Figure 6.5, a linear response of the standard antigen concentrations can also be observed. It is important to note that the minimum detectable limit for the ELISA as stated in the supporting information is estimated to be 0.05 ng ml^{-1}, although this could not be detected efficiently when carrying out experiments, whereas the detection capabilities of the SECM is 1 – 200 pg ml^{-1} in concentration. Mackness *et al* (2010), reported improvement in the detection range by using fluorescence in place of a colourmetric change and found an 8 – 15 fold improvement in sensitivity, enabling detection limits at 0.13 and 0.63 ng ml^{-1}. This was initially performed in buffered samples when repeated with human serum (Mackness and McDonald, 2010) detection limits of 0.63 ng ml^{-1} were also reported.

6.3 Conclusions

The main aim of this chapter was to explore the ability of the SECM to characterise a previously optimised impedance based immunosensor developed within the group (Barton *et al* 2008b). It was previously demonstrated that the immunosensor gave a "corrected" linear-type response from 1 to 100 pg ml^{-1} with saturation occurring above this concentration. The limit of detection of the affinity immunosensor was found to be 1 pg ml^{-1} with an ability to discriminate at 5 pg ml^{-1} PSA.

A polyelectrolyte film was constructed using biotinylated PEI, exposed to neutravidin and then the biotinylated antibody of interest, which in this case was PSA. The platform was interrogated by SECM by undertaking an area scan of the biotinylated PEI/biotinylated antibody array before and after exposure to a variety of concentrations of the complementary antigen PSA. After exposure to the antigen a decrease in current was observed over the modified areas, whereas little change was observed over the non-modified carbon surface, thus indicating the binding of PSA to the modified regions. As the antigen concentration being exposed to the array increased there was also an increase in the changes in tip current observed. To ensure that the binding events were specific to the antigen of interest ,scans were also conducted before and after exposure to the non-complementary antigen NSE showing a low level of non-specific binding over the entire array not just specific to the modified regions.

The limits of detection for PSA in this experiment are comparable to those obtained in previous work (Barton *et al*, 2008b) based upon an ac impedance protocol; Barton *et al* (2008b) showed that at concentrations above 100 pg ml^{-1} the sensor began to plateau as it approached saturation. The limit of detection of the PSA immunosensor system was found to be 1 pg ml^{-1} and there was an ability to discriminate at 5 pg ml^{-1} PSA. The results observed using the SECM were also able to detect binding events at concentrations as low as 1 pg ml^{-1} but it was possible to show discrimination at higher concentrations than those

previously observed with detection of up to 200 pg ml^{-1}. A corrected linear response was demonstrated with an R^2 value of 0.83 between 1 – 200 pg ml^{-1}, increasing to 0.94 when looking at 1 – 100 pg ml^{-1}.

Currently ELISA permits the quantification of elevated levels of PSA approximately 0.05 - 100 ng ml^{-1} (μg L^{-1}) (Canag Diagnostics, Diagnostic Automation, Inc, USA). The low limits of detection for PSA illustrate the potential use of the SECM for the labeless detection of markers for cancers as results are of clinical significance.

Chapter 7
Characterisation of an immunosensor for the detection of NTx by SECM

7. Characterisation of an immunosensor for the detection of NTx by SECM

7.1 Introduction

In the ageing population of western countries bone diseases, such as osteoporosis or bone metastases, are a continuously growing problem. Osteoporosis for example represents one of the most common age related diseases overall effecting about 75 million people in Europe, USA and Japan (Lindsay, 1997; Lippuner *et al*, 2005). The total number of fragility fractures, and hence the cost to society, will increase dramatically over the next 50 years as a result of demographic changes in the number of elderly (Walker-Bone *et al*, 2002). Thus, prevention, early diagnosis and management of bone disease are major issues.

At present, the diagnosis of osteoporosis is mainly based on the measurement of bone mineral density (BMD) by dual X-ray absorptiometry (DEXA) and the anamnesis of previous fragility fracture (Kanis, 2002). However, diagnosing bone diseases by low BMD and a positive fracture anamnesis is limited by the fat that the diagnosis can only be made in an advanced disease stage, when many of the disease related osseous modifications are irreversible. In addition, BMD has to be considered as a cumulative marker of bone metabolism over a long period that contributes only about 60-80% to the prediction of fracture risk (Small, 2005; Briot and Roux, 2005). However, the onset of many bone diseases precedes measurable changes of BMD by years. Consequently, there is a large scope to improve the diagnosis of many bone diseases. Beside BMD, macro- and microscope architecture of bone tissue, bone remodelling and the constitution of extracellular bone matrix (e.g. collagen cross-linking) are major determinants of bone strength (Oxlund *et al*, 1995, 1996; Banse *et al*, 2002a, 2002b; Felsenberg and Boonen, 2005; Chavassieux *et al*, 2007).

In recent years, great efforts have been made to develop biochemical markers of bone metabolism as comparatively inexpensive tools to monitor the current status of bone turnover. If used correctly, these indices have great potential to improve the management of many bone diseases. At present, there are more than ten different bone turnover markers commercially available. Bone alkaline phosphatase (BAP), osteocalcin (OC) and the N- and C-terminal procollagen type I propeptides (PINP, PICP) are the most commonly used biochemical markers of bone formation. All of these are synthetic products of the active osteoblast. In contrast, most of the current bone resorption markers are degradation products of collagen type I which may be measured in serum and/or urine. Due to their diverse mechanisms of release and elimination, the clinical performance of these markers can differ significantly depending on the clinical situation (Delmas *et al*, 2000; Fall *et al*, 2000; Seibel, 2006). These differences between seemingly similar molecules and parameters have caused considerable confusion and uncertainty within the scientific and clinical community.

This chapter will focus exclusively on one of the major macro-molecular collagen degradation markers the N-terminal cross-linked telopeptide of type I collagen (NTx-I). This compound can be measured in serum and urine, and the assay has been adapted to automated analysers permitting the rapid analysis of large series of samples.

In the early 1990s, a competitive inhibition ELISA has been developed for the measurement of NTx-I fragments in the urine (Hanson *et al*, 1992). This assay is based on a monoclonal antibody that specifically recognises an epitope embedded in the α-2 chain of the N-telopeptide fragment. The peptide has the sequence QYDGKGVG, where K is involved in a trivalent cross-linking site. The compound still contains the pyridinium crosslink, but the antibody does not recognise the pyridinoline or deoxypyridinoline *per se*. Thus, the antibody appears to react only with a conformational epitope, which is specific for the cross-linking of bone collagen and the presence of a pyridinium cross-link is not essential for reactivity (Hanson *et al*, 1992). Collagen must be broken down to small cross-linked peptides that contain the exact sequence before antibody binding occurs with the NTx-I antigen. Furthermore, the antibody also recognises such peptides in culture

medium conditioned by osteoclasts that are resorbing human bone particles *in vitro* (Eyre, 1995; Apone *et al*, 1998). These data suggest that the NTx-I peptide is a direct product of osteoclastic proteolysis and appears not to be metabolised further (Hanson *et al*, 1992; Apone *et al*, 1998).

The NTx-I assay is calibrated using standard amounts of human bone collagen digested with bacterial collagenases. The intra and inter-assay variability, expressed as a coefficient of variation, is on average 8% and 10% respectively, or higher at low concentration, and the sensitivity is 20-25 ng ml^{-1} (Gertz *et al*, 1994; Garnero *et al*, 1995; Ju *et al*, 1997).

This chapter describes the development of an immunosensor and its interrogation using the scanning electrochemical microscope. The fabrication of this immunosensor is described in the material and methods section. By interrogating the same system using SECM, valuable insights may be obtained regarding the fabrication of the immunosensor and the applicability of SECM to detecting antibody/antigen interactions. SECM offers a route for non-contact electrochemical interrogation, negating the need for hard-wired electrodes; this in turn offers the potential for developing an array based approach which may be interrogated via a scanning probe tip.

7 .2 Results and Discussion

7.2.1 Detection of antigen/antigen binding by SECM

Binding experiments were performed by soaking the modified antibody dotted arrays in solutions of varying concentrations of the complementary antigen for 30 mins, followed by scanning in fresh mediator solution. Binding experiments were carried out using NTx solution with concentrations ranging from 1 nM - 1000 nM in buffer solutions provided by the ELISA kit (Wampole Laboratories, USA). Detailed results are presented for the exposure to 100 nM. Figure 7.1a depicts the scan over the dotted array before incubation, with Figure 7.1b showing the scan taken after exposure to 100 nM NTx.

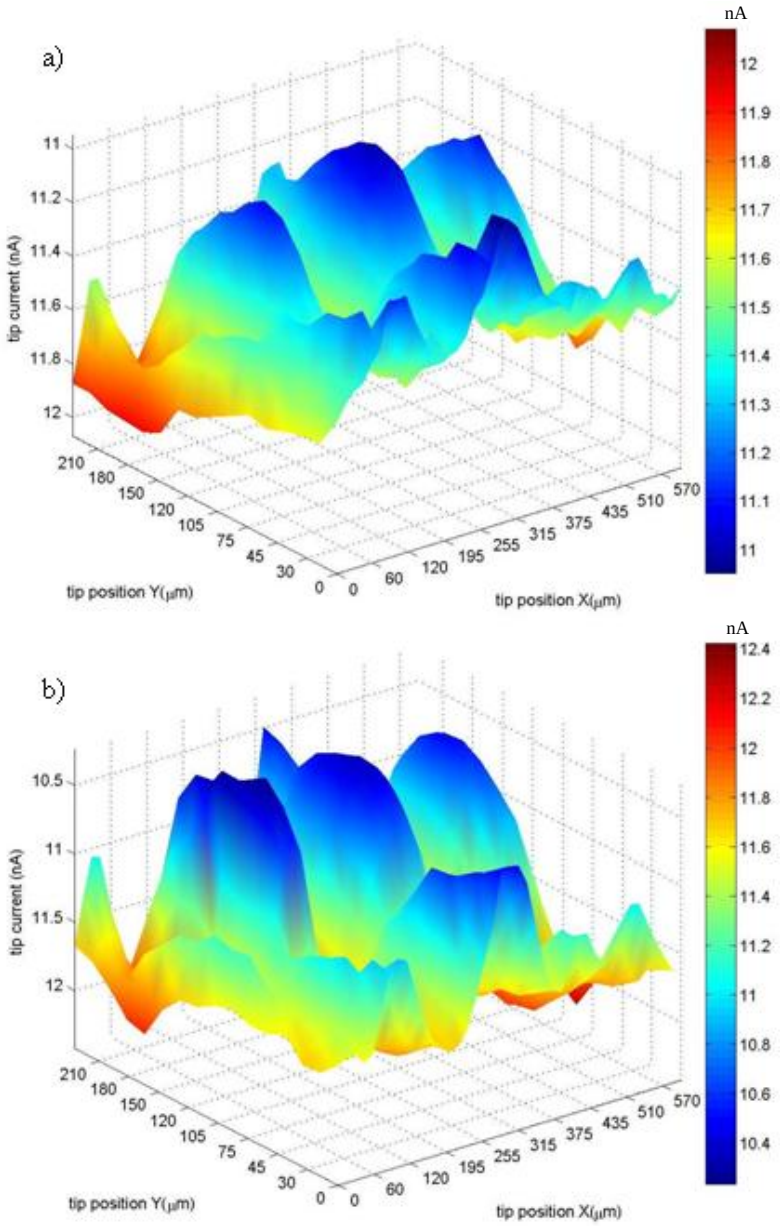

Figure 7.1: 3D representation of the data obtained from a SECM scan of a PEI/neutravidin/biotinylated antibody array on a screen-printed carbon electrode; (a) following exposure to biotinylated antibody NTx, (b) following further exposure to complementary NTx antigen at 100 nM.

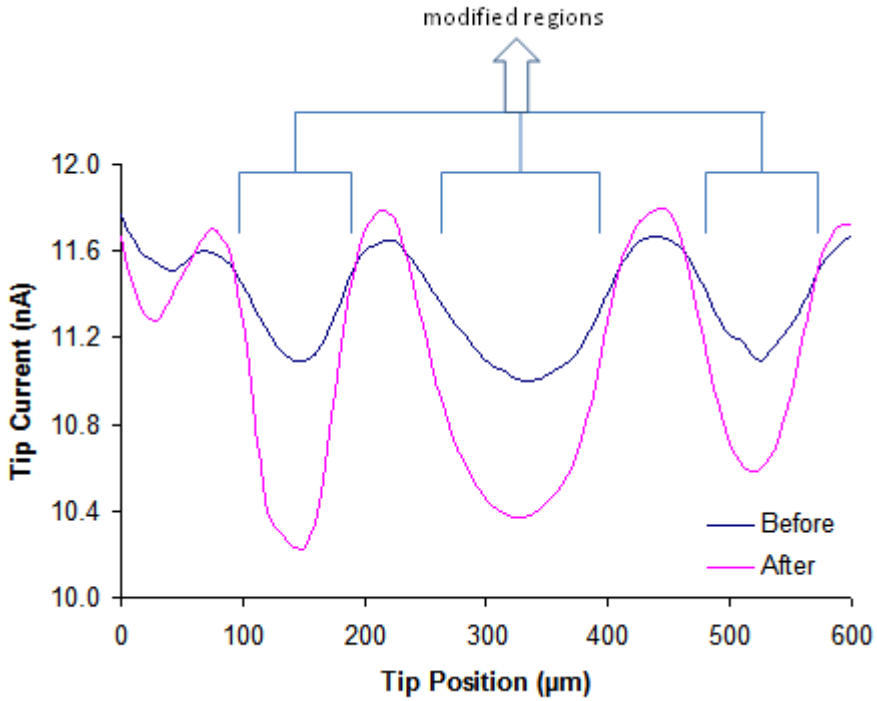

Figure 7.2: Line plot of a PEI/neutravidin/biotinylated antibody array on a screen-printed carbon electrode; before and after exposure to complementary NTx antigen at 100 nM.

Figure 7.2 is a line plot showing the difference between the two scans. It is clear that there are changes to the tip current over the modified dotted substrate, with a clear decrease in current measured being observed. Also it is worth noting that only very small changes in current are observed on the untreated carbon surface. Figure 6.3a shows the absolute change in feedback across the whole array while Figure 6.3b shows the absolute change in feedback of the line plots shown in Figure 6.2.

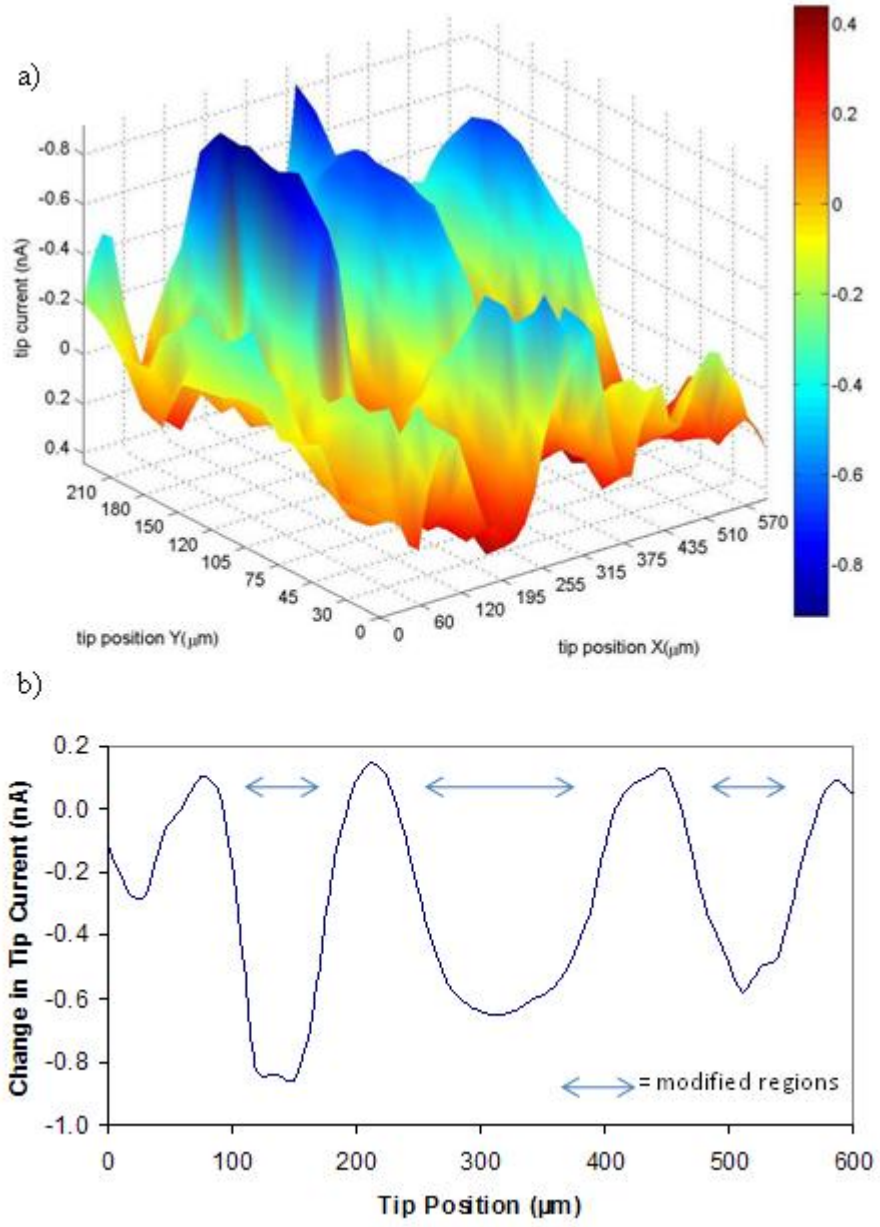

Figure 7.3: (a) 3D representation of the data obtained from a SECM scan of a PEI/neutravidin/biotinylated antibody array on a screen-printed carbon electrode, showing absolute change in feedback after exposure; (b) line plot of absolute change in feedback after exposure to NTx antigen at 100 nM.

In each investigation, an array of twelve dots were imaged with a surface profile being obtained for each separate dot. The twelve profiles could be combined to give a mean peak magnitude response for these dots. Figure 7.4a shows the mean trace for a number of samples which have been exposed to a variety of concentrations of NTx and it is clear that an increase in binding as the concentration of antigen increases can be seen. This results in a change in the current being measured with a decrease being observed over the modified areas. This is to be expected as binding of the protein to the modified areas will result in a decrease in flux to the tip resulting in the observed decreases in current observed. Figure 7.4b depicts a calibration profile obtained by plotting the peak mean dot responses with respect to antigen concentration. A linear relationship ($R^2 = 0.94$) can be seen between the response and the log of the concentration in the range 1 nM to 300 nM which decreases to 0.85 when including 1000 nM.

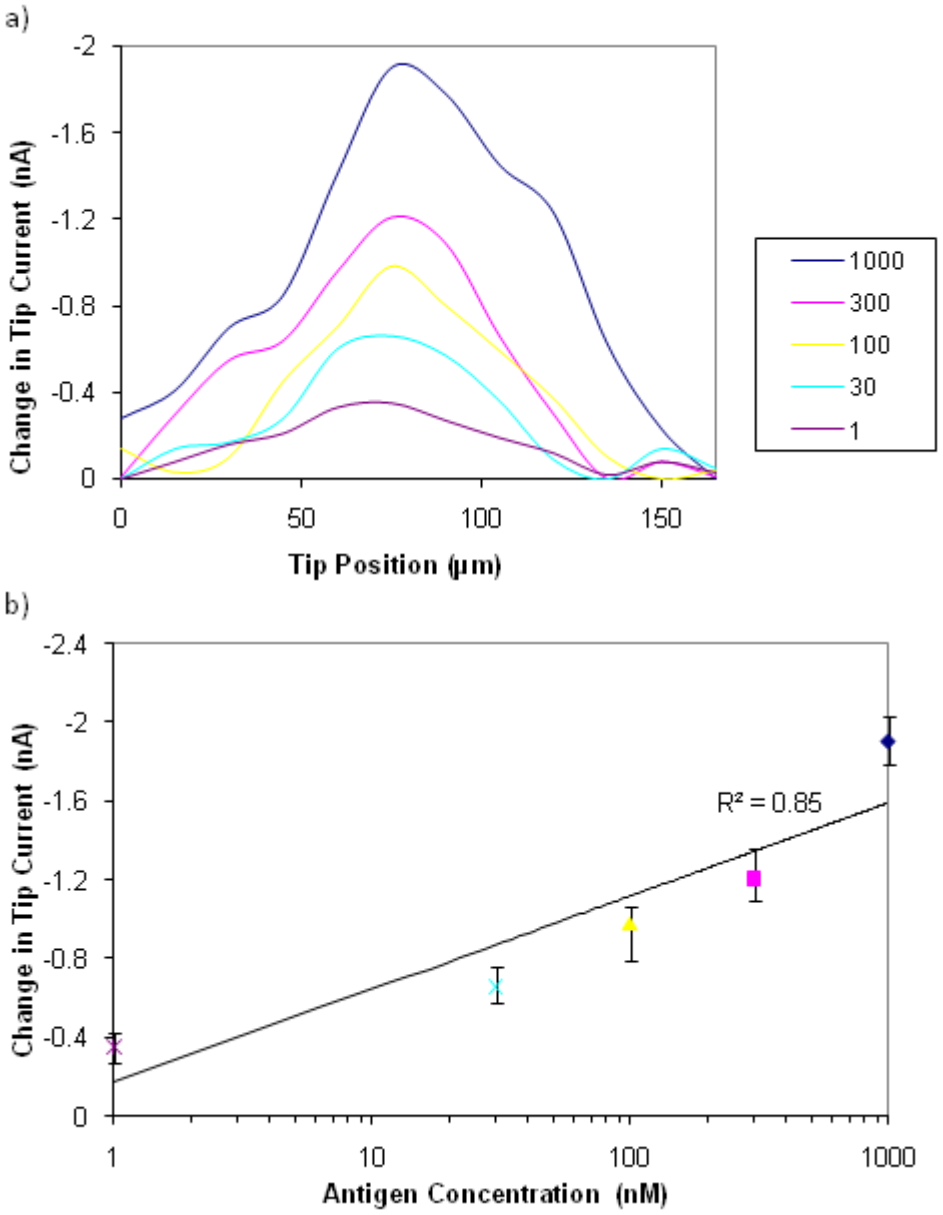

Figure 7.4: (a) Mean changes of a twelve dot array scan (n = 12) taken over PEI/neutravidin/biotinylated antibody surface area to various antigen concentrations (no error bars are included for clarity); (b) Calibration plot showing changes in current measured (n = 12) vs. NTx concentration.

7.2.2 Detection of non-specific antigen/antigen binding by SECM

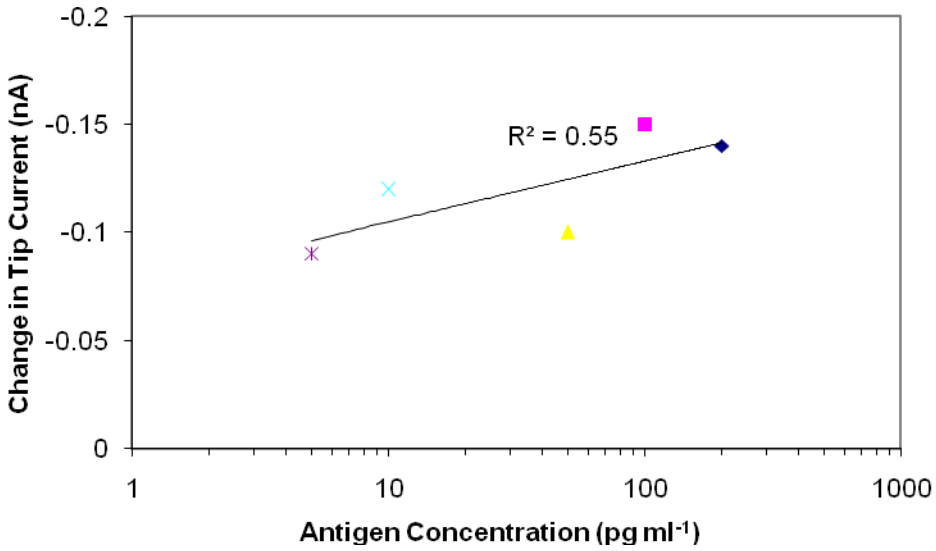

Figure 7.5: Calibration plot showing changes in current measured vs. non-complementary PSA antigen concentration.

To ensure that changes observed in the current were specific and not due to anything other than the binding of the antigen to the modified antibody array region experiments were also conducted exposing the NTx antibody array system to a variety of concentrations of PSA. As can be observed from Figure 7.5 when the biotinylated antibody array of NTx is exposed to a non-complementary (PSA) antigen, a small change in current is observed over the modified regions this is not unexpected as although the area has been blocked a small amount of non-specific binding is possible and this is what is being observed in the changes in current. However, this is to a much smaller extent when compared to the results observed when it is exposed to its complementary antigen. Also it is important to note that there is no linear response observed as the concentration increases unlike that observed when investigating the complementary NTx antigen. This is further evidence that the changes in current observed are related to the binding of the antigen onto the modified regions and shows that the arrays are specific to the antigens under interrogation.

7.3 Conclusions

The main aim of this chapter was to demonstrate the ability of the SECM to detect NTx and is directly comparable to the commercially available ELISA kit.

A polyelectrolyte film was constructed using biotinylated PEI, exposed to neutravidin and then the biotinylated antibody of interest, which in this case was NTx. The platform was interrogated by SECM by undertaking an area scan of the biotinylated PEI/neutravidin/biotinylated antibody array before and after exposure to a variety of concentrations of the complementary antigen NTx. After exposure to the antigen a decrease in current was observed over the modified areas, whereas little change was observed over the non-modified carbon surface, thus indicating the binding of NTx to the modified regions. As the antigen concentration being exposed to the array increased there was also an increase in the changes in tip current observed. To ensure that the binding events were specific to the antigen of interest scans were also conducted before and after exposure to the non-complementary antigen PSA showing a low level of non-specific binding over the entire array not just specific to the modified regions.

The sensors showed a clear linear response with an increase in the change of current observed as the antigen concentration increased. The detection levels investigated in this work were 1 nM – 1000 nM although there is a potential for this to be taken to a lower detection limit as demonstrated in previous chapters. However, it is worth noting that these levels are in the same range as those of the ELISA demonstrating the saturation of the array does not seem to be of a limiting factor.

Chapter 8
Characterisation of an immunosensor for the detection of ciprofloxacin by SECM

8. Characterisation of an immunosensor for the detection of ciprofloxacin by SECM

8.1 Introduction

Due to the recent problems arising from the increase of antibiotic resistance, the EU has established guidelines regarding the use of antibiotics by humans for animals (Bishai, 2002; Bogialli *et al*, 2009). Fluoroquinolones, an example of which is ciprofloxacin, are a group of antibiotics that have been found in food substances, however current detection methods involve the use of ultraviolet (UV) detection (Vallee *et al*, 1986; Groeneveld and Broewers, 1986), whereas others use expensive fluorescence detection (Borner *et al*, 1986; Lovdahl *et al*, 1993), a method that is not commonly available in every laboratory. However AC impedance analysis is a promising tool for the detection of anti-fluoroquinolones in food products (Mello and Kubota 2002).

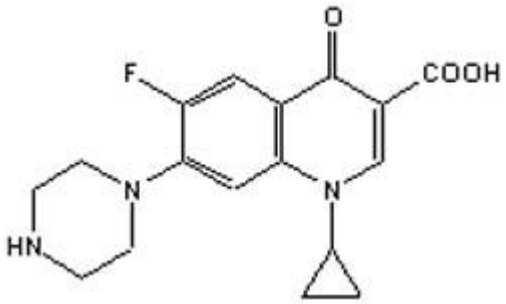

Figure 8.1: Chemical structure of ciprofloxacin

With the emergence of bacterial resistance and some adverse biological effects that in some cases have been severe, quinolones are a group of antibiotics which have been used for some time as they have been shown to have great antibacterial activity and broad spectrum of action (Blondeau, 2004). Quinolones are synthesised from a 3-quinolone carboxylic acid and constitute a relatively new class of antibiotics. They have a broad antibacterial spectrum against both gram negative and gram positive bacteria. They are

involved in disrupting DNA replication, recombination, decatenation and repair this is achieved by the inhibition of DNA gyrase and DNA topoisomerase. Some quinolones, such as danofloxacin and enrofloxacin were specifically developed for the treatment of enteric and respiratory infections in cattle (Bogialli *et al*, 2008). By the addition of fluorine in the carbon six position to the internal quinolone structure, a new group of antibiotics were developed which had similar properties to the quinolones; this was carried out as the quinolones had limited activity and showed early development of bacterial resistance. Flouroquinolones have been seen to have excellent tissue penetration as well as strong interactions with outer membrane proteins.

In the mid 1980s the first fluoroquinolone to be approved for clinical medicine was ciprofloxacin. In general quinolones can be classified into three generations. The first generation includes nalidixic acid and oxolimic acid alongside others, which have been found to have limited activity against *E. coli* and other gram negative bacteria. Additionally, they display poor oral bioavailability and limited distribution into systemic tissues. The second generation fluoroquinolones include ciprofloxacin and danofloxacin. These compounds, developed in the 1980s, displayed increased activity against gram negative *Enterobacteriacaea* as well as some activity against gram positive bacteria such as *P. aeriginosa*. They further displayed improved oral bioavailability. The third generation quinolones displayed similar activity to second generation drugs but showed enhanced antibacterial activity against gram positive bacteria. They also displayed better oral bioavailability alongside lower toxicity and longer serum half-life (Martinez *et al*, 2006; Ball, 2000).

Ciprofloxacin has a broad spectrum of activity against particularly gram negative and some gram positive bacteria. For decades it has been extensively used for the treatment of urinary and respiratory tract infections; however, there have been reports of failure when used for the treatment of pneumonococol infections. Ball (2000) reported that gemifloxacin appears to be the most effective compound for use against *S. pneumoniiae* also showing the least potent adverse biological reactions. Hartmann *et al* (1999), studied

the concentration of ciprofloxacin in hospital wastewaters using high performance liquid chromatography (HPLC) and correlated this with DNA damaging effects. The levels of detected ciprofloxacin ranged from 0.7 ng – 124.5 ng ml^{-1} and genotoxicity was observed from levels as low as 5.2 ng ml^{-1}. The therapeutic range of ciprofloxacin lies between 0.57 – 2.3 µg ml^{-1} in serum and 1.26 – 4.03 µg ml^{-1} in tissue (Licitra *et al*, 1987).

The importance of fluoroquinolones in the medical industry and the potent biological effects of some of these drugs on human health and environmental welfare have made it a necessity to develop methods for their fast detection and reliable determination of their concentration in food products e.g. diary milk. Torriero *et al* (2006), describe a horseradish peroxidise sensor for the detection of ciprofloxacin based on the inhibition of catechol oxidation, however, existing piperazine compounds may interfere with the detection process.

This chapter describes the development of an immunosensor and its interrogation using the scanning electrochemical microscope. The fabrication of this immunosensor is described in the material and methods section. By interrogating the same system using SECM, valuable insights may be obtained regarding the fabrication of the immunosensor and the applicability of SECM to detecting antibody/antigen interactions. SECM offers a route for non-contact electrochemical interrogation, negating the need for hard-wired electrodes; this in turn offers the potential for developing an array based approach which may be interrogated via a scanning probe tip.

In brief, the aim of the work presented in this chapter is to conduct a preliminary investigation into whether SECM may be used to detect ciprofloxacin at low concentrations in both buffer and milk.

8.2 Results and Discussion

8.2.1 Detection of antigen/antigen binding in buffer by SECM

Binding experiments were performed as previously described in Chapter 5. Scans were conducted of the modified antibody dotted arrays and then exposed to varying concentrations of the complementary antigen for 30 mins, followed by a second scan in fresh mediator solution. Binding experiments were carried out using ciprofloxacin solution with concentrations ranging from 100 pg ml^{-1} - 100 ng ml^{-1} in a phosphate buffer solution. Changes in the absolute feedback in current at the tip are shown (Figure 8.2) for the exposure to 100 pg ml^{-1}. Figure 8.2a depicts the scan over the dotted array showing the change in the feedback measured, with Figure 8.2b showing a line plot of the changes observed when exposed to 100 pg ml^{-1} ciprofloxacin.

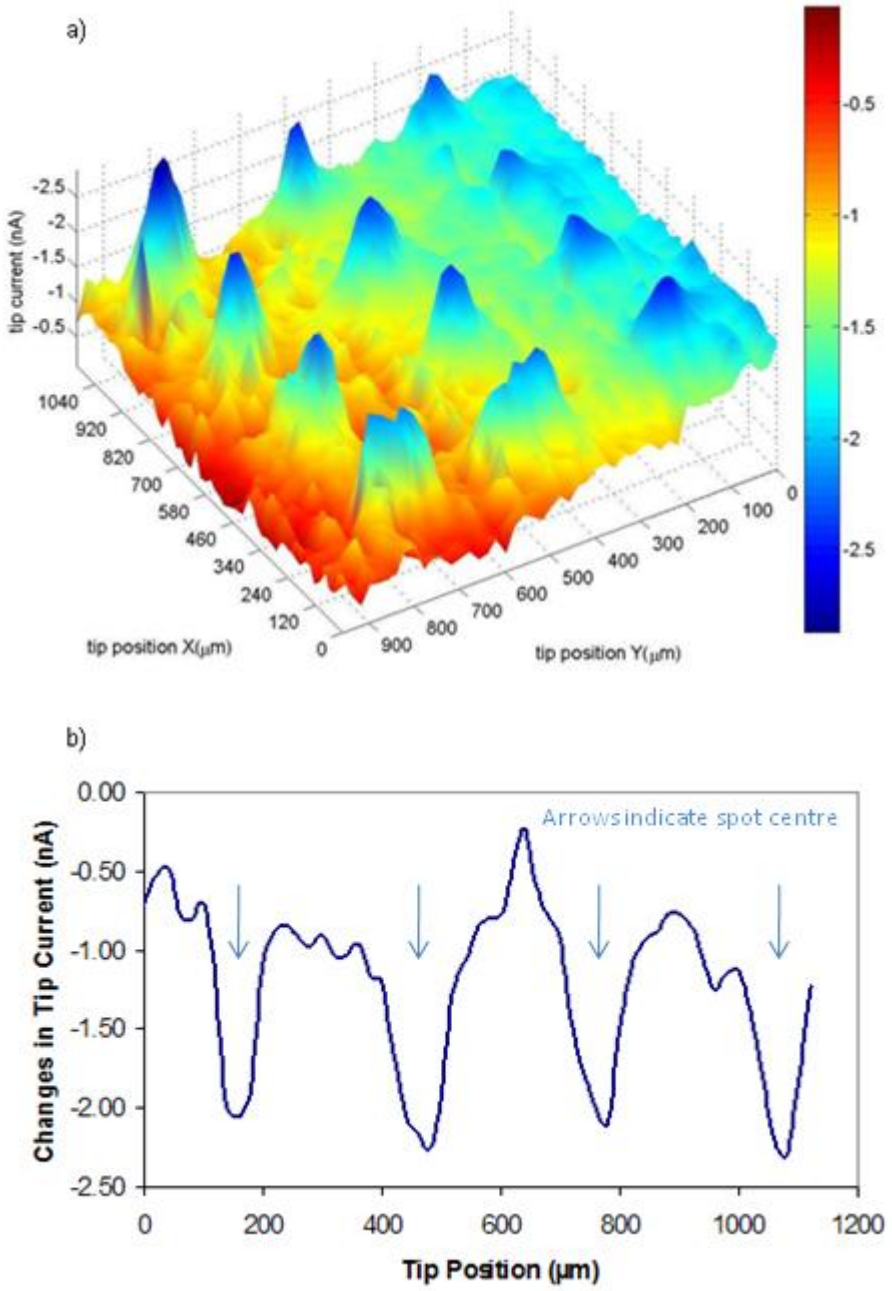

Figure 8.2: (a) 3D representation of the data obtained from a SECM scan of a PEI/neutravidin/biotinylated antibody array on a screen-printed carbon electrode, showing absolute change in feedback after exposure; (b) line plot of absolute change in feedback after exposure to ciprofloxacin antigen at 100 pg ml^{-1}.

It is clear from Figure 8.2a that there are changes to the tip current over the modified dotted substrate, with a clear decrease in current measured being observed. Also it is worth noting that only very small changes in current are observed on the untreated carbon surface. The results demonstrate that ciprofloxacin is bound at the surface in greater concentration in the modified areas, indicating that specific binding is indeed occurring. There appears to be very little non-specific binding occurring as demonstrated by the lack of change in current over the unmodified carbon surface. Further confirmation was obtained by control experiments with PSA which showed a low level of non-specific binding over the entire surface but no specific binding to the anti-ciprofloxacin; this is demonstrated in Figure 8.3a.

In each investigation, an array of twelve dots were imaged with a surface profile being obtained for each separate dot. The twelve profiles could be combined to give a mean peak magnitude response for these dots. Figure 8.3a shows the mean trace for a number of samples which have been exposed to a variety of concentrations of ciprofloxacin and it is clear that an increase in binding as the concentration of antigen increases can be seen. For 100 ng ml^{-1}, the dot profile appears to be getting larger and this is believed to be due to saturation of the area which can result in a greater level of non-specific binding being observed. Figure 8.3b shows a calibration profile obtained by plotting the peak mean dot responses with respect to antigen concentration. A linear relationship ($R^2 = 0.96$) can be seen between the response and the log of the concentration in the range 100 pg ml^{-1} to 100 ng ml^{-1}. A logarithmic relationship has also been found between AC impedance and antigen concentration in previous immunosensor work (Garifallou *et al*, 2008). This demonstrates the potential for this technique to detect and quantify the presence of a target in solution.

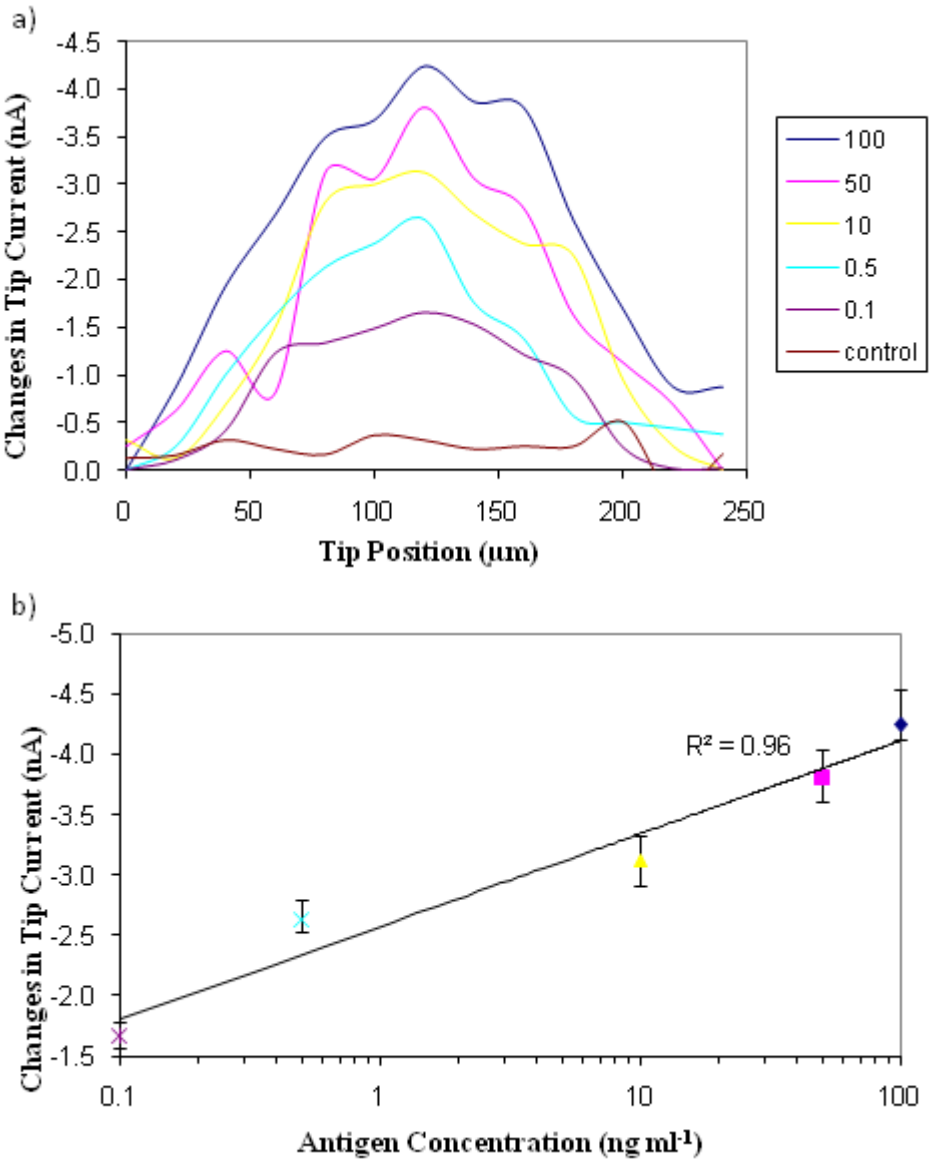

Figure 8.3: (a) Mean changes of a twelve dot array scan (n = 12) taken over PEI/neutravidin/biotinylated antibody surface area to various antigen concentrations (no error bars are included for clarity); (b) Calibration plot showing changes in current measured (n = 12) vs. ciprofloxacin concentration.

8.2.2 Detection of antigen/antigen binding in milk by SECM

For the method previously described to be of practical use further investigations were undertaken using a consumable food. It was therefore decided to detect ciprofloxacin at various concentrations in semi-skimmed milk. The maximum allowed concentration of ciprofloxacin in milk products has been limited to no greater than 100 ng ml^{-1} by the European Union.

Milk is a complete matrix of various constituents including proteins, salts and a plethora of other components. It can therefore be understood that the response detected would be more limited and that there could be a greater degree of non-specific binging events. Figure 8.4 shows the absolute change in tip current for an array exposed to 500 pg ml^{-1} ciprofloxacin in milk. It is clear that there has been a change of current observed over the non-modified carbon region, resulting in an overall decrease in current. However, the modified regions show an increase in current observed compared to the non-modified carbon region; this differs from the results obtained when investigating ciprofloxacin in PBS buffer, where a decrease in tip current was measured.

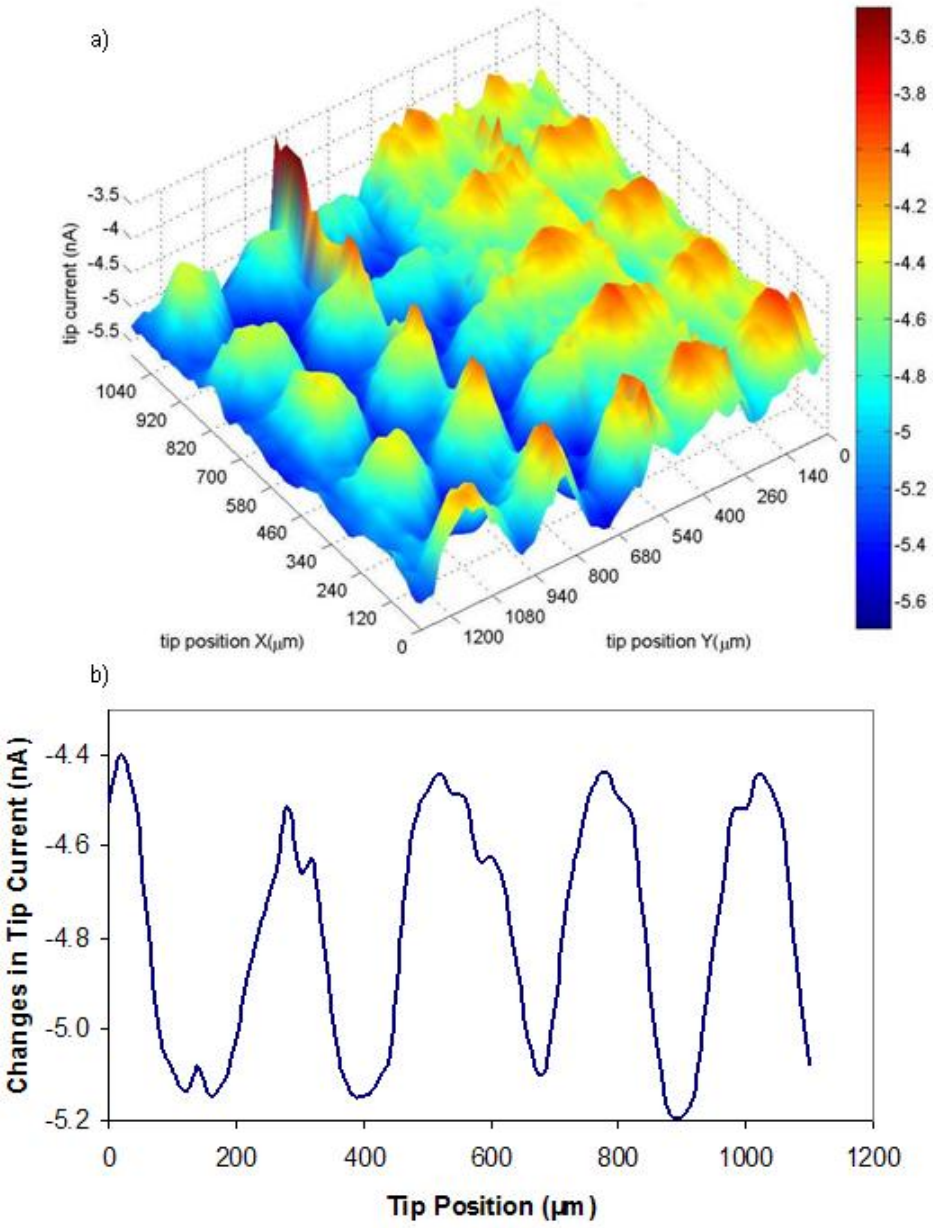

Figure 8.4: (a) 3D representation of the data obtained from a SECM scan of a PEI/neutravidin/biotinylated antibody array on a screen-printed carbon electrode, showing absolute change in feedback after exposure; (b) line plot of absolute change in feedback after exposure to ciprofloxacin antigen at 500 pg ml^{-1}.

To understand the changes observed over the carbon region a CV was carried out on an untreated screen-printed carbon electrode. This was then exposed to semi-skimmed milk for 30 mins before a second CV (Figure 8.5a). These results show that there is some absorbance of the products from the milk onto the carbon surface decreasing the conductivity of the carbon surface. This corresponds with the results observed with the SECM scans, but it is important to establish that there is no effect on the modified dots so that the changes can be related directly to the binding events of the antibiotic to the antibody. Therefore a screen-printed carbon electrode was homogenously treated with biotinylated PEI and a CV was carried out before and after a 30 min exposure to milk (Figure 8.5b). As can be seen a small degree of absorbance from the milk products onto the surface can be observed but to a much smaller degree than that shown on the untreated carbon surface. Also this would result in a further decrease in the current observed over the modified regions whereas - we actually see an increase in the current over the modified regions once exposed to the milk containing ciprofloxacin.

Ciprofloxacin is known to form chelation complexes with the calcium ions present in milk. These complexes consist of two ciprofloxacin units attached to one calcium ion (Katz and Wilner, 2003; Upadhyay *et al*, 2006). The binding of these complexes onto the modified surface would contribute to an increase in the current observed at the microelectrode tip explaining the results observed when measuring the various ciprofloxacin concentrations in the semi-skimmed milk.

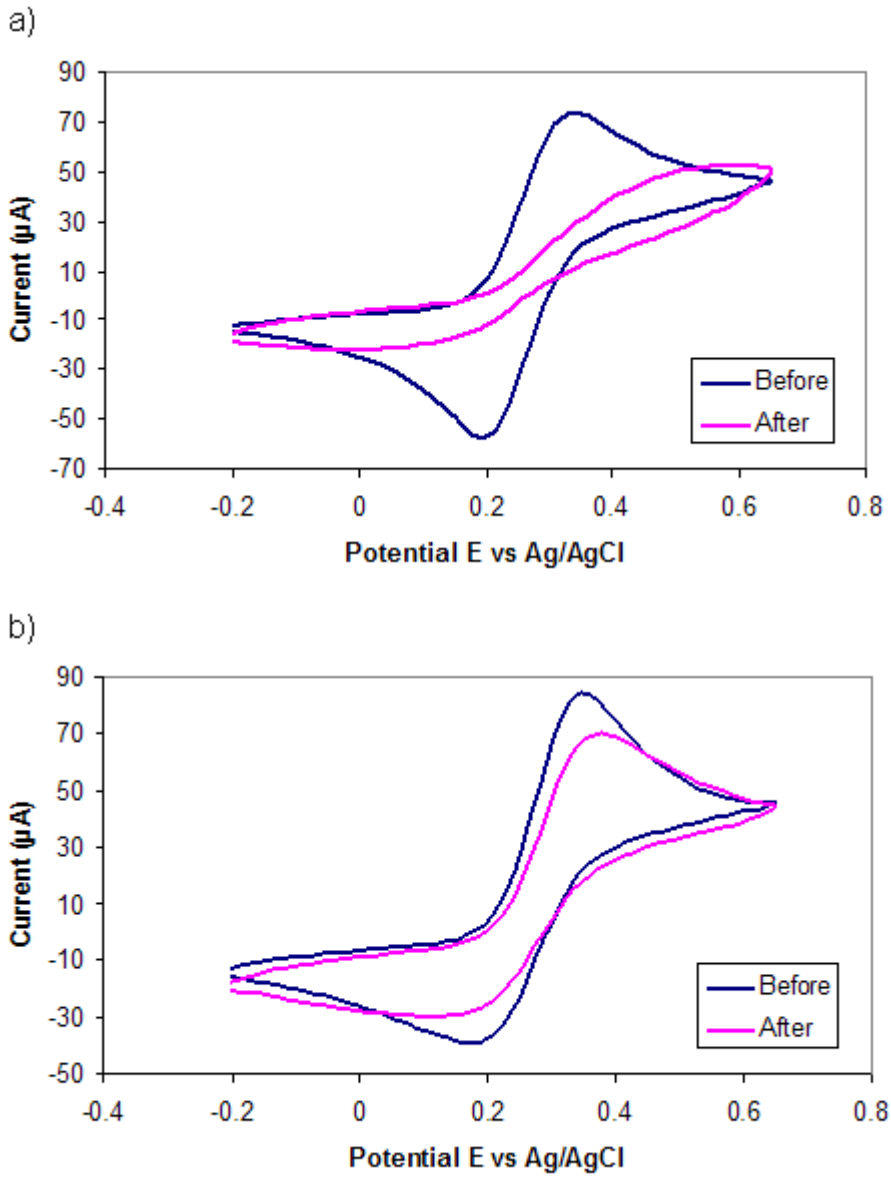

Figure 8.5: Shows cyclic voltammograms of screen printed carbon electrodes before and after exposure to semi-skimmed milk a) shows results for bare carbon surface b) shows results attained aftert the carbon surface has been coated with biotinylated PEI.

As with the ciprofloxacin measured in buffer, an array of twelve dots were imaged with a surface profile being obtained for each separate dot. The twelve profiles were combined giving a mean peak magnitude response for these dots. Figure 8.6a shows the mean trace for a number of samples which have been exposed to a variety of concentrations of ciprofloxacin in milk and it is clear that an increase in binding as the concentration of antigen increases can be seen. Whereas the current decreased as concentration increased with the ciprofloxacin in buffer, with the ciprofloxacin in milk the current is shown to increase as the concentration increases. However, it is worth noting that the magnitude of the current changes observed is smaller than that when investigated in the PBS buffer. This is most probably due to the interference of all the other constituents that are present in milk, such as proteins, salts, fats and enzymes. Once again to ensure changes in current were specific to binding of the complementary antigen to the antibody, a control was used (PSA) which showed a low level of non-specific binding over the entire surface - but no specific binding to the anti-ciprofloxacin; this is demonstrated in Figure 8.6a.

Figure 8.6b shows a calibration profile obtained by plotting the peak mean dot responses with respect to antigen concentration. A linear relationship (R^2 = 0.95) can be seen between the response and the log of the concentration in the range 100 pg ml^{-1} to 50 ng ml^{-1} but the R^2 value drops to 0.77 when inclusive of 100 ng ml^{-1}. A logarithmic relationship has also been found between AC impedance and antigen concentration in milk in previous immunosensor work (Garifallou *et al*, 2007).

Previous work has reported the use of liquid chromatography based methods for the detection of fluoroquinolones in milk (Rodriguez-Diaz *et al*, 2006). The assay described employed luminescence detection with liquid chromatography and reported a linear range of 8 ng – 3.5 µg ml^{-1}, with a detection limit of 3 ng ml^{-1}. ELISA based assays detecting fluoroquinolones in milk have also been reported but with detection limits in the range of several ng ml^{-1} (Duan and Yuan, 2001; Bucknall *et al*, 2003).

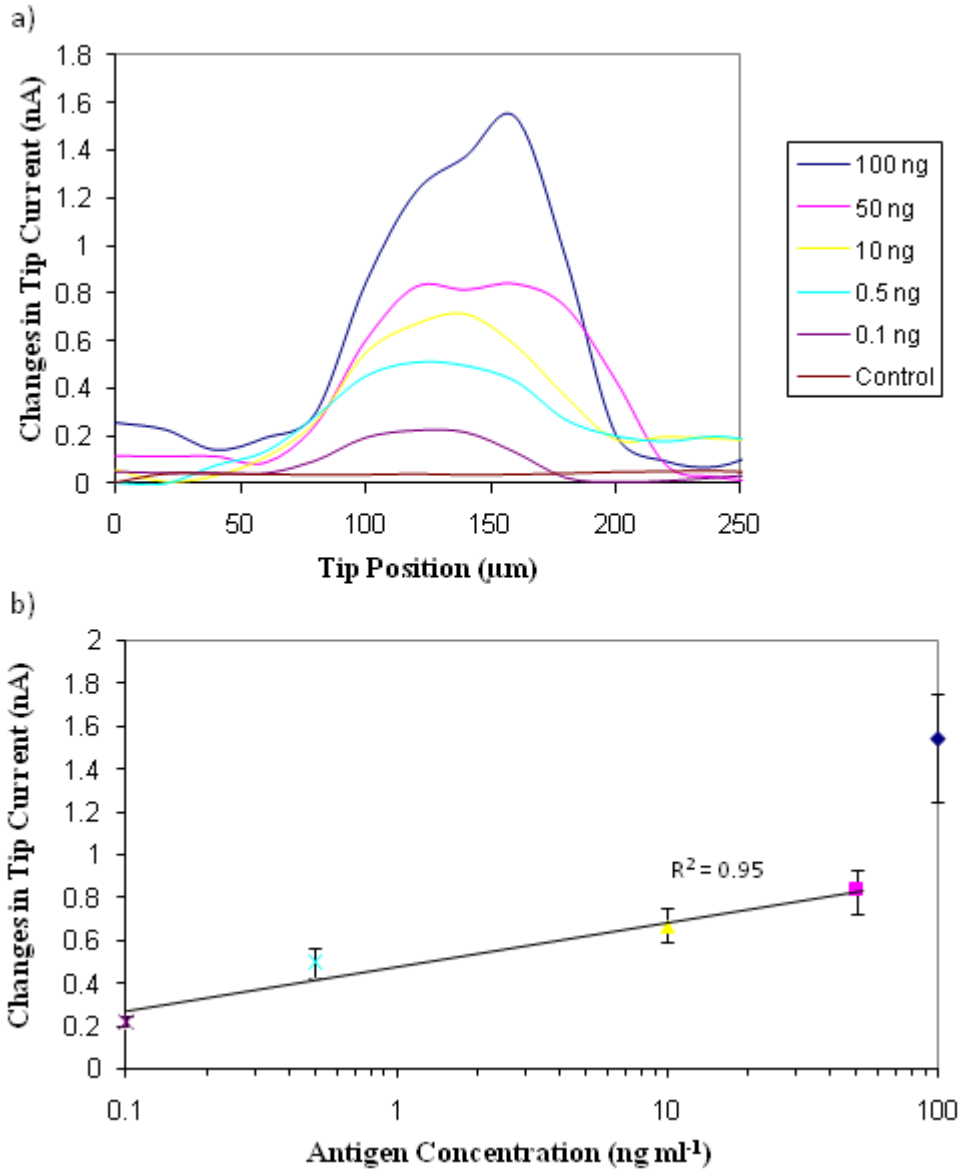

Figure 8.6: (a) Mean changes of a twelve dot array scan (n = 12) taken over PEI/neutravidin/biotinylated antibody surface area to various antigen concentrations (no error bars are included for clarity); (b) Calibration plot showing changes in current measured (n = 12) vs. ciprofloxacin concentration in milk. (Note, the y scale is inverted compared to that in Figure 8.3b).

8.3 Conclusions

The main aim of this chapter was to explore the ability of the SECM to characterise a previously optimised impedance based immunosensor developed within the group (Tsekenis *et al*, 2008a). It was previously demonstrated that a linear increase of the impedance change with the $\log^{10}$ of concentration (R^2 = 0.98) was observed between concentrations of 0.1 - 100 ng mL^{-1}.

A polyelectrolyte film was constructed using biotinylated PEI, exposed to neutravidin and then the biotinylated antibody of interest, which in this case was ciprofloxacin. The platform was interrogated by SECM by undertaking an area scan of the biotinylated PEI/neutravidin/biotinylated antibody array before and after exposure to a variety of concentrations of the complementary antigen ciprofloxacin. After exposure to the antigen in PBS buffer a decrease in current was observed over the modified areas, whereas little change was observed over the non-modified carbon surface, thus indicating the binding of ciprofloxacin to the modified regions. As the antigen concentration being exposed to the array increased there was also an increase in the changes in tip current observed. To ensure that the binding events were specific to the antigen of interest scans were also conducted before and after exposure to the non-complementary antigen PSA showing a low level of non-specific binding over the entire array and not just specific to the modified regions.

These experiments were then repeated but instead of the ciprofloxacin antigen being in a buffer it was exposed to the array within a milk solution. Once again after exposure to the antigen, changes in the tip current were observed over the modified region, however, there was also a degree of change observed over the non-modified carbon surface of the array. This was due to absorbance of products from the milk onto the carbon surface resulting in a decrease in the conductivity of the carbon surface. Whereas the absorbance of products onto the carbon surface resulted in a decrease in tip current, changes over the modified regions resulted in an increase of tip current change; this was due to the formation of positively charged chelation complexes.

The limits of detection for ciprofloxacin in this experiment are comparable to those obtained in previous work (Tsekenis *et al*, 2008a) based upon an AC impedance protocol. The results observed using the SECM were also able to detect binding events at concentrations as low as 0.1 ng ml^{-1} and was able to detect the free ciprofloxacin in PBS and the chelated ciprofloxacin present in the milk. The results indicate that the antigen concentration could be extended further to higher concentrations. A corrected linear response was demonstrated with an R^2 value of 0.96 for the antigen in buffer between 0.1 - 100 ng ml^{-1}, this dropped to an R^2 value of 0.77 for the antigen in buffer between 0.1 – 100 ng ml^{-1} when looking at the antigen in semi-skimmed milk. However, an R^2 value of 0.95 can be observed when looking at antigen concentrations in milk between the values of 0.1 – 50 ng ml^{-1}.

Chapter 9
Characterisation of DNA biosensor by SECM

9. Characterisation of DNA biosensor by SECM

9.1 Introduction

This chapter describes the use of scanning electrochemical microscopy for the further characterisation of a DNA biosensor previously developed within the group (Davis *et al*, 2005; Roberts *et al*, 2009). The work successfully demonstrates the usefulness of the technique in biosensor development, whilst also highlighting the possibility of using SECM for the label-less detection of DNA hybridisation.

The ability to detect specific DNA sequences in real time is currently being utilised in diagnostic tests used within various sectors such as forensic science, environmental regulation, food sciences and in the health sector. (MacPherson *et al*, 1993; Wang, 1997; Lucarelli *et al*, 2002; Babkina, 2004).

In 1993 Millan and Mikkelsen first introduced the concept of a DNA biosensor. The DNA biosensor works by recognising a DNA hybridisation event and converts it into a detectable signal which is then interpreted by the analytical device (see Figure 9.1). In most systems a single stranded DNA sequenced is immobilised onto a surface which is then exposed to a hybridisation solution which may contain the target sequences. If the solution does contain the complementary sequence, complementary binding may occur. A transducer will then detect the binding event – which may be based on gravimentric, optical or electrochemical approaches (Okumura 2005).

The ability to use electrochemical techniques for the detection of DNA hybridisation offers many advantages over the current alternative DNA assaying techniques. Electrochemical detection could potentially offer much higher sensitivity and are compatible with modern microfabrication technologies.

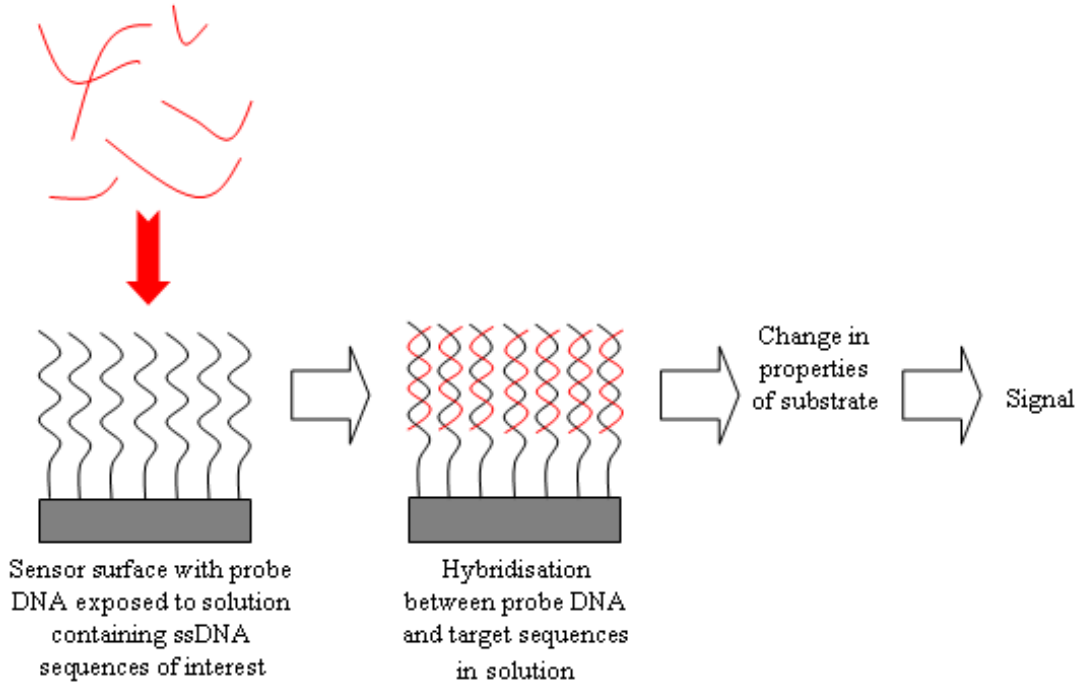

Figure 9.1: Schematic illustrating principle of DNA biosensor.

In the majority of electrochemical strategies for detecting DNA hybridisation a redox-active hybridisation indicator is used, the indicator has a greater affinity for double stranded over single stranded DNA (e.g. Hashimoto, 1994). In these systems a single stranded oligonucleotide sequence is funtionalised onto the electrode, which is then exposed to a solution which may contain the opposite target sequence. On the formation of the duplex, the indicator (which may be a groove binder, intercalator or cationic metal complex) preferentially binds to the double stranded region, which results in an increase in the local concentration of the indicator at the surface of the electrode. This can now be detected by electrochemical approaches such as chronoamperometric or cyclic voltammetry (Hashimoto *et al*, 1994; Millan and Mikkelsen, 1993; Kelley *et al*, 1997).

Zhou *et al* (2005), recently reported danthron (1,8-dihydroxy-anthraquinone) as having the ability to intercalate with DNA discriminating between DNA in its single and double stranded forms. A more well characterised intercalator, daunomycin, is known to bind to the guanine residue within the DNA duplex – limits of detection of 2.3 x 10^{-14} mol/L of target oligonucleotide using daunomycin and mercaptoacetic acid coated magnetite nanoparticles haven previously been reported (Cheng *et al*, 2005).

Whilst electrochemical labelling has potential in the development of a rapid sensing technology, there is greater scope for the direct, label-less detection of DNA hybridisation by electrochemical methods. By removing the necessity for labelling, sensors would be capable of offering faster responses, requiring fewer reagents, which would result in them becoming an extremely attractive route of investigation. The label-free detection of DNA hybridisation by doping electropolymerised conducting (poly)pyrrole films and monitoring the current-time profiles on the addition of complementary DNA sequences to the system was successfully developed by Wang *et al* (1999). In a similar system, detection limits of 1.6 fmol of complementary oligonucleotide target in 0.1ml was reported by Komarova *et al* (2005).

Within this chapter, further to a DNA biosensor previously developed within the group and interrogated by scanning electrochemical microscopy (Davis *et al* 2005; Roberts *et al*, 2009) the possibility of detecting the binding event of short oligonucleotides is investigated. The biosensor is based on the modification of a carbon electrode with a biotinylated oligonucleotide/polyelectrolyte film which is then exposed to a solution containing either non-complementary or complementary single stranded oligonucleotides.

Previously, when looking at whole genomic DNA, changes in the charge transfer properties of the film were monitored by impedimetric approaches. It was found that on exposing a carbon electrode modified with a polyethylenimine (PEI)/ssDNA film to a solution containing complementary ssDNA, the impedance of the system dropped approximately 10% over the course of three hours, after which time the impedance was

observed to plateau. In contrast, on exposing the ssDNA/PEI film to non-complementary DNA, the impedance of the system increased slightly. When interrogated with SECM it was found that on exposure to the complementary genomic DNA, the charge transfer properties of the ssDNA/PEI film were enhanced. This was also true for non-complementary exposure, although to a lesser degree.

By interrogating a similar system incorporating shorter oligonucleotides sequences, valuable insights may be obtained regarding the fabrication of this biosensor and the applicability of SECM to detecting DNA hybridisation. SECM offers a route for non-contact electrochemical interrogation, negating the need for hard-wired electrodes; this in turn offers the potential for developing an array based approach which may be interrogated via a scanning probe tip.

The aim of the work presented in this chapter is to conduct a preliminary investigation into whether SECM may be used to differentiate between non-complementary and complementary short oligonucleaotide hybridisation.

9.2 Results and Discussion

9.2.1 Detection of oligonucleotide binding by SECM

As described in the methods section (Chapter 3) the patterned array was achieved using the SECM micro-positioning XYZ stage. A capillary was filled with the biotinylated polyelectrolyte (PEI) and lowered towards the carbon substrate. By observing the small meniscus at the tip of the pulled capillary, it was possible to determine the point at which contact was made and when the deposition of the PEI droplet was achieved. After deposition, the tip was retracted and moved in the X or Y direction respectively and the process repeated. This array was then exposed to the biotinylated oligonucleotide Sp_cap1 (sequence 5' – 3' TTTTAACAGCCCCTCGACAC (20)).

A screen-printed carbon electrode substrate with the array was placed in a plastic Petri dish and exposed to 5 mmol l^{-1} mediator solution (ferrocenecarboxylic acid). The SECM working electrode tip and counter and reference electrodes were then immersed into the mediator solution. Prior to undertaking an area scan over the biotinlyated oligonucleotide/PEI functionalised regions, an approach curve experiment was conducted over the polycarbonate - non-conductive region of the substrate to estimate the tip-to-substrate distance (Tip Potential (E) = +0.45 V vs. Ag/AgCl; step size = 10 µm). The tip was positioned at a distance at which the measured current was half that of the observed current with the tip a few mm distant from the surface of the screen printed electrode (effectively infinite on this scale); this was to allow for the variation in topography and the height differential between this non-carbon region and the slightly raised carbon electrode surface - while also serving to reduce the risk of tip crash. After tip positioning, an area scan over the functionalised region was conducted with a step size of 10 µm. At no point in the experiment was the substrate touched; this allowed any change in the observed tip current to be attributed solely to changes in the charge transfer properties of the surface. In all cases the tip diameter was 8.5µm; the scan rate used was 10 µm per step throughout and there was no potential applied to the substrate.

After the first area scan experiment was conducted, the tip was retracted a known safe distance from the substrate. The mediator solution was then removed and the substrate gently rinsed with UHQ water before applying a solution containing either the complementary oligonucleotide Sp_rep1 (sequence 5' – 3' GTGTCGAGGGGCTGTTAAAA (20)) or the non-complementary oligonucleotide Sp_rep2 (sequence 5' – 3' GATAGACTCGCAGTTTCTAGAC (22)). After exposure for 30 mins, the antigen solution was then removed and the substrate again rinsed before the re-introduction of fresh mediator solution. A second area scan experiment was then conducted over the same functionalised area as measured previously. The tip current data from the area scan before exposure was then subtracted from the tip current data following this exposure. Throughout all these experiments the sample substrate does not move at all, i.e. all exposures, rinsing steps etc are performed with the sample *in situ.* It is worth noting here that after each exposure and rinsing step the Petri dish is refilled with fresh mediator solution and the tip exactly repositioned, made possible using the XYZ micro-positioning stage of the SECM270. This allows precise and reproducible imaging of the same area of the electrode. Differences in the pH of samples tested would have very little effect as the area of interest is rinsed well and the scan is conducted in the coupled buffer solution.

Changes in the absolute feedback in current at the tip are shown (Figure 9.2) for the exposure to the complementary oligonucleotides sequence Sp_rep1 (sequence 5' – 3' GTGTCGAGGGGCTGTTAAAA (20)). Figure 9.2a depicts the scan over the dotted array showing the change in feedback measured, with Figure 9.2b showing a line plot of the before and after scans indicating the changes observed when the array was exposed to the complementary sequence. It is clear from these line plots that there are changes to the tip current over the modified dotted substrate, with a clear increase in current measured being observed. This is further demonstrated in when looking at the absolute change in current measured for the area scan. Figure 9.2a clearly depicts an increase in current observed over the modified regions of the carbon; it is also worth noting that only very small changes in current are observed on the untreated carbon surface resulting in a small drop in the current measured.

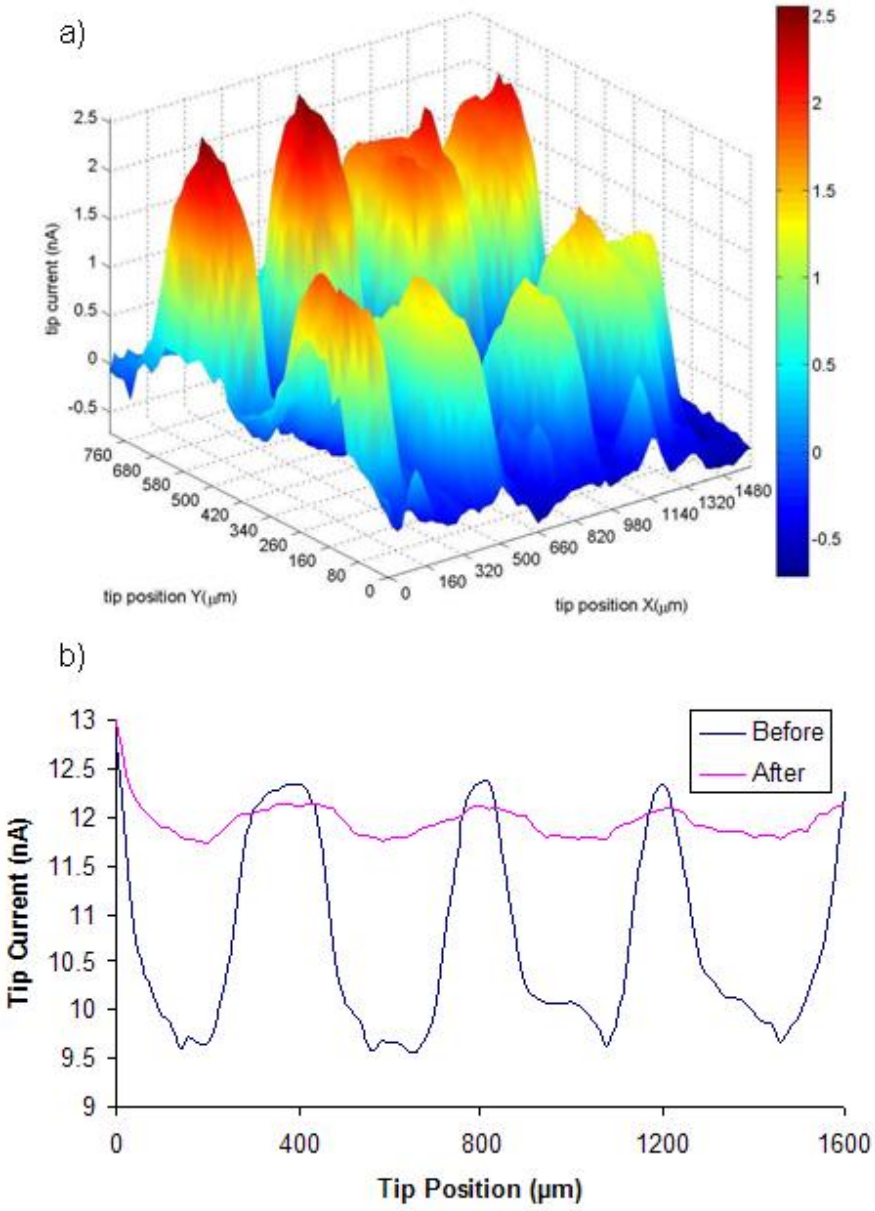

Figure 9.2: (a) 3D representation of the data obtained from a SECM scan of a PEI/avidin/biotinylated oligonucleaotide array on a screen-printed carbon electrode showing absolute change in feedback after exposure to complementary oligonucleotide sequence; (b) Line plot of a PEI/avidin/biotinylated oligonucleotide array on a screen-printed carbon electrode; before and after exposure to complementary oligonucleotide sequence.

Changes in the absolute feedback in current at the tip are shown (Figure 9.3) for the exposure to the complementary oligonucleotides sequence Sp_rep2 (sequence 5' – 3' GATAGACTCGCAGTTTCTAGAC (22)). Figure 9.3a depicts the scan over the dotted array showing the change in feedback measured, with Figure 9.3b showing a line plot of the before and after scans indicating the changes observed when the array was exposed to the non-complementary sequence. Once again there are changes to the tip current over the modified dotted substrate, with an increase in current measured being observed. This is also shown when looking at the absolute change in current measured for the area scan. However, it is also clear that those changes observed are to a much smaller degree than when the array was exposed to the complementary sequence. Figure 9.2a depicts the increase in current observed over the modified regions of the carbon; it is also worth noting that as with the complementary oligonucleotide exposure only very small changes in current are observed on the untreated carbon surface resulting in a small drop in the current measured.

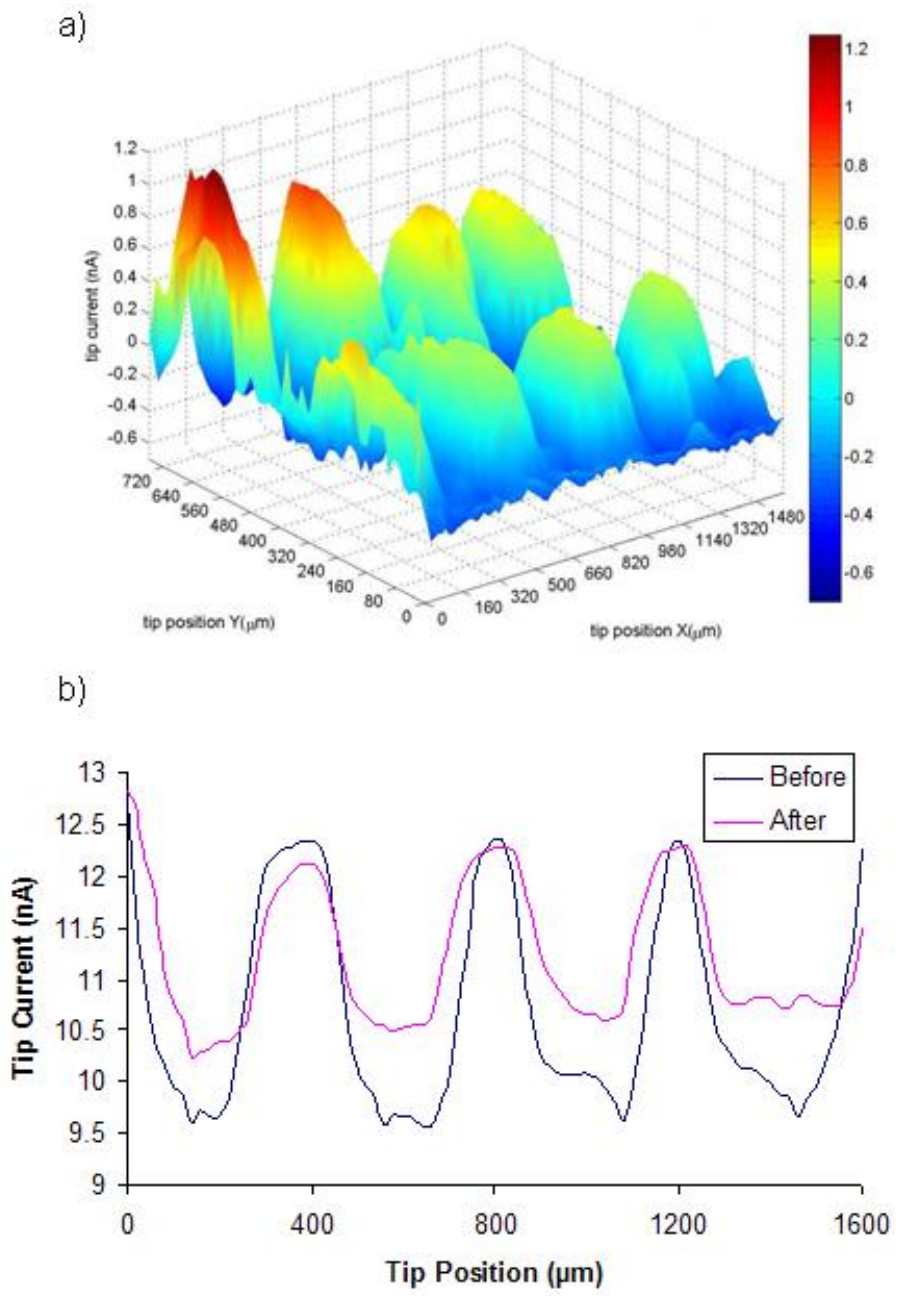

Figure 9.3: (a) 3D representation of the data obtained from a SECM scan of a PEI/avidin/biotinylated oligonucleaotide array on a screen-printed carbon electrode showing absolute change in feedback after exposure to non complementary oligonucleotide sequence; (b) Line plot of a PEI/avidin/biotinylated oligonucleotide array on a screen-printed carbon electrode; before and after exposure to non-complementary oligonucleotide sequence.

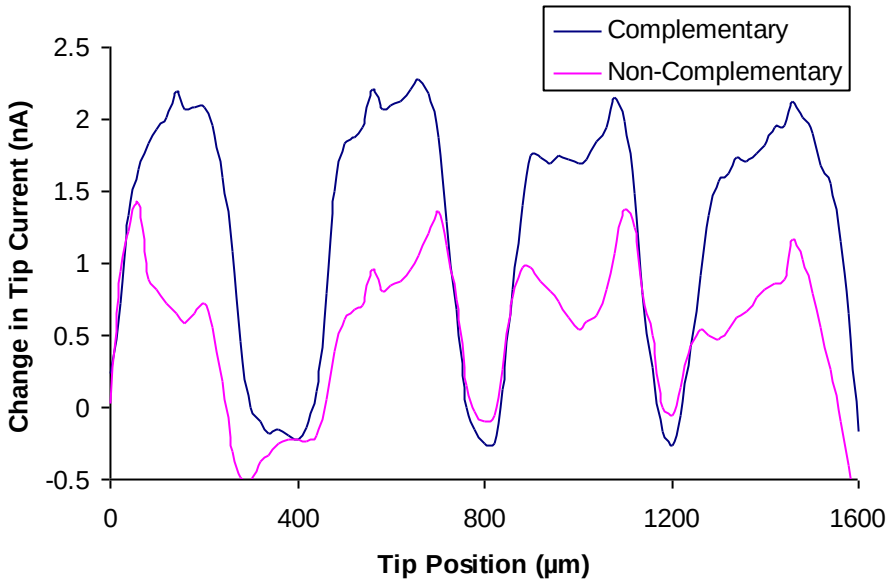

Figure 9.4: Linescans illustrating difference in feedback response after exposure to complementary and non-complementary oligonucleotide sequences.

The data presented in Figure 9.4 are the representative linescans from the arrays formed by the subtraction of the array data obtained before and following the exposure of the PEI/avidin/biotinylated oligonucleotide array to complementary and non-complementary oligonucleotide sequences plotted together on the same axis. It may be observed that the magnitude of change is more pronounced in the complementary experiment. This result would suggest that on exposure of the PEI/avidin/biotinylated oligonucleotide film to a hybridisation solution containing the complementary oligonucleotide sequence, a more significant effect on the feedback response of the polyelectrolyte film is observed than the exposure of the film to non-complementary oligonucleotide sequence.

A possible suggestion as to why the changes in feedback current were observed is based on the ability of DNA in conducting charge. Kara *et al* (2002), carried out a series of differentiated pulse voltammetry techniques on both ssDNA and dsDNA in methylene blue (MB). Their results suggested that ssDNA produced an increased voltametric reduction

signal of the MB when compared to the dsDNA. It was suggested that these results were contributed to the availability of guanine bases, since the interaction of MB and guanine bases have been previously well described.

It is assumed that on exposure to the solution containing complementary oligonucleotide sequence, complementary binding occurs, where regions of PEI/avidin/biotinylated oligonucleotide have been previously immobilised. This complementary pairing results in regions of double stranded DNA forming on the surface of the sensor which resulted in an increase of signal when interrogated with the SECM. It could be possible that the smaller enhancements observed with the non-complementary experiments are due to a lesser degree of binding occurring between non-complementary strands and mis-matching which may occur when non-complementary binding occurs. This would result in their still being a change in signal occurring but to a much lesser degree.

Evidence for this type of behaviour comes from earlier work on DNA where the charge on the mediator is found to determine the electrochemical response at the surface. DNA is an anionic polymer due to the presence of phosphate groups and when an anionic mediator is utilised (ferricyanide), increasing the amount of DNA at the surface by hybridisation led to a decrease in current transfer due to repulsion and inhibition of mediator diffusion (Turcu *et al*, 2004a). However when a cationic hexaamine ruthenium mediator was used, increasing the amount of DNA led to an increase in current transfer (Roberts *et al*, 2009). This is thought to be due to the cationic mediator associating with the anionic DNA, thereby increasing the local concentration of mediator at the surface and enhancing electron transfer between the surface and the probe tip.

9.3 Conclusions

The main aim of this chapter was to explore the ability of the SECM to further characterise a previously optimised impedance based DNA biosensor developed within the group (Davis *et al* 2007, Roberts *et al*, 2009). It was previously demonstrated that the impedance of the sensor dropped by approximately 10% in 3 hrs when exposed to a hybridisation solution containing single stranded complementary genomic DNA. When the sensor was exposed to a buffered solution of non-complementary single stranded DNA, the impedance was observed to marginally increase.

A polyelectrolyte film was constructed using biotinylated PEI, exposed to neutravidin and then the biotinylated oligonucleotide sequence Sp_cap1 (sequence 5' – 3' TTTTAACAGCCCCTCGACAC (20)). The platform was interrogated by SECM by undertaking an area scan of the PEI/neutravidin/biotinylated oligonucleotide array before and after exposure to a complementary and non-complementary oligonucleotide sequence (Sp_rep1 sequence 5' – 3' GTGTCGAGGGGCTGTTAAAA (20) and Sp_rep2 sequence 5' – 3' GATAGACTCGCAGTTTCTAGAC (22), respectively). After exposure to the complementary oligonucleotide sequence an increase in current was observed over the modified areas, whereas little change was observed over the non-modified carbon surface, thus indicating the binding of the oligonucleotide sequence to the modified regions. After exposure to the non-complementary oligonucleotide sequence, an increase in current was also observed of smaller magnitude due to a lesser degree of binding occurring between non-complementary strands and mis-matching which may occur when non-complementary binding occurs.

Chapter 10
General Conclusions

10. General Conclusions

Scanning electrochemical microscopy (SECM) is a scanning probe technique which allows the interrogation of the electrochemical and topographical properties of a variety of surfaces. The technique has been used in a variety of fields and its application to studying biological systems is well documented. Within this work the optimisation of microelectrode fabrication and characterisation of carbon ink surfaces was conducted.

The first aim of this work involved the fabrication and characterisation of microelectrodes leading to the production of robust, reproducible and cost-effective microelectrodes to be used in conjunction with the SECM. The fragile nature of the Pt-quartz fibres used, made polishing exceptionally difficult and problems were encountered at times with getting an electrical connection between the Pt-quartz fibre and the wire which was to be connected to the potentiostat cabling. The geometry of the tips produced was relatively consistent as there was very little deviation in the fibres position relative to the insulating glass surround during sealing with the technique applied. The robust construction of the probes allowed them to be used on the SECM270 without undue damage occurring due to the clamping system for holding the probe in position. By taking aspects of existing electrode designs and incorporating them into a single model, an electrode with a unique combination of desirable qualities has been produced.

The second SECM application explored in this project involved the characterisation of a variety of immunosensors previously.

In the immunosensors previously developed within our group, cyclic voltammetry was utilized to deposit polyaniline films on the carbon electrodes. This was deemed inappropriate for the preparation of electrodes to be interrogated by SECM as it was not possible to compare a modified region with an unmodified region. Any changes in the tip current obtained may have been due to fluctuations in the background current and not due to changes in the charge transfer properties of the modified substrate. Therefore, it was

necessary for the polyelectrolyte film to be patterned in an array dot format. By producing this pattern, background effects in the measured current were eliminated and any changes in the current over the modified surface contrasted with the current over regions of unmodified carbon. It was not possible to use polyaniline in this format and therefore, PEI which has previously been used within the group when interrogating DNA arrays with SECM was utilised.

It has successfully been demonstrated within this thesis for the potential of utilising the SECM to image arrays of immobilised antibodies and furthermore detect the binding of the antigen using a label-free protocol. For NSE a clear relationship between the antigen concentration and the changes in the signals obtained for binding to the arrays was observed. A calibration profile showed a clear correlation of change in current with respect to antigen concentration with detection limits of 0.5 pg ml^{-1} to 200 pg ml^{-1}. A clear relationship was also observed when looking at the relationship between PSA concentration and the changes in the signals obtained. The results observed showed the detection of binding events at concentrations as low as 1 pg ml^{-1} and the possibility of discrimination at higher concentrations than those previously observed with detection of up to 200 pg ml^{-1}. When investigating the binding events of NTx the sensors showed a clear linear response with an increase in the change of current observed as the antigen concentration increased. The SECM detection levels were within the same range as the ELISA standards demonstrating that saturation does not seem to occur and act as a limiting factor. For the detection of ciprofloxacin it was demonstrated that the presence of the antigen could be detected in both a buffer and in milk showing that it was possible to detect both free and chelated ciprofloxacin. Once again clear relationships were observed as anigen conacentration increased to the change in current response. This was demonstrated in both the free ciprofloxacin and the chelated format.

The results obtained within this work demonstrate the feasibility of using the SECM to analyse surface binding of antigens. This technique although slower than fluorescent

methods, has a significantly lower cost base and does not require labelling of any kind, including fluorescence of samples.

The final SECM application explored the characterisation of the PEI/neutravidin/biotinylated oligonucleotide sequence array and the detection of hybridisation of both complementary and non-complementary oligonucleotide sequences. It was found that on exposure to the complementary oligonucleotide sequence, the charge transfer properties of the modified array increased. This was also demonstrated however, when the array was exposed to the non-complementary oligonucleotide sequences although it was to a lesser degree.

This work demonstrates the applicability of SECM to detecting changes in the charge transfer properties of a film and highlights the potential of the technique to feature in the development of a label-less approach to detecting DNA hybridisation. Although the technique currently has limitations in comparison to the fluorescence technique for example, it holds great promise in terms of providing a sensitive, cost effective platform for detecting DNA hybridisation and also, characterising DNA biosensors based on electrochemical techniques.

Table 10.0: Table indicating the limits of detection of commercial ELISA kits compared to those demonstrated by the SECM

Antigen	SECM LOD	ELISA LOD
NSE	0.5 pg ml^{-1}	1.9 ng ml^{-1}
PSA	1 pg ml^{-1}	1 ng ml^{-1}
Ciprofloxacin	0.1ng ml^{-1}	6 ng g^{-1}

Chapter 11

Suggestions for Further Work

11. Suggestions for Further Work

Development of SECM as an antibody/antigen microarray platform

The works reported in Chapters 5-8 were focused towards the characterisation of a carbon ink surface which could become a platform for a label free based antibody/antigen interaction sensor using a variety of antibodies. With the aim of developing this technique as a high throughput hybridisation technology, further work may include:

- multiple antibodies for a variety of specific disease states onto one array platform.
- platform to include positive and negative controls to determine reliability of test
- to investigate the possibility of developing a method for quantifying results on one array rather than the need to carry out an number of repeats
- to investigate the different antibody interactions to have a fuller understanding of the effect on electrochemical changes.
- the investigation of the hybridisation of same system using another, non-electrochemical analytical technique – such as, lateral flow, ELISA or fluorescence microscopy.
- a study of the use of alternative, topographically flat substrates to serve as an immobilisation platform for the bio-polyelectrolyte film.

Development of SECM as a high throughput DNA microarray platform

The work reported in Chapter 9 was focused towards the characterisation of a carbon ink surface which could become a platform for a label free based DNA hybridisation sensor using short oligonucleotides. With the aim of developing this technique as a high throughput hybridisation technology, further work may include:

- a number of known oligonucleotides sequences for a variety of specific disease states onto one array platform.
- to investigate different length oligonucleotides to have a fuller understanding of the effect of length on electrochemical changes.
- the investigation of the hybridisation of same system using another, non-electrochemical analytical technique – such as, for example, QCM or fluorescence microscopy.
- a study of the use of alternative, topographically flat substrates to serve as an immobilisation platform for the bio-polyelectrolyte film.

Chapter 12

References

Adams, B.L., Vlahou, A., Semmes, O.J. and Wright, G.L. (2001) Proteomic approaches to biomarker discovery in prostate and bladder cancers. *Proteomics*, **1**, 1264-1270.

Adams, R.N. (1958) Carbon Paste Electrodes. *Analytical Chemistry*, **30**, 1576-1576.

Adamson, J., Beswick, A. and Ebrahim, S. (2004) Is stroke the most common cause of disability? *Journal of Stroke and Cerebrovascular Diseases*, **13**, 171-177.

Alvarez-Icaza, M. and Bilitewski, U. (1993) A mediated amperometric enzyme electrode using tetrethiafulvalene and L-glutamate oxidase for the determination of L-glutamic acid. *Analytica chimica acta*, **282**, 353-361.

Amemiya, S., Guo, J., Xiong, H. and Gross, D.A. (2006) Biological applications of scanning electrochemical microscopy: Chemical imaging of single living cells and beyond. *Analytical and Bioanalytical Chemistry*, **386**, 3, 458-471.

Apone, S., Fevold, K., Lee, M. and Eyre, D.R. (1998) A rapid method for quantifying osteoclast activity in vitro. *J. Bone Miner. Res.*, **9**, S178.

Ball, P. (2000) Quinolone generations: natural history or natural selection? *Journal of Antimicrobial Chemotherapy*, **46**, 17-24.

Banse, X., Devogelaer, J.P., Lafosse, A., Sims, T.J., Grynpas, M. and Bailey, A.J. (2002a) Cross-link profile of bone collagen correlates with structural organization of trabeculae. *Bone*, **31**, 70-76.

Banse, X., Sims, T.J. and Bailey, A.J. (2002b) Mechanical properties of adult vertebral cancellous bone: correlation with collagen intermolecular cross-links. *J. Bone Miner. Res.*, **17**, 1621-1628.

Bard, A.J. and Faulkner, L.R., (2001) Electrodhemical Methods, Fundamentals and Applications (2nd Ed.) John Wiley & Sons, Inc.

Bard, A.J. and Mirkin, M.V. (2001) Scanning Electrochemical Microscopy. Printed by Marcel Dekker, Inc. New York.

Bard, A.J., Denault, G., Friesner, R.A., Dornblaser, B.C. and Tuckerman, L.S. (1991) Scanning electrochemical microscopy: Theory and application of the transient (chronoamperometric) SECM response. *Analytical Chemistry*, **63**, 1282-1288.

Bard, A.J., Denault, G., Lee, C., Mandler, D. and Wipf, D.O. (1990) Scanning electrochemical microscopy: A new technique for the characterization and modification of surfaces. *Accounts of Chemical Research*, **23**, 357-363.

Bard, A.J., Fan, F.R., Kwak,J. and Lev, O. (1989) Scanning electrochemical microscopy. Introduction and principles. *Analytical Chemistry*, **61**, 132-138.

Bard, A.J., Mirkin, M.V., Unwin, P.R. and Wipf, D.O. (1992) Scanning electrochemical microscopy. 12. Theory and experiment of the feedback mode with finite heterogeneous electron-transfer kinetics and arbitrary substrate size. *Journal of Physical Chemistry*, **96**, 1861-1875.

Barton, A.C., Collyer, S.D., Davis, F., Garifallou, G.Z., Tsekenis, G., Tully, E., O'Kennedy, R., Gibson, T., Millner, P.A. and Higson, S.P.J (2009) Labeless AC impedimetric antibody-based sensors with pgml(-1) sensitivities for point-of-care biomedical applications. *Biosens. Bioelectron.*, **24(5)**, 1090-5.

Barton, A.C., Davis, F., Higson, S.P.J. (2008a) Labeless Immunosensor Assay for the Stroke Marker Protein Neuron Specific Enolase Based upon an Alternating Current Impedance Protocol**.** *Anal. Chem.*, **80**, 9411-9416.

Barton, A.C., Davis, F., Higson, S.P.J. (2008b) Labeless Immunosensor Assay for Prostate Specific Antigen with Picogram per Milliliter Limits of Detection Based upon an ac Impedance Protocol. *Anal. Chem.*, **80**, 6198-6205.

Barton, D., Bradley, J.W., Steele D.A. and Short, R.D. (1999) Investigating radio frequency plasmas used for the modification of polymer surfaces. *Journal of Physical Chemistry*, **103**, 4423-4430.

Bath, B.D., Scott, E.R., Phipps, J.B. and White, H.S. (2000) Scanning electrochemical microscopy of iontophoretic transport in hairless mouse skin. Analysis of the relative contributions of diffusion, migration, and electroosmosis to transport in hair follicles. *Journal of Pharmaceutical Science*, **89**, 1537-1549.

Belldegrun, A.S., Franklin, J.R., O'Donnell, M.A., Gomella, L.G., Klein, E., Neri, R., Nseyo, U.O., Ratliff, T.L. and Williams, R.D. (1998) Superficial bladder cancer: the role of interferon-alpha. *J Urol.*, **159(6)**, 1793-1801.

Berger, C.E.M., Rathod, H., Gillespie, J.I., Horrocks, B.R. and Datta, H.K. (2001) Scanning electrochemical microscopy at the surface of bone-resorbing osteoclasts: Evidence for steady-state disposal and intracellular functional compartmentalization of calcium. *Journal of Bone and Mineral Research*, **16**, 2092-2102.

Bishai, W. (2002) Current issues on resistance, treatment guidelines, and the appropriate use of fluoroquinolones for respiratory tract infections. *Clinical Therapeutics* **24**, 838-850.

Blondeau, J. M. (2004) Fluoroquinolones: Mechanism of action, classification, and development of resistance. *Survey of ophthalmology*, **49**, 73-78.

Bogialli, S., D'Ascenzo, G., Di Corcia, A., Lagana, A. and Nicolardi, S. (2008) A simple and rapid assay based on hot water extraction and liquid chromatography-tandem mass spectrometry for monitoring quinolone residues in bovine milk. *Food Chemistry*, **108**, 354-360.

Bollo, S., Yáñez, C., Sturm, J., Núñez-Vergara, L. and Squella, J.A (2003) Cyclic Voltammetric and Scanning Electrochemical Microscopic Study of Thiolated β-Cyclodextrin Adsorbed on a Gold Electrode. *Langmuir*, **19(8)**, 3365–3370.

Borner, K., Lode, H., Hoffken, G., Prinzing, C., Glatzel, P. and Wiley, R. (1986) Liquid chromatographic determination of ciprofloxacin and some metabolites in human body fluids. *J. Clin. Chem. Clin. Biochem.*,**24**, 325-331.

Bosch, J.L.H., Hop, W.C.J, Kirkels, W.J. and Schoder, F.H. (1995) Natural history of benign prostatic hyperplasia: appropriate case definition and estimation of its prevalence in the community. *Urology*, **46**, 34-46.

Briot, K. and Roux, C. (2005) What is the role of DXA, QUS and bone markers in fracture prediction, treatment allocation and monitoring? *Best Pract. Res. Clin. Rheumatol.*, **19**, 951-964.

Bruckenstein, S. (1987) Ohmic Potential Drop at Electrodes Exhibiting Steady-State Diffusion Currents. *Analytical chemistry*, **59**, 2098-2101.

Bucknall, S., Silverlight, J., Coldham, N., Thorne, L. and Jackman, R., (2003). Antibodies to the quinolones and fluoroquinolones for the development of generic and specific immunoassays for detection of these residues in animal products *Food Additives and Contaminants*, **20**, 221-228.

Cannes, C., Kanoufi, F. and Bard, A.J. (2002) Cyclic Voltammetric and Scanning Electrochemical Microscopic Study of Menadione Permeability through a Self-Assembled Monolayer on a Gold Electrode. *Langmuir*, **18 (21)**, 8134–8141.

Carano M., Holt K.B. and Bard A.J. (2003) Scanning Electrochemical Microscopy. 49. Gas-Phase Scanning Electrochemical Microscopy Measurements with a Clark Oxygen Ultramicroelectrode. *Analytical Chemistry*, **75**, 5071-5079.

Chai, G., Brewer, J.M., Lovelace, L.L., Aoki, T., Minor, W., Lebioda, L. (2004) Expression, purification and the 1.8 angstroms resolution crystal structure of human neuron specific enolase. *J. Mol. Biol.*, **341**, 1015-21.

Chan, D.W. and Sokoll, L.J. (1999) Prostate-specific antigen: advances and challenges. *Clin. Chem.*, **45(6 Pt 1)**, 755-756.

Chapman, D.L. (1913) A contribution to the theory of electrocapilliarity. *Philosophical Magazine*, **25**, 475-481.

Chavassieux, P., Seeman, E. and Delmas, P.D. (2007) Insights into material and structural basis of bone fragility from diseases associated with fractures: how determinants of the biomechanical properties of bone are comprised by disease. *Endocr. Rev.*, **28**, 151-164.

Claypool, S.M., Dickinson, B.L., Yoshida, M., Lencer, W.L. and Blumberg, R.S. (2002) Functional reconstitution of human FcRn in madin-darby canine kidney cells requires co-expressed human β_2-microglobulin. *Journal of Biological Chemistry*, **277**, 28038-28050.

Clements, J.A., Rohde, P., Allen, V., Hyland, V.J., Samaratunga, M.L., Tilley, W.D., Lavin, M.F. and Gardiner, R.A. (1999) Molecular detection of prostate cells in ejaculate and urethral washings in men with suspected prostate cancer. *J Urol.*, **161(4)**, 1337-1343.

Compton, R.G., Coles, B.A., Gooding, J.J., Fisher, A.C. and Cox, T.I. (1994) Chronoamperometry at Channel Electrodes. Experimental Applications of Double Electrodes. *J. Phys. Chem.*, **98(9)**, 2446–2451.

Conyers, J.L. and White, H. S. (2000) Electrochemical Characterisation of Electrodes with Submicrometer Dimensions. *Analytical Chemistry*, **72**, 4441-4446.

Cosnier, S. (1999) Biomolecule immobilisation on electrode surfaces by entrapment or attachment to electrochemically polymerised films. A review. *Biosensors and Bioelectronics*. **14**, 443-456.

Csoka, B., Kovacs, B. and Nagy, G. (2003a) Scanning electrochemical microscopy inside the biocatalytic layer of biosensors: investigation of a double function complex multienzyme reaction layer, *Electroanalysis*, **1**5**(15–16)** 1335–1342.

Csoka, B., Kovacs, B. and Nagy, G. (2003b) Investigation of concentration profiles inside operating biocatalytic sensors with scanning electrochemical microscopy (SECM), *Biosensors and Bioelectronics*, **18(2–3)**, 141–149.

Davis, F., Nabok, A.V. and Higson, S.P.J. (2005) Species differentiation by DNA-modified carbon electrodes using an ac impedimetric approach. Biosensors and *Bioelectronics*, **20(8)**, 1531-1538.

Dayton, M.A., Brown, J.C., Stutts, K.J. and Wightman, R.M. (1980) Faradaic electrochemistry at microvoltammetric electrodes. *Analytical Chemistry*, **52**, 946-950.

Decher, G., Hong, J.D. and Schmitt, J. (1992) Build up of ultrathin multilayer films by a self-assembly process. 3. Consecutively alternating adsoption of anionic and cationic polyelectrolytes on charges surfaces, *Thin Solid Films*, **210**, 831-835.

Delmas, P.D., Eastell, R., Garnero, P., Seibel, M.J. and Stepan, J. (2000) The use of biochemical markers of bone turnover in osteoporosis. Committee of scientific advisors of the international osteoporosis foundation. *Osteoporos. Int.*, **11(6)**, S2-17.

Demaille, C., Brust, M., Tsionsky, M. and Bard A.J (1997) Fabrication and characterisation of self-assembled spherical gold UMEs. *Analytical Chemistry*, **69(13)**, 2323-2328.

Diamandis, E.P. (1998) Prostate-specific antigen or human kallikrein 3? Recent developments. *Tumour Biol.*, **19(2)**. 65-67, discussion 67-68.

Dobson, P.S. Weaver, J.M.R. and Holder, M.N. (2005) Characterisation of batch-microfabricated scanning electrochemical-atomic force microscopy probes. *Analytical chemistry*, **77(2)**, 424-434.

Duan, J. and Yuan, Z. (2001) Development of an Indirect Competitive ELISA for Ciprofloxacin Residues in Food Animal Edible Tissues, *Journal of Agricultural Food Chemistry*, **49**, 1087-1089.

Edwards, M.A., Martin, S., Whitworth, A.L., Macpherson, J.V. and Unwin, P.R. (2006) Scanning electrochemical microscopy: principles and applications to biophysical systems. *Physiological Measurement*, **27**, R63-R108.

Engstrom, R.C., Weber, M., Wunder, D.J., Burgess, R. and Winquist, S. (1986) Measurements within the diffusion layer using a microelectrode probe. *Analytical Chemistry*, **58**, 844-848.

Evans, S.A.G., Brakha, K., Billon, M., Mailley, P. and Denuault, G. (2005) Scanning electrochemical microscopy (SECM): Localized glucose oxidase immobilization via the direct electrochemical microspotting of polypyrrole-biotin films. *Electrochemistry Communications*, **7 (2)**, 135-140.

Eyre, D.R. (1995) The specificity of collagen cross-links as markers of bone and connective tissue degradation. *Acta, Orthop. Scan. Suppl.*, **266**, 166-170.

Fall, P.M., Kennedy, D., Smith, J.A., Seibel, M.J. and Raisz, L.G. (2000) Comparison of serum and urine assays for biochemical markers of bone resorption in postmenopausal women with and without hormone replacement therapy and in men. *Osteoporos. Int.*, **11**, 481-485.

Felsenberg, D. and Boonen, S. (2005) The bone quality framework: determinants of bone strength and their interrelationships, and implications for osteoporosis management. *Clin. Ther.*, **27**, 1-11.

Feng, W.J., Rotenberg, S.A. and Mirkin, M.V. (2003) Scanning electrochemical microscopy of living cells. 5. Imaging of fields of normal and metastatic human breast cells. *Analytical Chemistry*, **75**, 4148-4154.

Fernandez, J.L. and Bard, A.J (2003) Scanning Electrochemical Microscopy. 47. Imaging Electrocatalytic Activity for Oxygen Reduction in an Acidic Medium by the Tip Generation−Substrate Collection Mode. *Analytical Chemistry*, **75**, 2967-2974.

Fernandez, J.L. and Bard, A.J (2004) Scanning Electrochemical Microscopy 50. Kinetic Study of Electrode Reactions by the Tip Generation−Substrate Collection Mode. *Analytical Chemistry*, **76**, 2281-2289.

Fernandez, J.L., Mano, N., Heller, A. and Bard, A.J. (2004) Optimization Of Wired Enzyme O_2-Electroreduction Catalyst Compositions by Scanning Electrochemical Microscopy. *Angewandte Chemie*, **116**, 6515-6517.

Fleishmann, M., Ghoroghchian, J. and Pons, S. (1985) Electrochemical Behaviour of Dispersions of Spherical Ultramicroelectrodes. 1. Theoretical Considerations. *Journal Physical Chemistry*, **89**, 5530-5536.

Fonseca, S.M., Barker, A.L., Ahmed, S., Kemp, T.J. and Unwin, P.R. (2003) Direct observation of oxygen depletion and product formation during photocatalysis at a TiO2 surface using scanning electrochemical microscopy. *Chem commum*, **8**, 1002-1003.

Garay, M.F., Ufheil, J., Borgwarth, K., Heinze, J., (2004) Retrospective chemical analysis of tree rings by means of the scanning electrochemical microscopy with shear force feedback. *Physical Chemistry Chemical Physics*, **6**, 4028-4033.

Garifallou, G-Z., Tsekenis, G., Davis, F., Millner P.A., Pinacho, D. G., Sanchez-Baeza, F., Marco, M-P., Gibson, T. D., Higson, S. P. J. (2007) Labeless Immunosensor Assay for Fluoroquinolone Antibiotics based upon an AC Impedance Protocol. *Anal. Lett*., **40**, 1412-1442.

Garnero, P., Gineyts, E., Arbault, P., Christiansen, C. and Delmas, P.D. (1995) Different effects of bisphosphonate and estrogen therapy on free and peptide-bound bone cross-links excretion. *Journal of Bone and Mineral Res.*, **10**, 641-649.

Gaspar, S., Mosbach, M., Wallma, L., Laurell, T., Csoregi, E. and Schumann, W. (2001) A method for the design and study of enzyme microstructures formed by means of a flow-through microdispenser. *Analytical Chemistry*, **73**, 4254-4261.

Gertz, B.J., Shao, P., Hanson, D.A., Quan, H., Harris, S.T., Genant, H.K., Chesnut III, H.K. and Eyre, D.R. (1994) Monitoring bone resorption in early postmenopausal women by an immunoassay for cross-linked collagen peptides in urine. *Journal of Bone and Mineral Res.*, **9**, 135-142.

Gewirth, A. A. and Bard, A.J. (1988) In situ scanning tunneling microscopy of the anodic oxidation of highly orientated pyrolytic graphite surfaces. *Journal of Physical Chemistry*, **92(20)**, 5563-5566.

Gilmartin, M. and Hart, J.P. (1995) Development of one-shot biosensors for the measurement of uric-acid and cholesterol. *Analytical Proceedings*, **32(8)**, 341-345.

Gitlin, G., Bayer, E.A. and Wilchek, M. (1988a) Studies on the biotin-binding site of avidin. Tryptophan residues involved in the active site. *Biochemical Journal*, **250**, 291-294.

Gitlin, G., Bayer, E.A. and Wilchek, M. (1988b) Studies on the biotin-binding site of streptavidin. Tryptophan residues involved in the active site. *Biochemical Journal*, **256**, 279-282.

Glover, B.P. and McHenry. C.S. (2001) The DNA Polymerase III holoenzyme: an asymmetric dimeric replicative complex with leading and lagging strand polymerases. *Cell*, **105**, 925-934.

Goldstein, M.M. and Messing, E.M. (1998) Prostate and bladder cancer screening. *J Am. Coll. Surg.*, **186(1)**, 63-74.

Gonsalves, M., Macpherson, J.V., O'Hare, D., Winlove, C.P. and Unwin, P.R. (2000) High resolution imaging of the distribution and permeability of methyl viologen dication in bovine articular cartilage using scanning electrochemical microscopy. *Biochimica et Biophysica Acta (BBA) - General Subjects*, **1524 (1)**, 66-74.

Grahame, D.C. (1947) The electrical double layer and the theory of electrocapillarity. *Chemical reviews*, **41**, 441-501.

Gray, H. (1994) Gray's anatomy. Male Generative organ pp671-672. Edited by Parker JW & Son. The promotional reprint ltd.

Green, N.M. (1964) Molecular weight of avidin, *Biochemical Journal*, **92**, 16C-17C.

Green, N.M., Konieczny, L., Toms, E.J. and Valentine, R.C. (1971) The use of bifunctional biotinyl compounds to determine the arrangement of subunits in avidin. *Biochemical Journal*, **125**, 781-791.

Grennan, B., Killard, A.J. and Smyth, M.R. (2000) Physical characteristics of a screen printed electrode for use in an amperometric biosensor system. *Electroanalysis*, **13(8-9)**, 745-750.

Gretch, D.R., Suter, M. and Stinksi, M.F. (1987) The use of biotinylated monoclonal antibodies and streptavidin affinity chromatography to isolate herpes virus hydrophobic proteins or glycoproteins. *Analytical Biochemistry*, **163**, 270-277.

Groeneveld, A.J. and Brouwers, J.R. (1986) Quantitative determination of ofloxacin, ciprofloxacin, norfloxacin and perfloxacin in serum by high performance liquid chromatography. *Pharm. Weekb.*, **8**, 79-84.

Guo, Y., Guettouche, T., Fenna, M., Boellmann, F., Pratt, W.B., Toft, D.O., David F. Smith, D.F. and Voellmy, R. (2001) Evidence for a mechanism of repression of heat shock factor 1 transcriptional activity by a multichaperone complex. *J. of Bio.Chem*., **276**, 45791-45799.

Gyurcsanyi, R.E., Jagerszki, G., Kiss, G. and Toth, K. (2004) Chemical imaging of biological systems with the scanning electrochemical microscope. *Bioelectrochemistry*, **63 (1-2)**, 207-215.

Hanks, G.E. and Scardino, P.T. (1996) Does screening for prostate cancer make sense? *Sci. Am.*, **275(3)**, 114-115.

Hanson, D.A., Weis, M.A., Bollen, A.M., Maslan, S.L., Singer, F.R. and Eyre, D.R. (1992) A specific immunoassay for monitoring human bone resorption: quantitation fo type I collagen cross-linked N-telopeptides in urine. *J. Bone Miner. Res.*, **7**, 1251-1258.

Hartmann, A., Golet, E.M., Gartiser, S., Alder, A.C., Koller, T. and Widmer, R. M. (1999) Primary DNA Damage But Not Mutagenicity Correlates with Ciprofloxacin Concentrations in German Hospital Wastewaters. *Archives of Environmental Contamination and Toxicology*, **36,** 115-119.

Hiller, Y., Gershoni, J.M., Bayer, E.A. and Wilchek, M. (1987) Biotin binding to avidin. Oligosaccharide side chain not required for ligand association. *Biochemical Journal*, **248**, 167-171.

Isgro, F., Schmidt, C.H., Pohl. P. and Saggau.W. (1997) A predictive parameter in patients with brain related complications after cardiac surgery, *European Journal of Cardiothoracic Surgery*, **11**, 640-644.

Ju, H.S., Leung, S., Brown, B., Stringer, M.A., Leigh, S., Scherrer, C., Shepard, K., Jenkins, D., Knudsen, J. and Cannon, R. (1997) Comparison of analytical performance and biological variability of three bone resorption assays. *Clin. Chem.*, **43**, 1570-1576.

Jung, K., Meyer, A., Lein, M., Rudolph, B., Schnorr, D. and Loening, S.A. (1998) Ratio of free-to-total prostate specific antigen in serum cannot distinguish patients with prostate cancer from those with chronic inflammation of the prostate. *J. Urology*, **159**, 1595-1598.

Kanis, J.A. (2002) Diagnosis of osteoporosis and assessment of fracture risk. *Lancet*, **359**, 1929-1936.

Kara, P., Kerman, K., Ozkan, D., Meric, B., Erdem, A., Ozkan, Z. and Ozsoz, M. (2002) Electrochemical genosensor for the detection of interaction between methylene blue and DNA. *Electrochemistry Communications*, **4**, 705-709.

Kasai, S., Shiku, H., Torisawa, Y-S., Noda, H., Yoshitake, J., Shiraishi, T., Tomoyuki, Y., Watanabe, T., Matsue, T., Yoshimura, T. (2005) Real-time monitoring of reactive oxygen species production during differentiation of human monocytic cell lines (THP-1). *Analytica Chimica Acta*, **549 (1-2)**, 14-19.

Katemann, B.B. and Schuhmann, W. (2002) Fabrication and characterisation of needle-type Pt-disk nanoelectrodes. *Electroanalysis*, **14**, 22-28.

Katz, E. and Willner, I. (2003) Probing Biomolecular Interactions at Conductive and Semiconductive Surfaces by Impedance Spectroscopy: Routes to Impedimetric Immunosensors, DNA-Sensors, and Enzyme Biosensors, *Electroanalysis*, **15**, 913-947.

Kaya, T., Nishizawa, M., Yasukawa, T., Nishiguchi, T., Onouchi, T. and Matsue, T. (2001) A microbial chip combined with scanning electrochemical microscopy.

Biotechnology and Bioengineering, **76**, 391-394.

Kelley, S.O., Barton, J.K., Jackson, N.M. and Hill, M.G. (1997) Electrochemistry of methylene blue bound to a DNA-modified electrode. *Bioconjugate Chemistry*, **8**, 3-37.

Kierszenbaum, A.L. (2002) Keratins: unraveling the coordinated construction of scaffolds in spermatogenic cells. *Mol. Reprod. Dev.*, **61(1)**, 1-2.

King, C.R. (2000) Patterns of prostate cancer biopsy grading: trends and clinical implications. *Int. J Cancer*, **90(6)**, 305-311.

Korri-Youssoufi, H., Garnier, F., Srivasta, P., Godillot, P. and Yassar, A. (1997) Toward bioelectronics: specific DNA recognition based on an oligonucleotide-functionalised polypyrrole. *Journal of the American Chemical Society*, **119**, 7388-7389.

Kranz, C., Lotzbeyer, T., Schmidt, H.-L. and Schuhmann, W. (1997) Mapping of enzyme activity by detection of enzymatic products during AFM imaging with integrated SECM-AFM probes. *Biosensors and Bioelectronics*, **12 (4)**, 257-266.

Kwak, J.B. and Bard, A.J. (1989a) Scanning Electrochemical Microscopy. Apparatus and two dimensional scans of conductive and insulating substrates. *Analytical Chemistry*, 1794-1799.

Kwak, J.B. and Bard, A.J. (1989b) Scanning Electrochemical Microscopy. Theory of the feedback mode. *Analytical Chemistry*, **61**, 1221-1227.

Kwiatkowski, T.G., Libman, R.B., Frankel, M., Tilley, B., Morgenstern, L.B., Lu, M., Broderick, J., Marler, J., Brott, T and the NINDS t-PA Stroke Study Group. (1999) The NINDS rt-PA stroke study: Effects of tissue plasminogen activator for acute ischemic stroke at one year. *New England Journal of Medicine*, **340**, 1781-1787.

Laskowitz, D.T., Grocott, H., Hsia, A. and Copeland, K.R. (1998) Serum markers of cerebral ischemia. *Journal of Stroke and Cerebrovascular Disease*, **7**, 234-241.

Lee, C., Kwak, J. and Bard, A.J. (1990) Application of SECM to biological samples. *PNAS USA*, **87**, 1740-1743.

Lee, C., Miller, C.J. and Bard, A.J. (1991) Scanning electrochemical microscopy: Preparation of sub-micrometer electrodes. *Analytical chemistry*, **63(1)**, 78-83.

Lee, Y., Ding, Z.F. and Bard, A.J. (2002) Combined Scanning Electrochemical/Optical Microscopy With Shear Force and Current Feedback. *Analytical Chemistry*, **74**, 3634-3643.

Licitra, C.M., Brooks, R.G. and Sieger, B.E. (1987) Clinical efficacy and levels of ciprofloxacin in tissue in patients with soft tissue infection. *Journal of Antimicrobial Agents and Chemotherapy*, **31**, 805–807.

Liljeroth, P., Johans, C., Slevin, C.J., Quinn, B.M. and Kontturi, K. (2002) Micro Ring-Disk Electrode Probes for Scanning Electrochemical Microscopy. *Electrochemistry Communications*, **4**, 67-71.

Lindsay, R. (Chairman) (1997) Who are candidates for prevention and treatment for osteoporosis? *Osteoporos. Int.*, **7**, 1-6.

Lippuner, K., Golder, M. and Greiner, R. (2005) Epidemiology and direct medical costs of osteoporotic fractures in men and women in Switzerland. *Osteoporos Int*, **16**, S8-17.

Liu, B., Cheng, W., Rotenberg, S.A. and Mirkin, M.V. (2001) Scanning Electrochemical Microscopy of Living Cells - Part 2. Imaging Redox and Acid/Basic Reactivities. *J. Electroanalytical Chem.*, **500**, 590-597.

Liu, B., Rotenburg, S.A. and Mirkin, M.V. (2000) Scanning electrochemical microscopy of living cells: different redox activities of non-metastatic and metastatic human breast cells. *PNAS*, **97**, 9855-9860.

Liu, H.-Y., Fu-Ren, F.F., Lin, C.W. and Bard, A.J. (1986) Scanning Electrochemical and Tunnelling Ultramicroelectrode Microscope for High-Resolution Examination of Electrode Surfaces in Solution. *Journal of the American Chemical Society*, **108**, 3838-3839.

Lovdahl, M., Steury, J., Russlie, H. and Canafax, D.M. (1993) Determination of ciprofloxacin levels in chinchilla middle ear effusion and plasma by high performance liquid chromatography with fluorescence detection. *J. Chromatogr.*, **617**, 329-333.

Mackness, B.C. and McDonald M.J. (2010) Serum-based ALYGNSA immunoassay for the prostate cancer biomarker, total prostate-specific antigen (tPSA). *Anal. Bioanal. Chem.*, **397(7)**, 3151-4.

Mackness, B.C., Chourb, S., Farris, L.R. and McDonald, M.J. (2010) Polymer-protein-enhanced fluoroimmunoassay for prostate-specific antigen. *Anal. Bioanal. Chem.*, **396(2)**, 681-6.

Macpherson, J.V. and Unwin, P.R. (2000) Combined Scanning Electrochemical-Atomic Force Microscopy. *Analytical Chemistry*, **72**, 276-285.

Macpherson, J.V. and Unwin, P.R. (2005) Scanning Electrochemical Microscopy as an In Vitro Technique for Measuring Convective Flow Rates Across Dentine and the Efficacy of Surface Blocking Treatments. *Electroanalysis*, **17**, 197-204.

Marler, J.R. (1999) Early stroke diagnosis saves time. *Journal of the Annals of Emergency Medicine*, **33**, 450-451.

Marler, J.R., Tilley, B.C., Lu, M., Brott, T.G., Lyden, P.C., Grotta, J.C., Broderick, J.P., Levine, S.R., Frankel, M.P., Horowitz, S.H., Haley, E.C., Lewandowski, C.A. and Kwiatkowski, T.P. (2000) Early stroke treatment associated with better outcomes, The NINDS rt-PA Stroke Study. *Neurology*, **55**, 1649-1655.

Martens, P., Raabe, A. and Johnsson, P. (1998) Serum S-100 and neuron-specific enolase for prediction of regaining consciousness after global cerebral ischemia. *Stroke*, **29**, 2363-2366.

Martinez, M., McDermott, P. and Walker, R. (2006) Pharmacology of the fluoroquinolones: A perspective for the use in domestic animals. *The Veterinary Journal*, **172**, 10-28.

McCreery, R.L. (1991) Carbon electrodes: Structural effects on electron transfer kinetics, Dekker, New York, US.

Mello, L.D. and Kubota, L.T. (2002) Review of the use of biosensors as analytical tools in the food and drink industries. *Food Chemistry*, **77**, 237-256.

Miles, D.T., Knedlik, A. and Wipf, D.O. (1997) Construction of Gold Microbead Ultramicroelectrodes. *Analytical Chemistry*, **69**, 1240-1243.

Mirkin, V. and Bard, A.J. (1992) Simple analysis of quasi-reversible steady-state voltammograms. *Analytical Chemistry*, **64(19)**, 2293-2302.

Missler, U., Wiesmann, M., Friedrich, C. and Kaps, M. (1997) S-100 protein and neuron specific enolase concentrations in blood as indicators of infarction volume and prognosis in acute ischemic stroke. *Stroke*, **28**, 1956-1960.

Munteanu, F.D., Mano, N., Kuhn, A. and Gorton, L. (2002) Mediator-modified electrodes for catalytic NADH oxidation: high rate constants at interesting overpotentials. *Bioelectrochemistry*, **56**, 67-72.

Myers, R.A. (2006) Encyclopedia of analytical chemistry: applications, theory and instrumentation, Wiley.

Nash, A.F. and Melezinek, I. (2000) The role of prostate specific antigen measurement in the detection and management of prostate cancer. *Endocr. Relat. Cancer*, **7(1)**, 37-51.

Naslund, M.J. (1993) Prostate gland Microsoft® Encarta Microsoft® Online Encycloprdia 2006 http://encarta.msn.com.

National Institute of Neurological Disorders and Stroke rt-PA Stroke Study Group. (1995) Tissue plasminogen activator for acute ischemic stroke. *New England Journal of Medicine*, **333**, 1581-1587.

Niculescu, M., Gaspar, S., Schulte, A., Csoregi, E. and Schuhmann, W. (2004) Visualization of micropatterned complex biosensor sensing chemistries by means of scanning electrochemical microscopy. *Biosensors and Bioelectronics*, **19**, 1175-1184.

Niwa, O. and Tabei, H. (1994) Voltammetric mesurements of reversible and quasi-reversible redox species using carbon film based interdigitated array microelectrodes. *Analytical Chemistry*, **66**,285-289.

Office of National Statistics Health Statistics Quarterly (12) Winter. (2001), *Stroke incidence and risk factors in a population based cohort study*. London, UK.

Oldham, K.B. and Zoski, C.G. (1988) Comparison of voltammetric steady states at hemispherical and disc microeletrodes. *Journal of electroanalytical chemistry*, **256**, 11-19.

Ouerghi, O., Touhami, A., Jaffreiz-Renaul, N., Martelet, C., Ben Ouada, H. and Cosnier, S. (2002) Impedimetric immunosensor using avidin-biotin for antibody immobilization. *Bioelectrochemistry*, **56**, 131-133.

Oxlund, H., Barckman, M., Ortoft, G. and Andreassen, T.T. (1995) Reduced concentrations of collagen cross-links are associated with reduced strength of bone. *Bone*, **17**, 365S-371S.

Oxlund, H., Mosekilde, L. and Ortoft, G. (1996) Reduced concentration of collagen reducible cross links in human trabecular bone with respect to age and osteoporosis. *Bone*, **19**, 479-484.

Oyamatsu, D., Hirano, Y., Kanaya, N., Mase, Y., Nishizawa, M. and Matsue, T. (2003a) Imaging of enzyme activity by scanning electrochemical microscope equipped with a feedback control for substrate-probe distance. *Bioelectrochemistry*, **60**, 115-121.

Oyamatsu, D., Kanaya, N., Hirano, Y., Nishizawa, M. and Matsue, T. (2003b) Area-Selective Immobilization of Multi Enzymes by Using the Reductive Desorption of Self-Assembled Monolayer. *Electrochemistry*, **71**, 439-441.

Pannek, J., Rittenhouse, H.G., Evans, C.L., Finlay, J.A., Bruzek, D.J., Cox, J.L., Chan, D.W., Subong, E.N. and Partin, A.W. (1997) Molecular forms of prostate-specific antigen and human kallikrein 2 (hK2) in urine are not clinically useful for early detection and staging of prostate cancer. *Urology*. **50(5)**, 715-721.

Parra, A., Casero, E., Vazquez, L., Jin, J., Pariente, F. and Lorenzo, E. (2006) Microscopic and voltammetric characterisation of bioanalytical platforms based on lactate oxidase. *Langmuir*, **22**, 5443-5450.

Pendley, B.D. and Abruna, H.D. (1990) Construction of submicrometer voltammetric electrodes. *Analytical Chemistry,* **62,** 782-784.

Penner, R.M., Heben, M.J. and Lewis, N.S. (1989) Preparation and Electrochemical Characterisation of Conical and Hemispherical Ultramicroelectrodes. *Analytical Chemistry*, **61**, 1630-1636.

Ponchon, J-L., Gespuglio, R., Gonon, F., Jouvet, M. and Pujol, J-F., (1979) Normal Pulse Polarography. *Analytical Chemistry*, **51**, 1483-1486.

Quinn, G.B., Reeves, I.G. and Day, I.N. (1994) Mapping of antigenic sites in human neuron-specific enolase by expression subcloning. *Clinical Chemistry*, **4**, 790-795.

Quinn, M. and Babb, P. (2002) Patterns and trends in prostate cancer incidence, survival, prevalence and mortality. Part II: individual countries. *BJU Int.*, **90(2)**, 174-184.

Roberts, W. S., Davis, F., Higson, S. P. J. (2009) Scanning electrochemical microscopy of genomic DNA microarrays - study of adsorption and subsequent interactions. *Analyst*, **134**, 1302-1308.

Rockel, H., Huber, J., Gleiter, R .and Schuhmann, W. (1994) Synthesis of functionalized poly(dithienylpyrrole) derivatives and their application in amperometric biosensors. *Advanced Materials*, **6**, 567-571.

Rodriguez-Diaz, R. C., Fernandez-Romero, J. M., Aguilar-Caballos, M. P. and Gomez-Hens, A. (2006) Determination of Fluoroquinolones in Milk Samples by Postcolumn Derivatization Liquid Chromatography with Luminescence Detection. *Journal of Agricultural and Food Chemistry*, **54 (26)**, 9670-9676.

Roehrborn, C.G., McConnell, J.D., Lieber, M., Kaplan, S., Geller, J., Malek, G.H., Castellanos, R., Coffield, S., Saltzman, B., Resnick, M., Cook, T.J. and Waldstreicher, J. (1999) Serum prostate-specific antigen concentration is as powerful predictor of acute urinary retention and need for surgery in men with clinical benign prostatic hyperplasia. *Urology*, **53(3)**, 473-480.

Rous, S.N. (1988) The prostate book, published by Penguin books Canada Ltd.

Scheller, F. and Renneberg, R. (1983) Glucose-Eliminating Enzyme Electrode for Direct Sucrose Determination in Glucose-Containing Samples. *Analytica Chimica Acta***, 152**, 265-269.

Schönhoff, M., (2003) Self-assembled polyelectrolyte multilayers. *Curr. Opin Coll. Inter. Sci.*, **8**, 86-95.

Schuhmann, W., Huber, J., Mirlach, A. and Daub, J. (1993) Covalent binding of glucose oxidase to functionalized polyazulenes. The first application of polyazylenes in amperometric biosensors. *Advanced Materials*, **5**, 124-126.

Schuhmann, W., Lammert, R., Uhe, B. and Schmidt, H.L. (1990) Polypyrrole, a new possibility for covalent binding of oxidoreductases to electrode surfaces as a base for stable biosensors. *Sensors and Actuators B,* **1**, 537-541.

Seibel, M.J. (2006) Biochemical markers of bone turnover part II: Clinical applications in the management of osteoporosis. *Clin. Biochem. Rev.*, **27**, 123-138.

Shao, Y. and Mirkin, M.V. (1998) Probing Ion Transfer at the Liquid/Liquid Interface by Scanning Electrochemical Microscopy (SECM). *Journal Physical Chemistry*, **102**, 9915-9921.

Small, R.E. (2005) Uses and limitations of bone mineral density measurements in the management of osteoporosis. *MedGenMed*,, **7**, 3.

Spence, R.A. and Johnson, P.G. (2001) Oncology. Oxford handbook of clinical medicine.

Stenman, U.H., Leinonen, J., Alfthan, H., Rannikko, S., Tuhkanen, K. and Alfthan, O. (1991) A complex between prostate-specific antigen and alpha 1-antichymotrypsin is the major form of prostate-specific antigen in serum of patients with prostatic cancer: assay of the complex improves clinical sensitivity for cancer. *Cancer Res.*, **51(1)**, 222-226.

Stern, O. (1924) Zur theorie der elektrolytischen doppelschicht. Zietschrift *Elektrochemia*, **30**, 508-516.

Strike, D., Hengstenberg, A., Quinto, M., Kurzawa, C., Koudelka-Hep, M. and Schuhmann, W. (1999) Localized visualisation of chemical cross-talk in microsensor arrays by using SECM (Scanning Electrochemical Microscopy). *Microchimica Acta*, **131**, 47-55.

Sun, P., Laforge, F.O. and Mirkin, M.V. (2007) Scanning electrochemical microscopy in the 21st century. *Physical Chemistry Chemical Physics*, **21,9 (7)**: 802-23.

Sun, P., Zhang, Z., Guo, J. and Shao, Y. (2001) Fabrication of Nanometer-Sized Electrodes and Tips for Scanning Electrochemical Microscopy. *Analytical Chemistry*, **73**, 5346-5351.

Suter, M. and Butler, J.E. (1986) The immunochemistry of sandwich ELISAs. II. A novel system prevents the denaturation of capture antibodies, *Immunology Letters*, **13**, 313.

Svancara, I. and Vytras, K. (2000) Physico-chemical processes in analytical electrochemistry with carbon paste electrodes. An overview. *Chemija*, **11(1)**, 18-27.

Svancara, I., Hvizdalova, M. and Vytras, K. (1996b) A microscopic study on carbon paste electrodes. *Electroanalysis*, **8(1)**, 61-65.

Svancara, I., Kalcher, K. and Diewald, W. (1996a) Voltammetric determination of silver at ultratrace levels using a carbon paste electrode with improved surface characteristics. *Electroanalysis*, **8(4)**, 336-342.

Takahashi, Y., Shiku, H., Murata, T., Yasukawa, T. and Matsue, T. (2009) Transfected Single-Cell Imaging by Scanning Electrochemical Optical Microscopy with Shear Force Feedback Regulation. *Anal. Chem.*, **81**, 9674–9681.

Takahashi, Y., Hirano, Y., Yasukawa, T., Shiku, H., Yamada, H. and Matsue, T. (2006) Topographic, electrochemical, and optical images captured using standing approach mode scanning electrochemical/optical microscopy. *Langmuir*, **22 (25)**, 10299-10306.

Takii, Y., Takoh, K., Nishizawa, M. and Matsue, T. (2003) Characterization of Local Respiratory Activity of Pc12 Neuronal Cell by Scanning Electrochemical Microscopy. *Electrochimica Acta*, **48**, 3381-3385.

Thiebaud, P., Beuret, C., Rooij, N.F.D. and Koudelka-Hep, M. (2000) Microfabrication of PT-tip Microelectrodes. *Sensors and Actuators*, **70**, 51-56.

Torriero, A. J. A., Ruiz-Diaz, J. J. J., Salinas, E., Marchevsky, E. J., Sanz, M. I. and Raba, J. (2006) Enzymatic rotating biosensor for ciprofloxacin determination. *Talanta*, **69**, 691-699.

Tsekenis, G., Garifallou, G-Z., Davis, F., Millner, P. A., Gibson, T. D., Higson, S. P. J. (2008b) Label-less Immunosensor Assay for Myelin Basic Protein Based upon an ac Impedance Protocol. *Anal. Chem*., **80**, 2058-2062.

Tsekenis, G., Garifallou, G-Z., Davis, F., Millner, P. A., Pinacho, D. G., Sanchez-Baeza, F., Pilar Marco, M., Gibson, T. D., Higson, S. P. J. (2008a) Detection of Fluoroquinolone Antibiotics in Milk via a Labeless Immunoassay Based upon an Alternating Current Impedance Protocol. *Anal. Chem*., **80**, 9233-9239.

Tsionsky, M., Cardon, Z.G., Bard, A.J. and Jackson, R.B. (1997) Photosynthetic Electron Transport in Single Guard Cells as Measured by Scanning Electrochemical Microscopy. *Analytical Chemistry*, **113**, 895-901.

Turcu, F., Hartwich, G., Schafer, D. and Schuhman, W. (2005) Ink-Jet Microdispensing for the formation of gradients of immobilised enzyme activity. *Macromolecular rapid Communications*, **26**, 325-330.

Turcu, F., Schulte, A., Hartwich, G. and Schuhmann, W. (2004a) Imaging immobilised ssDNA and detecting DNA hybridisation by means of the repelling mode of scanning electrochemical microscopy (SECM). *Biosensors and Bioelectronics*, **20(5)**, 925-932.

Turcu, F., Schulte, A., Hartwich, G. and Schuhmann, W. (2004b) Label-free electrochemical recognition of DNA hybridization by means of modulation of the feedback current in SECM. *Angewandte Chemie-International Edition*, **43**, 3482-3485.

Turner, A.P.F., Karube, I. and Wilson, G.S. (1987) Biosensors: Fundamentals and Applications, Oxford University Press.

Uitto, O.D. and White, H.S. (2003) Electroosmotic Pore Transport in Human Skin. *Pharmaceutical Research*, **20**, 646-652.

Unson, M.D., Newton, G.L., Arnold, K.F., Davis, C.E. and Fahey, R.C. (1999) Improved methods for immunoassay of mycothiol. *Journal of Clinical Microbiology*, **37**, 2153-2157.

Unwin, P.R. and Bard A.J (1991) Scanning electrochemical microscopy. 9. Theory and application of the feedback mode to the measurement of following chemical reaction rates in electrode processes. *Journal of Physical Chemistry*, **95**, 7814-7824.

Upadhyay, S. K., Kumar, P. and Arora, V. (2006) Complexes of quinolone drugs norfloxacin and ciprofloxacin with alkaline earth metal perchlorates. *Journal of Structural Chemistry*, **47**, 1078-1083.

Vallee, F., LeBel, M. and Bergeron, M.G. (1986) Determination of ciprofloxacin in biological samples by reversed-phase high performance liquid chromatography. *Ther. Drug Monit.*, **8**, 340-345.

Van der Cruijsen-Koeter, I.W., Wildhagen, M.F., De Koning, H.J. and Schroder, F.H. (2001) The value of current diagnostic tests in prostate cancer screening. *BJU International*, **88**, 458-466.

Vermette, P., Gengenbach, T., Divisekera, U., Kambouris, P.A., Griesser, H.J. and Meagher, L. (2003) Immobilization and surface characterization of NeutrAvidin biotin-binding protein on different hydrogel interlayers. *Journal of Colloid and Interface Science*, **259**, 13-26.

Wain, A.J. and Zhou, F. (2008) Scanning Electrochemical Microscopy Imaging of DNA Microarrays Using Methylene Blue as a Redox-Active Intercalator. *Langmuir*, **24**, 5155-5160.

Walker-Bone, K., Walter, G. and Cooper, C. (2002) Recent developments in the epidemiology of osteoporosis. *Curr. Opin. Rheumatol.*, **14**, 411-415.

Wang, J. (2001) Analytical Electrochemistry, 2nd edn.

Wang, J. and Zhou, F.M. (2002) Scanning electrochemical ,microscopic imaging of surface- confined DNA probes and their hybridization via guanine oxidation. *Journal of Electroanalytical Chemistry*, **537**, 95-102.

Wang, J., Song, F.Y. and Zhou, F.M. (2002) Silver-Enhanced Imaging of DNA Hybridization at DNA Microarrays With Scanning Electrochemical Microscopy. *Langmuir*, **18**, 6653-6658.

Wang, M.C., Valenzuela, L.A., Murphy, G.P. and Chu, T.M. (1979) Purification of a human prostate specific antigen. *Invest. Urology*, **17(2)**, 159-163.

Wang, X.L., Shi, Y.X., Bai, Z.L. and Jin, W.R. (2004) Chinese Chemical Letters, **15(2)**, 214-215.

Wijayawardhana, C.A., Wittstock, G., Halsall, H.B. and Heinman, W.R. (2000a) Electrochemical Immunoassay with Microscopic Immunomagnetic Bead Domains and Scanning Electrochemical Microscopy. *Electroanalysis*, **12**, 640-644.

Wijayawardhana, C.A., Wittstock, G., Halsall, H.B. and Heinman, W.R. (2000b) Spatially Addressed Deposition and Imaging of Biochemically Active Bead Microstructures by Scanning Electrochemical Microscopy. *Analytical Chemistry*, **72**, 333-338.

Wilchek, M. and Bayer, E.A. (1988) The avidin-biotin complex in bioanalytical applications. *Analytical Biochemistry*, **171**, 1-32.

Wilchek, M. and Bayer, E.M. (1990) Methods in Enzymology. 184, 123 Academic Press, New York, USA.

Wilhelm, T. and Wittstock, G. (2002) Generation of Periodic Enzyme Patterns by Soft Lithography and Activity Imaging by Scanning Electrochemical Microscopy. *Langmuir*, **18**, 9485-9493.

Wilhelm, T. and Wittstock, G. (2003) Analysis of interaction in patterned multienzyme layers by using scanning electrochemical microscopy. *Angewandte Chemie-International Edition*, **42**, 2247-2250.

Willner, I., Katz, E., Lapidot, N. and Bauerle, P. (1992) Bioelectrocatalysed reduction of nitrate utilizing polythiophene bipyridinium enzyme electrodes. *Bioelectrochemistry and Bioenergetics*, **29**, 29-45.

Wittstock, G. (2001) Modification and characterisation of artificially patterned enzymatically active surfaces by scanning electrochemical microscopy. *Fresenius Journal of Analytical Chemistry*, **370**, 303-315.

Wittstock, G., Burchardt, M., Pust, S.E., Shen, Y. and Zhao, C. (2007) Scanning electrochemical microscopy for direct imaging of reaction rates. *Angewandte Chemie International Edition*, **46**, 1584-1617.

Wittstock, G., Yu, K.J., Halsall, H.B., Ridgway, T.H. and Heineman, W.R. (1995) Imaging of immobilized antibody layers with scanning electrochemical microscopy. *Anal. Chem.*, **67(19)**, 3578-82.

Wojciechoski, M., Sundseth, R., **Moreno, M. and Henkens, R. (1999)** Multichannel Electrochemical Detection System for Quantitative Monitoring of PCR Amplification. *Clinical Chemistry*, **45**, 1690-1693.

Wring, S.A. and Hart, J.P. (1990) Development of screen-printed carbon electrodes, chemically modified with cobalt phthalocyanine, for electrochemical sensor applications. *Analytica Chimica Acta*, **231**, 203-212.

Xue, Y., Ding, L., Lei, J., Yan, F. and Ju, H. (2010) In Situ Electrochemical Imaging of Membrane Glycan Expression on Micropatterned Adherent Single Cells. *Anal. Chem.*, **82 (17)**, 7112–7118.

Yamashita, K., Takagi, M., Uchida, K., Kondo, H. and Takenaka, S. (2001) Visualization of Dna Microarrays by Scanning Electrochemical Microscopy (SECM). *Analyst*, **126**, 1210-1211.

Yasukawa, T., Kondo, Y., Uchida, T. and Matsue, T. (1998) Imaging of cellular activity of single cultured-cells by scanning electrochemical microscopy. *Chemistry Letters*, 767-768.

Yotter, R.A. and Wilson, D.M. (2004) Sensor technologies for monitoring metabolic activity in single cells - Part II: Nonoptical methods and applications. *Ieee Sensors Journal*, **4**, 412-429.

Zhang, H., Gao, Y.G., Vandermarel, G.A., Vanboom, J.H., and Wang, A.H.J. (1999) Simultaneous incorporation of 2 anticancer drugs into DNA – the structures of formaldehyde-cross-linked adducts of daunorubicin-d(CG(ARAC)GCG) and doxorubicin-d(CA(ARAC)GTC) complexes at high resolution. *Journal of Biological Chemistry*, **268**, 10095-10101.

Zhang, X. and Kanatzidis, M.G. (1994) AMTeS3 (A = K, Rb, Cs, M = Cu, Ag): A New Class of Compounds Based on a New Polychalcogenide Anion, TeS32-. *Journal of the American Chemical Society*, **116 (5)**, 1890-1898.

Zhang, X., Peng, X. and Wenrui, J. (2006) Scanning Electrochemical Microscopy with enzyme immunoassay of the cancer-related antigen CA15-3. *Analytica Chimica Acta*, **558**, 110-114.

Zhao, C. and Wittstock, G. (2004a) Scanning Electrochemical Microscopy of Quinoprotein Glucose Dehydrogenase. *Analytical Chemistry*, **76**, 3145-3154.

Zhao, C. and Wittstock, G. (2004b) An SECM Detection Scheme with Improved Sensitivity and Lateral Resolution: Detection of Galactosidase Activity with Signal Amplification by Glucose Dehydrogenase. *Angewandte Chemie*, **43**, 4170-4172.

Zhao, C. and Wittstock, G. (2005) Scanning electrochemical microscopy for detection of biosensor and biochip surfaces with immobilized pyrroloquinoline quinone (PQQ)-dependent glucose dehydrogenase as enzyme label. *Biosensors and Bioelectronics*, **20 (7)**, 1277-1284.

Zhao, G., Giolande, J.R. and Kirchoff, J. (1995) Chemical Vapor Deposition Fabrication and Characterization of Silica-Coated Carbon Fiber Ultramicroelectrodes. *Analytical Chemistry*, **67**, 2592-2598.

Zhou F., Unwin P.R. and Bard A.J. (1992) Scanning electrochemical microscopy. 16. Study of second-order homogeneous chemical reactions via the feedback and generation/collection modes. *Analytical Chemistry*, **96**, 4917-4924.

Zhou, H.F., Kasai, S. and Matsue, T. (2001) Imaging Localized Horseradish Peroxidase on a Glass Surface With Scanning Electrochemical/Chemiluminescence Microscopy.

Analytical Biochemistry, **290**, 83-88.

Zhu, R., Macfie, S.M. and Ding, Z. (2005) Cadmium-induced plant stress investigated by scanning electrochemical microscopy. *Journal of Experimental Botany*, **56**, 2831-2838.

Zoski, C.G. (1990) A survey of steady state microelectrode and experimental approaches to a voltammetric steady state. *Jounral of electroanalytical chemistry*, **296(2)**, 317-333.

Zoski, C.G. (2002) Ultramicroelectrodes: design, fabrication and characterisation. *Electroanalysis*, **14(15-16)**, 1041-1051.

Zoski, C.G. and Rodgers, R.S. (2000) Current amplification with signal averaging at steady state microelectrodes. *Electroanalysis*, **12(6)**, 420-424.

Appendices

Appendix 1: Analytica Chimica Acta Paper

G Model
ACA-230978; No. of Pages 6
ARTICLE IN PRESS
Analytica Chimica Acta xxx (2011) xxx–xxx
Contents lists available at ScienceDirect
Analytica Chimica Acta
journal homepage: www.elsevier.com/locate/aca

A new application of scanning electrochemical microscopy for the label-free interrogation of antibody–antigen interactions

Joanne L. Holmes, Frank Davis, Stuart D. Collyer, Séamus P.J. Higson*
Cranfield Health, Cranfield University, Cranfield, MK43 0AL, UK

ARTICLE INFO
Article history:
Received 24 September 2010
Received in revised form 6 January 2011
Accepted 14 January 2011
Available online xxx
Keywords:
Scanning electrochemical microscopy
Neuron specific enolase
Label-free
Antibody

ABSTRACT
Within this work we present a 'proof of principle' study for the use of scanning electrochemical microscopy (SECM) to detect and image biomolecular interactions in a label-free assay as a potential alternative to current fluorescence techniques. Screen-printed carbon electrodes were used as the substrate for the deposition of a dotted array, where the dots consist of biotinylated polyethyleneimine. These were then further derivatised, first with neutravidin and then with a biotinylated antibody to the protein neuron specific enolase (NSE). SECM using a ferrocene carboxylic acid mediator showed clear differences between the array and the surrounding unmodified carbon. Imaging of the arrays before and following exposure to various concentrations of the antigen showed clear evidence for specific binding of the NSE antigen to the antibody derivatised dots. Non-specific binding was quantified. Control experiments with other proteins showed only non-specific binding across the whole of the substrate, thereby confirming that specific binding does occur between the antibody and antigen at the surface of the dots. Binding of the antigen was accompanied by a measured increase in current response, which may be explained in terms of protein electrostatic interaction and hydrophobic interactions to the mediator, thereby increasing the localised mediator flux. A calibration curve was obtained between 500 fg mL^{-1} to 200 pg mL^{-1} NSE which demonstrated a logarithmic relationship between the current change upon binding and antigen concentration without the need for any labelling of the substrate.

1. Introduction

In recent years there has been an increasing demand for the development of parallel analytical testing platforms and this has led to increased research into miniaturised biosensors, biosensor arrays, and chip based testing systems. Within the commercial market it is already possible to obtain DNA-based testing systems, however there is still an unmet need when considering the use of proteins as the functional units. This is possibly due in part to proteins being less stable and also their characteristic to denature once in contact with the surface to which they are immobilized.

The incorporation of antibodies into conducting polymer films was first reported in 1991 [1]. Anti-human serum albumin (anti-HSA) was incorporated into a (poly)pyrrole film, which was galvonostatically polymerized onto a platinum wire substrate. When the pyrrole anti-HSA was exposed to 50 μg mL^{-1} HSA for 10 min, a new reduction peak was observed at a potential of +600 mV vs. Ag/AgCl. Since this preliminary work there has been an increase in the development of electrochemical immunosensors, as reviewed previously elsewhere [2–4].

Previous work within our group has shown that up to 2–3 μg of antibodies for bovine serum albumin (BSA) and digoxin may be successfully incorporated into conducting polymer films by entrapment in an electrochemically grown (poly)pyrrole film with no detrimental effect to antibody activity [5]. Further work utilized an ac impedance protocol as the method for interrogation for these films [6]. A protocol was then developed for immobilizing antibodies onto polyaniline-coated screen printed carbon electrodes which utilized the classical avidin–biotin interaction. This enabled the construction of immunosensors for the antibiotic ciprofloxacin [7,8], the heart drug digoxin [9] and for myelin basic protein [10] – which could detect their respective targets with detection limits of 1 ng mL^{-1} of the target species. Later work utilized polyaniline microarrays as a substrate for the assembly of immunosensors for prostate specific antigen (PSA) [11] and the stroke marker proteins neuron specific enolase (NSE) [12] and S100[β] [13], with greatly lowered limits of detection down to the level of 1 pg mL^{-1} of the target.

Biotin/avidin chemistry has been used extensively to modify electrode surfaces by protein immobilization. The attachment of a biotin molecule allows the immobilization of any biomolecule of the avidin family. Neutravidin protein is a deglycosylated version of avidin with four identical binding sites. It has a near neutral isoelectric point (IEP) which minimizes non-specific interaction and

* Corresponding author.
E-mail address: s.p.j.higson@cranfield.ac.uk (S.P.J. Higson).

0003-2670/$ – see front matter © 2011 Elsevier B.V. All rights reserved.
doi:10.1016/j.aca.2011.01.033

Please cite this article in press as: J.L. Holmes, et al., A new application of scanning electrochemical microscopy for the label-free interrogation of antibody–antigen interactions, Anal. Chim. Acta (2011), doi:10.1016/j.aca.2011.01.033

G Model
ACA-230978; No. of Pages 6
ARTICLE IN PRESS
2 J.L. Holmes et al. / Analytica Chimica Acta xxx (2011) xxx–xxx

like avidin itself has a strong affinity with biotin ($kD = 10^{-15}\ M^{-1}$) [14,15]. Due to this strong interaction, the complex formation is nearly unaffected by extremes of pH or temperature, organic solvents, and denaturing agents. The tetravalent binding of neutravidin to biotin allows the construction of a molecular sandwich effect where the bound neutravidin is free to couple to a biotinylated antibody with the appropriate characteristics needed for the construction of a biosensor.

Enolase is a 78 kDa homo- or heterodimeric cytosolic protein produced from [α], [β], and [γ] subunits. The [γ][γ] enolase isoform is most specific for neurons, and is referred to as NSE. Elevations of NSE in serum can be attributed to cerebral injury due to physical damage or ischemia caused by infarction or cerebral haemorrhage, coupled with increased permeability of the blood brain barrier. The serum concentration of NSE has also been reported to correlate with the extent of damage (infarct volume) and neurological outcome [16]. Additionally, a secondary elevation of serum NSE concentration may be an indicator of delayed neuronal injury resulting from cerebral vasospasm [17]. NSE, which has a biological half-life of 48 h and is normally detected in serum at an upper limit of 12.5 ng mL^{-1} (160 pM), is typically elevated after stroke and cerebral injury. Serum NSE is elevated after 4 h from onset, with concentrations reaching a maximum between 1 and 3 days after onset [18]. After the serum concentration reaches its maximum (maybe >300 ng mL^{-1}, 3.9 nM), it gradually decreases to normal concentrations over approximately one week.

Scanning electrochemical microscopy (SECM) is a surface scanning probe technique that allows for the collection of high resolution electrochemical data on a variety of surfaces and has previously been used successfully to investigate various biological systems including cells [19–23], enzymes [24–27], and DNA [28–30].

We have, within this work, attempted to utilize the SECM to detect the binding of antibody layers to electrodes and to determine if these systems can be used for the label-free detection of NSE. This work is intended as a 'proof of principle' study to show the feasibility of antigen adsorption and imaging rather than the fabrication of either a sensitive antigen sensor or the detailed examination of the polymer and biomolecular films absorbed. Once a proof of principle has been demonstrated we will in future work move towards studying a range of antigens of various molecular sizes and investigate the possibility of fabricating one array containing a number of different antibodies of interest.

2. Experimental

2.1. Chemicals and reagents

Ferrocene carboxylic acid, biotinylation kit (part no. BK101), neutravidin, polyethyleneimine (PEI) (MW = 50000) and BSA were purchased from Sigma–Aldrich (Gillingham, Dorset, UK). Disodium hydrogen orthophosphate monohydrate, sodium dihydrogen orthophosphate 12-hydrate and sodium chloride (all 'AnalaR' grade) were purchased from BDH (Poole, Dorset, UK). All reagents were used without further purification. Commercial screen-printed carbon electrodes were obtained from Microarray Ltd. (Manchester, UK). NSE and monoclonal antibody against NSE – both with sodium azide preservative, and PSA were supplied by Canag Diagnostics, Ltd. (Gothenburg, Sweden).

For antibody and PEI biotinylation, the procedure outlined in the BK101 kit was followed (see manufacturer's instructions for details). Biotinylated antibodies were kept frozen in aliquots of 200 μL at a concentration of 0.2 mg mL^{-1} until required.

All water used was purified with an ELGA Purelab UHQ-II water system (Elga, High Wycombe, UK). Phosphate buffer (PBS), pH 7.0 contained NaH_2PO_4 (4 mmol mL^{-1}), Na_2HPO_4 (6 mmol mL^{-1}) and NaCl (132 mmol mL^{-1}).

SECM experiments were carried out using a Uniscan SECM270 (Uniscan Instruments Ltd, Buxton, UK). The SECM instrument (shown schematically in Fig. 1a) is composed of (1) an electrochemical cell, (2) a translational stage capable of high resolution movement in the *X*, *Y* and *Z* planes (sub-micron), (3) a bipotentiostat for the accurate control of the potential applied at the tip and/or substrate, (4) a hardware interface enabling the control of (1) and (2), and (5) a PC which provides an interface with the hardware – and allows the operator to accurately control the parameters of the SECM procedure. Pt counter electrodes and Ag/AgCl reference electrodes were also utilized as shown in Fig. 1b. Ferrocene carboxylic acid (5 mmol L^{-1} in pH 7.0 phosphate buffer) was used as the mediator (Fig. 1c).

2.2. Substrate patterning

In the immunosensors previously developed within our laboratory, cyclic voltammetry was utilized to deposit polyaniline films on the carbon electrodes [7–13]. This was deemed inappropriate for the preparation of electrodes to be interrogated by SECM as it is not possible to compare a modified region with an unmodified region. Any changes in the tip current obtained may be due to fluctuations in the background current and not due to changes in the charge transfer properties of the modified substrate. It was therefore decided that for SECM interrogation, the polyelectrolyte film should be patterned in an array dot format. By producing this pattern, background effects in the measured current could therefore be eliminated and any changes in the current over the modified surface would contrast with the current over regions of unmodified carbon. Since it would not be possible to use polyaniline in this format it was decided to use PEI which has previously been used within the group when interrogating DNA arrays with SECM [30].

A borosilicate glass capillary was pulled to an internal diameter of 80–100 μm using a Narishige PP-830 pipette puller (Narishige International Limited, London, UK) and the tip polished to a flat finish. This capillary was then filled with a 1% biotinylated PEI solution and, using the micropositioning stage on the Uniscan SECM270, used to fabricate a biotinylated PEI array (Fig. 2). Each of the dots was distanced 300 μm centre to centre and approximately 200 μm in diameter. After patterning, the substrate was then rinsed with UHQ water. Once the area was dry 20 μL of neutravidin (10 mg mL^{-1} in water) was placed on the dotted microarray for 1 h, followed by rinsing with water. 20 μL of biotinylated antibody (0.2 mg mL^{-1} in water, 1 h) was then added followed by further rinsing. Finally non-specific interactions were blocked by BSA (10^{-6} mol L^{-1} in PBS, 1 h).

2.3. SECM studies

A screen-printed carbon electrode substrate was placed in a plastic Petri dish and exposed to 5 mmol L^{-1} mediator solution. The SECM working electrode tip and counter and reference electrodes were then immersed into the mediator solution. Prior to undertaking an area scan over the antibody/PEI functionalised regions, an approach curve experiment was conducted over the polycarbonate, non-conductive region of the substrate to estimate the tip-to-substrate distance (tip potential (E) = +0.45 V vs. Ag/AgCl; step size = 10 μm). The tip was positioned at a distance at which the measured current was half that of the observed current with the tip a few mm distant from the surface of the screen printed electrode (effectively infinite on this scale) (approximately 70 μm

Please cite this article in press as: J.L. Holmes, et al., A new application of scanning electrochemical microscopy for the label-free interrogation of antibody–antigen interactions, Anal. Chim. Acta (2011), doi:10.1016/j.aca.2011.01.033

G Model
ACA-230978; No. of Pages 6
ARTICLE IN PRESS
J.L. Holmes et al. / Analytica Chimica Acta xxx (2011) xxx–xxx

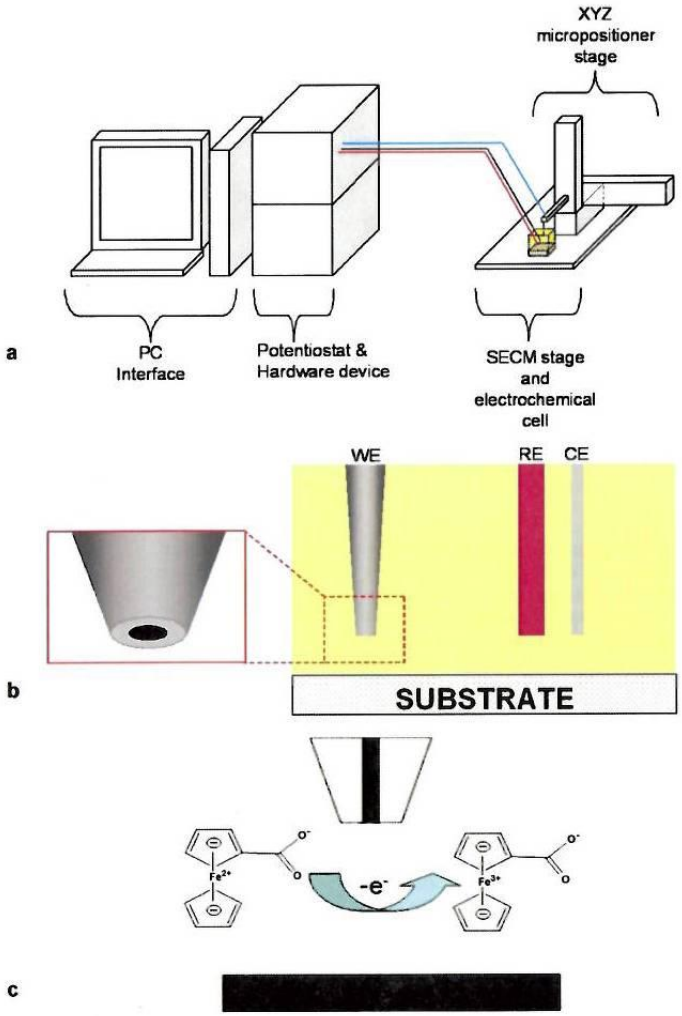

Fig. 1. (a) Schematic representation of SECM instrumentation – the microelectrode probe is clamped into a high resolution *XYZ* micropositioning device and scanned across the sample surface. Scan parameters and tip electrochemistry are controlled via a PC interface. (b) The arrangement of electrodes in the electrochemical cell – i.e. WE, RE and the CE. (c) Redox coupling of ferrocene carboxylic acid between the microelectrode tip and the substrate.

from substrate surface); this was to allow for the variation in topography and the height differential between this non-carbon region and the slightly raised carbon electrode surface – while also serving to reduce the risk of tip crash. After tip positioning, an area scan over the functionalised region was conducted with a step size of 10 μm. At no point in the experiment was the substrate touched; this allowed any change in the observed tip current to be attributed solely to changes in the charge transfer properties of the surface. In all cases the tip diameter was 8.5 μm; the scan rate used was 10 μm per step throughout and there was no potential applied to the substrate.

After the first area scan experiment was conducted, the tip was retracted a known safe distance from the substrate. The mediator solution was then removed and the substrate gently rinsed with UHQ water before applying a solution containing complementary antigen over a range of concentrations or a non-complementary antigen. After exposure for 1 h, the antigen solution was then removed and the substrate again rinsed before the re-introduction of fresh mediator solution. A second area scan experiment was then conducted over the same functionalised area as measured previously. The tip current data from the area scan before exposure was then subtracted from the tip current data following this exposure. Throughout all these experiments the sample substrate does not move at all, i.e. all exposures, rinsing steps etc. are performed with the sample *in situ*. It is worth noting here that after each exposure and rinsing step the Petri dish is refilled with fresh mediator solution and the tip exactly repositioned, made possible using the *XYZ* micro-positioning stage of the SECM270. This allows precise and reproducible imaging of the same area of the electrode.

Please cite this article in press as: J.L. Holmes, et al., A new application of scanning electrochemical microscopy for the label-free interrogation of antibody–antigen interactions, Anal. Chim. Acta (2011), doi:10.1016/j.aca.2011.01.033

GModel
ACA-230978; No. of Pages 6
ARTICLE IN PRESS
4 J.L. Holmes et al. / Analytica Chimica Acta xxx (2011) xxx–xxx

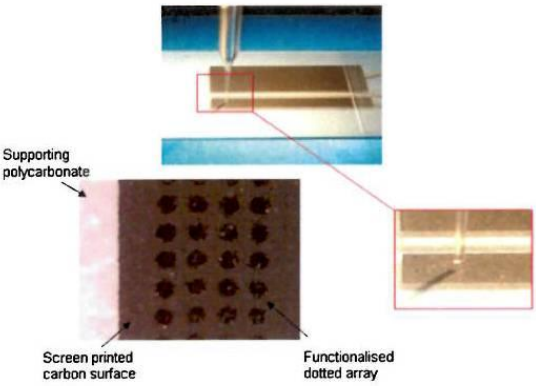

Fig. 2. Photograph of biotinylated PEI deposition on carbon electrode by pulled microcapillary using the *XYZ* micro-positioning stage of the SECM270 and of the final array pattern on the screen printed carbon electrode surface (dot size ~200 μm).

3. Results and discussion

To ensure that changes occurring on the sensor surface were directly related to the hybridization of antibody and antigen, and not due to interference of mediator solution or poor stability of the substrate, surface scans were undertaken of the antibody modified dotted arrays (Fig. 3a). The modified surface displays an array of peaks which correspond to decreases in the tip current. This can be accounted for by the polymer/antibody composite acting as a barrier to mediator diffusion to the surface, thereby diminishing the current since polyelectrolytes are known to act as barriers to ion migration [31].

After this initial scan, samples were incubated in purified water for 30 min in parallel to the immunochemical exposures but in the absence of antigen. Following rinsing, fresh mediator solution was introduced. A scan of this surface is shown in Fig. 3b. Subtraction of Fig. 3a from b (Fig. 3c) clearly shows only minimal variations, indicating that minimal changes in background current are seen and that there is no loss of material from the surface. Other techniques employed to dot down the array were investigated. These included the direct dotting of antibody onto the carbon surface, however, these proved to be unstable and deterioration of the array could be visualised as the scan progressed.

Binding experiments were performed by soaking the modified antibody dotted arrays in solutions of varying concentrations of the complementary antigen for 30 min, followed by scanning in fresh mediator solution. A control was also run using 5 pg mL^{-1} PSA to ensure changes could be related to specific antigen/antibody binding rather than simple non-specific absorption of proteins to surfaces. Binding experiments were carried out using NSE solution with concentrations ranging from 500 fg mL^{-1} to 200 pg mL^{-1} in water. Detailed results (Fig. 4a–c) are presented for the exposure to 200 pg mL^{-1}. Fig. 4a depicts the scan over the dotted array before incubation, with Fig. 4b showing the scan taken after exposure to 200 pg mL^{-1} NSE. Fig. 4c shows the difference between the two scans indicating changes to the tip current over both the carbon surface and the dotted substrate. Fig. 4c shows that across the whole of the array there is a general increase in measured tip current. The change in tip current is, however, seen to be much greater in the areas of the PEI/biotinylated antibody dots than for the untreated carbon surface.

NSE is known to have both positively and negatively charged areas on the surface of the protein [32]. The cationic areas of the protein are capable of electrostatically attracting the ferrocene carboxylic acid (which is anionic at pH 7 due to ionisation of the acid group), thereby increasing the flux of the mediator to the microelectrode tip. There is also the possibility of hydrophobic interactions between the ferrocene unit and any hydrophobic regions of the NSE protein. These could effectively increase the concentration of ferrocene carboxylic acid at the surface and thus enhance the current flow.

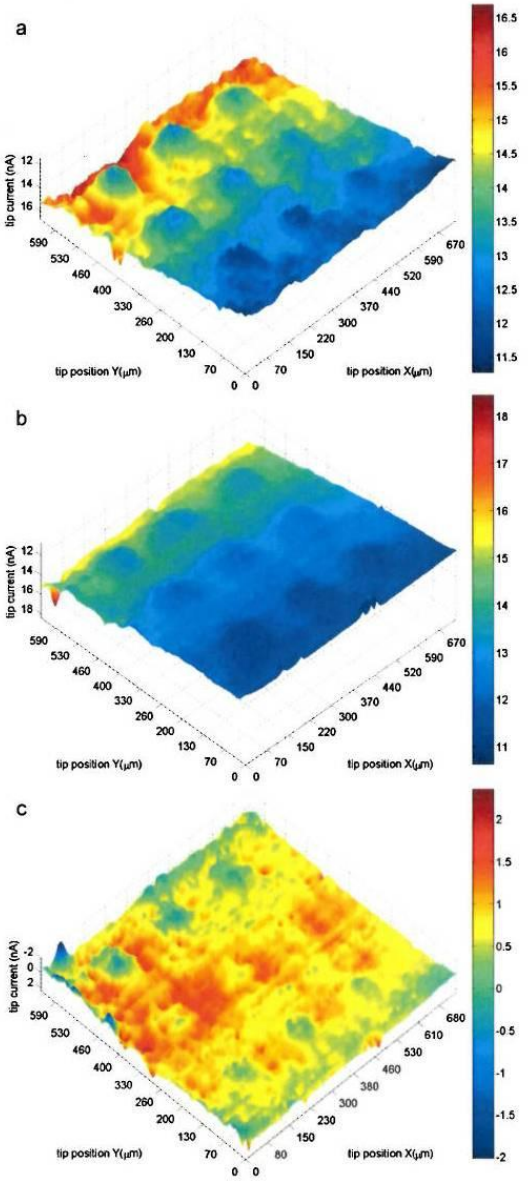

Fig. 3. Area scan of PEI/avidin/biotinylated antibody arrays on screen printed carbon electrode (a) before and (b) following rinsing and 30 min exposure to water; (c) absolute change in measured current. (Scan rate was 10 μm per step.) (Note *Z* axis scales are in reverse for visual aid.)

Please cite this article in press as: J.L. Holmes, et al., A new application of scanning electrochemical microscopy for the label-free interrogation of antibody–antigen interactions, Anal. Chim. Acta (2011), doi:10.1016/j.aca.2011.01.033

G Model
ACA-230978; No. of Pages 6
ARTICLE IN PRESS
J.L. Holmes et al. / Analytica Chimica Acta xxx (2011) xxx–xxx

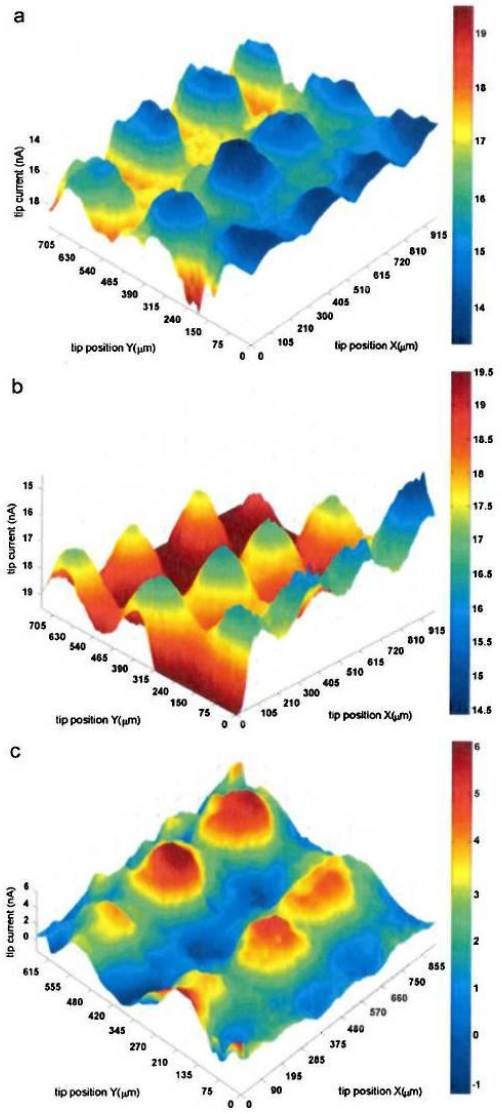

Fig. 4. SECM scan of a PEI/avidin/biotinylated antibody array on a screen-printed carbon electrode; (a) following exposure to biotinylated antibody NSE, (b) following further exposure to complementary NSE antigen at 200 pg mL^{-1}, and (c) absolute change in measured current. (Scan rate was 10 μm per step.) (Note Z axis scales are in reverse for visual aid).

Evidence for this type of behaviour comes from earlier work on DNA where the charge on the mediator is found to determine the electrochemical response at the surface. DNA is an anionic polymer due to the presence of phosphate groups and when an anionic mediator is utilized (ferricyanide), increasing the amount of DNA at the surface by hybridisation led to a decrease in current transfer due to repulsion and inhibition of mediator diffusion [33]. However

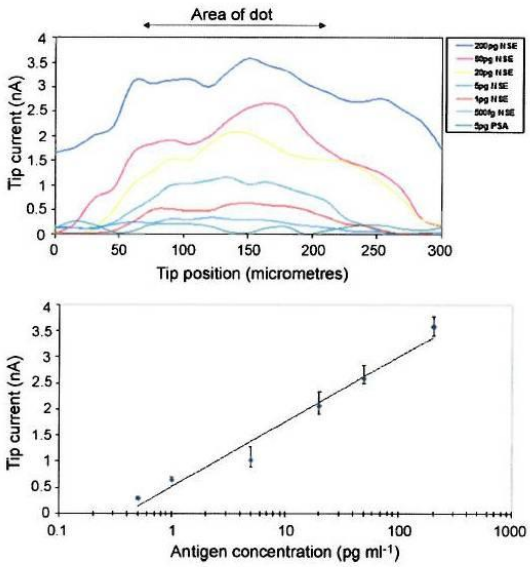

Fig. 5. (a) Mean changes of a 12 dot array scan ($n = 12$) taken over PEI/avidin/biotinylated antibody surface area to various antigen concentrations (no error bars are included for clarity, data points on individual curves represent the tip current values taken in different sites of the dots); (b) Calibration plot showing changes in current measured ($n = 12$) vs. NSE concentration. Equation is $y = 0.54 \ln(x) + 0.51$, $R^2 = 0.97$ and the error bars show the standard deviation between the 12 individual dots.

when a cationic hexamine ruthenium mediator was used, increasing the amount of DNA led to an increase in current transfer [30]. This is thought to be due to the cationic mediator being bound by the anionic DNA, thereby increasing the local concentration of mediator at the surface and enhancing electron transfer between the surface and the probe tip. In a similar fashion we believe the binding of antigen causes a localised increase of mediator (in this case ferrocene carboxylic acid) by the same principle and leads to increased current transfer.

The results demonstrate that NSE is bound at the surface in greater concentration in the modified areas, indicating that specific binding is indeed occurring. There appears to be some non-specific binding as shown by the increase in current over the unmodified carbon surface however, this non-specific binding was only observed at the highest concentration of 200 pg mL^{-1} and not when investigating the lower antigen concentrations. This confirms our earlier results obtained with microelectrode arrays [9]. Further confirmation was obtained by control experiments with PSA which showed a low level of non-specific binding over the entire surface but no specific binding to the anti-NSE; this is demonstrated in Fig. 5a.

In each investigation, an array of 12 dots was imaged with a surface profile being obtained for each separate dot. The 12 profiles could be combined to give a mean peak magnitude response for these dots. Fig. 5a shows the mean traces for 12 dotted samples, exposed to a variety of concentrations (0.5–200 pg mL^{-1}) of NSE and it is clear that an increase in tip current as the concentration of antigen increases occurs over the modified regions. For 200 pg mL^{-1} the dot profile appears larger and this is believed to be due to saturation of the area resulting in a much greater level of non-specific binding to the carbon being observed. There is also

Please cite this article in press as: J.L. Holmes, et al., A new application of scanning electrochemical microscopy for the label-free interrogation of antibody–antigen interactions, Anal. Chim. Acta (2011), doi:10.1016/j.aca.2011.01.033

G Model
ACA-230978; No. of Pages 6
ARTICLE IN PRESS
6 J.L. Holmes et al. / Analytica Chimica Acta xxx (2011) xxx–xxx

sign of the dot swelling in size at 20 and 50 pg mL^{-1} antigen concentration however, at the lower concentrations (0.5–5 pg mL^{-1}) there is clearly very little change in current to the carbon region. Fig. 5b shows a calibration profile obtained by plotting the peak mean dot responses with respect to antigen concentration. A linear relationship can be seen between the response and the log of the concentration in the range 0.5–200 pg mL^{-1}. A logarithmic relationship has also been found between ac impedance and antigen concentration in previous immunosensor work [8,10]. This demonstrates the potential for this technique to detect and quantify the presence of a target in solution.

The limits of detection for NSE in this experiment (0.5–200 pg mL^{-1}) are comparable to those obtained with sonochemically microfabricated arrays (0.5 pg mL^{-1}) [12] – and substantially lower than we obtained for similar systems based on macroelectrodes [7,8,10]. Previous work has succeeded in imaging layers of immobilized antibodies [34], however their technique required the use of enzyme modified antigens and also only reported the use of excess labelled antigen whereas our technique is label-free and is capable of producing a calibration curve. The sensitivity of our method also compares well with fluorescence based assays, for example, when microarrays on silicon were utilized, antibody–peptide specific interactions could be observed with a detection limit of 0.5–1 ng mL^{-1} [35,36].

The key significance of this work is that for the first time we have demonstrated the feasibility of SECM antibody based arrays for the development of high throughput label-free affinity based analysis. This highly simplified approach could in some contexts directly challenge the fluorescence based approach for molecular diagnostic and/or other applications.

4. Conclusions

We have within this paper demonstrated the potential for utilizing the SECM to image arrays of immobilized antibodies and furthermore detect binding of the antigen using a label-free protocol. A clear relationship between the antigen concentration and the changes in the signals obtained for binding to the arrays is observed. A calibration profile showed a clear correlation of change in current with respect to antigen concentration with detection limits of 0.5–200 pg mL^{-1}. The low (pg mL^{-1}) limits of detection will aid in the analysis of physiological samples since they can be diluted before use therefore diminishing the effects of interferents.

The results obtained within this work demonstrate the feasibility of using the SECM to analyse surface binding of antigens. This technique although slower than fluorescent methods, has a significantly lower cost base and does not require labelling of any kind, including fluorescent labelling of samples. Further work to be conducted will include the improvement of the preparation of arrays to increase the number of samples being tested at one time and also to allow for 'control dots' being incorporated within an array.

Acknowledgements

The authors would like to thank Dr Michael Cauchi and Dr Lee Larcombe for helping in imaging and formatting scan surfaces as well as Cranfield Health for funding a PhD project for JLH.

References

[1] R. John, M. Spencer, G.G. Wallace, M.R. Smyth, Anal. Chim. Acta 249 (1991) 381–385.
[2] S. Cosnier, Electroanalysis 17 (2005) 1701–1715.
[3] M. Diaz-Gonzalez, M.B. Gonzalez-Garcia, A. Costa-Garci, Electroanalysis 17 (2005) 1901–1918.
[4] S. Rodriguez-Mozaz, M.J.L. de Alda, D. Barcelo, Anal. Bioanal. Chem. 386 (2006) 1025–1041.
[5] S. Grant, F. Davis, J.A. Pritchard, K.A. Law, S.P.J. Higson, T.D. Gibson, Anal. Chim. Acta 495 (2003) 21–32.
[6] S. Grant, F. Davis, K.A. Law, A.C. Barton, S.D. Collyer, S.P.J. Higson, T.D. Gibson, Anal. Chim. Acta 537 (2005) 163–168.
[7] G.-Z. Garifallou, G. Tsekenis, F. Davis, P.A. Millner, D.G. Pinacho, F. Sanchez-Baeza, M.-P. Marco, T.D. Gibson, S.P.J. Higson, Anal. Lett. 40 (2007) 1412–1442.
[8] G. Tsekenis, G.-Z. Garifallou, F. Davis, P.A. Millner, D.G. Pinacho, F. Sanchez-Baeza, M. Pilar Marco, T.D. Gibson, S.P.J. Higson, Anal. Chem. 80 (2008) 9233–9239.
[9] A.C. Barton, S.D. Collyer, F. Davis, G. Garifallou, G. Tsekenis, E. Tully, R. O'Kennedy, T.D. Gibson, P.A. Millner, S.P.J. Higson, Biosens. Bioelectron. 24 (2009) 1090–1095.
[10] G. Tsekenis, G.-Z. Garifallou, F. Davis, P.A. Millner, T.D. Gibson, S.P.J. Higson, Anal. Chem. 80 (2008) 2058–2062.
[11] A.C. Barton, F. Davis, S.P.J. Higson, Anal. Chem. 80 (2008) 6198–6205.
[12] A.C. Barton, F. Davis, S.P.J. Higson, Anal. Chem. 80 (2008) 9411–9416.
[13] A.C. Barton, F. Davis, S.P.J. Higson, Anal. Lett. 43 (2010) 2160–2170.
[14] M. Wilchek, E.A. Bayer, Anal. Biochem. 171 (1988) 1–32.
[15] P. Pantano, T.H. Morton, W.G. Kuhr, J. Am. Chem. Soc. 113 (1991) 1832–1833.
[16] P. Martens, A. Raabe, P. Johnsson, Stroke 29 (1998) 2363–2366.
[17] D.T. Laskowitz, H. Grocott, A. Hsia, K.R. Copeland, J. Stroke Cerebrovasc. Dis. 7 (1998) 234–241.
[18] U. Missler, M. Wiesmann, C. Friedrich, M. Kaps, Stroke 28 (1997) 1956–1960.
[19] T. Yasukawa, T. Kaya, T. Matsue, Anal. Chem. 71 (1999) 4637–4641.
[20] W. Feng, S.A. Rotenberg, M.V. Mirkin, Anal. Chem. 75 (2003) 4148–4154.
[21] Y. Torisawa, T. Kaya, Y. Takii, D. Oyamatsu, M. Nishizawa, T. Matsue, Anal. Chem. 75 (2003) 2154–2158.
[22] R.T. Kurulugama, D.O. Wipf, S.A. Takacs, S. Pongmayteegul, P.A. Garris, J.E. Baur, Anal. Chem. 77 (2005) 1111–1117.
[23] Y. Torisawa, N. Ohara, K. Nagamine, S. Kasai, T. Yasukawa, H. Shiku, T. Matsue, Anal. Chem. 78 (2006) 7625–7631.
[24] T. Wilherm, G. Wittstock, Langmuir 18 (2002) 9485–9493.
[25] D. Oyamatsu, Y. Hirano, N. Kanaya, Y. Mase, M. Nishizawa, T. Matsue, Bioelectrochemistry 60 (2003) 115–121.
[26] M. Suzuki, T. Yasukawa, Y. Mase, D. Oyamatsu, H. Shiku, T. Matsue, Langmuir 20 (2004) 11005–11011.
[27] H. Yamada, H. Fukumoto, T. Yokoyama, T. Koike, Anal. Chem. 77 (2005) 1785–1790.
[28] B. Liu, A.J. Bard, C. Li, H. Kraatz, J. Phys. Chem. 109 (2005) 5193–5198.
[29] E. Fortin, P. Mailley, L. Lacroix, S. Szunerits, Analyst 131 (2006) 186–193.
[30] W.S. Roberts, F. Davis, S.P.J. Higson, Analyst 134 (2009) 1302–1308.
[31] M. Schönhoff, Curr. Opin. Colloid Interf. Sci. 8 (2003) 86–95.
[32] G. Chai, J.M. Brewer, L.L. Lovelace, T. Aoki, W. Minor, L. Lebioda, J. Mol. Biol. 341 (2004) 1015–1021.
[33] F. Turcu, A. Schulte, G. Hartwich, W. Schuhmann, Biosens. Bioelectron. 20 (2004) 925–932.
[34] G. Wittstock, K.-J. Yu, H.B. Halsall, T.H. Ridgway, W.R. Heineman, Anal. Chem. 67 (1995) 3578–3582.
[35] M. Cretich, F. Damin, R. Longhi, C. Gotti, C. Galati, L. Renna, M. Chiari, Methods Mol. Biol. 669 (2010) 147–160.
[36] M. Cretich, G. di Carlo, R. Longhi, C. Gotti, N. Spinella, S. Coffa, C. Galati, L. Renna, M. Chiari, Anal. Chem. 81 (2009) 5197–5203.

Please cite this article in press as: J.L. Holmes, et al., A new application of scanning electrochemical microscopy for the label-free interrogation of antibody–antigen interactions, Anal. Chim. Acta (2011), doi:10.1016/j.aca.2011.01.033

Appendix 2: Poster of Work presented at 1st Biosensing Technology Conference, Bristol, 2009.

Cranfield UNIVERSITY

Cranfield Health

DNA Detection – from electrochemistry to imaging.

Joanne L. Holmes, Frank Davis, William S. Roberts, Séamus P. J. Higson

Introduction

We have previously described a simple and novel DNA hybridisation based AC impedimetric biosensor capable of differentiating, in the first instance, between differing species of fish[1] (Fig 1). Later work used this technique to detect single gene DNA with greatly enhanced (fg ml^{-1}) sensitivities[2] (Fig 2) and further studies using complimentary optical techniques confirmed hybridisation[3] (Fig 3). We now utilise a novel imaging method, Scanning Electrochemical Microscopy[4] (SECM) to directly image DNA hybridisation at electrode surfaces.

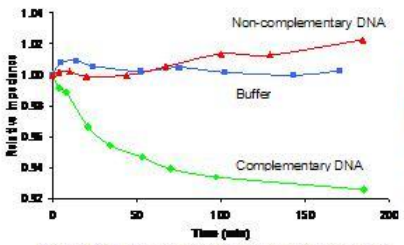

Figure 1. Hybridisation of complementary and non-complementary DNA at electrode surface

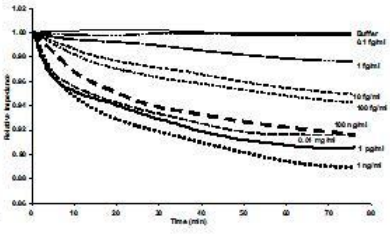

Figure 2. Hybridisation of single gene DNA at electrode surface

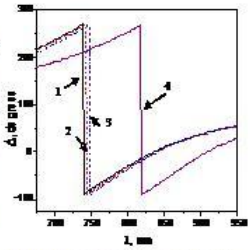

Figure 3. Confirmation of DNA hybridisation by TIRE (1. bare Au 2. PEI 3. DNA 4. Complementary DNA)

Methods/Materials

SECM experiments (Fig 4) were carried out using an Uniscan SECM270 (Uniscan Instruments Ltd, Buxton, UK). Hexaammine ruthenium chloride (5mM in phosphate buffer) was used as a charge transfer mediator. In-house fabricated working electrodes were made using 8µm platinum wire encased in quartz capillaries along with a platinum wire counter electrode and a Ag/AgCl reference electrode. Carbon electrodes were patterned with a microdot array of cationic polyethylenimine (PEI).

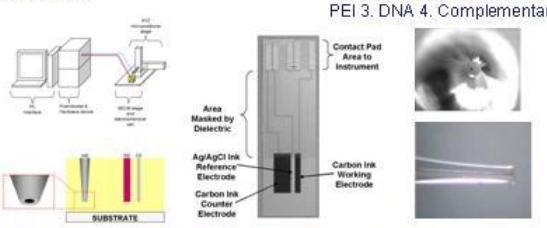

Figure 4. Schematic of the SECM equipment, carbon screen-printed electrodes and Pt/quartz working microelectrodes.

Results

Figure 5 displays a SECM scan of an array of PEI microdots on a screen-printed carbon electrode which have been modified with (a) single stranded DNA and (b) complementary DNA resulting in (c) an increase in tip current. Figure 5(d) shows the changes in current across three microdots on binding of complementary DNA and (e) the same for non-complementary DNA. Figure 5(f) shows the relative changes and clearly demonstrates the enhanced hybridisation of complementary DNA in comparison to non-complementary DNA.

Conclusions

The significance of this work is that we have demonstrated the potential of SECM for the direct label-free electrochemical interrogation of DNA microarrays – as a simplified alternative to other existing techniques.

References
1. "Species Differentiation by DNA-modified Carbon Electrodes using an AC Impedimetric Approach", F. Davis, A. V. Nabok and S. P. J. Higson, Biosens. Bioelec., (2004) 20 1531.
2. "Single Gene Differentiation by DNA-modified Carbon Electrodes using an AC Impedimetric Approach", F. Davis, A. R. Cossins, M. A. Hughes and S. P. J. Higson, Anal. Chem., (2007), 79, 1159-1167.
3. "The study of DNA adsorption and subsequent interactions using Total Internal Reflection Ellipsometry", A. V. Nabok, A. Tsargorodskaya, F. Davis, S. P. J. Higson. Biosens. Bioelec., (2007), 23, 377-383.
4. W.S. Roberts, D.J. Lonsdale, J. Griffiths, S. P. J. Higson, Biosens. Bioelec., 2007, 23, 301-318.

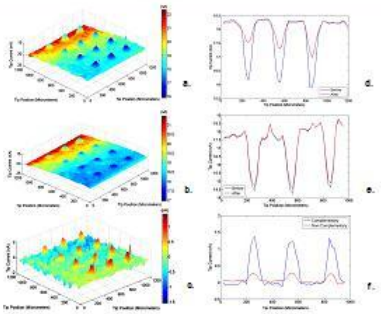

Figure 5. SECM scan of an array of (a) PEI/single stranded herring DNA, (b) after further exposure to complementary single stranded DNA, (c) absolute change in feedback current., (d) feedback currents before and after exposure to complementary DNA, (e) feedback currents before and after exposure to non-complementary DNA, (f) absolute changes in feedback current.

J.L.Holmes.05@cranfield.ac.uk

www.cranfield.ac.uk/health

Appendix 3: Poster of Work presented at 20th World Congress on Biosensors, Glasgow, 2010.

Cranfield UNIVERSITY

Cranfield Health

Scanning Electrochemical Microscopy Of Oligonucleotide DNA Microarrays As An Approach To Challenge Conventional Fluorescent Microarray Technology.

Joanne L. Holmes, Frank Davis and Séamus P. J. Higson

Introduction

Scanning electrochemical microscopy (SECM) is a novel, scanning probe technique which allows for the collection of high resolution electrochemical data at a range of surfaces. We previously described a simple and novel AC impedance based sensor to directly image DNA hybridisation at electrode surfaces to allow differentiation of DNA between differing species of fish[1]. This work, utilising SECM, demonstrates electrochemical recognition of the presence and hybridisation of nucleic acids 20 base pairs long which could ultimately challenge conventional fluorescent DNA microarray approaches.

Methods/Materials

SECM measurements (Figure 1) were performed using a Uniscan SECM270 (Uniscan Instruments Ltd, Buxton, UK). Ferrocene carboxylic acid (5mM in phosphate buffer) was used as a charge transfer mediator. In-house fabricated working electrodes were made using 8µm Pt wire encased in quartz capillaries along with a Pt wire counter electrode and a Ag/AgCl reference electrode. Screen-printed carbon surfaces were patterned with a microdot array of biotinylated polyethylenimine (PEI) which was first exposed to neutravidin and then the biotinylated oligonucleotide of interest.

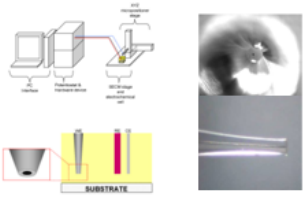

Figure 1. Schematic of the SECM equipment, and Pt/quartz working microelectrodes.

Results

Figure 2 displays a SECM scan of absolute change in feedback current of an array of polyethyleneimine microdots on screen-printed carbon modified with a biotinylated oligonucleotide sequence exposed to (a) complementary and (b) non-complementary oligonucleotide sequences. Figure 2(c) shows the changes in current across four microdots on binding of complementary and (d) non-complementary oligonucleotide sequences. Figure 2(e) shows the relative changes and clearly demonstrates the enhanced hybridisation of a complementary oligonucleotide sequence in comparison to a non-complementary oligonucleotide; tip currents changes of 2.5nA are observed for complementary and 1nA for non-complementary oligonucleotide sequences.

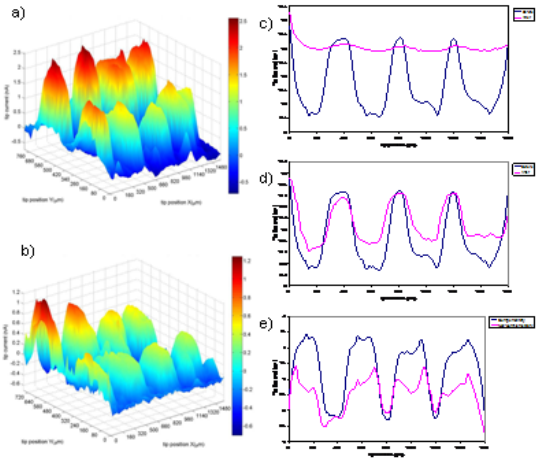

Figure 2. SECM scan of an array of (a) absolute change in feedback current to a complementary oligonucleotide sequence (b) absolute change in feedback current to non-complementary oligonucleotide sequence (c) feedback currents before and following exposure to a complementary oligonucleotide sequence, (d) feedback currents before and following exposure to a non-complementary oligonucleotide sequence, (e) absolute changes in feedback current.

Conclusions

The significance of this work is that we have demonstrated the capacity of SECM to detect changes in the charge transfer properties of a film when using short oligonucleotide sequences as well as differences between complementary and non-complementary sequences that vary by only a few mis–match pairs. This highlights the potential of the technique for the development of a highly simplified label-less approach for monitoring DNA hybridisation. This technique holds great promise in terms of providing a highly sensitive, cost effective platform for detecting DNA hybridisation via an approach that could ultimately compete with conventional DNA fluorescent based micro-array techniques[2].

J.Holmes05@cranfield.ac.uk

References
1. "Scanning Electrochemical Microscopy of Genomic DNA Microarrays – Study of Adsorption and Subsequent Interactions". W. S. Roberts, F. Davis, S. P. J. Higson, Analyst, 2009, 134, 1302.
2. "Advances in the Application of Scanning Electrochemical Microscopy to Bioanalytical Systems", W. S. Roberts, D. J. Lonsdale, J. Griffiths, S. P. J. Higson, Bioseins. Bioelec., 2007, 23, 301.

www.cranfield.ac.uk/health

Appendix 4: Programme written in MatLab for 3D Visualization of SECM sloping Marco Scan Results

```
%import excel files and view surface plots
clear
clc
close all
warning off

%import file from excel
[filename, pathname] = uigetfile('*.xls', 'select excel file');

A = xlsread([pathname '\' filename]);
disp(sprintf('The dimensions of the matrix from file %s are: %d by
%d',strrep(filename,'.xls',''),size(A)))
% START WHILE LOOP
LOOP1 = 2;
while LOOP1 == 2
    %crop data to remove unecessary sloping - get user inputs
    RowCol = [];
    while isempty(RowCol)
        RowCol = input('Enter the row and column to start cropping from,
separated by columns (row,col): ','s');
        RowCol = str2num(RowCol);
        if length(RowCol) ~= 2
            disp('I say again, please...')
            RowCol = [];
        else
            disp(sprintf('Removing first %d rows and %d
columns',RowCol(1),RowCol(2)))
            X = A(RowCol(1):end, RowCol(2):end);
        end
    end

    % Perform mean-centring
    MC = input('Mean-Centre? (y/n): ','s');
    if (isempty(MC) | MC ~= 'y')
        disp('Skipping...')
        if exist('Xorig') == 1
            X = Xorig;
        end
    else
        disp('Mean-centring data...')
        if exist('Xorig') == 0
            Xorig = X;
        end
        X = mncn(X);
    end

    spkn1 = input('Enter a negative value to remove spikes or hit Enter
for defaults: ');
    if isempty(spkn1)
        disp('Defaulting to fixed respective parameters...')
```

```
        spknN = -0.5;
        spksN = [num2str(spknN) 'pA'];
    end

    spkn2 = input('Enter a positive value to remove spikes or hit Enter
for defaults: ');
    if isempty(spkn2)
        disp('Defaulting to fixed respective parameters...')
        spknP = 0.5;
        spksP = [num2str(spknP) 'pA'];
    end

    %converting to current measurement mA, nA, pA
    disp('Choose units: pA (1); nA (2); mu-A (3)')
    currmeas = input('Choice: ');
    if isempty(currmeas)
        currmeas = 4;
    end
    switch (currmeas)
        case 1
            disp('picoAmps..')
            X = X*1E12;
            unts = '(pA)';
            if exist('spkn1') == 1
                spknN = spkn1;
                spksN = [num2str(spkn1) 'pA'];
            end

            if exist('spkn2') == 1
                spknP = spkn2;
                spksP = [num2str(spkn2) 'pA'];
            end
        case 2
            disp('nanoAmps..')
            X = X*1E9;
            unts = '(nA)';
            if exist('spkn1') == 1
                spknN = spkn1;
                spksN = [num2str(spkn1) 'nA'];
            end

            if exist('spkn2') == 1
                spknP = spkn2;
                spksP = [num2str(spkn2) 'nA'];
            end

        case 3
            disp('microAmps..')
            X = X*1E6;
            unts = '(\mum)';
            if exist('spkn1') == 1
                spknN = spkn1;
                spksN = [num2str(spkn1) '\muA'];
            end

            if exist('spkn2') == 1
```

```
                spknP = spkn2;
                spksP = [num2str(spkn2) '\muA'];
            end
        otherwise
            disp('Defaulting to picoAmps..')
            X = X*1E12;
            unts = '(pA)';
            if exist('spkn1') == 1
                spknN = spkn1;
                spksN = [num2str(spkn1) 'pA'];
            end

            if exist('spkn2') == 1
                spknP = spkn2;
                spksP = [num2str(spkn2) 'pA'];
            end
    end



    % remove negative spikes
    remNspike = input(['Remove negative spikes below ' spksN ' (y/n):
'],'s');
    if (isempty(remNspike) | remNspike ~= 'y')
        disp('Negative spikes not removed...')
    else
        disp('Removing spikes...')
        % use for loops and if - else statements...
        X2 = zeros(size(X,1),size(X,2));
        for i = 1:size(X,1)
            for j = 1:size(X,2)
                if X(i,j) < spknN
                    X2(i,j) = spknN;
                else
                    X2(i,j) = X(i,j);
                end
            end
        end
        % Update X
        X = X2; clear X2
    end

    remPspike = input(['Remove psoitive spikes above ' spksP ' (y/n):
'],'s');
    if (isempty(remPspike) | remPspike ~= 'y')
        disp('Positive spikes not removed...')
    else
        disp('Removing spikes...')
        % use for loops and if - else statements...
        X2 = zeros(size(X,1),size(X,2));
        for i = 1:size(X,1)
            for j = 1:size(X,2)
                if X(i,j) > spknP
                    X2(i,j) = spknP;
                else
                    X2(i,j) = X(i,j);
```

```
                end
            end
        end
        % Update X
        X = X2; clear X2
    end

    %creating distance vectors
    scanint = input('Enter the scan interval (Default = 20): ');
    if isempty(scanint)
        disp('Defaulting to 20..')
        scanint = 20;
    end

    distx = 0:scanint:size(X,2)*scanint;
    disty = 0:scanint:size(X,1)*scanint;

    %view surface plot
    figure (1)
    disp('viewing surface plot')
    surf(X,'FaceColor','interp','EdgeColor','none')
    shading interp
    colorbar
    xlabel('tip position X(\mum)')
    ylabel('tip position Y(\mum)')
    zlabel(['tip current ' unts])
    title(['surface plot of ' strrep(filename,'.xls','') ' (INT: '
int2str(scanint) '\mum)'])
    axis tight

    set(gca,'XTick', 1:length(distx)/10:length(distx));
    set(gca,'XTickLabel',distx(1:length(distx)/10:length(distx)))
    set(gca,'YTick', 1:length(disty)/10:length(disty));
    set(gca,'YTickLabel',disty(1:length(disty)/10:length(disty)))

    % Display second plot with range-scaled values
    figure (2)
    % Calculate range-scaled matrix
    Xrs = rangescaleJo(X);
    surf(Xrs,'FaceColor','interp','EdgeColor','none')
    shading interp
    colorbar
    xlabel('tip position X(\mum)')
    ylabel('tip position Y(\mum)')
    zlabel('RELATIVE PERCENT OF TIP CURRENT')
    title(['surface plot of ' strrep(filename,'.xls','') ' (INT: '
int2str(scanint) '\mum)'])
    axis tight

    set(gca,'XTick', 1:length(distx)/10:length(distx));
    set(gca,'XTickLabel',distx(1:length(distx)/10:length(distx)))
    set(gca,'YTick', 1:length(disty)/10:length(disty));
    set(gca,'YTickLabel',disty(1:length(disty)/10:length(disty)))

    % Option to reverse z-axis for hexamine!
    LOOP = 1;
```

```
    but0 = 1;
    while LOOP == 1
        rev1 = input('Reverse Z-axis? (y/n): ','s');
        if (isempty(rev1) | rev1 ~= 'y')
            disp('Skipping...')
            LOOP = 0;
        else
            if isodd(but0)
                figure (1)
                set(gca,'ZDir','Reverse')
                figure (2)
                set(gca,'ZDir','Reverse')
            else
                figure (1)
                set(gca,'ZDir','Normal')
                figure (2)
                set(gca,'ZDir','Normal')
            end
            but0 = but0+1;
            LOOP = 1;
        end
    end

    %reminder to save
    repeat = input('save image? (y/n): ','s');
    if (isempty(repeat) | repeat ~='y')
        disp('Not saved.')
    else
        savename = input('Enter new filename: ','s');
        if isempty(savename)
            disp('Not saving image...')
        else
            figure (1)
            print(gcf,'-djpeg70',[savename '_' strrep(filename,'.xls','')
'FIG1.jpg'])
            figure (2)
            print(gcf,'-djpeg70',[savename '_' strrep(filename,'.xls','')
'FIG2.jpg'])
        end
    end

    % Repeat?
    GoAgain = input('Repeat again? (y/n): ','s');
    if (isempty(GoAgain) | GoAgain ~= 'y')
        disp('Quitting...')
        LOOP1 = 0;
    else
        LOOP2 = 1;
        clear spkn1 spkn2
    end
end
%END WHILE LOOP
```